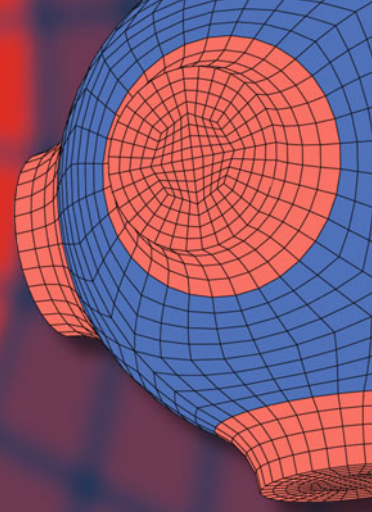


Advanced Structured Materials

Azman Ismail
Fatin Nur Zulkipli
Syajaratunnur Yaakup
Andreas Öchsner *Editors*



Materials and Technologies for Future Advancement

 Springer


Advanced Structured Materials

Volume 193

Series Editors

Andreas Öchsner, Faculty of Mechanical Engineering, Esslingen University of Applied Sciences, Esslingen, Germany

Lucas F. M. da Silva, Department of Mechanical Engineering, Faculty of Engineering, University of Porto, Porto, Portugal

Holm Altenbach , Faculty of Mechanical Engineering, Otto von Guericke University Magdeburg, Magdeburg, Sachsen-Anhalt, Germany

Common engineering materials are reaching their limits in many applications, and new developments are required to meet the increasing demands on engineering materials. The performance of materials can be improved by combining different materials to achieve better properties than with a single constituent, or by shaping the material or constituents into a specific structure. The interaction between material and structure can occur at different length scales, such as the micro, meso, or macro scale, and offers potential applications in very different fields.

This book series addresses the fundamental relationships between materials and their structure on overall properties (e.g., mechanical, thermal, chemical, electrical, or magnetic properties, etc.). Experimental data and procedures are presented, as well as methods for modeling structures and materials using numerical and analytical approaches. In addition, the series shows how these materials engineering and design processes are implemented and how new technologies can be used to optimize materials and processes.

Advanced Structured Materials is indexed in Google Scholar and Scopus.

Azman Ismail · Fatin Nur Zulkipli ·
Syajaratunnur Yaakup · Andreas Öchsner
Editors

Materials and Technologies for Future Advancement

 Springer

Editors

Azman Ismail
Centre for Women Advancement
and Leadership, Malaysian Institute
of Marine Engineering Technology
Universiti Kuala Lumpur
Lumut, Perak, Malaysia

Syajaratunnur Yaakup
Malaysian Institute of Marine Engineering
Technology
Universiti Kuala Lumpur
Lumut, Perak, Malaysia

Fatin Nur Zulkipli
Information Science Studies, College
of Computing, Informatics,
and Mathematics
Universiti Teknologi MARA, Kelantan
Branch
Machang, Malaysia

Andreas Öchsner
Faculty of Mechanical Engineering
Esslingen University Applied Sciences
Esslingen am Neckar, Germany

ISSN 1869-8433

Advanced Structured Materials

ISBN 978-3-031-38992-4

<https://doi.org/10.1007/978-3-031-38993-1>

ISSN 1869-8441 (electronic)

ISBN 978-3-031-38993-1 (eBook)

© The Editor(s) (if applicable) and The Author(s), under exclusive license to Springer Nature Switzerland AG 2023

This work is subject to copyright. All rights are solely and exclusively licensed by the Publisher, whether the whole or part of the material is concerned, specifically the rights of translation, reprinting, reuse of illustrations, recitation, broadcasting, reproduction on microfilms or in any other physical way, and transmission or information storage and retrieval, electronic adaptation, computer software, or by similar or dissimilar methodology now known or hereafter developed.

The use of general descriptive names, registered names, trademarks, service marks, etc. in this publication does not imply, even in the absence of a specific statement, that such names are exempt from the relevant protective laws and regulations and therefore free for general use.

The publisher, the authors, and the editors are safe to assume that the advice and information in this book are believed to be true and accurate at the date of publication. Neither the publisher nor the authors or the editors give a warranty, expressed or implied, with respect to the material contained herein or for any errors or omissions that may have been made. The publisher remains neutral with regard to jurisdictional claims in published maps and institutional affiliations.

This Springer imprint is published by the registered company Springer Nature Switzerland AG
The registered company address is: Gewerbestrasse 11, 6330 Cham, Switzerland

Paper in this product is recyclable.

Preface

This book is a platform to publish new progress in the field of materials and technologies that can offer significant developments with the possibility of changing the future. These emerging developments will change the way we live now at an unprecedented pace across our society. It is important to note that such modern developments are no longer restricted to a single discipline, but are the outcome of a multidisciplinary approach, which combines many different engineering disciplines. This book explores the new technology landscape that will have direct impact on production-related sectors, individually and in combination with different disciplines. A major driver for this actual research is efficiency, many times connected with a focus on environmental sustainability.

Lumut, Malaysia
Machang, Malaysia
Lumut, Malaysia
Esslingen am Neckar, Germany

Azman Ismail
Fatin Nur Zulkipli
Syajaratunnur Yaakup
Andreas Öchsner

Contents

1	Analysis of the Natural Hydraulic Lime Mortar’s Properties Under Accelerated Tropical Climate Conditions	1
	Nadia Razali, Alan M. Forster, Nurriswin Jumadi, and Nadlene Razali	
1.1	Introduction	1
1.2	Methodology	2
1.2.1	Specimens Manufacturing	2
1.2.2	Curing Process	3
1.2.3	Chemical and Physical Testing	3
1.3	Results and Discussions	5
1.3.1	Potential Hydrogen—pH	5
1.3.2	Carbonation Depth	6
1.3.3	Flexural Strength	7
1.3.4	Compressive Strength	8
1.3.5	Sorptivity	9
1.3.6	Physical Pore Structure Analysis	10
1.4	Conclusion	10
	References	11
2	Design of a Rebung Bookshelf	15
	Muhamad Aiman Hamizan Abd Halim and Nur Syazana Osman	
2.1	Introduction	15
2.2	Methodology	16
2.3	Results and Discussion	17
2.4	Conclusion	19
	References	20
3	Modelling a Temperature Based Speed Control of a Fan	21
	Noor Ikmal Hakim Noor Azmi and Mohd Zain Ismail	
3.1	Introduction	21
3.2	Literature Review	22

3.2.1	Development of an Automatic Person Detection Systems to Control an AC Fan and Room Lights	22
3.2.2	Automatic Temperature Controlled Household Electric Ceiling Fan	22
3.2.3	Smarty Smart Fan	22
3.2.4	Modelling and Simulation of a Microcontroller Based Temperature Control in a Ventilation System	23
3.2.5	Temperature Based Speed Control a of Fan by Using an Arduino	23
3.2.6	The Development of Arduino Based Automatic Fan Control System Using PIR Sensor	23
3.3	Methodology	24
3.4	Results and Discussion	26
3.5	Conclusion	27
	References	28
4	Development of an Automated Segregator for Solid Waste	29
	Muhammad Sufi Johari, Ainul Hakimah Karim, and Siti Hafshar Samseh	
4.1	Introduction	29
4.2	Methodology	30
4.3	Results and Discussion	30
4.3.1	Electronic Circuit Design	30
4.3.2	Sensor Behavior	31
4.3.3	Monitoring System	35
4.3.4	Error for Classification	36
4.3.5	Discussion	36
4.4	Conclusion	37
	References	37
5	Design and Development of an Efficient Meat Smoker	39
	Ahmad Qamarul Arifin Rahman and Faiza Mohamed Nasir	
5.1	Introduction	39
5.2	Methodology	40
5.2.1	Conceptual Designs	40
5.2.2	CFD Simulations	40
5.2.3	Decision Analysis	41
5.2.4	Fabrication and Assembly	41
5.3	Results and Discussion	44
5.4	Conclusion	45
	References	45

- 6 Between Batik and Fiberglass: The Hybrid-Technology of Boat Construction** 47
Aizat Khairi, Shaiful Bakri Ismail,
and Shamsul Effendy Abdul Hamid
 - 6.1 Introduction 47
 - 6.2 Methodology 49
 - 6.3 Results and Discussion 49
 - 6.3.1 The Evolution of Boat Making Techniques: From Wood to Fiberglass 49
 - 6.3.2 Batik Application in the Process of Making Fiberglass Boat in UniKL MIMET 50
 - 6.3.3 First Stage (Planning) 50
 - 6.3.4 Second Stage (Boat Construction) 51
 - 6.3.5 Third Stage (Analysis of Batik-Based Fiberglass Boat) 51
 - 6.4 Conclusion 52
 - References 53

- 7 Conceptual Design of a Mini Houseboat for Local Inland Water Use** 55
Muhammad Nasuha Mansor, Iwan Zamil Mustaffa Kamal,
Zaimi Zainal Mukhtar, Anis Akmal Zulkefle,
and Ainul Bahri Roslan
 - 7.1 Introduction 55
 - 7.2 Literature Review 56
 - 7.3 Research Methodology 58
 - 7.4 Results and Discussion 58
 - 7.5 Conclusion 67
 - References 67

- 8 Effect of Barnacle Fouling on Ship Resistance Using MATLAB Image Processing** 69
Shaiful Bakri Ismail, Zulzamri Salleh, Mohd Faizal Abdul Razak,
Aizat Khairi, Mohd Zaifulrizal Zainol,
and Muhammad Azrin Muhammad Azhar
 - 8.1 Introduction 69
 - 8.2 Literature Review 70
 - 8.3 Research Methodology 71
 - 8.3.1 Flowchart of Image Processing in MATLAB and C++ Programing 71
 - 8.4 Results and Discussion 73
 - 8.4.1 Raw Image of Barnacles 73
 - 8.4.2 Image Processing of Barnacles 75
 - 8.4.3 Result of Fouling Coefficient and Ship Resistance 75
 - 8.4.4 Result of Fouling Resistance 76

8.4.5	Result of Total Resistances	76
8.5	Conclusion and Recommendation	79
	References	81
9	Finite Element Analysis on Enhancement of Contactless Power Transfer by Using Metamaterials—A Review	83
	Mohd Zaifulrizal Zainol, Mohd Faizal Abdul Razak, and Shaiful Bakri Ismail	
9.1	Introduction	83
9.2	Finite Element Analysis	84
9.3	Finite Element Analysis of Enhancement Contactless Power System by Using Metamaterials	85
9.3.1	What is a Metamaterial	85
9.3.2	Finite Element Analysis Setup and Result	86
9.4	Finite Element Analysis of Contactless Power Transfer and Its Losses in Air Gaps	87
9.4.1	Effect on Mutual Inductance and Coupling Coefficient	87
9.4.2	Effect on Magnetic Flux Distribution Ratio	90
9.5	Finite Element Analysis of Contactless Power with Different Types of Coils and Shapes	92
9.6	Latest Research Development	94
9.7	Conclusion	94
	References	95
10	Flexural Characteristic of Carbon Powder Bio-composite with Different Matrix Layer Sandwich Panels	99
	Zulzamri Salleh and Muhammad Azmil Syafuan Mazlan	
10.1	Introduction	99
10.2	Methodology	101
10.3	Results and Discussion	103
10.4	Conclusion	103
	References	106
11	Risk Assessment of Marine High-Speed Diesel Engine Failures Onboard Naval Vessels Using Failure Mode and Effect Analysis ...	107
	Muhammad Syafiq Naquiddin Mohd Zuki, Izuan Ishak, Iwan Mustaffa Kamal, Muhammad Nasuha Mansor, and Yaseen Adnan Ahmed	
11.1	Introduction	107
11.2	Methodology	110
11.3	Results and Discussion	112
11.4	Conclusion	116
	References	119

12 Prediction of the Fibre-Reinforced Polymer Hull on the Wave Slamming Impact	121
Roslin Ramli, Mohd Hisbany Mohd Hashim, Anizahyati Alisibramulisi, Suhailah Mohamed Noor, and Noorlee Boonadir	
12.1 Introduction	122
12.2 Methodology	122
12.2.1 Material	123
12.2.2 Created Hull	123
12.2.3 Wave Components	125
12.2.4 Hydrodynamic Diffraction—FSI	126
12.3 Results and Discussion	127
12.4 Conclusion	128
References	129
13 The Effect of Welding Parameters of Flux Core Arc Welding by Utilizing Robotic Welding	131
Intan Ramli, Mohd Faizal Abdul Razak, Mohd Zaifulrizal Zainol, and Shaiful Bakri Ismail	
13.1 Introduction	131
13.2 Methodology	133
13.2.1 Robotic Arm Welding Setting	133
13.2.2 Experimental Preparation	133
13.2.3 Analysis Preparation	134
13.2.4 Hardness Test	134
13.3 Results and Discussion	136
13.3.1 Microstructure Testing	136
13.4 Conclusion	138
References	138
14 Membranes Technology Development and Challenges in Oily Wastewater Treatment: A Brief Review	141
Nurshahnawal Yaacob	
14.1 Introduction	141
14.2 Nanocomposite Membranes	142
14.3 Photocatalytic Membranes	142
14.4 Photocatalytic Membrane Reactors	143
14.5 Challenges	144
14.6 Conclusion	144
References	144
15 Compliance to IMO Sulphur Cap Regulations for Vessels of 10 Years of Age and Below	147
Kogulan Murugan and Aminuddin Md Arof	
15.1 Introduction	147
15.2 Methodology	148

15.2.1	Cost Benefit Analysis	148
15.2.2	Scenarios for Analysis	148
15.2.3	Interview with Industry Experts	149
15.3	Results and Discussion	150
15.3.1	Cost Benefit Analysis Result	150
15.3.2	Discussion	150
15.4	Conclusion	152
	References	152
16	Investigation of Impact of Various Oceanographic Variables on Offshore Platforms Behavior	155
	Md. Redzuan Zoolfakar, Muizzuddin Abdullah, and Sarah Nadiah Rashidi	
16.1	Introduction	155
16.2	Methodology	157
16.2.1	Parameter	157
16.2.2	Preparation of Offshore Model and Wave Tank	157
16.2.3	Identify Software and Set Data Value	158
16.2.4	Simulation Using Wave Tank	159
16.2.5	Data Collection and Analysis	161
16.3	Results and Discussion	161
16.4	Conclusion	164
	References	165
17	Soil Nutrient and Management in Oil Palm Plantations and Agronomic Potential of Biochar	167
	Arasu Uttran, Soh Kheang Loh, Muhammad Ahmad, and Robert Thomas Bachman	
17.1	Introduction	167
17.2	Nutrient Management in Oil Palm Plantations	168
17.2.1	Nutrient Uptake Mechanism	170
17.2.2	Organic Nutrients in Oil Palm Plantations	171
17.2.3	Inorganic Nutrients in Oil Palm Plantations	172
17.2.4	Nutrient Application System in Oil Palm Plantations	173
17.2.5	Nutrient Movement and Losses	173
17.3	Biochar as a Tool in Soil Nutrient Management	179
17.3.1	Oil Palm Biomass as Biochar Sources	179
17.3.2	Biochar Effects on Nutrient Leaching	179
17.3.3	Biochar Effect on Crop Yield	181
17.3.4	Biochar Effect on Microbial Population and Activity	181
17.4	Conclusion	183
17.5	Recommendations	183
	References	184

18	Performance Analysis on an Arduino-Based Low-Cost Active Dual-Axis Solar Tracking System	189
	Noor Hasyimah Abu Rahim, Muhammad Adam Saifuddin, and Mohamad Maaroff Bahurdin	
18.1	Introduction	189
18.2	Methodology	190
18.3	Results and Discussion	192
18.3.1	Tracker Efficiency	197
18.4	Conclusion	197
	References	198
19	Rapid Small-Scale Column Test of Oil Palm Frond Biochar Potential as Heavy Metal Adsorbent	199
	Amelia Md. Som, Zhenzen Wang, Yemi Akinyugha, Padmini Karananidi, Radzi Samsunanwar, and Robert Thomas Bachmann	
19.1	Introduction	199
19.2	Methodology	202
19.3	Results and Discussion	203
19.4	Conclusion	206
	References	206
20	Effect of <i>Zingiber officinale</i> on Blood Glucose Level, Pancreas, Liver and Kidney Histology Evaluated in Diabetic Induced Dawley Rats: A Systematic Review	209
	Nurul Farisya Abd Aziz, Nur Athirah H. Abdullah, Nur Jannah Crustia Mohd Halil, Zuhaida Embi, and Ahmad Najib Hasan	
20.1	Introduction	209
20.1.1	Background	209
20.1.2	Problem Statement	210
20.1.3	Research Objective	211
20.1.4	<i>Zingiber Officinale</i>	211
20.2	Methodology	212
20.2.1	Research Design	212
20.2.2	Inclusion and Exclusion Criteria	212
20.2.3	Data Analysis	212
20.3	Results and Discussion	214
20.3.1	Blood Glucose Level	214
20.3.2	Kidney Histology	214
20.3.3	Pancreas Histology	215
20.3.4	Liver Histology	215
20.3.5	Discussion	215
20.4	Conclusion	217
	References	217

21 The Development of Simulation to Improve the Production Process Efficiency 219
 Emilyya Azrien Samri, Helmi Adly Mohd Noor,
 Syed Muhammad Shamin Syed Roslee, Rahimah Kassim,
 Fauziah Abdul Rahman, and Zirawani Baharum

21.1 Introduction 219
 21.1.1 Problem Statement 221
 21.1.2 Research Objective 221

21.2 Methodology 222
 21.2.1 Research Design 222

21.3 Results and Discussion 222
 21.3.1 Research Objective 1 223
 21.3.2 Research Objective 2 223
 21.3.3 Research Objective 3 223

21.4 Conclusion 230
 21.4.1 Overview of the Study 230
 21.4.2 Recommendation 230

References 231

22 The Effect of Oil Spill from Current Oil Spill Incidents in Malaysia 233
 Ismila Che Ishak, Aminuddin Md Arof, Md Redzuan Zoolfakar,
 Mohd Fairoz Rozali, Hayatul Safrah Salleh,
 Ahmad Shahrul Nizam Isha, and Nur Aqilah Mohd Sabri

22.1 Introduction 233
 22.1.1 Data on the Oil Spill Incidents 234

22.2 Literature Review 235
 22.2.1 The Effects of Oil Spill 235

22.3 Methodology 236
 22.3.1 The Pilot Test 236
 22.3.2 Likert Scale 236
 22.3.3 The Proposed Summary of Theoretical Framework 236

22.4 Result and Discussion 237
 22.4.1 The Qualitative Analysis of the Effect of the Oil Spill from the Current Oil Spill Incidents 237
 22.4.2 The Quantitative Analysis of the Effect of the Oil Spill from the Current Oil Spill Incidents 237

22.5 Conclusion 239

References 240

- 23 Optimization of the Effect of Hydraulic Hot-Pressing: Process Parameters on Tensile Properties of Kapok Fiber Nonwoven Web Based on Taguchi Experimental Design** 243
 - Muhammad Abdul Mun’aim Mohd Idrus, Aniq Danish Azli, Md Redzuan Zoolfakar, Raa Khimi Shuib, and Asmalina Mohamed Saat
 - 23.1 Introduction 243
 - 23.2 Methodology 245
 - 23.2.1 Materials 245
 - 23.2.2 Kapok Fiber Web Production 246
 - 23.2.3 Hydraulic Hot-Pressing Process: Experimental Design 247
 - 23.2.4 Morphology Analysis 248
 - 23.2.5 Tensile Test 248
 - 23.3 Results and Discussion 250
 - 23.3.1 Data Analysis from Table 23.3: Taguchi Analysis: Tensile Strength (MPa) Versus Temperature, Time, and Pressure 250
 - 23.3.2 S/N Ratio Analysis 251
 - 23.3.3 Analysis of Variance 251
 - 23.3.4 Surface Morphology 252
 - 23.3.5 Confirmation Experiment 252
 - 23.3.6 Regression Analysis 253
 - 23.4 Conclusion 253
 - References 254

Chapter 1

Analysis of the Natural Hydraulic Lime Mortar's Properties Under Accelerated Tropical Climate Conditions



Nadia Razali, Alan M. Forster, Nurriswin Jumadi, and Nadlene Razali

1.1 Introduction

The worldwide physical and literature evidence of lime mortar since the ancient civilization clearly states the favourable character of its setting properties and strength (Hughes and Válek 2003; Holmes and Wingate 2002). Current literature demonstrates the scientific advantages of lime over modern cement, which proves lime is greener than ordinary Portland cement (OPC). Lime requires a lower firing temperature during manufacturing and emits fewer greenhouse emissions per unit weight than OPC (Imbabi et al. 2012; Mahasenan et al. 2003). In addition, during the setting process, lime sequester carbon dioxide (CO₂), thus reducing its carbon footprint impact.

Understanding climatic conditions is a critical ‘first-order’ concern in planning and building functional and efficient buildings because climate substantially impacts the function, operation, life duration, and overall durability of a building/structure

N. Razali (✉) · N. Jumadi

Universiti Kuala Lumpur Malaysian Institute of Chemical and Bioengineering Technology, 78000 Alor Gajah, Melaka, Malaysia
e-mail: nadiarazali@unikl.edu.my

N. Jumadi

e-mail: nurriswin@s.unikl.edu.my

A. M. Forster

School of Energy, Geoscience, Infrastructure and Society, Heriot-Watt University, EH144AS, Edinburgh, Scotland, UK

e-mail: A.M.Forster@hw.ac.uk

N. Razali

Faculty of Mechanical Engineering, Universiti Teknikal Melaka Malaysia, 76100 Durian Tunggal, Melaka, Malaysia

e-mail: nadlene@unikl.edu.my

(Forster et al. 2014; Jelle 2012; Rathore et al. 2020). However, material deterioration from poor weather circumstances such as temperature fluctuations, solar radiation, atmospheric gases, humidity, rainfall, and the wind is less considered in the construction guidelines (Oliver 2008; Lomas and Porritt 2017; Mizzi et al. 2018). Lime mortar is temperature sensitive, affecting the development of hydration products and the creation of calcite compounds (Schroder and Ogletree 2010). These outputs are important in defining the strength and long-term durability and, hence, resistance to deteriorating features.

Due to changes in the construction industry landscape and lime mortar's sensitivity towards the atmosphere, most contemporary buildings in tropical Asia use Portland cement (PC) (Rasiah et al. 2017). Further widespread use of PC-based mortars is related to the benefits of the comparatively dense materials' impermeability or "waterproofing" qualities (Prezant et al. 2008). This viewpoint is largely criticized, particularly in historic structures (Banfill and Forster 1999). Lime mortars are crucial in these nations because they allow the structure to "breathe" by preventing the wall from holding moisture (Lawrence 2006). Numerous buildings and homes are constructed with PC-bound concrete because it is resistant to severe rains. In a hot-humid climate, biological growth from penetrating rain, evaporation, condensation, air pollution, dehydration, and thermal stress typically causes faults in rendering and mortars (de Oliveira et al. 2021).

1.2 Methodology

In this study, the mortar specimens were made from St. Astier NHL 3.5 lime, sand aggregates, and purified water. In order to guarantee that any salts and other contaminants were eliminated from the water, distillation was performed on it.

1.2.1 Specimens Manufacturing

The rheological characteristics of the mortars were determined using a manually controlled flow table device (BS EN 459-2:2010). The binder: aggregate volume ratio of 1:3 was chosen, and the mixing was designed based on the relative bulk density (RBD) principles, as shown in Table 1.1 (Razali et al. 2020).

Table 1.1 Mortar manufactures constituents and flows value

NHL density (g/L)	Constituent amounts of materials in the mortar used in the slump test			Flow value (mm \pm 2 mm)
	Mass of NHL (g)	Mass of sand (g)	Mass of water (g)	
650	207.9	1564.0	332.0	165

The 'dry mixing' approach was chosen, in which the binder and aggregates were mixed for three minutes using a mechanical mixer before adding water and mixing for another three minutes (Allen et al. 2003; Ball et al. 2009). The mixture then being poured into 160 × 40 × 40 mm moulds. Afterwards, an automated vibrating table was utilized to compact the samples and remove trapped air (BS 459-2: 2010).

1.2.2 Curing Process

The curing process was conducted in an environmental chamber using accelerated tropical climatic simulations of temperature (°C) and relative humidity (RH) of (i) 20 °C–60%RH; (ii) 27 °C–90%RH; and (iii) 33 °C–90%RH. Seven days after being placed inside the curing chamber, the samples were de-moulded. The samples were covered with damp hessian fabric to minimize moisture loss during the early phases of the specimen set. A CO₂ injection system was devised to ensure enough carbonation, permitting a continuous CO₂ concentration of 450–500 ppm.

1.2.3 Chemical and Physical Testing

As recommended by Hanley and Pavia (2008), a 56-day test period was chosen as an acceptable alternative to the 365-day primary test duration.

1.2.3.1 Potential Hydrogen—pH

The pH value is important to ascertain the alterations that took place during the hydration process. Rasanen and Penttala (2004) used the approach to determine the hardened mortar. In order to prevent measurement errors caused by carbonation and variations in moisture content gradient, the mortar samples were manually cut at a depth of 40 mm from the surface. Afterwards, the samples were run through a crushing press to turn them into fine powdery particles. Following the crushing step, 15 g of the specimen was mixed into 15 mL of purified water.

1.2.3.2 Carbonation Depth

The samples were sprayed with 0.1% phenolphthalein solution, in which the colour pink denotes uncarbonated mortar. The stained area was measured using a digital calliper (± 0.01 mm) and photographed with a digital single-lens reflex camera for the record.

1.2.3.3 Mortar Strength Tests

The mortar samples were tested for three-point flexural strength (flexural response) using universal testing machine at low loading rates of 2 mm/min (Apostolopoulou et al. 2020). On the other hand, the compressive strength test applied load compresses the sample between the platens of the compression testing apparatus (BS EN 459-2:2010). The results' data were calculated using the standard flexural and compressive strength test formulas.

1.2.3.4 Sorptivity Test (Capillary Absorption)

Evaluating capillary absorption by adopting the direct gravimetric technique provides insight into porous structure and volume (Benachour et al. 2009; Hall and Hoff 2012). The surface of the specimens was then coated with resin except for the bottom surface (the surface that will come into contact with water). The specimen was immersed in water that had a height of 5 mm. Five weight gain readings are taken within the specified time interval. The data was then graphed, and the sorptivity value was calculated using the slope gradient, as shown in Eq. (1.1) (Dias 2000);

$$\text{Sorptivity, } i = k\sqrt{t} \quad (1.1)$$

A study by de Oliveira et al. (2006) measured the sorptivity coefficient, k , in $\text{kg}/\text{m}^2/\text{min}^{0.5}$. In this study, however, k values are given in terms of volume; volume (mm^3) absorbed across section (mm^2) per $\text{min} = \text{mm}/\text{mm}^{0.5}$.

1.2.3.5 Physical Pore Structure Analysis

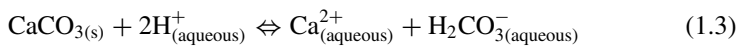
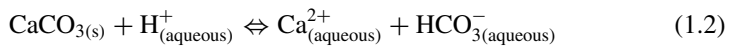
This study used an electron microscope to study further the pore structure of the mortar specimen. The scanning electron microscope (SEM) is superior to conventional microscopes in several ways. The SEM has a broad field depth, allowing a greater portion of a specimen to be in focus simultaneously. Additionally, the SEM has a lot better resolution, allowing for much greater magnification of closely spaced specimens.

1.3 Results and Discussions

1.3.1 Potential Hydrogen—pH

Figure 1.1 shows that the entire specimens read a high amount of alkalis of pH 14 on the day of casting and read pH 10–12 after a week. After 14 days, the pH of each specimen fell to 7. As a mortar exterior chemically reacts with CO_2 in the atmosphere, the $\text{Ca}(\text{OH})_2$ compound carbonates into calcite. Principally, the carbonation process, with time, lowers the pH value in the mortar by maximizing the number of Ca^{2+} ions. Although the pH values change is small, a clear trend can be distinguished.

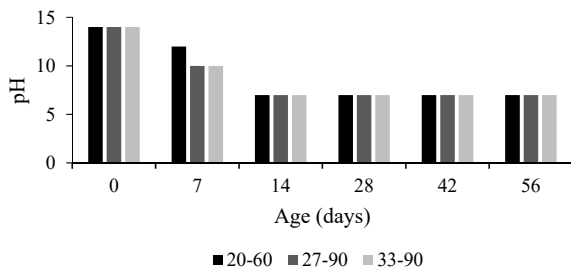
Based on the data obtained, it was determined that the neutralization process with its corresponding exothermic reaction had occurred per Eqs. (1.2) and (1.3) (Lottermoser 2010). The interaction between calcium hydroxide and carbon dioxide produces a mortar that hardens rather fast. However, the process can be reversed if the temperature, water loss, or carbon dioxide loss changes. The pH will decrease with the continued re-precipitation of carbonate, which releases hydrogen ions.



The pH value will decrease as the calcium inside the mortar solubility rises. The mortar exterior surface exhibited limited moisture vapour movement, resulting in greater pH variation and carbonation depth variation compared to the sample's opposite side. In this experiment that involves a high-humidity atmosphere, excessive moisture will transport more hydroxides (alkalis) to the surface, thus increasing the pH. This reaction may weaken the mortar since calcium ions (Ca^{2+}) are necessary to form hydrates.

Then again, the pH changes might be related to differences in material features and qualities, which had a commensurate effect on the degree of carbonation in the mortars. Carbonation is responsible for the overall decrease in pH over time. During the initial week of curing, the surfaces of all specimens were exposed to atmospheric

Fig. 1.1 pH of mortars



carbonation. The optimal CO_2 concentration promotes quick carbonation of mortar, hence lowering the pH levels.

The rate of hydration is accelerated by a high temperature, which also affects the pH. The extended exposure of the specimens probably resulted in higher pH alterations. Continuous measurements were conducted till the conclusion of the investigation to detect any pH value rise.

1.3.2 Carbonation Depth

This study's carbonation depth (Fig. 1.2) reveals that climate and curing time are vital variables determining the mortar carbonation rate. This creates an environment rich in carbonic acid, resulting in portlandite ($\text{Ca}(\text{OH})_2$) transition into calcite. The process results in the formation of calcium carbonate (CaCO_3), which aids in the mortar's hardening. Intriguingly, mortars cured at 27°C –90%RH demonstrated better carbonation than other studied climates, in which the mortars were fully carbonated in 14 days. In a lower-studied climate, the time required for complete carbonation was much longer (doubling to 28 days). On the other hand, a steady linear trend was observed during the 33°C –90%RH climate.

Due to lime's intrinsic thermodynamic features (high carbonation temperature, high CO_2 carrying capacity), carbonation rates increase as the temperature rises (Materic and Smedley 2011). As the temperature rises to 33°C , the water's contact with the solid surface increases, and the carbonation process begins swiftly. After prolonged contact with high temperatures, the materials become dehydrated, preventing the carbonation of $\text{Ca}(\text{OH})_2$. The carbonation process was continued in an atmosphere of 90%RH. This was a result of the detrimental effect of excessive humidity on carbonation. Importantly, the pace and magnitude of carbonation were generally independent of time but temperature-dependent (Materic and Smedley 2011). Lime hydration is reactivated when exposed to humid air at room temperature.

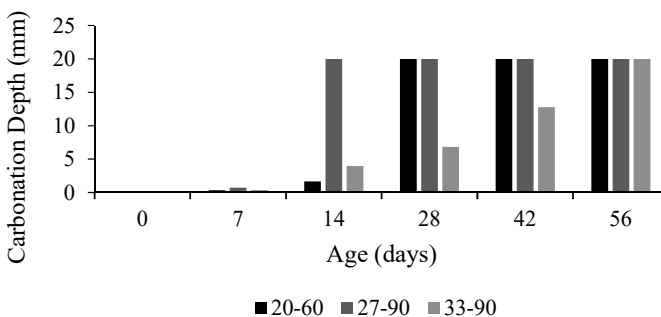


Fig. 1.2 Carbonation depth of mortars

The pace of carbonation is affected by several environmental conditions, including relative humidity, temperature, and the amount of CO_2 in the air. High CO_2 enhances calcite formation from $\text{Ca}(\text{OH})_2$. The presence of water adsorbed from the surface of calcium hydroxide (as a result of the spraying regime) significantly impacts calcium hydroxide's carbonation. The presence of water adsorbed by mortar controls the kinetics and significantly affects the carbonation progression of $\text{Ca}(\text{OH})_2$. Carbonation relies on the presence of water and happens fast near the surface. This is accentuated in a carbon dioxide-saturated environment.

1.3.3 Flexural Strength

Figure 1.3 demonstrates that the specimens' optimal curing conditions for flexural growth were at 20°C – $60\%RH$. This data illustrates both quicknesses of early strength (at 7 days) and the consistency of strong growth across 56 days. On the other hand, the strength developments in the 27°C – $90\%RH$ specimens were atypical, in which the specimens had a positive early strength development but suffered a 61% loss at 28 days. Even though curing at 33°C – $90\%RH$ experienced an early linear flexural strength growth of up to 42 days, the specimens had the weakest flexural strengths relative to specimens from different climate conditions.

The mortars improved their mechanical strength with extended curing times/ longer carbonation processes. Due to the rising binder content and porosity, which facilitates the transport of CO_2 into the mortar where portlandite ($\text{Ca}(\text{OH})_2$) is still available to undergo the carbonation process, the carbonation response was stronger with longer curing durations. This aligns with the generally acknowledged body of knowledge in this field (Hughes and Válek 2003; Holmes and Wingate 2002; Forster et al. 2014). This is true for specimens cured at 27°C – $90\%RH$. Mortars cured at the higher temperature of 33°C – $90\%RH$ exhibited the worst flexural strength, most likely due to a delayed carbonation rate impeded by very high and prolonged moisture levels that impeded CO_2 diffusion. Nonetheless, Cizer et al. (2007, 2008)

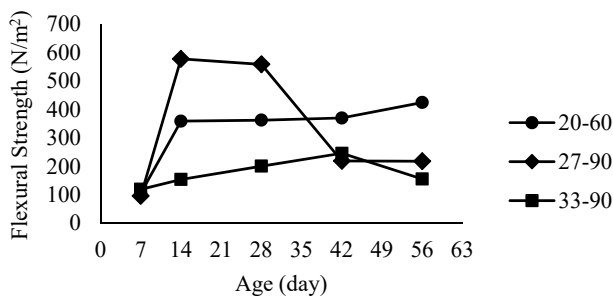


Fig. 1.3 Flexural strength of mortars

indicated that the flexural strength of modified mortar depended heavily on alternative ingredient(s), seeded material(s) and porosity.

In contrast, the flexural strengths found at the initial curing period of 28 days are inconclusive due to the fact that the specimens were greatly impacted by the water content used in the mix and humidity in the atmosphere, as there is a direct correlation between water ratio and strength. Lanas and Alvarez-Galindo (2006) developed a hypothesis that helps to explain this phenomenon by demonstrating that mortars have the best strength when a particular proportion of $\text{Ca}(\text{OH})_2$ stays uncarbonated. Observations corroborated this hypothesis on different testing days in all studied climates. A modest drop in uncarbonated $\text{Ca}(\text{OH})_2$ results in a small decrease in mortar strength. However, analytical analysis cannot precisely identify $\text{Ca}(\text{OH})_2$'s quantity.

1.3.4 Compressive Strength

Figure 1.4 illustrates the influence of temperature and curing time on the mortar's compressive strength. All specimens show an increase in strength with respect to time, even though the strength development varies according to the studied climates. It is reasonable that, while analyzing the growth of compressive strength, the variables impacting the quality of flexural strength would also be prominent. As discussed in flexural strength, carbonation rate determines strength development. The compressive strength improves over time by converting $\text{Ca}(\text{OH})_2$ to CaCO_3 (calcite). This is predicted and consistent with the recognized knowledge of the mechanics behind the development of strength in lime mortars during curing. According to Moropoulou et al. (1997), because crystalline calcite is present in the mortar, the porosity of the material is reduced, while at the same time, its strength is increased.

Mortars lost strength due to prolonged, high-temperature curing over extended periods because they exhibited a non-uniform distribution of hydration products due to rapid hydration. This resulted in an increase in porosity and a high compressive strength in the early stage. However, a decrease in longer strength development

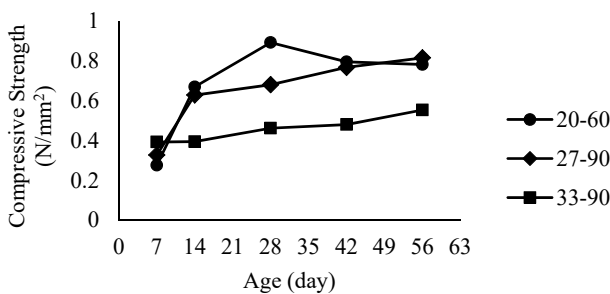


Fig. 1.4 Compressive strength of mortars

was observed in most accelerated climates. These findings correlated with Ezziane et al. (2007), who observed the strength loss evolution in elevated temperatures and proposed mineral admixtures in the mortar as a plausible solution. Some mineral admixtures in the mortar change the hydration kinetics, resulting in a decrease in heat evolution and the production of extra C–S–H.

1.3.5 Sorptivity

A substantial correlation between lime mortar and sorptivity highlights the significance of a mortar's absorption and transmission properties. Figure 1.5 demonstrates that the water absorption rate and sorptivity coefficient significantly affect the curing environment and time. The samples cured at the lower climate had a denser structure, as shown by their high sorptivity values. Additional research revealed that the 33 °C–90%RH specimens had the greatest k values, indicating an abundance of linked pores.

The mortar specimens in 20 °C–60%RH climate displayed the lowest sorptivity values. It is believed that the intricacy of matrix development in the structure is a consequence of composition and hygrothermal conditions that either promote or inhibit growth; an increase in sorptivity does not necessarily cause by a decrease in relative humidity. Based on microscopy investigation, the specimens cured at this climate observed crystal formations of unusual forms and sizes.

Even though the specimens were exposed to the same high humidity level, it was shown that the temperature impacts affected pore structure, resulting in increased sorptivity. This was likely the result of a conducive atmosphere for the development of hydration products. Once exposed outside the curing box, the temperature differential between the specimens and the ambient room temperature may have further altered the sorptivity. In order to achieve thermal balance with the surrounding air, the specimens would emit a certain quantity of moisture into the environment. As a result, moisture release and loss during equilibrium attempts would reduce the moisture content of the specimens. This would affect their absorption throughout the sorptivity

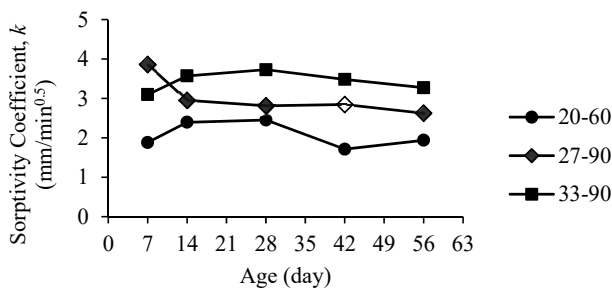


Fig. 1.5 Sorptivity coefficient, k of mortars

tests. Specimens treated at 33 °C–90%RH had a crystal structure that was smaller but more uniform and regular-shaped than those cured at 20 °C–60%RH. It is fair to conclude that these tests resulted in size discrepancies in the crystal formations, which led to a decrease in water absorption. Variations in the physical properties linked with cure led to variances in sorptivity. These findings are comparable to those of Kerr (2008), who proposed probable parameters that may influence the deterioration of the pore structure due to the formation of additional hydration products.

1.3.6 Physical Pore Structure Analysis

Figure 1.6 depicts SEM photographs of specimens. Clusters of needle-shaped (acicular) and hexagonal plate-shaped crystals can be found embedded in various places throughout the set matrix. Crystals that resemble needles (acicular) are indicative of the C–S–H morphology. Ettringite formation was also identified. Through its hydration process, ettringite hydrates fast, creating early strength and generating significant heat. Its creation might partially explain the strong outcomes of all lime mortars cured in tropical climates gaining rapid strength development but subsequently experiencing a strength loss afterwards.

1.4 Conclusion

The study shows that lime mortar specimens cured in accelerated tropical climates exhibited enhanced early-age strength development, but the strength qualities and pore structure deteriorated with time. These findings demonstrate the challenges of using NHL materials in high-temperature and high-humidity conditions, such as tropical climates. Specimens cured in accelerated tropical climates exhibited clusters of needle-shaped acicular and hexagonal plate-shaped crystals that led to unstable matrix formation. These results are critical because the pore structure's growth significantly impacts the hardened material's strength, permeability, and durability. This can potentially compromise the lime mortar's properties, leading to structural failure that could result in user safety. However, further studies should be made by studying the new mixture of NHL using other admixtures or additives to overcome the deficiency of lime mortar quality used in tropical climates.

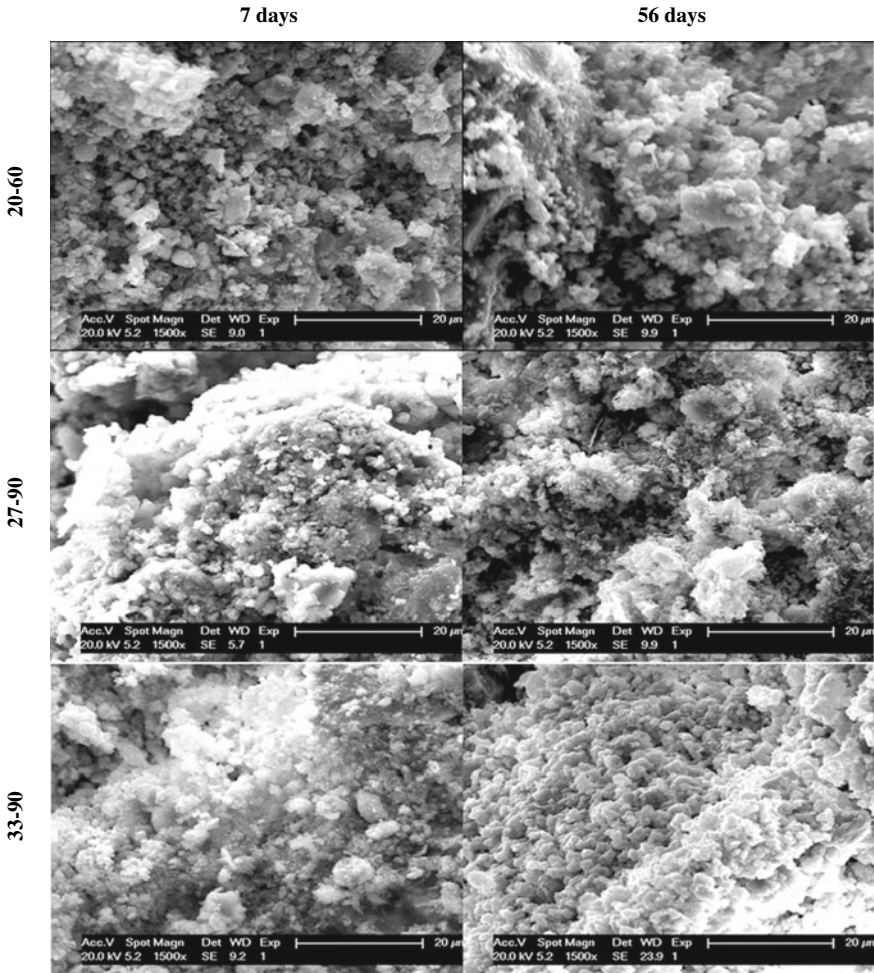


Fig. 1.6 SEM images of mortars

References

- Allen G, Allen J, Elton N, Farey M, Holmes S, Livesey P, Radonjic M (2003) Hydraulic lime mortar for stone. Donhead Publishing Ltd., Dorset, UK, Brick and Block Masonry
- Apostolopoulou M, Asteris PG, Armaghani DJ, Douvika MG, Lourenço PB, Cavaleri L, Bakolas A, Moropoulou A (2020) Mapping and holistic design of natural hydraulic lime mortars. *Cem Concr Res* 136:106167–106187
- Ball RJ, El-Turki A, Allen GC (2009) Influence of carbonation on the load dependent deformation of hydraulic lime mortars. In: Walker P et al (eds) 11th international conference on non-conventional materials and technologies (NOCMAT 2009), Bath, UK

- Banfill PFG, Forster AM (1999) A relationship between hydraulicity and permeability of hydraulic lime'. In: Bartos P, Groot C, Hughes JJ (eds) Proceedings PRO012: international RILEM workshop on historic mortars: characteristics and tests Paisley, Scotland, Edinburgh. RILEM, 11, United Kingdom
- Benachour Y, Davy CA, Skoczylas F, Houari H (2009) Effect of high calcite filler addition upon micro-structure and freeze/thaw resistance of a mortar. In: Tanabe T, Sakata K, Mihashi, H, Sato R, Maekawa K, Nakamura H (eds) Creep, shrinkage and durability mechanic of concrete and concrete structure. Taylor & Francis Group, London, UK
- Cizer O, Van Balen K, Van Gemert D, Elsen J (2007) Carbonation and hydrations of mortars with calcium hydroxide and calcium silicates binders. Taylor & Francis Group, Coventry, UK
- Cizer O, Van Balen K, Van Gemert D (2008) Blended lime-cement mortars for conservation purposes: microstructure and strength development structural analysis and historic construction. Taylor & Francis Group, London
- de Oliveira VC, Godinho JP, Grings KJO, de Oliveira RA, dos Santos EGF (2021) Performance as for water tightness of rendering mortars using admixtures. *Int J Build Pathol Adapt* 6(1):1–9
- de Oliveira LAP, de Castro Gomes JP, Gonilho Pereira CN (2006) Study of sorptivity of self-compacting concrete with mineral additives. *J Civil Eng Manag* 12(3): 215–220. <https://doi.org/10.1080/13923730.2006.9636395>
- Dias WPS (2000) Reduction of concrete sorptivity with age through carbonation. *Cem Concr Res* 30(8)
- Ezziane K, Bougara A, Kadri A, Khelafi A, Kadri E (2007) Compressive strength of mortar containing natural pozzolan under various curing conditions. *Cem Concr Compos* 29(8):587–593
- Forster AM, Szadurski EM, Banfill PFG (2014) Deterioration of natural hydraulic lime mortars, I: effects of chemically accelerated leaching on physical and mechanical properties of uncarbonated materials. *Constr Build Mater* 72:199–207
- Hall C, Hoff WD (2012) Water transport in brick. Spon Press, Oxon, UK, Stone and Concrete
- Hanley R, Pavia S (2008) A study of workability of natural hydraulic lime mortars and its influence on strength. *Mater Struct* 41(2):373–381
- Holmes S, Wingate M (2002) Building with lime: a practical introduction. ITDK, London
- Hughes JJ, Válek J (2003) Mortars in historic buildings: a review of the conservation, technical and scientific literature. Historic Scotland, Edinburgh
- Imbabi MS, Carrigan C, McKenna S (2012) Trends and developments in green cement and concrete technology. *Int J Sustain Built Environ* 1(2):194–216
- Jelle BP (2012) Accelerated climate ageing of building materials, components and structures in the laboratory. *J Mater Sci* 47(18):6475–6496
- Kerr EA (2008) Damage mechanism and reparability of high strength concrete exposed to heat, Unpublished thesis. The University of Notre Dame
- Lanas J, Alvarez-Galindo JI (2006) Masonry repair lime-based mortar: factors affecting the mechanical behaviours. *Cem Concr Res* 33(11):1867–1878
- Lawrence RMH (2006) A study of carbonation in non-hydraulic lime mortars, unpublished thesis. The University of Bath
- Lomas KJ, Porritt SM (2017) Overheating in buildings: lessons from research. *Build Res Inf* 45(1–2):1–18
- Lottermoser BG (2010) Mine wastes: characterization. Springer-Verlag, Berlin, Treatment and Environmental Impacts
- Mahasenan N, Smith S, Humphreys K (2003) The cement industry and global climate change: current and potential future cement industry CO₂ emissions. In: Greenhouse gas control technologies-6th international conference, Pergamon
- Materic V, Smedley SI (2011) High-temperature carbonation of Ca(OH)₂. *J Am Chem Soc* 50(10):5927–5932

- Mizzi B, Wang Y, Borg RP (2018) Effects of climate change on structures; analysis of carbonation-induced corrosion in reinforced concrete structures in Malta. *IOP Conf Series Mater Sci Eng* 442(1):12023–12038
- Moropoulou A, Biscontin G, Bakolas A, Bisbikou K (1997) Technology and behaviour of rubble masonry mortars. *Constr Build Mater* 11(2):119–129
- Oliver JE (ed) (2008) *Encyclopedia of world climatology*. Springer Science & Business Media
- Prezant B, Weekes DM, Miller JD (eds) (2008) *Recognition, evaluation, and control of indoor mold*. AIHA Publishing, Virginia
- Rasanen V, Penttala V (2004) The pH measurement of concrete and smoothing mortar using a concrete powder suspension. *Cem Concr Res* 34(5):813–820
- Rasiah R, Ahmed A, Al-Amin AQ, Chenayah S (2017) Climate change mitigation: comparative assessment of Malaysian and ASEAN scenarios. *Environ Sci Pollut Res* 24(3):2632–2642
- Rathore PKS, Shukla SK, Gupta NK (2020) Yearly analysis of peak temperature, thermal amplitude, time lag and decrement factor of a building envelope in tropical climate. *J Build Eng* 31:101459–101474
- Razali N, Azizan MA, Pa'ee KF, Razali N, Jumadi N (2020) Preliminary studies on calcinated chicken eggshells as fine aggregates replacement in conventional concrete. *Mater Today Proc* 31:354–359
- Schroder L, Ogletree V (2010) *Adobe homes for all climates: simple, affordable, and earthquake-resistant natural building techniques*. Chelsea Green Publishing, Vermont

Chapter 2

Design of a Rebung Bookshelf



Muhamad Aiman Hamizan Abd Halim and Nur Syazana Osman

2.1 Introduction

The objective of this project is to design a unique bookshelf for home office. Due to work from home trends during the COVID-19 pandemic, there is an increase demand on new home furniture (Global Market Insight 2021). The bookshelf is one of the furniture that can be found in everyone's home. Bookshelves have been created for ages as a form of storage. Till this day, human kept on developing new bookshelf design to meet customers need. From home to office and library, the bookshelf will always be the compulsory storage system to organize books and important files. However, the current market trends change how we use the bookshelf and how the consumers' needs change due to the current world situation.

Since the year 2020, a lot of companies forced their employee to work from home due to the COVID-19 outbreak. This is as a safety step to prevent virus spread. Several reports suggested that working from home has shifted human behaviors towards home furniture (LECTRA 2020). The environmental trends, along with a rising focus on the value of the house, are fortunate for furniture makers (LECTRA 2020). Consumers who have experienced COVID have a strong desire to improve their living area. COVID-19 caused roughly 58% of the world's population to stay at home, resulting in a surge in work-from-home, home schooling, and a slew of other "at-home" activities, such as church at home, dining at home, and more, all of which benefit from a boost in comfort and style (LECTRA 2020). Consumer expenditure

M. A. H. A. Halim (✉) · N. S. Osman

Department of Design Engineering Technology, Universiti Kuala Lumpur Malaysia Italy Design Institute, 199, Jalan 7/91, Taman Shamelin Perkasa, 56100 Kuala Lumpur, Malaysia
e-mail: aiman.halim07@s.unikl.edu.my

N. S. Osman

e-mail: nursyazana@unikl.edu.my

Fig. 2.1 The bamboo shoot or “pucuk rebung” served as the inspiration for this project



on furniture and home goods is projected to rise as social distance becomes the new normal (LECTRA 2020).

Based on the article by Lee in 2020, he also emphasizes the same matter. According to him, the need for pleasant and productive environments throughout the lockdown has created a huge potential for furniture manufacturers (Lee 2020). Companies that make the adaptive strategy might place themselves to profit handsomely both during and after the crisis. The challenge, as always, is understanding how to make the correct decisions and having the vision and determination to follow through. Current customer trends prove that furniture making for home will be the most beneficial out of other type of furniture for years to come. That is why it was decided to design a bookshelf for home office and not for an office or a library.

The study on the Malaysian craft was also carried out before the design process. By carrying out research on the Malaysian craft, it was decided to use the motif used on the Malay Songket which is the “pucuk rebung” motif (see Fig. 2.1).

2.2 Methodology

The research method for this project is by online observation, literature review, sketching development, and online survey. Online observation was done instead of physical observation due to the movement control order (MCO) during this pandemic. In the online observation, online articles and webpages were used as one of the guidelines to design this product. The first article to be reviewed covers on the furniture market trends during the COVID-19 (LECTRA 2020). Two articles discussing on the effect of wood furniture to human stress were also used for this research (Burnard and Kutnar 2020; Lipovac and Burnard 2020). Next, to come out with the best design

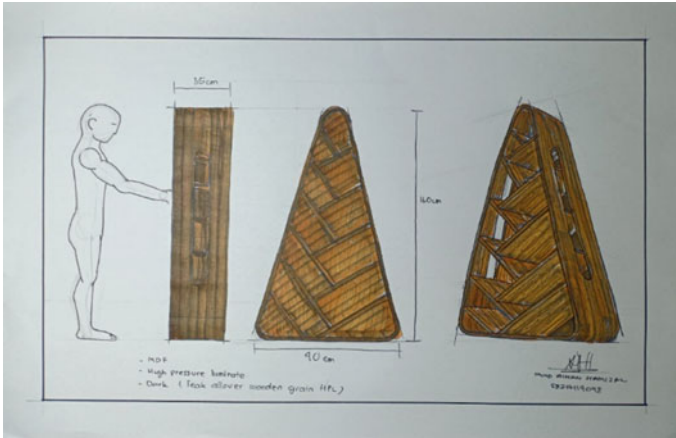


Fig. 2.2 The chosen sketch design of the Rebung bookshelf

concept, design and development sketches were made (see Fig. 2.2). Choosing the best design solution was done via a validation survey done between the student and lecturer. During the sketch development stage, the survey was also done to choose the best material for the product.

2.3 Results and Discussion

There is no doubt that the COVID-19 pandemic effected how humans behave towards home furniture. More people started to practice healthy lifestyle thus increasing the market size for eco-friendly furniture (LECTRA 2020). Demands on high-quality products, transparent pricing with helpful service increases over time. Many people have shifted to online furniture buying with an increase of 12% in the market (LECTRA 2020). When it comes to finding distinctive furniture designs that support and express their social ideals whilst still boosting the comfort and functioning of their homes, the majority of consumers go online (LECTRA 2020). This situation proves that people want to improve their home living style during the pandemic.

Wooden furniture has been the most preferred when creating a relaxed office ambiance. When designing a home furniture, factors such as psychophysiological health impact should be considered for better stress management (Burnard and Kutnar 2020). Based on the measurement of salivary cortisol concentration, it was demonstrated that wood furniture reduces stress reactions, thereby enhancing personal stress recovery (Burnard and Kutnar 2020). An office with wooden furniture has lower overall stress level between workers therefore providing a better working environment.

Stress can be widespread inside a working environment even during the absence of obvious stress-including occurrences. People tried various methods to reduce

stress such as physical exercise, meditation, and even cognitive-behavioral therapy. However, those actions cost more energy and time. That is why creating a passive intervention such as a relaxing workspace is useful to help to reduce the stress for most people (Lipovac and Burnard 2020). Nature or natural components, based on the most recent researchers, may be the greatest strategy for increasing emotional states, physiological arousal, and attentional skills (Lipovac and Burnard 2020). Therefore, providing an environment with wood elements will help create a relaxing ambiance that helps with reducing stress.

Next, after analyzing the market requirements and reviewing articles, design and development sketches were made. The design process started with the thumbnail sketches, followed by the design development, concept development and concept refinement. To proceed into making the final design a validation survey was done to choose the best design out of all refined sketches. The final design of the product was done using a computer aided design (CAD) software. CATIA was the software used to create the complete final 3D model. The 3D model is then imported into the Blender software for graphic rendering with the right material selection (see Fig. 2.3). Some changes were made towards the final design to make it more stable and for easy assembly (see Fig. 2.4). Wood is the preferred material for the final product design. The wood that was chosen is the pine wood due to its beautiful texture and color. In addition, pine wood is a solid and light wood which is great for home furniture (see Fig. 2.5).



Fig. 2.3 The final design of the Rebung bookshelf

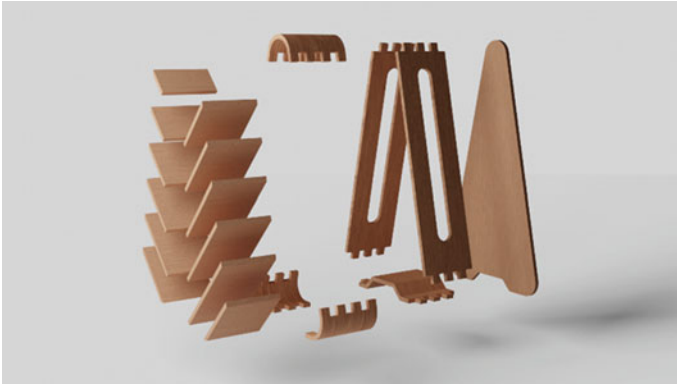


Fig. 2.4 An exploded overview of the product



Fig. 2.5 Environmental illustration of the final product

2.4 Conclusion

The Rebung bookshelf will always be one of my favourite designs projects. Not only it has a beautiful design, but it can also create an emotional value for the user. I hope that it can be made into a finished product so people can experience a different way of storing their books and enjoy the aesthetic values this product presents. Even though this is a great furniture, some improvement can be made to enhance this masterpiece.

Nowadays, the current furniture trends focus on sustainability and greener furniture product. To make the Rebung bookshelf shine in the market, the material of the product can be changed. Furniture companies are using recycled materials and low carbon emission material to meet with the upcoming furniture trends. By changing the material used on the Rebung bookshelf, it has the potential to become the best option for a bookshelf in the market.

Since the Rebung bookshelf is a home product, a more family friendly experience can be beneficial. By improving the bookshelf structure and assembly processes, we can produce a product that can be assembled by the customer themselves. When a modular product needs to be assembled by the customer, it can become a family activity. With a family activity like this, it will create an amazing customer experience and making the product more memorable for the family or friends. This will also cause the product to have emotional values.

In addition, the structure design of the bookshelf can be improved. The dowel connection can be replaced with a better type of fasteners to make it stronger. Improving the structure can also result in less product costing and quality. Modern innovations such as using a 3D printed jointing system will become future trends of furniture making. Thus, the same concept can be applied to this product to improve its design and capability to shine in future markets.

With all the improvements stated, it is believed that the Rebung bookshelf can become a revolutionary home furniture. Even if the customer trends kept on changing, a simple improvement can change how we perceive the product.

Acknowledgements I would like to convey my gratefulness to everyone who made it possible for me to work on this design project. A special gratitude I give to my supervisor Dr. Nur Syazana Osman, whose contribution in providing great and helpful suggestions and encouragement, which helped me improved my design for this project. Furthermore, I would like to acknowledge the crucial role of my family that show endless love and support throughout the hard times upon completing this project. Last but not least, many thanks to my friends that helped by giving their ideas and personal views on designing the final product.

References

- Burnard MD, Kutnar A (2020) Human stress responses in office-like environments with wood furniture. *Build Res Inf.* <https://doi.org/10.1080/09613218.2019.1660609>
- Global Market Insight (2021) Global furniture market growth, COVID impact, trends analysis report by 2026. *Global Trade.* <https://www.globaltrademag.com/global-furniture-market-growth-with-covid-impact-trends-analysis-report-by-2026/>. Accessed 22 March 2021
- LECTRA (2020) The furniture industry post COVID-19. *LECTRA.* <https://www.lectra.com/en/library/the-furniture-industry-post-covid-19>. Accessed 22 March 2021
- Lee J (2020) How furniture brands win in the age of COVID-19. *Adroll.* <https://www.adroll.com/blog/marketing/how-furniture-brands-win-in-the-age-of-covid-19>. Accessed 15 April 2021
- Lipovac D, Burnard MD (2020) Effects of visual exposure to wood on human affective states, physiological arousal and cognitive performance: a systematic review of randomized trials. *Indoor Built Environ.* <https://doi.org/10.1177/1420326X20927437>

Chapter 3

Modelling a Temperature Based Speed Control of a Fan



Noor Ikmal Hakim Noor Azmi and Mohd Zain Ismail

3.1 Introduction

Nowadays, the major problem each country near the equator experiences for three-quarters of the year is heating. Every home has different types of cooling appliances to reduce the heat within their houses. But there are two main cooling appliances which are the ordinary fan and air conditioner. The ordinary fans are still at their earlier ages and are not being innovated as any other appliances that are in the present technological world. Air conditioners are smart and being innovated but they require a lot of money to buy, fit and maintain throughout meanwhile suffering higher power consumption (Saad et al. 2014).

The only viable solution for a cheaper cooling appliance, which consists of more technologically advanced features, is to introduce an automatic fan throughout this research. This automatic fan consists of a variable number of technologically advanced features to the present day which enables it to use the Arduino component to work together to provide the users with a better experience of using the fan. Furthermore, with the use of the mobile application, the fan was enabled to be controlled with a simple tap. This fan was designed for a broader area of users which helped both normal individuals and people with disabilities to interact with the fan with more ease.

N. I. H. Noor Azmi (✉)

Electrical Technology Section, British Malaysian Institute, Universiti Kuala Lumpur, Selangor, Malaysia

e-mail: ikmal.azmi@s.unikl.edu.my

M. Z. Ismail

Communication Technology Section, British Malaysian Institute, Universiti Kuala Lumpur, Selangor, Malaysia

e-mail: mzain@unikl.edu.my

3.2 Literature Review

There has also been discussion on the basic concept of some related theories and frameworks for this project such as monitoring system, potential software, and component unit. This chapter will review the existing system that has been developed and has similarities with the modelling a temperature-based speed control of fan project.

3.2.1 Development of an Automatic Person Detection Systems to Control an AC Fan and Room Lights

In this paper, the microcontroller 16F887A and IR sensor are used in controlling the fan and lights. When a person is entering the room, he or she will be detected by an IR sensor. Then, the microcontroller will turn on the fan and the lights. The microcontroller also can control the temperature environment. When the fan is on, the microcontroller will check the temperature. In case the temperature increases the speed of the fan will increment in the same manner (Mishra et al. 2013).

3.2.2 Automatic Temperature Controlled Household Electric Ceiling Fan

According to this paper, the electric ceiling fan is controlled by the microcontroller of the Arduino Uno by applying the pulse width modulation (PWM) technique for changes in the fan speed. There are two types of sensors. The PIR sensor is used for detecting the human movement and functioning to switch on the fan. Meanwhile, the LM35 sensor is used to check the environment temperature. In Arduino Uno, a PWM is set accordingly to control the speed based on the temperature changes detected by the LM35 sensor (Oduah 2017).

3.2.3 Smart Smart Fan

A Raspberry Pi and Arduino Uno were used as a microcontroller in this system. The temperature is checked by using the DS18B20 digital temperature sensor (Supunya et al. 2016). The operation of the system consists of three modes, i.e. normal mode, auto mode, and security mode. The system can be controlled by using a smartphone.

3.2.4 Modelling and Simulation of a Microcontroller Based Temperature Control in a Ventilation System

The operation of this system used a microcontroller and LM35 temperature sensor. The temperature sensor detected the temperature of the environment. The microcontroller controlled the temperature by using the PID controller algorithm to convert the temperature to the desired electrical current that controls the fan. Then, the PWM will drive the relay to switch on and off the fan (Akpado et al. 2013).

3.2.5 Temperature Based Speed Control a of Fan by Using an Arduino

The temperature based speed control of fan using an Arduino is an innovation established in 2019 which developed the automatic fan speed control by the temperature. An Arduino-based temperature control fan is implemented. Thus, the speed of the fan is being controlled by using the PWM and the temperature is sensed by the DHT22 temperature and humidity sensor (Venkat and Kumar 2020).

The main idea for this project is to control the speed of the fan automatically by the sensor. This project uses the technique of PWM towards controlling the speed of fan using the sensed temperature. The system is working properly. Hence, the surrounding temperature will decide the speed of the fan and the user will not require to switch the fan speed manually by using the toggle button.

3.2.6 The Development of Arduino Based Automatic Fan Control System Using PIR Sensor

This project was invented in August 2019 by Ayesha Siddika and Sayeda Farzana Nasrin from the World University (Siddika and Farzana Nasrin 2018). Everyone already knows that today's technology requires an automatic system that easily helps the user. This project provided two functions to help the user. The first one is that this project uses human detection to switch on the fan rather than using the toggle button. Another function is to control the speed of a fan concerning the temperature set. This project uses the PIR sensor to switch on the fan and the LM35 temperature sensor to distinguish the encompassing temperature and control the speed of the fan.

The temperature sensing element was rigorously chosen to determine the room temperature, and the motion sensor is used to sensing the human movement to switch on/off the fan. Besides, the Arduino had been customized to manage the speed of fan. Therefore, the Arduino was with success programmed using C/C++ language to check the temperature in degree centigrade and control the speed of fan then to display the room temperature value on the LCD.

Moreover, the speed of the fan can mechanically increment if the temperature area is inflated. In conclusion, the system that was designed during this work was perform all right, for any action and may be classified as automatically management.

3.3 Methodology

Figure 3.1 shows the block diagram of the project which comprises of three different stages, i.e. input, process, and output. The main components involved are the DHT11 temperature sensor at the input phase. This project uses the DHT11 as the temperature sensor. The main component in the process phase is the NodeMCU ESP8266. The NodeMCU microcontroller is considered the main heart of the system.

A few components used at the output stage are the liquid crystal display (LCD), the 4 channel relay module and the light-emitting diode (LED). In the final phase, the output, every input received will be changed into output. The LCD module is used to show the surrounding temperature and the speed of the fan.

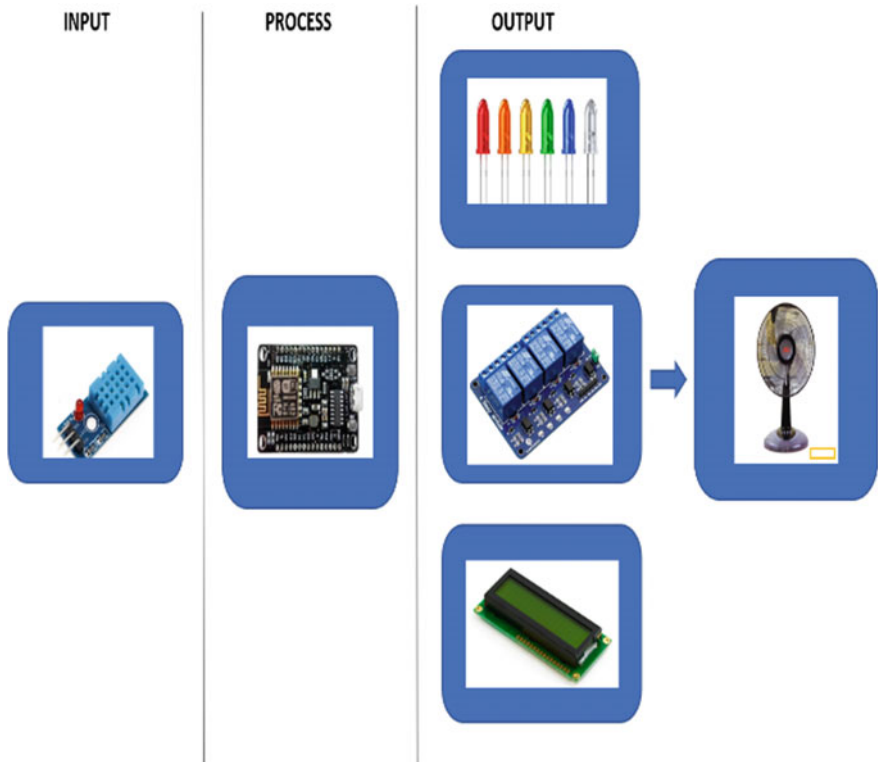


Fig. 3.1 Block diagram

Besides, the process created by the NodeMCU ESP8266 will be displayed through the application on the mobile device. The LED will show the output differently depending on the input it receives. In this project, a LED is used to act as an indicator to show the changes of fan speed. As an example, the green LED indicates the low speed of the fan, the yellow LED indicates the medium speed of the fan, and the red LED indicates the high speed of the fan. Last but not least, the relay 4 channel module is used in this project to replace the toggle speed button of a table fan.

Figure 3.2 shows the flowchart of the process of this project. Firstly, the system is initialized by the input and output of the project. Then, the NodeMCU ESP8266 and DHT11 is on simultaneously. If the DHT11 is detecting the temperature it will automatically switch on the LED and display it on the mobile phone. However, the process will be going on until the temperature is detected. Figure 3.3 shows the connection of the components and devices in the project.

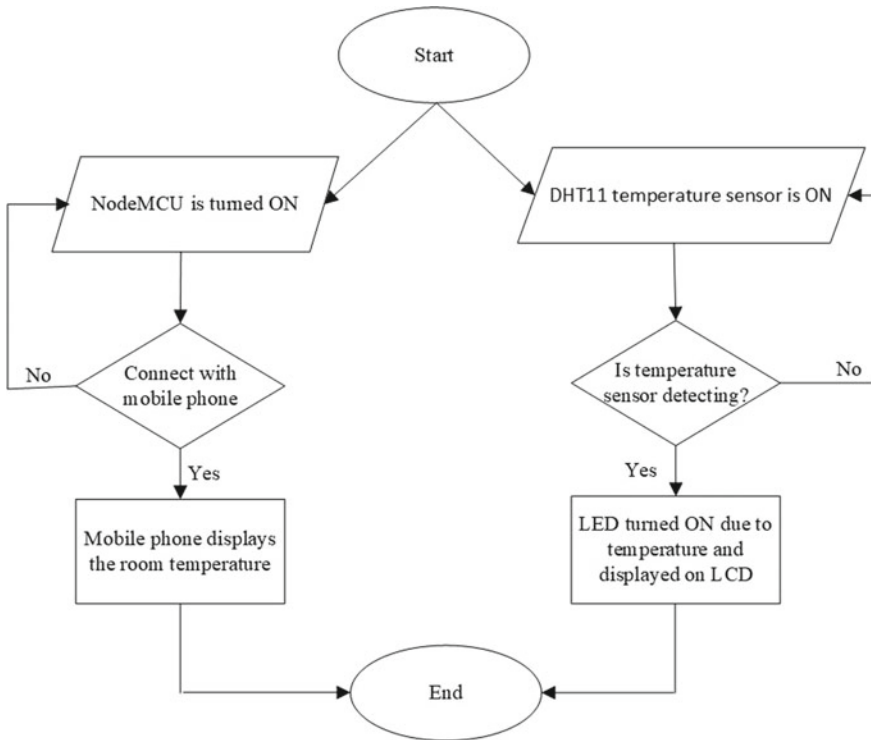


Fig. 3.2 Flowchart

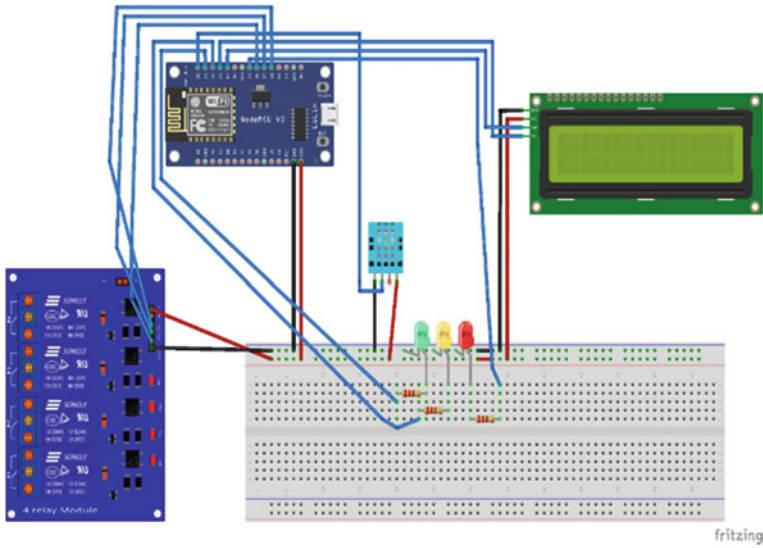


Fig. 3.3 Circuit diagram

3.4 Results and Discussion

Figure 3.4 shows the location of the temperature sensor DHT11 at the packaging of the project. The function of the temperature sensor detection system is to sense the changing of the surrounding temperature in various weather conditions. The temperature detected by the DHT11 temperature sensor will be converted into an analog signal. The analog signal will be converted into a digital signal by using ADC.

The value of the surrounding temperature that is being detected will be displayed on the liquid crystal display (LCD) as shown in Fig. 3.5. This temperature sensor detection system enables the fan to change the speed automatically based on the surrounding temperature. The speed monitoring system consists of 16×2 the LCD

Fig. 3.4 Temperature sensor detection system

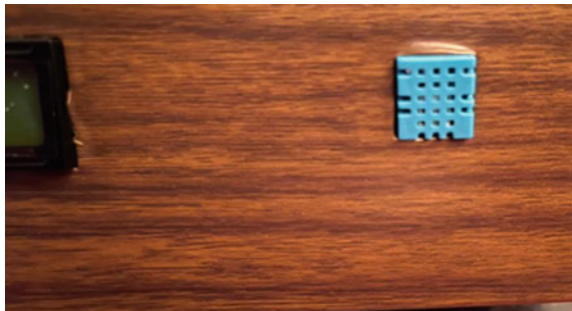




Fig. 3.5 Speed and LED monitoring system



Fig. 3.6 LCD display when detected changing of temperature and speed of fan

display and LED light as the output from the temperature sensor. Figure 3.5 also shows that LED will be turned ‘ON’ due to the speed and temperature that have been set.

Figure 3.6 shows the LED display and the three LED light of three conditions of temperature measures. For the low temperature, the speed of the fan is set to number one with the green LED light. For the medium temperature, the speed of the fan is number two with the yellow LED light. Finally, if the temperature displayed is high, it will change the speed of the fan into number three with red the LED light.

3.5 Conclusion

An efficient, cheap, automated temperature-controlled fan has been designed and built in this project. The fan blades running velocity automatically adapts to the ambient temperature with the useful resource of the temperature sensor which controls the fan regulator. A fan speed regulator controls the speed of an electric fan as needed by users that used embedded technology to control the system efficiently and reliably. As we already know, the current stand fan models in the market mostly need users to physically press the desired speed of the fan despite the temperature in a specific room.

This innovation focused on overcoming the demanding situations posed through the traditional table fan requiring that one wishes to be at alert all instances to switch the fan in reaction to unexpected unwanted fluctuations in the temperature of the environment. Such unexpected changes in temperature might also additionally rise because of changes in weather conditions due to rain, harmattan, heavy sun, wind, and others.

The constructed automatic temperature-controlled table fan is efficient and comparatively cheap. The mobile application system also proposes to send orders to operate the fan as ON or OFF from a distance. The automatic temperature-controlled fan is a welcome improvement inside the era in the industry nowadays and is predicted to replace the traditional manually regulated household electric powered fan as soon as it is produced commercially.

In a nutshell, the new design of fan reduces the power consumption when the speed of the fan is controlled automatically with the changes of the temperature state. The method of speed control of the fan seems to be suitable for the modern lifestyle where the manual traditional speed control regulator system is replaced with the self-regulatory mechanism. Finally, temperature-based automatic control systems are fitting for implementation of the internet of things (IoT), where real-life problems can be solved with the design of intricate electronic circuits.

Acknowledgements The authors would like to acknowledge the Communication Section for the assistance and support of the success of the project.

References

- Akpado KA, Ezeagwu CO, Ejiofor A, Nwokeke AO (2013) Design, modeling and simulation of a microcontroller based temperature control in a ventilation system
- Mishra R, Kumar P, Professor A (2013) Development of automatic person detection system to control AC fan & room lights. *Int J Innov Res Sci Eng Technol* 2
- Oduah U (2017) Automatic temperature controlled household electric ceiling fan suppression of intrinsic recombination in silicon solar cell. View project
- Saad M, Abdoalgader H, Mohamed M (2014) Automatic fan speed control system using microcontroller. In: 6th int'l conference on electrical, electronic & civil engineering
- Siddika A, Farzana Nasrin S (2018) Design and development of Arduino based automatic fan control system using PIR and LM35
- Supunya R, Madushani MI, Pathirana SUR, Abeyssekera NGCN, Supunya NHPR (2016) Smarty smart fan
- Venkat AA, Kumar D (2020) Temperature based fan speed controller

Chapter 4

Development of an Automated Segregator for Solid Waste



Muhammad Sufi Johari, Ainul Hakimah Karim, and Siti Hafshar Samseh

4.1 Introduction

According to the Solid Waste Management and Public Cleansing Corporation (SWCorp), Malaysians generated a whopping of 38,142 tonnes of waste per day, an increase from 19,000 tonnes of waste a day in 2005 [1]. Malaysia's population in 2020 is estimated at 32.7 million as compared to 32.5 million in 2019 with an annual growth rate of 0.4%. The decline of population growth rate is attributed to the decrease in the number of non-citizens from 3.1 million (2019) to 3.0 million (2020). This is in line with the closure of our national borders and the return of foreigners to their respective countries during the Movement Control Order following the spread of the COVID-19 pandemic worldwide. The growth rate of citizens remained stable at 1.1% with the population increasing from 29.4 million in 2019 to 29.7 million in 2020 [2].

In general, recycling is the method by which materials are gathered and recycled or otherwise be thrown away as waste and converted into new items. Recycling will help the environment and your neighborhood [3]. The recycling policy of Malaysia helps conserve valuable natural resources as it can save the biodiversity and the climate. Moreover, Malaysia recycle effort also generates jobs opportunities. It is a comparatively economical waste management process for urban areas because the process of recycling produces more jobs compared to landfills or incinerators. As

M. S. Johari · A. H. Karim (✉) · S. H. Samseh
Instrumentation and Control Engineering Section, Malaysian Institute of Industrial Technology,
Universiti Kuala Lumpur, Masai, Johor, Malaysia
e-mail: ainulhakimah.karim@unikl.edu.my

M. S. Johari
e-mail: sufi.johari@s.unikl.edu.my

S. H. Samseh
e-mail: sitihafshar@unikl.edu.my

landfills grow, there is not much space left in Malaysia's urban regions and the capital unless everyone has a minor landfill in their back yard. It also reduces the amount of solid waste that goes into landfills [4].

Based on previous work done by other researchers, this project proposes an automated segregator for solid waste powered by an Arduino microcontroller. The aim of this project is to automatically sort recycled waste into four separate compartments. The waste is sorted based on the type of material being detected. Thus, the consumer does not need to decide which bin is correct for the recycling waste. The recycling bin will focus exclusively on four different common materials that the students throw away, papers, aluminum cans, plastic bottles and glass. In addition, material sorting depends on the type of material detected by the sensors, where the metal detector sensor is used to detect cans of metal, the force sensor for glass weight detection, the LDR sensor for calculating the light intensity that is penetrated through plastic. If none of the sensors detects something, that material is classified as paper.

4.2 Methodology

Figure 4.1 shows the flowchart of waste classification through each sensor. The process flow of the system starts when the user puts the waste inside the bin. After that, the sensor detects continuously the waste, if the metal sensor senses the waste is metal, the bin will rotate and drop the waste inside the metal container and close the lids. For glass, it will be sensed by using the force sensor. The force sensor senses the weight of the waste either it is heavy or light. The bin will rotate to the glass container if the force sensor senses a heavy object and closes the lid. To verify that waste is paper, the LDR sensor is used. If the waste cannot be detected by sensors, the system declares the waste as paper.

4.3 Results and Discussion

4.3.1 *Electronic Circuit Design*

This part shows two electronic circuits that have been install on the prototype, which is the Arduino Mega circuit and the NodeMCU circuit.

Figure 4.2 show the schematic circuit for the process. It contains three sensors, which are the force sensor, metal sensor and LDR sensor. Other than that, there were three actuators which act as the servo motor. Besides that, two indicators where installed in the system.

Figure 4.3 shows the connection for the NodeMCU Esp8266, where there are four ultrasonic sensors connected to the NodeMCU. This system will be monitored by the Blynk application.

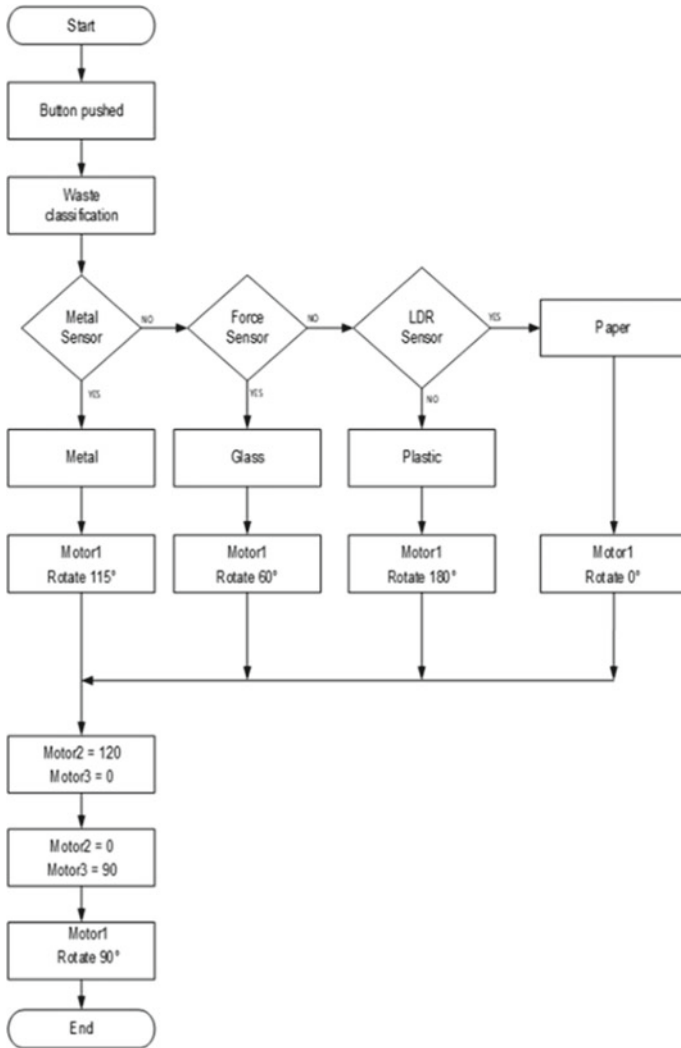


Fig. 4.1 Process flowchart

4.3.2 Sensor Behavior

This part shows the sensor behavior when it detects materials. There will be three sensors tested in this section which are the force sensor, metal sensor and LDR sensor.

Figure 4.4 shows the reading that has been taken by the force sensor for 8 s. The reading changes when there is a force applied on it, by using a glass bottle it creates some force from the weight of it.

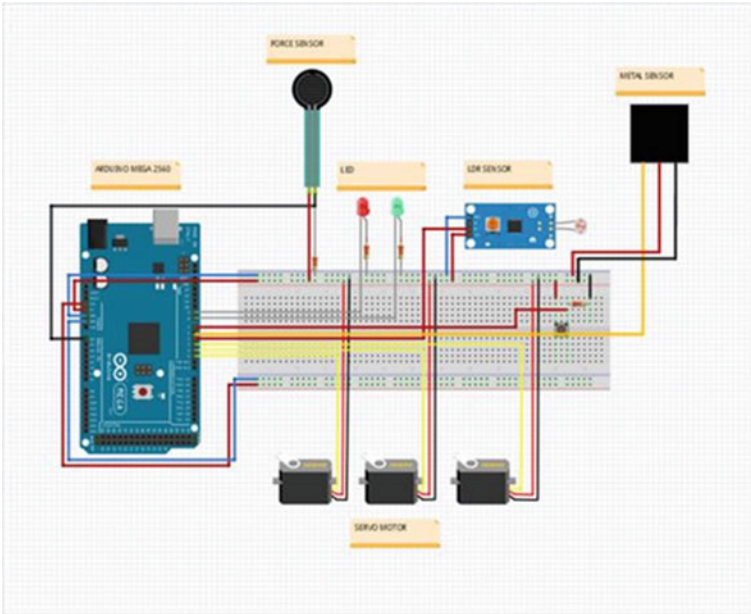


Fig. 4.2 Arduino Mega circuit

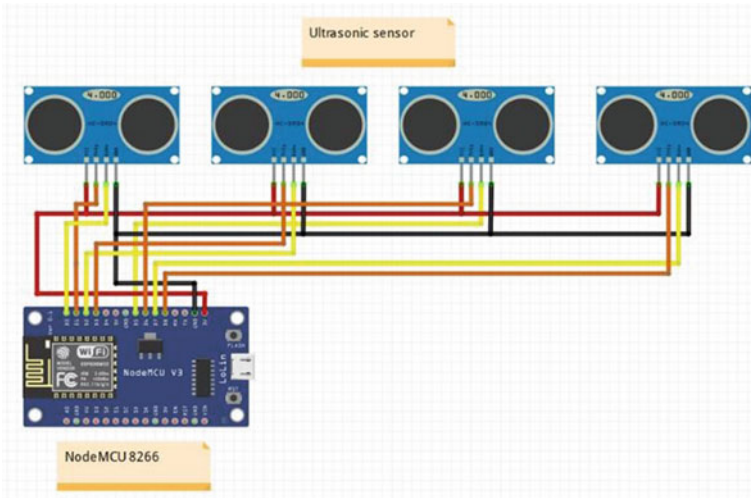


Fig. 4.3 NodeMCU Esp8266 circuit

Fig. 4.4 Force sensor reading

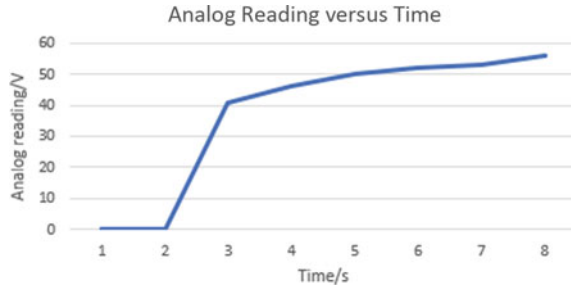


Figure 4.5 shows the metal sensor reading that occurs when there is metal type or conductive material. The fundamental principle is that the sensor will create an electromagnetic field around the object. The sensing range is 5 mm for this sensor. The digital value will be 0 if the sensor detects metal. Table 4.1 shows the conversion of digital output to voltage.

Figures 4.6 and 4.7 show two different types of materials used to test the LDR sensor. For Fig. 4.6 the sensor detects paper, the voltage turns to 0 when it detects the paper. Figure 4.7 shows that the sensor detects a plastic material. This happens because the LDR sensor detects the light intensity. The difference between these two types of material is that plastic is transparent and light can go through it, but paper

Fig. 4.5 Metal sensor reading

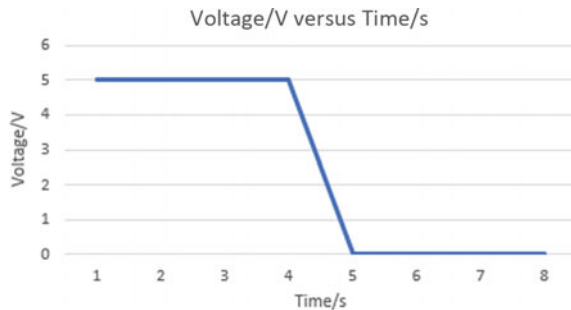
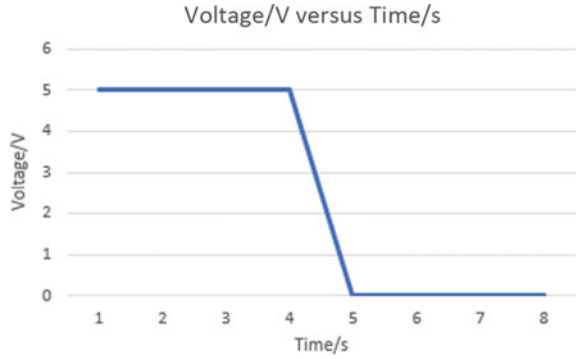


Table 4.1 Conversion of digital output to voltage for the metal sensor

Time/s	Digital output	Voltage/V
1	1	5
2	1	5
3	1	5
4	1	5
5	0	0
6	0	0
7	0	0
8	0	0

Fig. 4.6 Paper detection by LDR sensor



is an opaque type, so the light is hard to go through. Tables 4.2 and 4.3 show the conversion of digital output to voltage for the LDR sensor.

Fig. 4.7 Plastic detection by LDR sensor

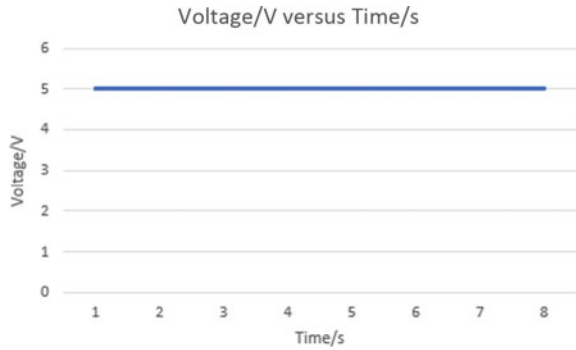


Table 4.2 Conversion of digital output to voltage for the LDR sensor in case of paper

Time/s	Digital output	Voltage/V
1	1	5
2	1	5
3	1	5
4	1	5
5	0	0
6	0	0
7	0	0
8	0	0

Table 4.3 Conversion of digital output to voltage for the LDR sensor in case of plastic

Time/s	Digital output	Voltage/V
1	1	5
2	1	5
3	1	5
4	1	5
5	1	5
6	1	5
7	1	5
8	1	5

4.3.3 Monitoring System

This part shows the monitoring system that has been applied by using the Blynk app to monitor the level of the material inside the dustbin.

Figure 4.8 shows the Blynk app for the dustbin monitor. Each of the bins has an ultrasonic sensor installed for measuring the height of the material inside the dustbin. Figure 4.9 also shows the notification that will be sent to our phone if the dustbin is full.

Fig. 4.8 Blynk apps



Fig. 4.9 Blynk notification

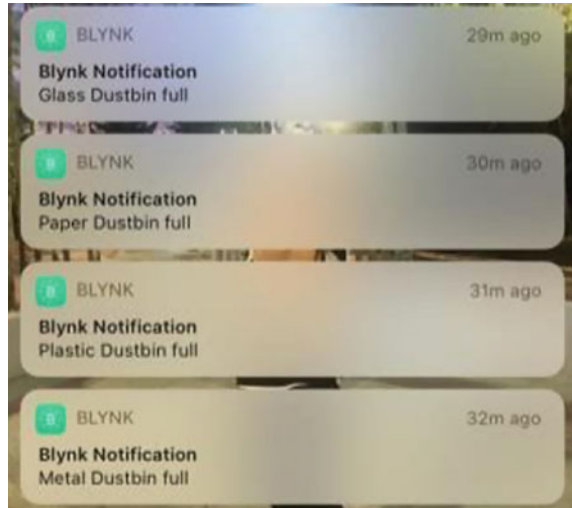


Table 4.4 Error for classification

Type of solid waste	Success	Fail
Metal	5	0
Plastic	4	1
Paper	4	1
Glass	3	2

4.3.4 Error for Classification

There are several tests that have been done to test the sensor sensibility for each material. For metal there is no error since the sensor will detect the presence of the metal. For plastic and paper there will be a slight error happening because there is a disturbance that may occur. The disturbance from the surrounding light will affect the measurement of the LDR sensor. Finally, the glass has some error happening because of the sensor itself.

The sensor will detect the force if the glass is placed at the correct position. From Table 4.4, it can be concluded among the four types of waste, metal could be automatic segregated and followed by paper and plastic but with a small error.

4.3.5 Discussion

Based on the data collected from the project outcome, the development of an automated segregator for solid waste can be summarized as a well functioning project. The classification of the solid waste based on their type was functioning well as the

servo motor rotates according to the type of solid waste class after the sensor sensed it. The detection of solid waste is based on the sensor behavior, i.e. the metal sensor will detect metal, force sensor will detect glass and the LDR sensor will detect paper or plastic. For the monitoring system, by using an ultrasonic sensor that is connected to NodeMCU and linked to the Blynk app to monitor the level of the solid waste inside the storage works well.

4.4 Conclusion

This study is about the design and development of an automated segregator for solid waste by using a non-contact technology. The main objective of this project prototype was achieved. The system is divided into several parameter controls which is the detection of metal, plastic, glass and paper waste. A few major components and devices are needed in order to create and develop this system. The crucial component is the sensor and the servo motor. The servo motor act as the output to open the lids and to rotate the waste storage based on the type of material that the sensor detects. This is done to ensure that the waste is separated according to their respective type, hence classifying it. For the monitoring part, the Blynk app is used to monitor the level of waste inside the bin and display it to the phone and give notification if the storage is full. There are three types of sensors used in detection of materials. The metal sensor was used to detect metal. The LDR sensor was used to detect plastic or paper. The force sensor was used to detect glass. All components may not function adequately without the Arduino Mega microcontroller that acts as the brain of the system.

Acknowledgements Thanks to all lecturers of Universiti Kuala Lumpur (MITEC) that supported this project.

References

- Chu MM (2019) Generating more waste than ever. <https://www.thestar.com.my/news/nation/2019/07/30/generating-more-waste-than-ever>. Accessed 5 May 2023
- Mahidin DS (2020) Department of statistic Malaysia: Press release current population estimates Malaysia 2020. <https://www.dosm.gov.my/portal-main/release-content/current-population-estimates-malaysia-2020#:~:text=Malaysia's%20population%20in%202020%20is,to%203.0%20million%20>. Accessed 5 May 2023
- Thanam (2013) The importance of waste and scrap recycling in Malaysia. <http://www.thanam.com>. Accessed 24 April 2023
- United States Environmental Protection Agency (2020) Recycling basics. <https://www.epa.gov>. Accessed 15 April 2023

Chapter 5

Design and Development of an Efficient Meat Smoker



Ahmad Qamarul Arifin Rahman and Faiza Mohamed Nasir

5.1 Introduction

Meat smokers are outdoor cooking appliances that can maintain a low cooking temperature for an extended period of time in order to produce smoke and trap heat. For a long time, people have used smoking to preserve and flavour food (Venema 2016; Adeyeye 2019). Before the food spoils, people have discovered that food that has been exposed to smoke lasts longer. Smoking has been around for a long time and is still popular all over the world (Yang and Po-Yuan 2019). This technique has been used in some countries to preserve fish and meat, especially in the fall to ensure a steady supply of protein throughout the winter and to reduce hunting activities.

In Malaysia, meat smokers are used by the hawkers at the night market and operated in an open environment. This exposes the meat to the environmental pollutants such as vehicle smoke, dust, bacteria and virus, raising concerns on the food hygiene. Furthermore, existing meat smokers require complex preparation and require large operating spaces. Existing meat smoker operations, as well as the heat source they impose, must be continuously monitored to avoid overheating, or else the food will be burnt. During the smoking process, the meat should be manually inspected to ensure that the smoking is complete. As a result, this operation necessitates a large number of working hours, making it ineffective in situations where a quick operation is required.

Meat can be cooked in two ways: directly or indirectly. Grilling meat involves using direct heat for a short period of time, whereas smoking involves using indirect

A. Q. A. Rahman · F. Mohamed Nasir (✉)
Universiti Kuala Lumpur Malaysian Spanish Institute, Kulim Hi-Tech Park, 09000 Kulim, Kedah, Malaysia
e-mail: faiza@unikl.edu.my

A. Q. A. Rahman
e-mail: aqamarul@s.unikl.edu.my

heat to cook meat at a low temperature for an extended period of time. Smokers and grills are, in essence, diametrically opposed. The indirect heat of the smoke is what distinguishes it. To put it another way, the meat is not cooked directly over a flame or heat source. Allow the heat and smoke from the fire to permeate the meat instead, keeping it away from flames or direct heat sources. Cooking with indirect heat is simple when one uses a dedicated smoker. Smokers are specifically designed to keep meat away from heat while allowing and absorbing smoke. Smokers are well-designed to allow smoke and heat to circulate freely around the meat to be cooked.

The designs available for smokers are quite limited. This is because most smokers are created by do-it-yourself enthusiasts who love to do it. A small number are used for commercial purposes. In this work, a meat smoker is designed, fabricated, assembled and tested. The meat smoker must be able to produce smoked meat with excellent taste, requires minimal intervention, operates hygienically in a shorter period of time.

5.2 Methodology

5.2.1 Conceptual Designs

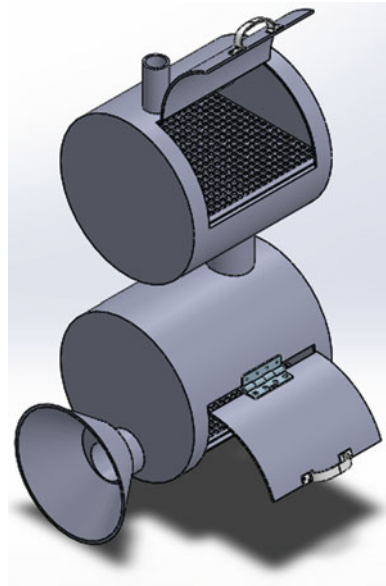
Six conceptual designs were developed, after benchmarking with different designs of smokers from do-it-yourself projects. Double barrel or double chamber design were chosen as the main concept as this design would allow better flow of heat and smoke for the meat while minimising the occurrence of burnt meat, compared to single barrel design.

In the double barrel design, there are two barrels or chambers placed on top of one another separated by a channel or connector. The top chamber is used to place the meat (cooking chamber) and the bottom chamber is for charcoal briquettes (Fig. 5.1). There are the air suction channel and air exhaust channels in the design, where the former is located at the bottom chamber and the latter is located at the top chamber or the cooking chamber.

5.2.2 CFD Simulations

The six conceptual designs of the meat smoker were modelled using the CAD software SOLIDWORKS. CFD simulations for the designs were conducted focusing on the fluid flow and the temperature distribution in the smoker. Results of the CFD simulations provide an initial overview of the effectiveness of the meat smoker without having to produce the actual product.

Fig. 5.1 Design concept for the meat smoker



5.2.3 Decision Analysis


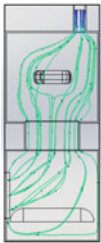

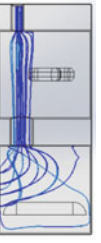

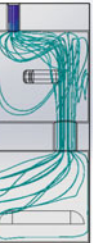
The selection of the final design of the meat smoker is based on the results of the CFD simulations. The results and the designs are illustrated in Table 5.1. Design 5 is the best design based on the results obtained from simulations (Fig. 5.1). It is observed that the temperature obtained at the bottom of the meat and the top of the meat is similar for this design of meat smoker. This allows the meat to be cooked evenly on both sides, top and lower and will not overcook on certain parts.

Once the analysis is done and the design is selected, a fabrication process is performed to test the effectiveness and accuracy of the data that has been obtained through the analysis method.

5.2.4 Fabrication and Assembly

The finished meat smoker is equipped with a temperature reading device in the cooking chamber to make it easier for users to monitor the temperature in the cooking chamber. In addition, it is also equipped with a funnel to direct ambient air by using a fan to ignite the combustion in the combustion chamber and control the temperature in the cooking chamber. The drawings for the final design are shown in Figs. 5.2 and 5.3. The finished meat smoker is shown in Fig. 5.4.

Table 5.1 Results for the CFD simulation

	Design 1	Design 2	Design 3	Design 4	Design 5	Design 6
Shape of chamber	Cylinder	Cuboid	Cylinder	Cuboid	Cylinder	Cuboid
Maximum temperature (K)	508.00	454.77	498.47	571.95	581.49	576.57
Air flow						

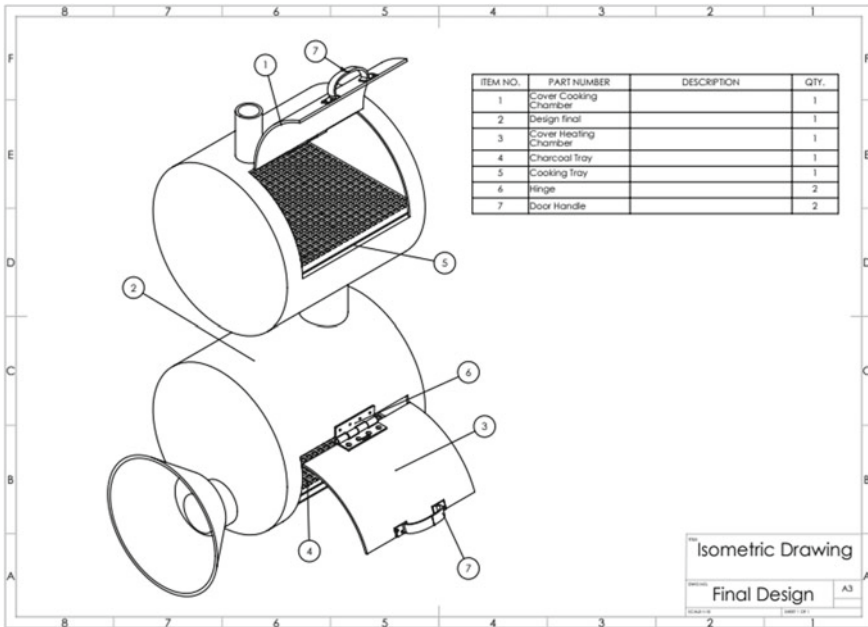


Fig. 5.2 Isometric drawing of the final design

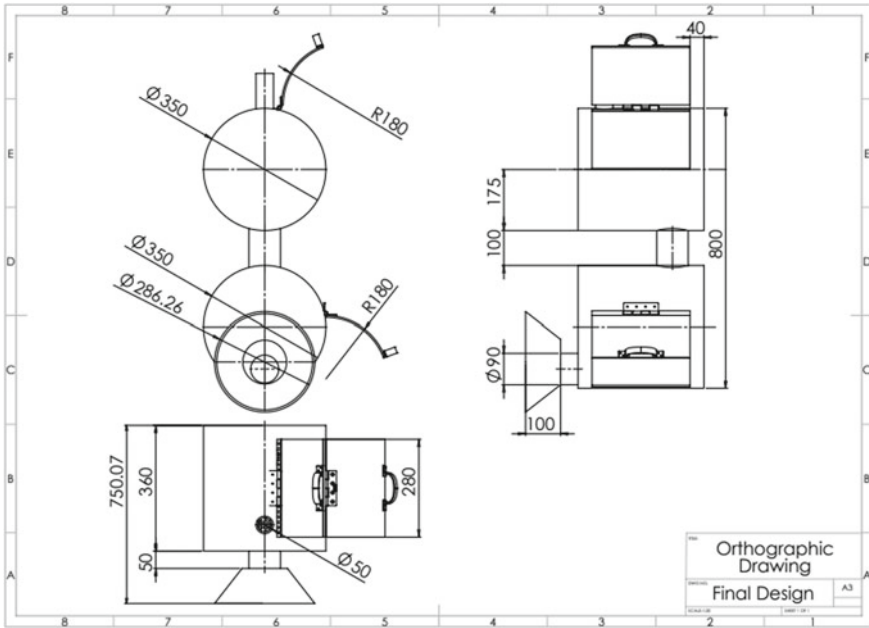


Fig. 5.3 Orthographic drawings of the final design

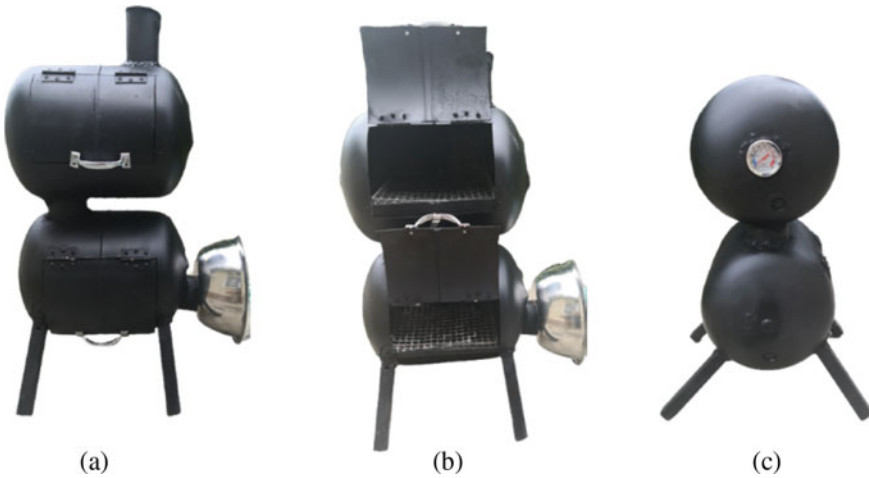


Fig. 5.4 The finished meat smoker **a** front view with the chamber openings closed, **b** front view with the chamber openings open and **c** side view

5.3 Results and Discussion

Testing of the meat smoker was conducted to ensure that it works as required. The meat smoking process was conducted by using the meat smoker or by using a conventional oven cooker. The meat was prepared and marinated using the same ingredients. Two samples of marinated meat with the same weight of 500 g were prepared and cooked. The time taken for the meat to be cooked was recorded. The conditions of the meat after every 30 min were also observed for both smoking methods.

Results indicate that the meat smoker was able to cook the marinated meat within 1 h and 30 min at a temperature of 225 to 250 °F. Under the same conditions, the oven took 2 h 30 min to 3 h to fully cook the marinated meat. This demonstrated the ability of the meat smoker to cook the meat at half the time required for the oven cooker.

Comparing the appearance of the cooked meat using both cooking methods, it is found that the oven-cooked meat looks a little darker and a little drier than the smoker's meat (Fig. 5.5). The meat cooked using the smoker looks tastier and the outside of the meat looks fresh.

When it comes to cooked meat tenderness, oven-cooked meat does not compare favourably to meat cooked in a smoker (Fig. 5.6). Because oven-cooked meat is drier on the inside, it is not as tender as meat that has been smoked in a smoker. Meat cooked in a smoker is tenderer and juicier than meat cooked in a conventional oven because it is not cooked over an open flame but rather over a smoke fire, thereby cooking it indirectly over an open flame where there is a source of heat.



Fig. 5.5 The appearance of **a** oven-cooked meat, **b** smoked meat

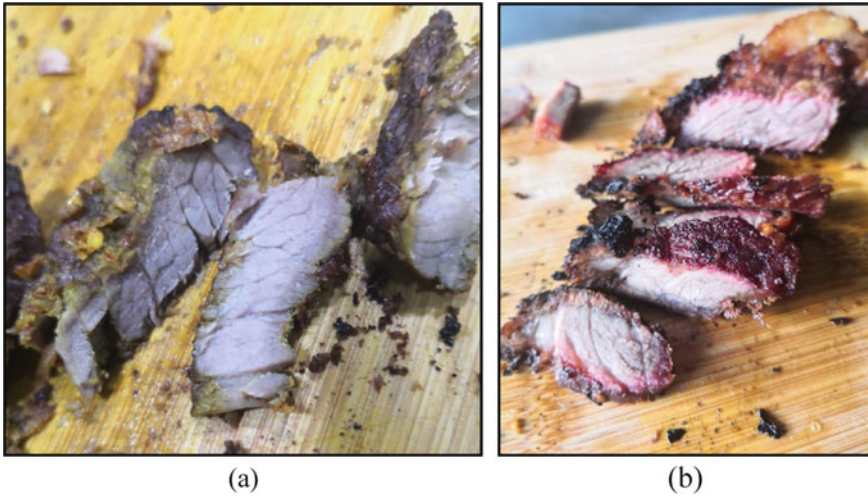


Fig. 5.6 Appearance of sliced meat cooked by **a** oven and **b** the meat smoker

5.4 Conclusion

The aim of this work was to successfully develop an efficient smoker that can reduce the time required to smoke and cook meat, operating with minimal supervision, maintaining high level of food hygiene while maintaining the uniqueness of smoke flavor itself. By employing a design process, a meat smoker was developed, fabricated, assembled and tested. Testing of the smoker indicated that it is capable of cooking the meat at half the time required by a conventional oven, with juicier appearance and tastier.

Acknowledgements We would like to acknowledge the support of UniKL MSI in completing this work successfully within the COVID-19 pandemic.

References

- Adeyeye SAO (2019) Smoking of fish: a critical review. *J Culin Sci Technol* 17:55–575
- Venema C (2016) Smoking as a food cooking method. https://www.canr.msu.edu/news/smoking_as_a_food_cooking_method. Accessed 25 Sep 2021
- Yang K-M, Po-Yuan C (2019) Effects of smoking process on the aroma characteristics and sensory qualities of dried longan. *Food Chem* 287:133–138

Chapter 6

Between Batik and Fiberglass: The Hybrid-Technology of Boat Construction



Aizat Khairi, Shaiful Bakri Ismail, and Shamsul Effendy Abdul Hamid

6.1 Introduction

Batik is one of the popular handicraft arts for the Malay community in Malaysia (Fauziah 1983). This handicraft art is a technique in designing fabrics using certain dyes to be used as clothing for both men and women. The batik weaving technique has gone through a process of development from conventional to modern practice. In Malaysia, batik is not only worn by Malays but also by non-Malays because of its pattern attractive and suitable to wear when attending formal or informal functions. Therefore, the demand for batik is increasing from time to time and this situation gives a good picture in improving the economic sector in the country.

The batik industry in Malaysia is also experiencing good development in the country (Chee 1990). For example, previously the batik industry was often associated with states on the East Coast such as Kelantan and Terengganu, but now there are also other states, such as Kedah, have begun to develop the batik industry to compete in healthy in producing batik products of different motifs and patterns (Azimi 2018). The batik industry is currently getting good demand not from local community only,

A. Khairi (✉)

General Study Department, Universiti Kuala Lumpur, Malaysian Institute of Marine Engineering Technology, Jalan Pantai Remis, 32200 Lumut, Perak, Malaysia

e-mail: aizat@unikl.edu.my

S. B. Ismail

Marine Electrical and Engineering Technology Section, Universiti Kuala Lumpur, Malaysian Institute of Marine Engineering Technology, Jalan Pantai Remis, 32200 Lumut, Perak, Malaysia

e-mail: shaifulbakri@unikl.edu.my

S. E. Abdul Hamid

Maritime Engineering Engineering Technology Section, Universiti Kuala Lumpur, Malaysian Institute of Marine Engineering Technology, Jalan Pantai Remis, 32200 Lumut, Perak, Malaysia

e-mail: shamsuleffendy@unikl.edu.my

© The Author(s), under exclusive license to Springer Nature Switzerland AG 2023

A. Ismail et al. (eds.), *Materials and Technologies for Future Advancement*,

Advanced Structured Materials 193,

https://doi.org/10.1007/978-3-031-38993-1_6

but also the international community also wears it due to the quality and finesse of its art of making (Yusoff and Abdullah 2018).

To promote batik, the government strives to hold various initiatives through its agencies. For example, the Ministry of Tourism and Culture takes the initiative by organizing the National Craft Day every year to promote and commercialize local handicraft products on the international level. National Craft Day also aims to make the local handicraft industry, including the production of batik, which is seen to be able to contribute to the improvement of the country's economic sector. In addition, the program is the best platform to give recognition and appreciation to local handicraft entrepreneurs and entrepreneurs who work hard in developing the handicraft industry, including the batik industry.

The art of batik handicrafts continues to be promoted to the international level based on two main purposes, namely, to highlight the culture and image of the country and attract foreign tourists to visit Malaysia to witness the production of batik traditionally and modernly. The initiative was undertaken by a group of students from the Faculty of Fashion and Creative Lifestyle, Limkokwing University who have brought their fabric design collection to London Fashion Week, United Kingdom (Muzdalifah 2018). Their design fabrics of batik managed to attract many visitors.

The Malaysian batik is traditionally produced through hand painting. The art of batik handicrafts is synonymous with the activity of weaving fabrics made from materials such as cotton to be used as fabric and then clothing for men and women. Batik-based clothing patterns and motifs are one of the efforts in maintaining the culture and identity in Malaysia, especially for the Malay community. Although the Malay community is rich in the treasures of handicrafts, but the art of batik handicrafts is one of the superior arts and is a symbol of the Malay identity that needs to be preserved and dignified.

Malaysian batik has its own identity in terms of manufacturing techniques, patterns and motifs. Such features also symbolize the Malay identity and culture which has its own uniqueness. In Malaysia, the batik industry continues to be preserved and fought for by the Malays in order to maintain the identity and culture of Malay -based handicrafts so as not to be swallowed up by the currents of modernity. In addition, the existence of the batik industry in Malaysia is indirectly able to contribute specially to improving the small and medium industrial sector for the rural community. Typically, the batik industry in Malaysia focuses on productivity based on the manufacture of textiles and clothing as well as other products such as souvenirs, appliances, and home decorations.

However, the batik-based products are seen as limited to textile-related enterprises only. The retention efforts of Malay cultural identity through batik must be expanded in various sectors or fields to be able to survive in the face of progress in today's globalized world (Rafeah 2012). In addition, batik-based art needs to undergo transformation and be flexible to further highlight the specialties and uniqueness found in batik (Akhir et al. 2016). Based on the argument, the batik industry is not only limited to the textile industry and has the potential to be developed in other sectors.

This initiative needs to be done not only to maintain the Malay identity and culture through batik, but also to be able to contribute to the economic resources

in the country. Therefore, a group of lecturers and students from Universiti Kuala Lumpur Malaysian Institute of Marine Engineering Technology (UniKL MIMET) sought to explore the potential application of batik in the construction of fiber boats as an initiative and alternative to maintain Malay cultural identity based on batik.

6.2 Methodology

The research method used is experimental and involves two main stages, namely prototype construction and analysis. The design of the study is based on design and development. Design and development refer to the activity of designing, developing and evaluating certain processes systematically against a product or material created (Richey and Klein 2007). In addition, the design and development methods involving hands-on or practical teaching and learning activities starting from project planning, material preparation, prototype construction and evaluation of the process and product.

Hence, this study involves an experimentation of the construction of a fiberglass boat prototype done by combining fabrics containing batik patterns through certain processes. Next, the fiberglass batik boat prototype was tested in terms of its strength to determine whether the prototype is safe to use or otherwise.

6.3 Results and Discussion

This section discusses about the techniques in boat making from wood to fiberglass as well as the process of making batik-based fiberglass boats. The process are divided into three stages which are planning, boat construction and analysis of batik-based fiberglass boats in order verify the quality and durability of the boats.

6.3.1 *The Evolution of Boat Making Techniques: From Wood to Fiberglass*

Boat construction using fiberglass material is a continuation of wood-based boat manufacturing technology. The history of boat making for the Malays began when the Malay settlement territories began to undergo a process of separation because of the melting of the ice that increased the sea level thousands of years ago (Ali 2009). Therefore, boats and ships are needed to help the Malays to travel and trade and visit relatives separated by the sea, especially in the Malay archipelago (Ingram 2007).

At that time, the Malays had used wood as the main material in the construction of boats and ships. The wood from *cengal* trees and wood from *resak* trees were

chosen by the Malays to be used to build boats and ships due to their durability and strength (Ingram 2007). The technique of making boats and ships based on wood is traditional based on the way of working that uses almost entirely human energy and this manufacturing knowledge is usually inherited from one generation to the next (Salam and Osozawa 2008).

Today, wood is still used in the manufacture of boats and ships for the Malays, but the rate is declining (Maidin 2003). As a result of the advancement of science and technology, this situation has affected the technology of making boats and ships and their building materials. Shipbuilding is now more focused on the use of iron-based materials, especially involving large-scale projects so that the ship is durable and strong for long-distance travel with heavy loads. Boat making is more focused on the use of fiberglass than the use of wood (Koto Munirah and Arief 2014).

Manufacture of fiberglass-based boats is more popular today because this material is easier to maintain and more durable than wood. Fiberglass material is lighter, can move fast on water is stable and can prevent the entry of water into the boat. Furthermore, the difficulty in obtaining a supply of *cengal* timber and its rising prices have prompted boat operators to switch to using fiberglass as an alternative material in the boat building process as the cost of the material is cheaper than wood (Shamsuddin 2003).

6.3.2 Batik Application in the Process of Making Fiberglass Boat in UniKL MIMET

To create a good learning environment and meet the standards of the study program, UniKL MIMET has provided laboratories and workshops for instructors and students so that they are able to carry out practical academic assignments. Thus, the fiberglass workshop is used as a location in the process of making batik-based fiberglass boats. The process is divided into three stages, namely planning, construction process and prototype analysis.

6.3.3 First Stage (Planning)

Referring to the planning activities, the first thing to do is to find a suitable existing boat mold. UniKL MIMET fiberglass workshop already has several types of boat molds available, and this situation provides convenience to lecturers and students in the process of building a boat without having to make a mold first. Then, the process of measuring the boat mold that has been selected needs to be done because the process will determine the amount and number of materials used during the boat construction process. Among the materials used are batik fabric, fiberglass fabric, resin, gel coat, flow coat and catalyst material known as MEKP catalyst.

6.3.4 Second Stage (Boat Construction)

When implementing the boat making process, the preparation of batik fabric must be done first. The batik fabric purchased must have the same color so that the final product looks beautiful and even. Batik cloth needs to be soaked in hot water to remove the remnants of batik wax and new cloth wax. After that, the fabric is washed using soap and then dried. Then, the batik fabric is rubbed to produce a neat surface. The cloth is cut to a small size measuring one foot square so that it is parallel to the curved shape of the boat. The second process in construction leads to the preparation of boat molds. At the initial stage, the existing boat molds that have been selected will be cleaned using soap and water and dried.

The next step is that the dried boat mold will be smeared with a polishing material known as mold release wax. The third process involves the manufacture of the boat hull or known as the hull. This process started by applying a gel coat mixed with a catalyst that is the catalyst MEKP which is translucent on the surface layer of the mold. After that, the layer is left to dry for about half an hour. Once dried, glue or polyester resin is applied to the gel coat layer. Then, a piece of batik cloth that has been cut is applied on the glue that is wet. Another layer of glue is applied on the batik fabric.

This process needs to be repeated by replacing the batik cloth with fiberglass material known as chopped strand mat (CSM 300), woven roving (WR 400) and CSM 300 again. Once four layers are ready, this boat mold is left overnight for the drying process. The fourth process deals with the work of detail work. The dried hull of the boat is removed from the mold using tools such as hammers and wedges. Once the hull is removed, the process of tidying and detailing is done using an electric saw and an electric grinder. Floors, banana transom wood and seating are then attached to the boat. The surface in the boat is coated again using batik cloth and coated with a material known as clear flow coat. After that, the detailing and tidying work is done again using sandpaper. Imperfect parts of the boat will be repaired and smeared with a flow coat.

6.3.5 Third Stage (Analysis of Batik-Based Fiberglass Boat)

The first analysis of a batik-based fiberglass boat is to do a driving test on water or known as a sea trial. This test is important to determine the stability of a boat built while on the surface of the water. In addition, this is also important to ensure the safety of drivers and passengers when using the boat. At UniKL MIMET, the batik boats produced are lowered into the sea via a ship platform (slip way). After that, the boat is driven to test for stability, comfort, and leakage. The second analysis is from the use of batik cloth in the production of fiberglass boats.

To produce a beautiful and neat batik exterior surface, more time is required compared to the usual fiberglass boat making process. The process of soaking hot

water, washing and batik fabric fixtures in the boat mold takes quite a long time. In addition, the batik fabric should be placed on the mold in a small size (one square foot) to reduce the risk of trapped air. The attached batik cloth should be pressed using a cotton roller to remove the trapped wind residue.

This action is important because wind trapped in the batik fabric will damage the durability and surface of the boat. The second analysis is in terms of costs and expenses. Estimated cost for batik fabric in terms of size, it is priced at RM9.00 for a size of 2 m, compared to fiberglass fabric, which is priced at RM10.00 for a size of 3.3 m. Therefore, the price differences are seen not far from each other and not very significant. Thus, the final product of batik boat can be sold at a higher price compared to without batik if this product can be commercialized.

The third analysis is more scientific through testing of the materials used including a combination of materials such as batik coating, CSM 300, WR 350, CSM 300 and batik fabric. The results of scientific test analysis found that batik boats meet the requirements of the standards that have been set in the manufacture of fiberglass boats in terms of tension test, water absorption test and fire-retardant test.

6.4 Conclusion

In summary, the batik-based fiberglass boat construction process is a new method in boat building technology. This process is an experiment to find out whether the quality and durability of batik-based fiberglass boats can compete with ordinary fiberglass boats. Based on the analysis done, batik fiberglass boats have the same durability and quality as fiberglass boats, but batik fiberglass boats have their own advantages. This is because the batik fiberglass boat has been covered with batik cloth and makes it more attractive and beautiful. Batik fiberglass boats can be used as an attraction in the water-based tourism industry such as cruise boats and fishing boats to attract tourists to try the boat.

Although batik fiberglass boats have their own uniqueness, there are some disadvantages in terms of time and cost. This is because if a regular fiberglass boat can be completed in four days, a batik fiberglass boat will need to take six days to complete, and this situation will involve increased costs in terms of material expenses and workers' wages. However, such challenges can be addressed if the construction of batik fiberglass boats is done commercially and involves the use of technology as an additional approach to boost the construction of batik fiberglass.

The construction of batik fiberglass boats is a new thing and has the potential to be developed in the future based on continuous efforts, research, and development. In addition, this activity is also an alternative effort to highlight the Malay identity and culture in the application of batik to survive as one of the Malay heritages for the next generation.

Acknowledgements This study sponsored by UniKL research grant UniKL/CoRI/str19056. We would like to express our special thanks of gratitude to Universiti Kuala Lumpur Malaysian Institute

of Marine Engineering Technology (UniKL MIMET) which provides us the golden opportunity to do this wonderful research project and publication.

References

- Akhir NMH, Ismail NW, Said R (2016) Creative craft: the uniqueness and potential of the Malaysian batik industry. *Int J Interact Mob Technol* 4:10–14
- Ali I (2009) The culture of outrigger boat in the Malay Archipelago: a maritime perspective. *Hist J* 1:57–70
- Azimi R (2018) Batik Kedah tampil keunikan motif, *Utusan Malaysia*. Accessed 20 April 2018. <http://www.utusan.com.my/gaya-hidup/fesyen/batik-kejahtampil-keunikan-motif-1.456616#ixzz4dS1fAFLX>
- Chee WT (1990) Industrial development, the new economic policy in Malaysia, and the international division of labour. *ASEAN Econ Bull* 1:106–119
- Fauziah A (1983) Sejarah perusahaan batek. Monograf, Kelantan, Malaysia
- Ingram K (2007) Keeping the tradition of boat building alive, Auckland, Australia
- Koto Munirah J, Arief DS (2014) Occupational safety in production of traditional fishing vessels in Indonesia. *J Ocean Mech Aerospace* 4:7–12
- Maidin P (2003) Tukang timbal membina perahu: Tradisi dan inovasi. *Sari UKM J*. 21:39–56
- Muzdalifah M (2018) Universiti pertama di pentas terkemuka, *Utusan Malaysia*. Accessed 20 April 2018. <http://www.utusan.com.my/pendidikan/kampus/universiti-pertama-di-pentas-terkemuka-1.459418>
- Rafeah L (2012) Malaysian batik sarongs: a study of tradition and change, PhD dissertation, Royal Melbourne Institute of Technology (RMIT), Melbourne, Australia
- Richey RC, Klein JD (2007) Design and development research, New Jersey, USA
- Salam A, Osozawa K (2008) Technological adaptation in the transformation of traditional boats in the Spermonde Archipelago, South Sulawesi. *J Southeast Asian Stud* 46:200–227
- Shamsuddin MZ (2003) A conceptual design of a fibre reinforced plastic fishing boat for traditional fisheries in Malaysia. Development Division Fisheries, Malaysia
- Yusoff SA, Abdullah NA (2018) Batik Malaysia pikat ratu dunia, *Utusan Malaysia*. Accessed 20 April 2018. http://ww1.utusan.com.my/utusan/info.asp?y=2010&dt=1229&pub=Utusan_Malaysia&sec=Feminin&pg=fe_01.htm#ixzz4dS0uHw53

Chapter 7

Conceptual Design of a Mini Houseboat for Local Inland Water Use



Muhammad Nasuha Mansor, Iwan Zamil Mustaffa Kamal,
Zaimi Zainal Mukhtar, Anis Akmal Zulkefle, and Ainul Bahri Roslan

7.1 Introduction

A houseboat is a boat that has been designed or modified to be used similarly as a home. It is a floating structure with a high load-carrying capacity and can accommodate numbers of people. Some houseboats are not motorized, because they are usually moored, kept stationary at a fixed point and often tethered to land to provide utilities. For a typical motorized one, the outboard engine is preferable to support for slow cruising on inland waters, offered the space and comfort as a home (Reymala 2012).

Over the years, houseboats have built an eco-tourism attraction with accessibility to many areas. Due to the deck size, hull shape and arrangement, a houseboat can carry a load almost similarly like a floating cabins. This new experience attracted and gained demands in tourism sector recently. The attraction of simplicity and the originality provided by the houseboat operator brought impressive feedback from tourists. They loved slow and leisurely movement in short term period more than the monotonous trip of the other typical boat shuttles and services. Malaysia, as a tropical country

M. N. Mansor (✉) · I. Z. Mustaffa Kamal · Z. Z. Mukhtar · A. A. Zulkefle · A. B. Roslan
Universiti Kuala Lumpur, Malaysian Institute of Marine Engineering Technology, Lumut, Perak,
Malaysia
e-mail: mnasuha@unikl.edu.my

I. Z. Mustaffa Kamal
e-mail: iwanzamil@unikl.edu.my

Z. Z. Mukhtar
e-mail: zaimi@unikl.edu.my

A. A. Zulkefle
e-mail: anis.zulkefle@s.unikl.edu.my

A. B. Roslan
e-mail: ainul.roslan@s.unikl.edu.my

surrounded by beautiful rainforest and inland waterways unescapably follows this trend of demand. Local tourists extended their interest to travel and explore the attractions offered by this new experience houseboat trip. Most of the existing houseboats in Tasik Kenyir and Tasik Banding have an overall length ranging from 15 to 25 m suitably to accommodate between 20 to 30 persons each trip. Depending on the duration, season and trip arrangement, the price of rental varies from RM1800 to RM 6500 per night. This existing situation creates restrictions especially for small groups and families to enjoy the similar experience with slight lower budget. As an alternative, there is a potential to explore the smaller size of houseboat with more flexible trip arrangement and affordable rental. The conceptual design for this so-called mini houseboat was initiated for this project. Hull form assessment is one of the main agenda for hull selection based on the mission requirement. The final outcome of the 3D rendered conceptual design was developed by taking into consideration of essential elements such as comfortability, safety as well as ergonomics.

7.2 Literature Review

A houseboat is a built structure that lies on the water surface, thus uniquely creates sensations portrayed by the moving water below and views surrounding them. To suit the role of the houseboat as a unique recreational experience and vacation styles on water, the hull is the most crucial design consideration in order to provide sufficient buoyancy for required overall weight and remain seaworthy in any common condition. Comparing to the floating house, the major difference between houseboat designs is the capability of self-moving and maneuverability (Merrington 2004). Since they are not intended to be kept stationary at fixed locations, they are mostly motorized and only moored using dock lines when necessary (Wang and Xu 2021). Most of the houseboats range in length from 15 to 25 m, and could be more in some countries like United States, as shown in Fig. 7.1. Commonly with shallow draft feature, they have living quarters in the superstructure, maximizing the windows for light and ventilation. These houseboats typically have broad decks, which provides an ideal space for home-looked design and arrangement. Although facilities and amenities selection inside are more compacted compared to a normal house, they combine the roominess and comfort of the houseboat with the convenience of so called cabin cruiser. This cabin built on the hull varies from single level up to three tiers deck to equipped vacation-need facilities such as beds, kitchen, bathroom, refrigerator, television room, living room, dining room and other recreational spaces.

In Malaysia, houseboats are receiving a lot of attention as new style of vacation among foreign and local tourists. Inland water such as Kenyir lake, Pedu lake and Banding lake is the most preferable operation area due to its suitability in terms of calm water and large size, surrounded by natural ambiance as well as spectacular flora and fauna. In common practice, the houseboat owners or operators are entirely responsible during the operation, including helmsman and tour guide. This



Fig. 7.1 Houseboats in Tasik Temenggor, Royal Belum, Perak (Holly Bluff Marina [2022](#))

scenario gained more attention and demand among tourists, with a peaceful experience throughout their houseboat vacation trip. According to Amarudin ([2022](#)), Kenyir lake recorded a significant increased numbers of visitors experiencing the houseboat trip. The growing numbers of tourists has reached more than ten thousands since 2010, which is showing that this activity becomes increasingly popular.

The typical houseboat design ideally consists of a hull that is partially submerged in water which allows the boat to move in the water with required speed and maneuverability. There are two major types of hull form design, the one with a mono hull that is curved and shaped to move through the water efficiently. The other has a pontoon base type that is wider in the water and contains at least two hull extrusions into the water, similarly with the feature of catamaran. This design is considered concerning on the bigger reserve buoyancy for more weight required but sacrificing cruising speed and less manoeuvrability through water. This design provides more deck space for the cabin above or within ‘twin’s’ hull and therefore better flexibility on the general arrangement. In faster single curved hulled boats, sleeping and living quarters are included in the hull of the boat, similarly like a yacht. The pontoon base design mostly creates shallower draft at corresponding displacement (Merrington [2004](#)).

Advantages from both types of design are listed and taken into consideration to produce the new conceptual design. The pontoon based type potentially could be improvised to achieve as much as possible catamaran look and features. By having advantages of catamaran over a mono hull in terms of wider layout, excellent stability and less wetted surface area, the conceptual design of a smaller size the so-called mini houseboat would be the main option (Hidayah and Radam [2014](#)). Hull form variations were developed based on mission requirement and individual assessment were further performed in this project.

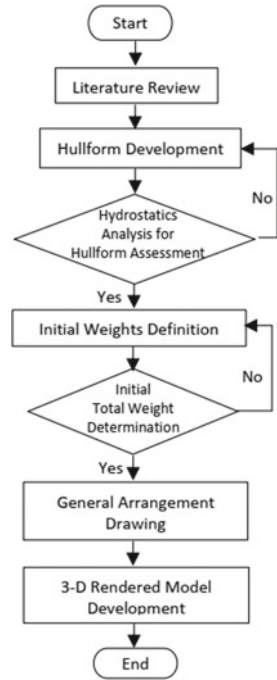
7.3 Research Methodology

The project was initiated with the development of potential hull forms. The overall flow of the project can be referred in Fig. 7.2. Based on the main dimensions and type of hull required, variations of hull form were developed by using a 3D modelling software, Maxsurf Bentley. Assessment of individual hull forms then is carried out to comply the mission and operation requirement. Parameters such as length of overall (LOA), shallow depth and draft, distance between both hulls and total displacement are among the crucial factors in finalizing the hull form. The hull form selected must ensure to provide sufficient reserve buoyancy to support the required total weight of the houseboat. At the same time, decision for deck width must be sufficient to accommodate the required cabin. Factors such as wetted surface area for less resistance, and height of freeboard for better stability also need to be borne in mind during hull form consideration. All these considerations are made based on assessment of the hydrostatics data produced. Hydrostatics particulars of each potential hull form were evaluated individually to determine the most suitable one, in terms of displacement required at acceptable design draft, sufficient depth and adequate deck area for cabin and equipment/outfitting arrangement. A decision matrix as suggested by (Jack 2022) was used to compare, evaluate and decide the most suitable one. Initial list of typical weights to be accommodated onboard were considered once the conceptual design of hull form has been finalized. There is a wealth of outsourcing information available such as catalogues and brochures for equipment and weight consideration. The maximum displacement based on hydrostatics result is the main reference in considering the total of potential weights. The total weight proposed ideally should be within the allowable displacement determined at a design draft. For the final outcome, a general arrangement drawing was produced to give the overall view of space and equipment distribution onboard. On top of that, a three-dimensional design by using Rhinoceros was developed for better visualization purpose as a proposed conceptual design of the mini houseboat.

7.4 Results and Discussion

As far as the conceptual design is concerned, the selection of a suitable hull form and main dimensions are the most important stage for the project. The hull form assessment based on the variations developed crucially needs to be considered to meet the initial mission and operation requirements. To propose the new concept of a houseboat for a smaller group of tourists having similar experience, with more affordable and flexible trip, new mission requirements were initially stated as given in Table 7.1. Based on a literature research made earlier, for the new requirement of the mini houseboat concept, the possible range of length overall is from 7.5 to 10 m. This is the common length for leisure boat activities involving between 6 and 8 persons. This range of numbers is an acceptable number for a small group of tourists

Fig. 7.2 Flowchart of the overall project



as well as a family. Similarly with the other existing houseboat operation, slow and leisure trip with speed from 6 to 8 knots is their preference. The conceptual design of the mini houseboat is also preferably having shallow depth, to give more flexibility for the area of operation. Not only lake, but the route of trip could also be extended to shallower water depth areas such as natural swamps and river mouths for new experience.

The variation of hull forms were developed and assessed in determining the most suitable one to be used as the conceptual design. The hydrostatics data produced was mainly used as main reference in analyzing the most suitable hull form for the mini houseboat concept. Variation of hull forms and the individual hydrostatics data can

Table 7.1 Mission requirements of mini houseboat

Particulars	Parameters
Length overall (LOA)	7.5–10 m
Number of passenger	6–8 person
Cruising speed	7–8 knots (typical houseboat)
Displacement	3.5–4 tonnes
Cabin for overnight stay	
Limited depth (with shallow draft)	

be referred in Figs. 7.3, 7.4, 7.5, 7.6 and 7.7. The Maxsurf Modeller software was used for the hull form development and hydrostatics analysis.

The length of overall is firstly highlighted so that the range is not too small to cater approximately 6–8 passengers but at same time, not too long to meet the ‘mini’ houseboat concept. Out of 5 hull forms developed, the first three, hull 1, hull 2 and hull 3 are potentially restricted the deck space for cabin arrangement and superstructure with an initiated overall length less than 10 m. hull 4 and hull 5 with length of overall 10.5 m were prioritized to accommodate conveniently the superstructure,

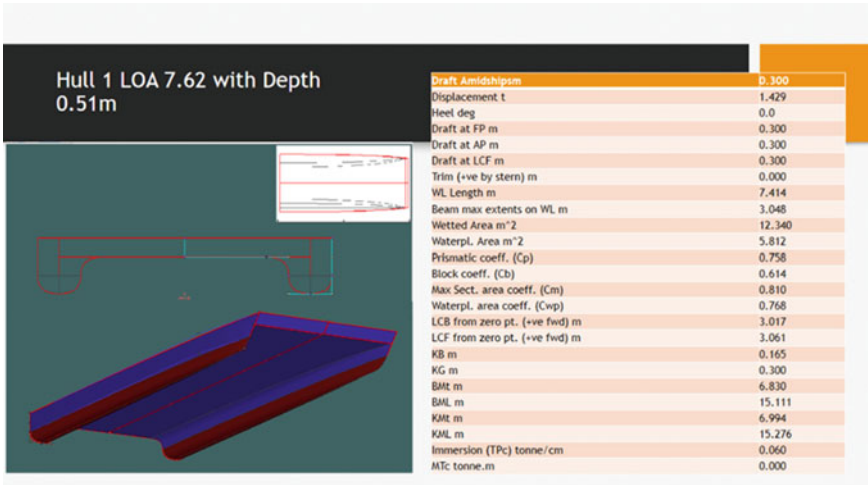


Fig. 7.3 Hull 1 design and hydrostatics particulars at design draft

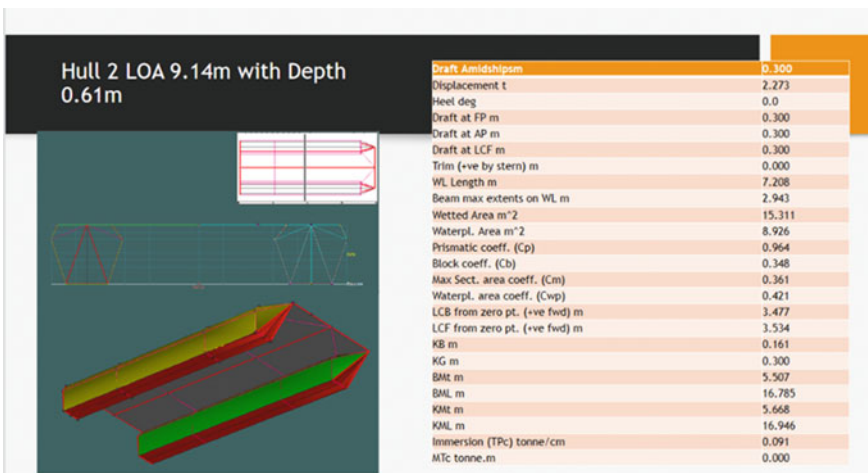


Fig. 7.4 Hull 2 design and hydrostatics particulars at design draft

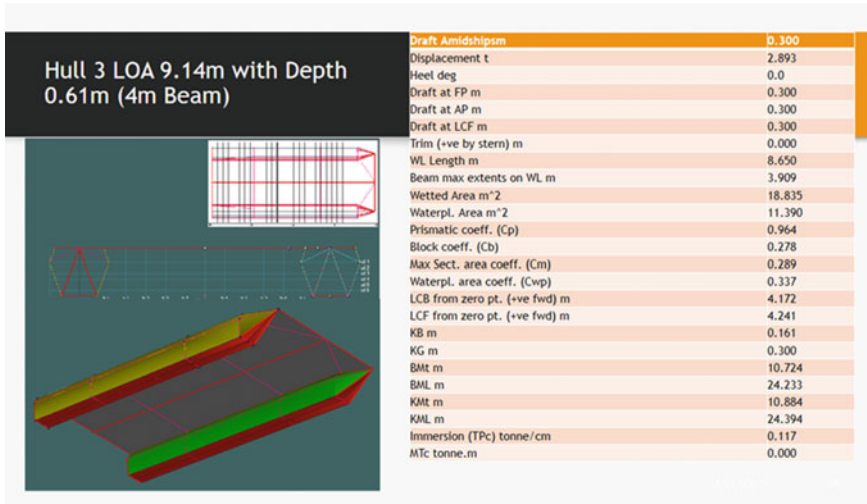


Fig. 7.5 Hull 3 design and hydrostatics particulars at design draft

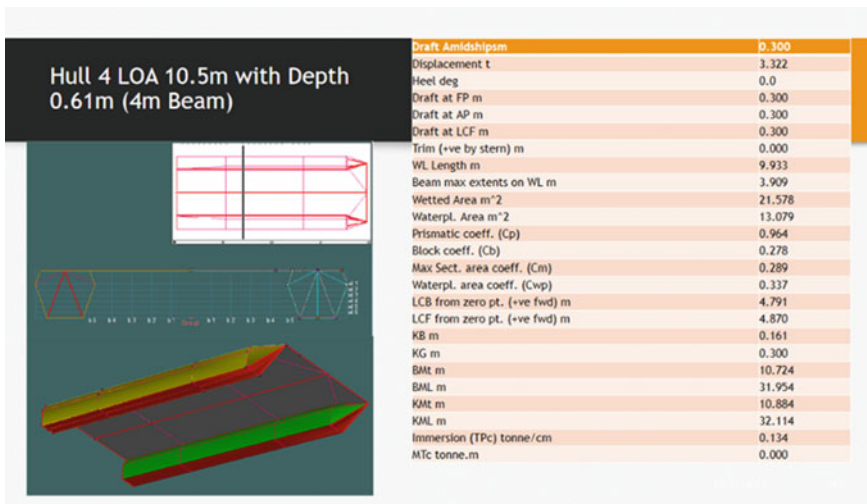


Fig. 7.6 Hull 4 design and hydrostatics particulars at design draft

with optimized width from 3 to 4 m. Concerning the mission requirement of shallow depth and draft, the depth decided for hull 5 improvised the variations proposed earlier in hull 1–4. Although an attempt was made to achieve as low as possible the depth, those designs could not provide sufficient draft to maximize the required displacement. A design with too low depth creates a restriction on the draft to have better reserve buoyancy, as well as freeboard height. Crucial evaluation between

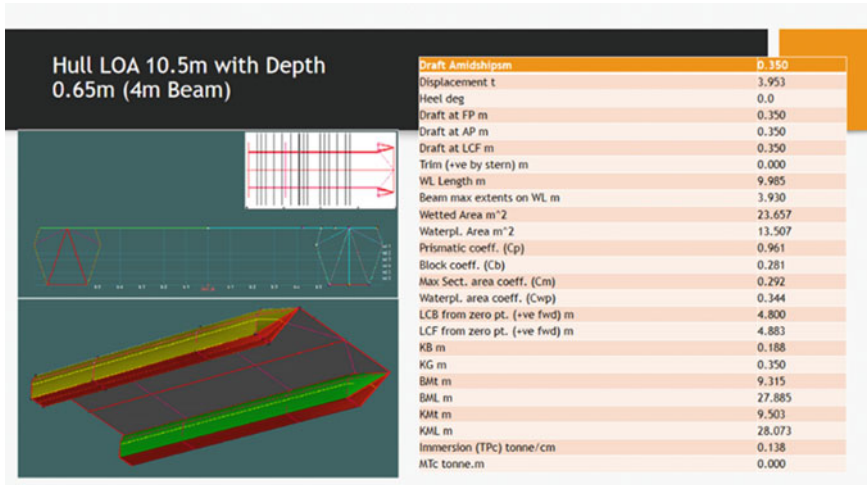


Fig. 7.7 Hull 5 design and hydrostatics particulars at design draft

lower depth (with shallow draft) and displacement requirement is needed, thus hull 5 gives an acceptable range of depth at 0.65 m and displacement nearly 4.0 tonnes (3.95 tonnes). Comparing to earlier hull 1, hull 2 and hull 3, although the size of LOA (7.6–9 m) and depth (0.5–0.6 m) suits within the range, the corresponding maximum displacement gained at appropriate draft is just less than 3 tonnes. The ideal concept of the mini houseboat with all basic facilities and equipment for up to 8 people requires at least 3.8–4 tonnes for full load displacement. With appropriate depth and draft, this range of displacement potentially could also provide better flexibility and stability in considering more than one deck of superstructure. With adequate control of weight and vertical center of gravity (VCG) distribution, a two-tiers deck was proposed for this conceptual design of the mini houseboat. Table 7.2 shows the decision matrix used to relatively compare the variations of the hull form design. The criteria specified are mainly based on the mission and operation requirements identified earlier. Though, weightage is specified to rate the importance and priority of the requirements. As a rating factor, weightage 1.0 is the most important, thus main dimensions selection, convenience of cabin and total displacement provided are in the list. Those criteria signify the compliance of initial mission requirements and success of the ideal mini houseboat.

The flexibility of the construction process also is preferable as a criteria of selection, but it is considered as the least important with weightage of 0.5. Out of 5 hull form designs, although the criteria of shallow depth and draft rated as the lowest, hull 5 still gained the highest in total of 12.5 and is considered as the winning concept. Its lowest criteria is still acceptable since it is categorized as the least important in considering the conceptual design. With additional of 0.5 m depth height from 0.6 m (hull 4) to 0.65 m (hull 5), it is still acceptable to operate in typical shallow water if necessary. With moderate score of main dimensions selection, the design provides

Table 7.2 Decision matrix for hull form conceptual design of mini houseboat

Criteria	Weightage	Hull 1		Hull 2		Hull 3		Hull 4		Hull 5	
Main dimension	1.0	3	3	2	2	2	2	2	2	2	2
Number of passenger	0.8	2	1.6	2	1.6	3	2.4	3	2.4	3	2.4
Convenience cabin for overnight stay	1.0	1	1	1	1	2	2	3	3	3	3
Shallow depth and draft	0.6	3	1.8	2	1.2	3	1.8	2	1.2	1	0.6
Total displacement	1.0	1	1	1	1	2	2	2	2	3	3
Hull fabrication process	0.5	1	0.5	3	1.5	3	1.5	3	1.5	3	1.5
Total with weightage			8.9		8.3		11.7		12		12.5

convenient cabin space for a maximum of 8 persons, a less-challenging process of hull fabrication and most importantly allows adequate buoyancy to maximize the total weight to be onboard.

Based on the allowable total displacement of 3.9 tonnes at 0.35 m draft for Hull 5 design, the initial weight breakdown has been considered and distributed as listed in Table 7.3. As a conceptual design stage, items and weight to be considered were based on the relevant reference of typical recreational boats. The prediction of weight is made by considering factors such as similar range of size and mission as well as relevant brochures and catalogues available in the market. There might be room for improvements in term of the accuracy once the design has been detailed out later.

The list of initial weight for this conceptual design was decided mainly based on the mission requirement as well as the basic needs and space for 8 persons such as:

- (i) Light weight material of hull by using aluminum
- (ii) High water resistance for superstructure by using wooden-looked cement fibre material planks
- (iii) As minimum as possible power of engine for light weight and low cruising speed
- (iv) Adequate cabin to cater for 8 persons
- (v) Galley and convenience space for dining
- (vi) Water closet and shower room
- (vii) Fresh water tank
- (viii) Space for recreational activities such as observation deck and water slide.

Table 7.3 Initial weight estimation for conceptual design

Item	Weight (kg)
Hull structure	650
Superstructure	530
Railing/pillars	290
Engine (engine mercury 30HP)	51
Cabin 1	
Single tier 1 and 2 (mattress and Pillow)	44
Locker 1	8
Fan	3
Window 2	6
Window 2	6
Cabin 2	
Single tier 3 (mattress and pillow)	22
Locker	8
Window 1	3
Cabin 3	
Queen bed matteress and pillow	44
Fan	6
Window 2	6
Galley	
Refrigerator	36
Dine table & chair (8)	70
Stove	2
Hanging cabinet	13
Storage and sink	42
Fan	3
Window	3
Deck flooring	680
Anchor and rope + railing rope	11
Steering and gear	10
Wood blind	62
Fuel oil	40
Fresh water tank	450
Toilet	
Bowl	35
Toilet door	9
Sink	16
Mirror	5
Crew	75

(continued)

Table 7.3 (continued)

Item	Weight (kg)
Passengers × 8	600
Galley accessories	50
Safety equipment	30
Water slides	30
Total weight	3949

As a conceptual design, spaces with all necessary equipment and items have been modelled by using the Rhinoceros 3D software for better visualization and can be seen Fig. 7.8.

In terms of the powering requirement, the drag of the hull 5 was estimated using the Holtrop method. The speed was calculated from 2 to 8 knots. At 8 knots the total effective power is at 15.2 kW. If we consider a propulsive efficiency of 70%, the delivered power required for hull 5 will be at 21.7 kW which is equivalent to 29.1 horsepower as shown in Fig. 7.9.

As a whole, the overall arrangement of spaces proposed mainly prioritizing the restriction area of the mini houseboat and lighter weight of equipment, without compromising the minimum requirement of safety, comfortability and ergonomic factor. The arrangement and distribution proposed can be referred in the general arrangement drawing as shown in Fig. 7.10.

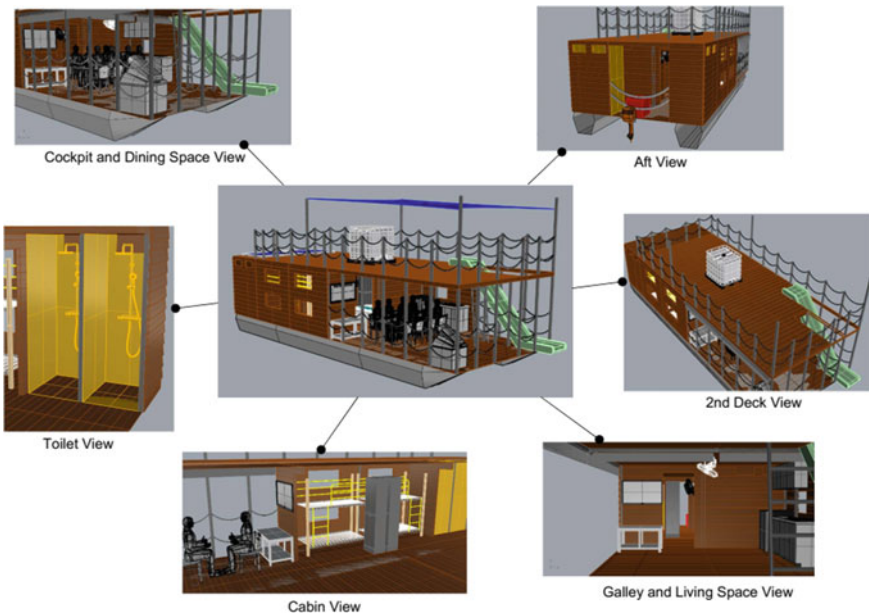


Fig. 7.8 3-dimensional views of conceptual design of mini houseboat

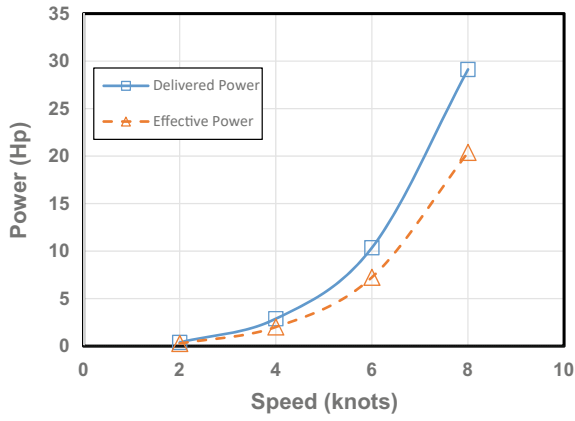


Fig. 7.9 The powering requirement for hull 5 from 2 to 8 knots

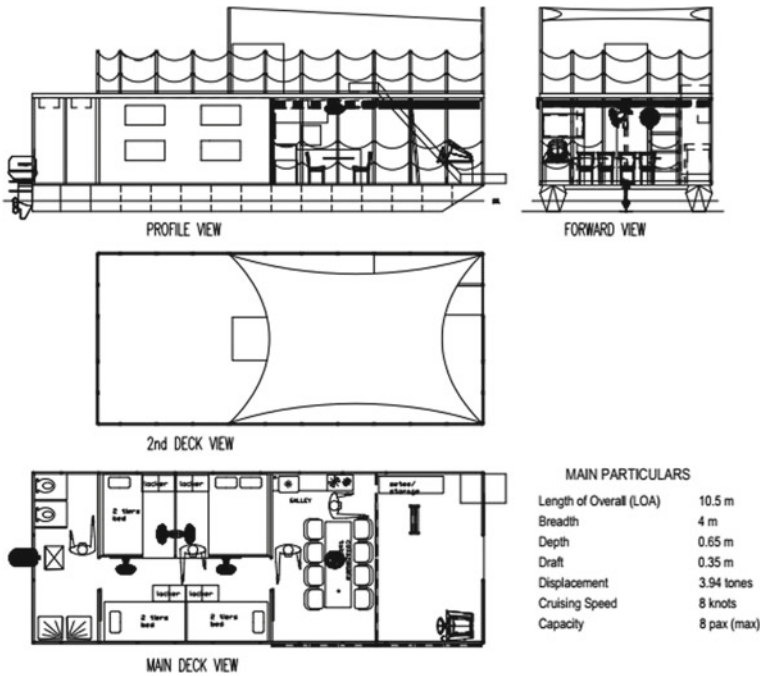


Fig. 7.10 General arrangement of conceptual design of mini houseboat

Table 7.4 Main particulars of conceptual design of mini houseboat

Particulars	Parameters
Length overall	10.5 m
Breadth	4.0 m
Depth	0.65 m
Design draft	0.35 m
Displacement (at design draft)	3.95 tonnes
Cruising speed	8 knots (approximately)
Capacity	8 persons

7.5 Conclusion

The conceptual design of a mini houseboat was completely developed as an alternative of existing houseboat with a larger size. Considering the restrictions as well as the mission and operation requirements, this new design not just caters for smaller size of tourists having similar experience, it also gives a more flexible trip with lower budget. They still can have a relaxing overnight trip with convenience cabin and facilities, more privacy close to nature trip and a safe adventurous tour. Concerning the mission and operation requirement, safety and ergonomics factors, Table 7.4 shows the main particulars for the conceptual design of the mini houseboat. This conceptual design potentially could be further detailed out for future research. Having the initial general arrangement drawing together with weight list, a detailed weight estimation could be performed next by taking into account the individual center of gravity. This will give a more convincing weight distribution and overall center of gravity for stability assessment purpose. Prior to that, scantling and structure weight calculation also need to be detailed out for the next preliminary design stage. Cost estimation and analysis then could be carried out later in determining the feasibility of this new concept of mini houseboat. The main factors to be highlighted at this stage include materials and equipment, man hours for construction and cost of operation such as fuel consumption, helmsman wages and potential rental fees.

References

- Amarudin SK (2022) Tasik Temenggor Royal Belum dibuka kepada pelancong mulai hari ini. Utusan Online. <https://www.utusan.com.my/berita/2021/10/tasik-temenggor-royal-belum-dibuka-kepada-pelancong-mulai-hari-ini/>. Accessed 14 Sep 2022
- Holly Bluff Marina: Houseboat amenities [Online]. Available: <https://www.hollybluff.com/houseboat-amenities/> Accessed 14 Sep 2022
- Hidayah WN, Radam A (2014) Using choice experiments to understand visitors preferences for the man-made lake ecotourism services in Terengganu. *J Int Consum Mark* 4:41–50
- Jack H (2022) Engineering design, planning, and management, 2nd edn. Academic Press
- Merrington E (2004) Arch 684 sustainable case studies, University of Waterloo School of Architecture

- Reymala M (2012) Houseboats in Kerala—constructional features and environmental issue. *IOSR J Environ Sci Toxicol Food Technol* 1(6):31–34
- Wang X, Xu SY (2021) Exploit the ocean for extra housing supply: a comparison between the floating house and houseboat. *Int J Eng Adv Technol* 2(2):37–39

Chapter 8

Effect of Barnacle Fouling on Ship Resistance Using MATLAB Image Processing



Shaiful Bakri Ismail, Zulzamri Salleh, Mohd Faizal Abdul Razak, Aizat Khairi, Mohd Zaifulrizal Zainol, and Muhammad Azrin Muhammad Azhar

8.1 Introduction

Barnacles are attached to the hull of the ship and makes the ship to slow down and will result in 40% increases of fuel consumption (Demirel et al. 2017). This is because the barnacle fouling led to a loss of power for the ship to maintain at a constant speed thus increases of the fuel consumption. This statement also is supported (Alghamdi and Quijada 2019) in which it is stated that the ship that is covered by the barnacle will

S. B. Ismail (✉) · M. Z. Zainol

Marine Electrical and Engineering Technology Section, Universiti Kuala Lumpur, Malaysian Institute of Marine Engineering Technology, Jalan Pantai Remis, 32200 Lumut, Perak, Malaysia
e-mail: shaifulbakri@unikl.edu.my

M. Z. Zainol

e-mail: mzaifulrizal@unikl.edu.my

Z. Salleh · M. F. Abdul Razak

Maritime Engineering Engineering Technology Section, Universiti Kuala Lumpur, Malaysian Institute of Marine Engineering Technology, Jalan Pantai Remis, 32200 Lumut, Perak, Malaysia
e-mail: zulzamri@unikl.edu.my

M. F. Abdul Razak

e-mail: mfaizalar@unikl.edu.my

A. Khairi

General Study Department, Universiti Kuala Lumpur, Malaysian Institute of Marine Engineering Technology, Jalan Pantai Remis, 32200 Lumut, Perak, Malaysia
e-mail: aizat@unikl.edu.my

M. A. Muhammad Azhar

Maritime Management Section, Universiti Kuala Lumpur Malaysian Institute of Marine Engineering Technology, 32200 Lumut, Perak, Malaysia
e-mail: mazrin.azhr@s.unikl.edu.my

utilize more fuel thus this research will provide an explanation and proves towards the problem stated by the past researcher. This research objective is to measure the growth rate of the barnacle by using image processing in MATLAB (Gerald and Maurice 2014) and to analyze the effect of barnacle fouling towards the ship performance. To achieve these objectives, a research question is provided which is how to measure the growth rate of the barnacle and how to analyze the effect of barnacle fouling on ship resistance and powering.

8.2 Literature Review

The term of fouling can be defined as the attachment of an organism on the surface of the hull whether the hull of the ship, boat or any kind of transportation that is floating on the surface of the sea water that can bring negative impact on the vessels. These organisms can also hide and live at the area in which the area is protected or niche such as the sea chest (Bressy and Lejars 2014). The fouling of the hull also can be called vessel fouling or biofouling. There are many kinds of example of organisms that are being attached on the surface of the hull such as the barnacle (Larsson et al. 2010; Sulaiman et al. 2018). The hull will be colonized by the organism whenever the vessels reach from one port to another port or bioregion to the next by means of invasions when these organisms release their larvae into the water (Deshner 2018; Lau 2018).

There are several effects or impacts of the barnacle on the ship. Authors of Desher (2018) described that these barnacles are one of the examples of macrofouling organisms that accumulated and attached the hull in which it brings a very significant problem to the vessel's hull. Whenever these barnacles accumulate and increase their colony on the surface area of the hull, the hydrodynamic volume of the ship is increased thus the drag of the ship increases (Song et al. 2019). According to Bocchetti et al. (2015) the barnacle which is attached to the surface of the hull will causing the fuel consumption to increase.

The following are the formulae that are being used to calculate the ship resistance.

Total Resistance

The total resistance obtained four components which is the frictional resistance, residual resistance, air resistance and fouling resistance causing the resistance to occur on the ship during the movement of the ship through the water. Authors of Lau (2018), Birk (2019) indicate the equation for the total resistance.

$$R_T = R_{foul} + R_{aw} + R_{air} + R_{calm} \quad (8.1)$$

Frictional Resistance

The frictional resistance occurs when the water flows along the surface of the ships (Birk 2019). Equation (8.2) is the equation for the frictional resistance.

$$R_{aw} = WSA \cdot f \cdot V^{1.825} \quad (8.2)$$

Residual Resistance

The residual resistance is the pressure or force in which pushed the water aside (Birk 2019). The equation for this residual resistance is as Eq. (8.3).

$$R_v = C_v \cdot (0.5) \cdot \rho \cdot V^2 \cdot S \quad (8.3)$$

Air Resistance

The air flow that passes through or flows around the superstructure of the ship (Seok and Park 2020). Equation (8.4) shows the relation for air resistance.

$$R_{air} = (0.5) \rho S V^2 C_A \quad (8.4)$$

Fouling Resistance

The following is the formula for calculating the fouling resistance (8.5) of the ship by using the data gained from the image processing. Fouling is causing the ship to add more resistance towards the ship (Lau 2018).

$$C_{foul} = R_{foul} / (0.5 \cdot \rho \cdot WSA \cdot V^2) \quad (8.5)$$

8.3 Research Methodology

The images of the barnacle were taken each week and there is a total of three locations which is located at the KL Sauh UniKL MIMET. The images are the data for the image processing in MATLAB. The process of the image processing is shown in Fig. 8.1. Then, the data of the image processing will be the input to be used in the mathematical modelling realized using C++. The result is the resistance of the ship based on the coefficient of fouling.

8.3.1 Flowchart of Image Processing in MATLAB and C++ Programing

In MATLAB, the image processing tools are used to code the process of converting the image from the original image into black and white picture. From that black and white pixel picture, the images are analyzed by calculating the ratio between the

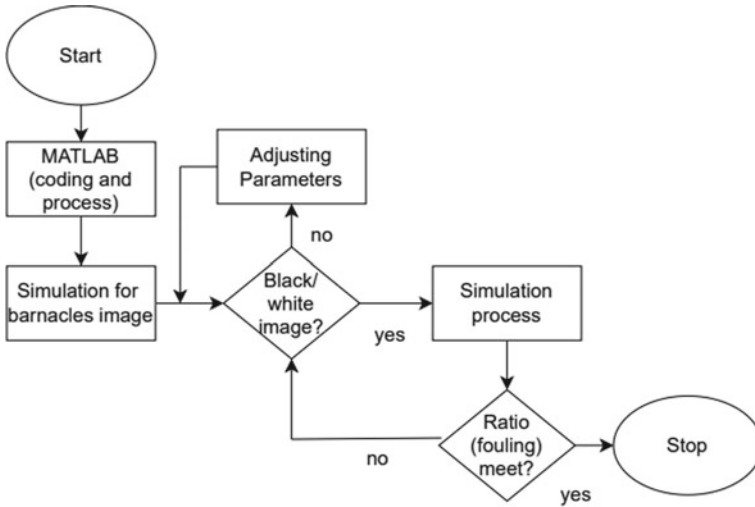


Fig. 8.1 Flowchart of MATLAB programming

black and white pixel to get the ratio as it represents as the coefficient of fouling. Meanwhile, by using C++ programming, the formula of the resistance is coded to get the result of the calculation based on the data of the ship and the data from the image processing in MATLAB which is the coefficient of fouling (Fig. 8.2).

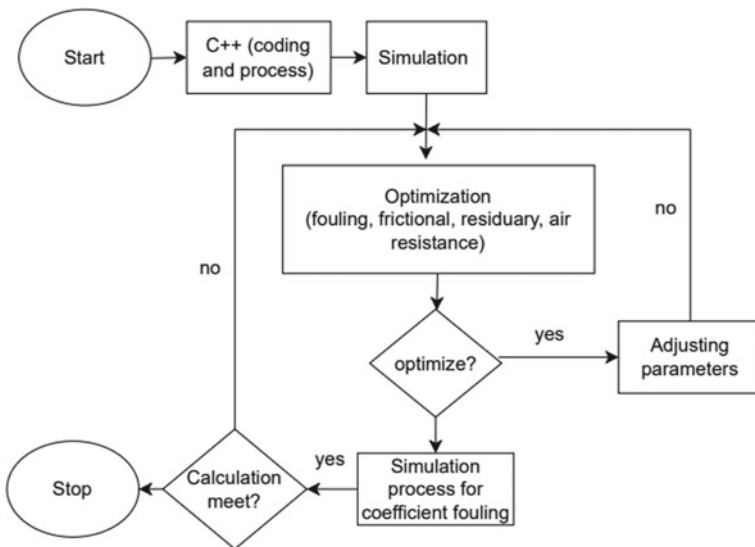


Fig. 8.2 Flowchart of C++ programming process

8.4 Results and Discussion

8.4.1 Raw Image of Barnacles

There is a total of four stages of image processing. Figures 8.3, 8.4, 8.5, 8.6, 8.7 and 8.8 are the result from the image processing MATLAB coding. Figure 8.3 shows the location 1 and location 2 of the barnacle image while Fig. 8.4 shows the image of location 3.

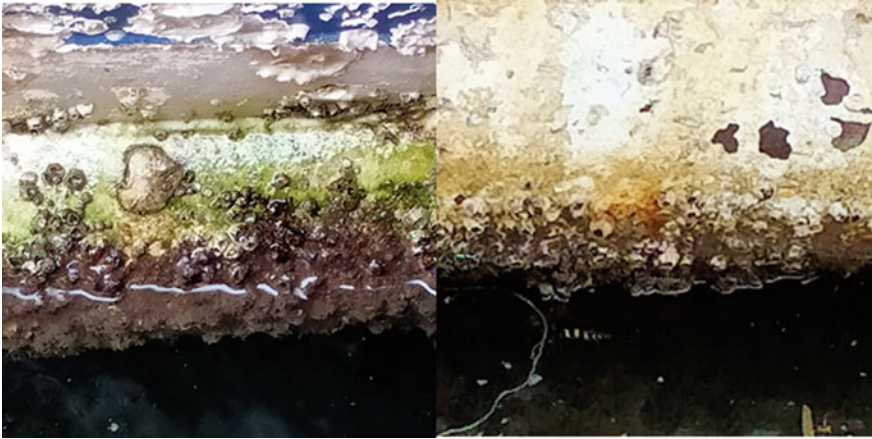


Fig. 8.3 Image at location 1 and location 2



Fig. 8.4 Image at location 3

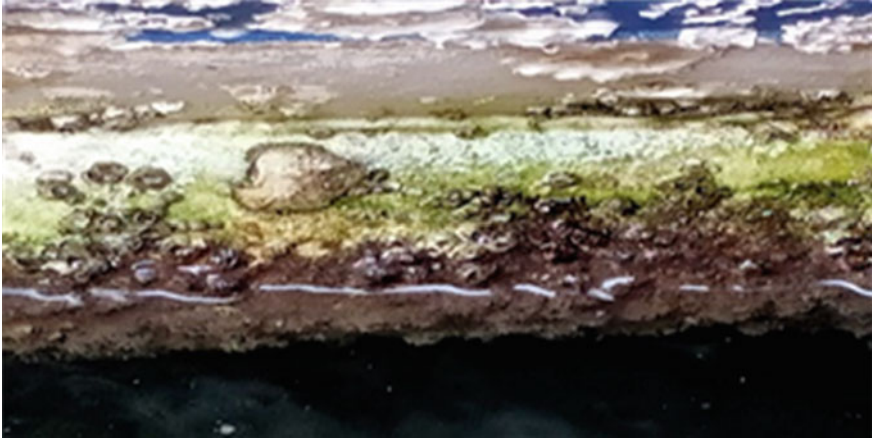


Fig. 8.5 Displaying image

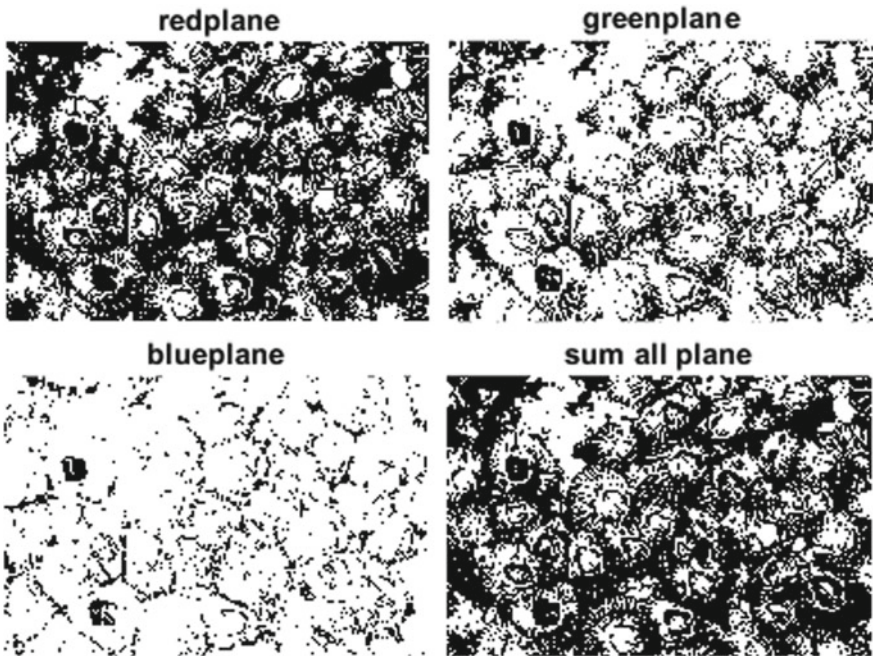


Fig. 8.6 RGB image



Fig. 8.7 Gray scaling image



Fig. 8.8 Final result of image

8.4.2 Image Processing of Barnacles

The first process is the displaying of the image taken which is the image of the barnacle. Figure 8.5 shows the original image that is being taken from each week and Fig. 8.6 shows each format of color into separate images. Each image of color format is then converted into grayscale and different types of color produce different image of grayscale as shown in Fig. 8.7. The result of the image is as shown on Fig. 8.8. The fouling coefficient, fouling resistance, total resistance and the effective power of the ship is tabulated, and a graph is plotted to analyze the result.

8.4.3 Result of Fouling Coefficient and Ship Resistance

This process calculates the total area of the image then the total of white pixel is divided with the total pixel area of the image to get the ratio of the white pixel. The white pixel result will be considered as the area of the barnacle or the coefficient of barnacle fouling. From Table 8.1, the value of the coefficient ratio which is the area of the barnacle compared to the area of the hull for location 1 is 0.6505 meanwhile location 2 and location 3 have a value of 0.5366 and 0.7443. This data is the initialization for the growth rate of the barnacle starting from week 5 which is considered as the first week of the barnacle image being taken until the final week which is in

Table 8.1 Result coefficient of fouling

Name of image	Coefficient ratio
Location 1	0.6505
Location 2	0.5366
Location 3	0.7443

week 12. The growth rate of the barnacle is monitored and analyzed each week in order to determine the growth rate of the barnacle.

The result from the image processing of each location of the barnacles is used as mathematical tabulated data in C++ programming. The results are shown in Table 8.2. Table 8.3 shows the result of growth rate per day for each location from week 5 until week 12 from three locations of barnacles. The area of barnacles represents the white number of pixels from the result of image processing (MATLAB). As for the coefficient of fouling, it is the ratio between the number of white pixels and black pixels. From Table 8.3, the coefficient of fouling significantly increases from 0.6505 to 0.7468. As a result, there is an increase of 14.8% for the barnacle growth rate at hull of the ship from week 5 until week 12 with a total percentage of 0.3% per day for location 1. Meanwhile, the coefficient of fouling growth rate is slightly increased for barnacles at location 2 and 3 are 0.2% and 0.04% per day, respectively.

8.4.4 Result of Fouling Resistance

The value of the fouling resistance at each different location is tabulated as shown on Table 8.4 and Fig. 8.9. Fouling resistance can be measured by using the value of fouling coefficient. The result for the fouling resistance will be divided into each location of the images which is fouling resistance for location 1, location 2 and location 3.

8.4.5 Result of Total Resistances

Table 8.5 and Fig. 8.10 show the total resistance of the ship in accordance to the barnacle growth rate at the hull of the ship which is the fouling coefficient. All the resistance occurring at the ship will be summed up such as the fouling resistance, air resistance, sea water pressure and water plane area pressure thus producing the total resistance of the ship. To analyze the impact of the fouling coefficient which is represent by the number of barnacles attached at the hull of the ship, the total resistance of the ship is calculated and estimated by using the mathematical modelling in the C++ software. There is an increase in percentage of the total average resistance up to 17.65–22.78% for three locations. This percentage of increase can be gained by doing the calculation of percentage increase. Location 2 stated the highest value of

Table 8.2 Result of estimation of resistance for each location

Location	Coefficient fouling	Fouling resistance	Sea water resistance	Air resistance	Area waterplane resistance	Total resistance	Effective power	% increase of resistance
1	0.6505	671.607	$4,28153 \times 10^{-10}$	532.977	2061.81	3266.4	20,162.8	20,5611
2	0.5366	554.011	$4,28153 \times 10^{-10}$	532.977	2061.81	3148.8	19,436.9	17,5943
3	0.7443	768.45	$4,28153 \times 10^{-10}$	532.977	2061.81	3363.24	20,760.6	22,8485

Table 8.3 Result of fouling coefficient at all location until week 12

Week	Location 1	Location 2	Location 3
	Fouling coefficient	Fouling coefficient	Fouling coefficient
5	0.6505	0.5366	0.7443
7	0.5895	0.4103	0.7182
8	0.7014	0.5774	0.768
9	0.6872	0.5315	0.7234
10	0.7533	0.5528	0.7849
11	0.6934	0.5803	0.6956
12	0.7468	0.5897	0.7573

Table 8.4 Result of fouling resistance

Week	Location 1	Location 2	Location 3
	Fouling resistance (kn)	Fouling resistance (kn)	Fouling resistance (kn)
5	671.607	554.011	768.45
7	608.627	423.613	741.503
8	724.158	596.135	792.919
9	709.497	548.745	746.872
10	777.742	570.736	810.367
11	715.898	599.129	718.17
12	771.031	608.834	781.872

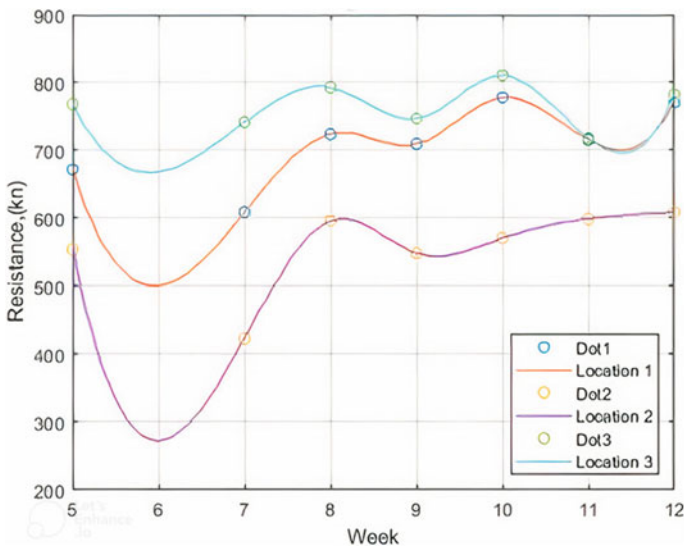


Fig. 8.9 Graph of fouling resistance

Table 8.5 Total resistance result

Week	Location 1	Location 2	Location 3
	Total resistance (kn)	Total resistance (kn)	Total resistance (kn)
5	3266.4	3148.8	3363.24
7	3203.42	3018.4	3336.29
8	3318.95	3190.93	3387.71
9	3304.29	3143.54	3341.66
10	3372.53	3165.53	3405.16
11	3310.69	3193.92	3312.96
12	3365.82	3203.63	3376.66

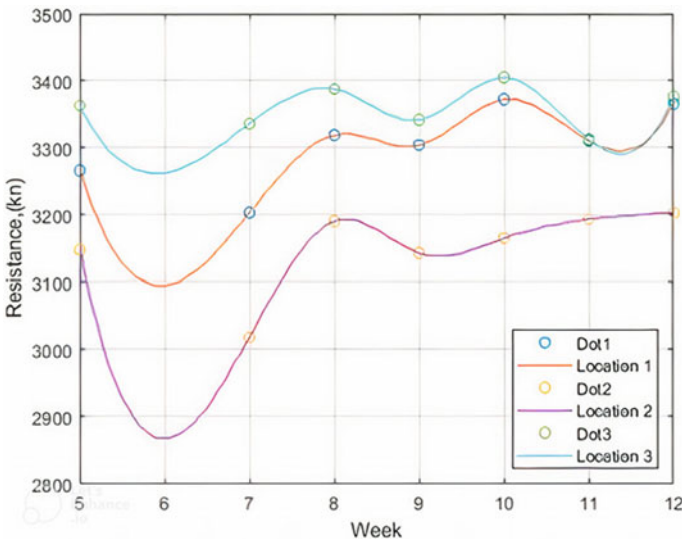


Fig. 8.10 Graph of total resistance

average resistance due to several reasons such as surface of the ship, seawater depth and reaction of organic substances.

8.5 Conclusion and Recommendation

In conclusion, both the objectives of this research are achieved which is to analyze the growth rate of the barnacle and to estimate the effect of the ship resistance caused by the barnacle fouling. Three different locations of barnacle image provide different values of growth rate and it shows that the barnacle grows for about 0.3021, 0.202

and 0.0356% per day. Hence, this barnacle growth brings impact to the increases of ship resistance for location 1 is about 21.49%, location 2 is 17.65% and location 3 is 22.78%.

Other than that from the result, the value of effective power is calculated and estimated so that the powering of the ship can be analyzed. The result indicated that the effective power significantly increases to 20,776.5 kW, 19,775.3 kW and 20,843.5 kW for each location respectively. There is an increase in percentage of the total resistance up to 20.56%. The ship structures that are covered by the barnacle will utilize more fuel and the fuel consumed by the delivery business is a huge supporter of worldwide carbon emission.

In the future, this result and scope can be widened which means not only calculated and estimated at the surface area of the barnacle but also consider the height of the barnacle. The data of these two different factors will be compared and the accuracy of the growth rate of the barnacle also the resistance of the ship can be further improved.

Acknowledgements We would like to express our special thanks of gratitude to Universiti Kuala Lumpur Malaysian Institute of Marine Engineering Technology (UniKL MIMET) which provides us the golden opportunity to do this wonderful research project and publication.

Nomenclature

C_v	Coefficient of viscous resistance
ρ	Water density
V	Velocity
S	Wetted surface area of the underwater hull
C_v	Coefficient of viscous resistance
C_F	Tangential (skin friction) component of viscous resistance
R_n	Reynolds number
L	Length of ship
V	Velocity
ν	Kinematic viscosity of water
C_{foul}	Coefficient of fouling
R_{foul}	Fouling resistance
ρ	Density of sea water
WSA	Wetted surface area
V	Velocity of the ship
R_{air}	Resistance of air
ρ	Density of air
C_A	Coefficient of air

References

- Alghamdi SA, Quijada CRA (2019) The impact of biofouling on marine environment: a qualitative review of the current antifouling technologies. Master's dissertation, Malmo, Sweden
- Birk L (2019) Fundamentals of ship hydrodynamics: fluid mechanics, ship resistance and propulsion. New Orleans, USA
- Bocchetti D, Lepore A, Palumbo B (2015) A statistical approach to ship fuel consumption monitoring. *J Ship Res* 59:162–171
- Bressy C, Lejars M (2014) Marine fouling: an overview. *JOT* 9:19–28. <https://doi.org/10.1080/08927014.2017.1364113>
- Demirel YK, Uzun D, Zhang Y, Fang HC, Day AH, Turan O (2017) Effect of barnacle fouling on ship resistance and powering. *Biofouling* 33(10):819–834. <https://doi.org/10.1080/08927014.2017.1364113>
- Deshler AA (2018) Biofouling impacts on the environment and ship energy efficiency. World Maritime University Dissertation, Malmo, Sweden
- Gerald B, Maurice M (2014) Digital signal and image processing using MATLAB. London, UK
- Larsson AI, Mattsson-Thorngren L, Granhag LM, Berglin M (2010) Fouling-release of barnacles from a boat hull with comparison to laboratory data of attachment strength. *J Exp Mar Biol Ecol* 392:107–114. <https://doi.org/10.1016/j.jembe.2010.05.015>
- Lau M (2018) Friction correction for model ship resistance and propulsion tests in ice. *Int J Nav Archit* 10:413–420. <https://doi.org/10.1016/j.ijnaoe.2018.01.002>
- Seok J, Park JC (2020) Comparative study of air resistance with and without a superstructure on a container ship using numerical simulation. *J Mar Sci Eng* 8:267. <https://doi.org/10.3390/jmse8040267>
- Song S, Demirel YK, Atlar M (2019) An investigation into the effect of biofouling on the ship hydrodynamic characteristics using CFD. *Ocean Eng* 175:122–137. <https://doi.org/10.1016/j.oceaneng.2019.01.001>
- Sulaiman MH, Mustafa Z, Saari MM (2018) Barnacles mating optimizer: a bio-inspired algorithm for solving optimization problems. *IEEE/ACIS*. <https://doi.org/10.1109/SNPD41920.2018>

Chapter 9

Finite Element Analysis on Enhancement of Contactless Power Transfer by Using Metamaterials—A Review



Mohd Zaifulrizal Zainol, Mohd Faizal Abdul Razak,
and Shaiful Bakri Ismail

9.1 Introduction

Wireless power transfer can be defined as the transmission of energy from one place to another without using wires. It started by Nikola Tesla in the late 1890s. Wireless technology has provided us the ability to have long-range communications that would not normally happen if wires were needed. The most common wireless power transfer technologies are electromagnetic induction and microwave power transfer (Rahman et al. 2014).

There are different types of the wireless power transfer systems. It can be categorized into the capacitive coupling and inductive coupling (Asheer et al. 2013). Capacitive coupling is usually used in the lower range of power transfer whereas inductive coupling is used in high power transmission. Inductive power is used widely compared to capacitive power because it has more advantages than capacitive. Inductive power transfer carries a lower risk of electric shock because there are no exposed conductors (Asheer et al. 2013).

In general, a wireless power system consists of a transmitter connected to a source of power such as a main power line, which converts the power to a time-varying electromagnetic field, and one or more receiver devices that receive the power and convert

M. Z. Zainol (✉) · M. F. Abdul Razak · S. B. Ismail
Universiti Kuala Lumpur Malaysia Institute of Marine Engineering Technology, Jalan Pantai
Remis, 32200 Lumut, Perak, Malaysia
e-mail: mzaifulrizal@unikl.edu.my

M. F. Abdul Razak
e-mail: mfaizalar@unikl.edu.my

S. B. Ismail
e-mail: shaifulbakri@unikl.edu.my

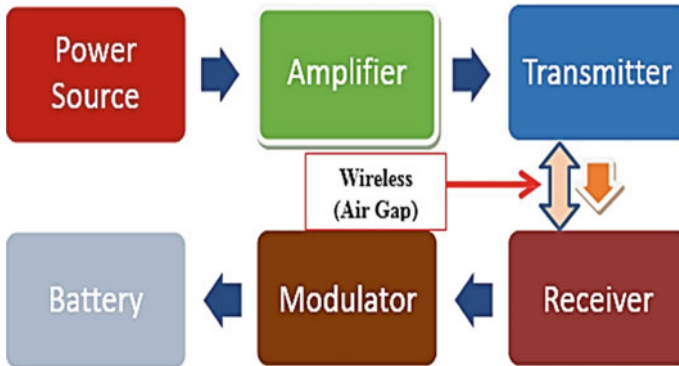


Fig. 9.1 The basic principle of contactless power transfer

it back to DC or AC electric current which is utilized by an electrical load (Shinohara 2014; Sun et al. 2013). Figure 9.1 shows the basic principle of contactless power transfer. This paper will review the finite element analysis method for contactless power transfer systems.

9.2 Finite Element Analysis

Finite element analysis (FEA) is a computer-based method of simulating or analyzing the behavior of engineering structures and components under a variety of conditions. It is the latest engineering tool that has been used to replace the old way which is by experimenting. FEA is widely accepted in almost all engineering disciplines. The process of analysis involves subdividing the complex structure or component into smaller more manageable (finite) elements. Figure 9.2 shows a simple explanation of how FEA works.

Like any other approximate numerical method, the solution produced by finite element analysis contains a certain amount of error. It is highly dependent on the parameter design in terms of size, type of use, and the similarity of the design with actual hardware. Validation of a FE model is carried out by comparison of the results with measured test data or by values obtained by other independent means such as hand calculations or other FEA programs (Nuttall 2011).

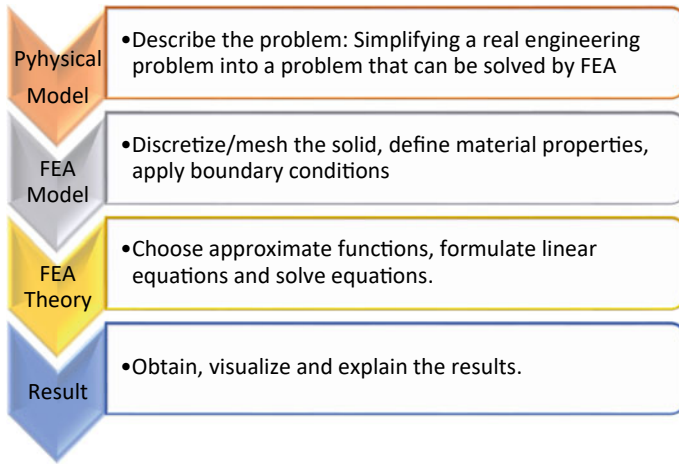


Fig. 9.2 How does FEA work (Bong 2004)

9.3 Finite Element Analysis of Enhancement Contactless Power System by Using Metamaterials

9.3.1 What is a Metamaterial

One of the earliest demonstrations of wireless energy transfer was the use of microwave radiation to power a small helicopter in 1964 (Brown 1984). Until now, there is still undergoing an evolution and many efforts have been made to improve this technology as well as its efficiency. There is much research on how to increase the efficiency of WPT.

One way to improve the efficiency of the WPT is by using metamaterials (Nishimura et al. 2014). In Nishimura et al. (2014), Yu (2014), Greegor et al. (2008), Wang et al. (2011, 2010), Chabalko et al. (2015), Wang and Teo (2012), there has been discussed the use of metamaterials in contactless power transfer. Due to their unique electromagnetic properties such as negative permeability, metamaterials can be used to enhance the evanescent waves of the near-field (Yu 2014). Metamaterials are engineered structures usually much smaller than the working wavelength whose electromagnetic properties are obtained from their structure rather than their chemical composition (Pendry et al. 2006).

Metamaterials are a new class of artificial material composed of man-made structures. Figure 9.3 shows how the setup of the circuit is done using metamaterials. The blocks of the metamaterial are much smaller in size than their working wavelength. Like other electromagnetic materials, the electromagnetic properties of metamaterials are described by macroscopic parameters such as permittivity ϵ and permeability μ (Yu 2014). When evanescent waves propagate in the air or other dielectric media, they can be enhanced (Greegor et al. 2008).

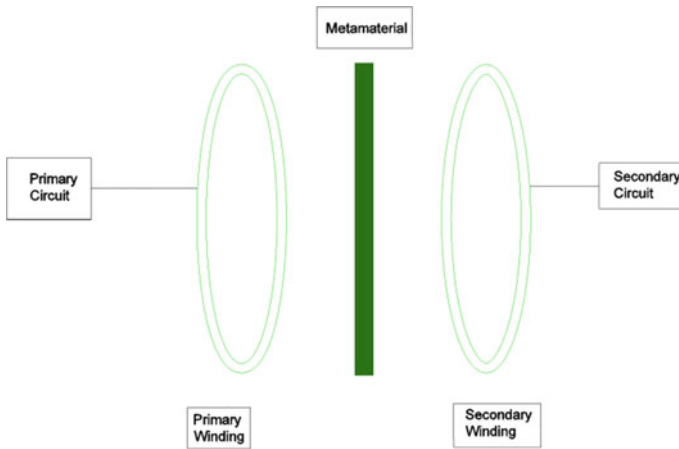


Fig. 9.3 Circuit setup using metamaterial

9.3.2 *Finite Element Analysis Setup and Result*

The metamaterial is placed between the two coils. Metamaterials are supposed to act as a magnetic super lens that concentrates the evanescent magnetic field around the slab enhancing the inductive. The result for secondary voltage with and without metamaterial in Nishimura et al. (2014) showed the difference.

Usually, the electromagnetic induction that was produced by the transmitter coil will spread randomly in the air medium. But using metamaterials can guide or focus the electromagnetic induction to increase the range of interactions between the receiver coil and electromagnetic induction produced by the transmitter coil. The result in Nishimura et al. (2014) shows that at the same transmitter and receiver gap, the efficiency of wireless transfer that uses metamaterials is higher compared to the efficiency of wireless transfer that does not use metamaterials.

It shows that the usage of the metamaterial in a system will improve the magnetic coupling strength. When using a metamaterial, the magnetic flux generated in the primary coil will focus on the secondary coil thus will increase the efficiency of the transfer. In Wang et al. (2011) the researchers have done a simulation on the effect of different distances of metamaterials from the windings. The simulation setup is shown in Fig. 9.4.

The position 'P' is shown as the distance between the transmitting coil and the metamaterial slab. The researchers changed the distance of 'P' in some different values. Figure 9.7 shows the simulation result of contactless power transfer with metamaterial with a different distance of 'P'.

There were five different distances of 'P' which are 5 cm, 10 cm, 15 cm, center between transmitter and receiver, and finally original which means no metamaterial was used. The result shows that the efficiency is highest when the metamaterial was placed at the center between the primary winding and secondary winding and the

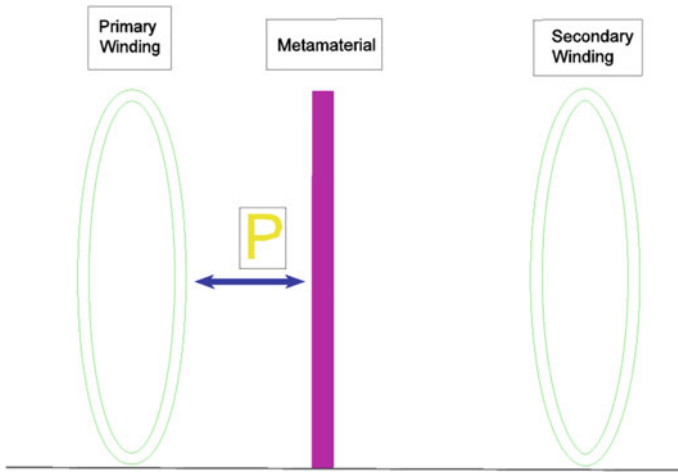


Fig. 9.4 Simulation setup for contactless power transfer with a different distance of metamaterial

second highest is when the distance of metamaterial is 15 cm. The lowest efficiency is when there is no use of metamaterial during the transfer process. This is because the field strength at metamaterial is lowest at the center, so power loss due to the metamaterial is lower compared to other positions, so more power is delivered (Wang et al. 2011). Thus, more magnetic flux was induced to the secondary winding or transmitter coil.

9.4 Finite Element Analysis of Contactless Power Transfer and Its Losses in Air Gaps

9.4.1 Effect on Mutual Inductance and Coupling Coefficient

Some different types of losses occur during the contactless power transfer process that has been discussed in Nguyen et al. (2014), Sibue et al. (2012), Tang and McDannold (2014). One of the main reasons for these losses to occur is because of an air gap that happens during the power transfer process. The air gap in wireless power transfer (WPT) cannot be avoided and will always happen in the WPT system. This is because in the basic concept of WPT, there is no contact between the power transmitter and power receiver during the transmission process. So, this air gap will influence the WPT system.

One of the effects that can be seen or measured is an inductance value or output power. The inductance value usually will influence the value of mutual inductance and coupling coefficient. Mutual inductance is the basic operating principle of the transformer, motors, generators, and any other electrical component that interacts

with another magnetic field. Mutual inductance can also be defined as a leakage inductance from a coil that can interfere with the operation of another adjacent component through electromagnetic induction. The mutual inductance (M) between the primary winding and secondary winding produce can be calculated by:

$$M = L_m(N_2/N_1) \quad (9.1)$$

or

$$M = (|L_{\text{ser}} - L_{\text{par}}|)/4 \quad (9.2)$$

where L_m is the magnetizing inductance, N_1/N_2 is the turn ratio between the primary and secondary winding, L_{ser} is the inductance in series and L_{par} is the inductance in parallel.

The value of mutual inductance produced depends on the positioning or gap between the two coils or windings. If the distance between two coils is small, so nearly all of the magnetic flux generated by the first coil will interact with the second coil turns inducing a relatively large electromagnetic force (emf) and therefore producing a large mutual inductance value. Otherwise, the amount of magnetic flux interacting between two coils will be weaker if the distance or gap between the coils is large. So it will produce a much smaller induced emf and therefore a much smaller mutual inductance value. The maximum efficiency of wireless power transfer depends on the value of mutual inductance (Nguyen et al. 2014).

Besides that, the coupling coefficient value also will influence the mutual inductance. The coupling coefficient can be derived as:

$$K = \frac{M}{L_1 L_2} \quad (9.3)$$

The coupling coefficient will be maximum when the entire flux in one coil links with the other. The maximum value of k is unity. Thus when $k = 1$, the coupled coils will be perfectly connected. The mutual inductance between the two coils will be maximum with $k = 1$. So the formula of mutual inductance with a maximum value of K will become:

$$M = \sqrt{(L_1 L_2)} \quad (9.4)$$

where L_1 is the self-inductance at primary circuit and L_2 is the self-inductance at secondary circuit.

When the distance or gap between the coils is larger, the value of k is very small. So the connection will be called a loosely coupled coil. In Zainol et al. (2016), the researchers have done the finite element analysis on a contactless battery charger. The simulation will be based on the magnetic field distributions of contactless battery chargers with different air gaps. Then the results were focused on the mutual inductance and coupling coefficient effect on the various air gap. Figures 9.5 and 9.6 show

the result of mutual inductance and coupling coefficient on the different air gaps by using the finite element analysis solution. The researchers were using the ANSOFT MAXWELL software as a method to get the result. The distance of air gap was tested at four different distances which were 1, 2, 3, and 4 cm. The parameter of the primary and secondary winding for experiment and simulation is the same to verify the data.

It is shown that as the gap becomes larger the mutual inductance and coupling coefficient of wireless power transfer will be small. This is because the existence of a large air gap between the primary coil and the secondary coil will weaker the mutual coupling inductance within the contactless power transfer.

Fig. 9.5 Mutual inductance with different distances (Zainol et al. 2016)

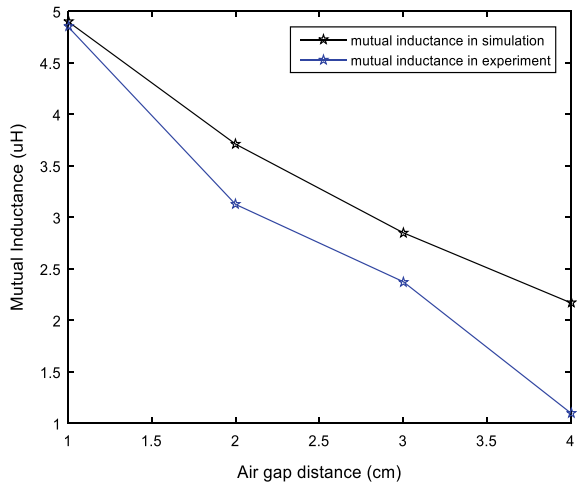
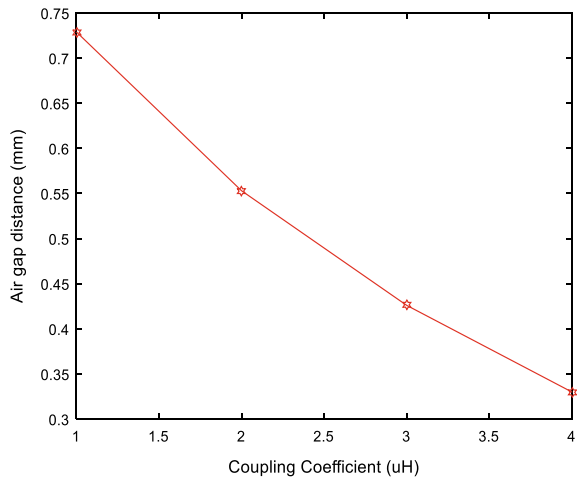


Fig. 9.6 Coupling coefficient with different distances (Zainol et al. 2016)



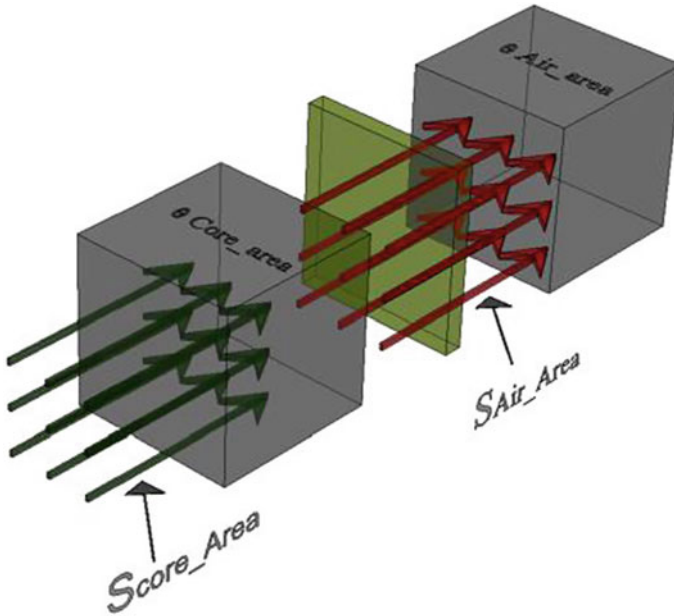


Fig. 9.7 Factor of flux ratio of magnetic core with air-gap

9.4.2 Effect on Magnetic Flux Distribution Ratio

In Jez and Polit (2014) the researchers have done a study about the effect of air gap on the magnetic flux distribution ratio by using the finite element analysis method. Due to the increasing distance of the air gap, the magnetic flux will spread out to the air medium and will cause an effect called the fringing effect. The fringing effect was discussed in Jez and Polit (2014), Nysveen and Hernes (1993), Fletcher et al. (2005). The best design of a contactless power system is when the fringing flux is at minimum and flux lines occupy the same cross-section in the air-gap area as in the magnetic core (Jez and Polit 2014). The situation is shown in Fig. 9.7.

Based on Fig. 9.10, the flux ratio formula can be derived as:

$$F_{FR} = \frac{\phi_{air_area}}{\phi_{core_area}} \tag{9.5}$$

where F_{FR} is the factor of magnetic fluxes ratio, Φ_{air_area} is the magnetic flux in an air-gap area with a cross-section like in a magnetic core and Φ_{core_area} is themagnetic flux in a core area with a cross-section of a magnetic core.

Then finite element analysis is done by researchers by using the COMSOL software to get the result of magnetic flux ratio with a different air gap. The simulation model is shown in Fig. 9.8.

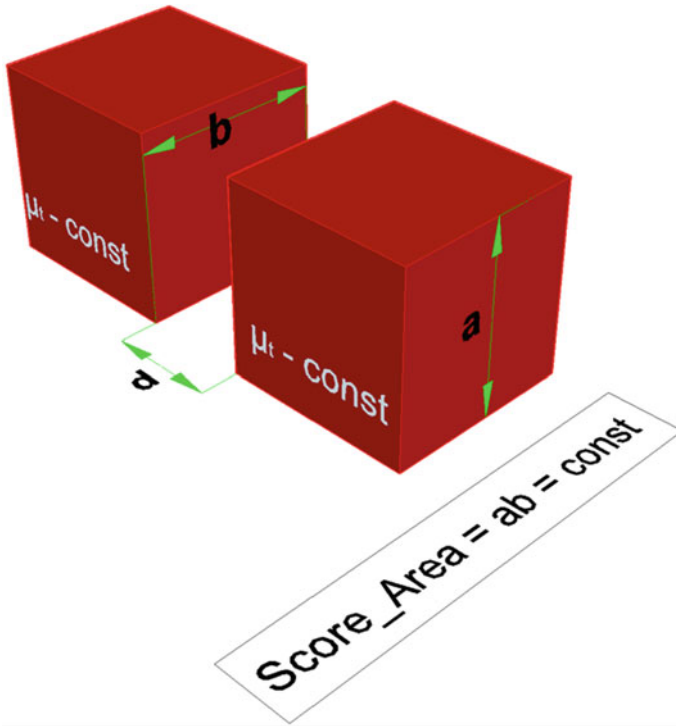


Fig. 9.8 Basic model of simulation analyses

Dimension ratio for ‘a’ and ‘b’ and the distance of air gap is changed. The gap distances (d) was tested on 1, 5, 10, 30, 70 and 90 mm. The result shows that factor of magnetic fluxes ratio is highest when the air gap is nearest which means at 1 mm. Its mean, the fringing effect is minimum when the air gap between the coils is close. But if the distance of gap is constant but only the dimension ratio for ‘a’ and ‘b’ is changed, the magnetic flux ratio is highest when the dimension ratio is nearer to one. Its mean, at dimension ratio 0.8, the factor of magnetic fluxes ratio (F_{FR}) was highest at each gap 1, 5, 10, 70 and 90 mm. That is because flux lines occupy the same cross-section in the air-gap area as in the magnetic core. As a result, the fringing effect will decrease the reluctance of the magnetic path and thus increases inductance of the winding so more magnetic flux will be transferred to the secondary winding.

9.5 Finite Element Analysis of Contactless Power with Different Types of Coils and Shapes

One of the most important things that need to be considered in designing a contactless power transfer system is the type of coil and the shape design of the coil. The effect of different types of coil and parameters of coil design on contactless power transfer systems has been discussed in Horigome et al. (2014), Ongayo and Hanif (2015), Kava et al. (2015), Sampath et al. (2014), Fincan and Üstün (2015). Rectangular coil and circular coil are the two most popular types that are usually used in a contactless power circuit system. The effect of using these two types of coils has been discussed in Ongayo and Hanif (2015) by using the finite element analysis method. Figure 9.9 shows the design of the coil that has been used in the simulation.

The efficiency between these two types of coils can be determined in many ways and one of them is by determining the value of mutual inductance and coupling coefficient for each coil under the same parameter experiment process. Figures 9.10 and 9.11 show the magnetic field density plot in circular coreless coil and rectangular coreless coil. The model design has been simulated using Ansys Maxwell from a 240 V, 20 kHz AC sinusoidal voltage (Ongayo and Hanif 2015).

The magnetic field density plot scale shows the range of the strength of the magnetic field density with the bottom blue representing the lowest value and the top red the highest value. That shows the induction is highest near the coil and becomes weaker when it moves further from the coil. The field density plot between the two coils has the same pattern. In order to determine which type of coil gives the better performance or efficiency, the researchers have done a simulation on both coils to get the value of inductance for each coil. Figure 9.12 shows the simulation result on the mutual inductance value for both coils.

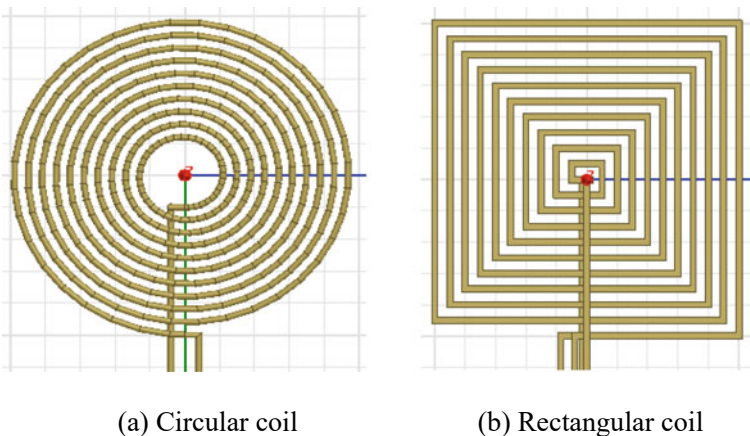


Fig. 9.9 Design of coil in ANSOFT MAXWELL simulation

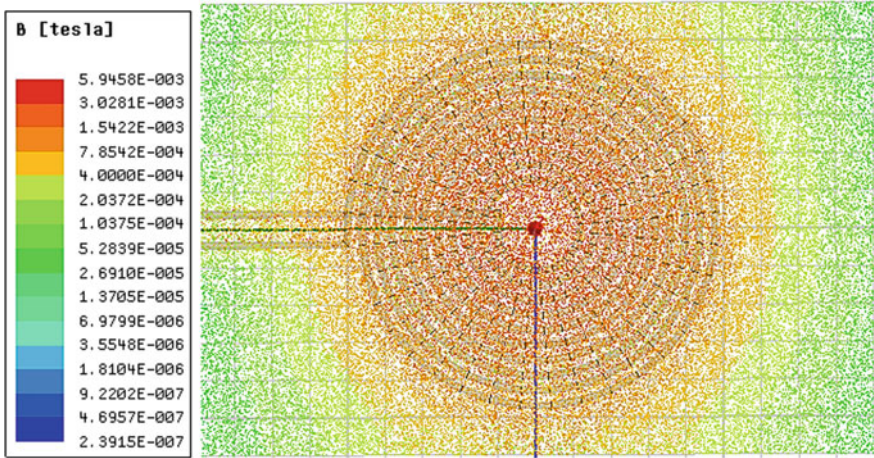


Fig. 9.10 Magnetic field density plot for circular coil

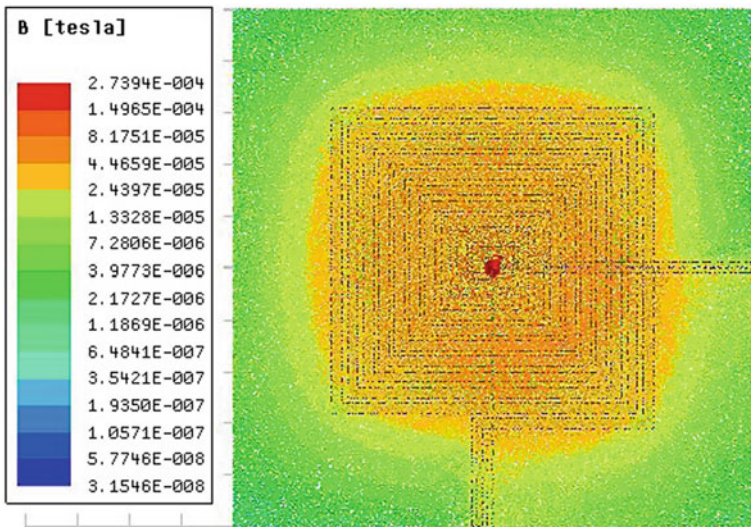
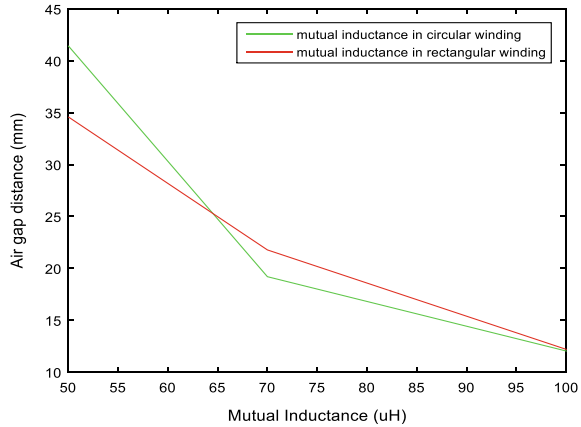


Fig. 9.11 Magnetic field density plot for rectangular coil

The result shows that mutual inductance in circular winding was higher than the mutual inductance in rectangular winding. This is because the rectangular coil geometry results in a longer conducting path as compared to circular coil (Ongayo and Hanif 2015). Therefore, the circular winding is more efficient to use in contactless power transfer systems compared to the rectangular winding because it can induce more power compared to rectangular winding.

Fig. 9.12 Value of mutual inductance for circular and rectangular coil for 50–100 mm air gap (Ongayo and Hanif 2015)



9.6 Latest Research Development

Currently, the enhancement of contactless power transfer using metamaterials have been developed widely. The displacement distributions on two typical plate-type structures have been introduced by Ma et al. (2017). The guidelines to design the optimal metamaterial with efficient power transfer, low cost, and high capability have been discussed in Dong et al. (2017). A metamaterial slab and the superconducting coil had been used in Sharma (2018) for electric vehicle charging to obtain a higher coupling coefficient of around 0.9. The challenges and opportunities for contactless power transfer using metamaterials have been explored in their properties (Bhattacharya et al. 2018) and design solutions (Lee et al. 2018). Two kinds of dual-band metamaterials were integrated to achieve negative and near zero permeability (Lu et al. 2020). A triplex layer with low metamaterial resulted in an efficiency enhancement of 26.8% (Liu et al. 2020). The metamaterial inclusion is investigated after using the evolutionary algorithm to optimize the design and geometry of the coil (Corrêa et al. 2019; Khafaga et al. 2022). The design is constructed with anisotropic Z magnetic metamaterials (Z-MM) to enhance the efficiency of contactless power transfer (Lu et al. 2021). In Adepoju et al. (2022) the finite element analysis of proposed metamaterials coupled with an equivalent circuit model is performed in ANSYS and validated in an experimental prototype.

9.7 Conclusion

In conclusion, this paper has reviewed the finite element analysis method for the enhancement of contactless power systems by using metamaterials. Then the paper evaluates the effect of air on the mutual inductance, coupling coefficient, and magnetic flux ratio. It is found that the effect of mutual inductance is very much

dependent upon the relative positions of the two coils. The position between the two coils also will create the air gap that will influence the magnetic field ratio. The simulation results have shown that a circular coil has relatively better coupling and gives better efficiency as compared to a rectangular one with more or less similar dimensions. All these situations have been verified by the finite element analysis method. The results of recent finite element analysis have proven the effectiveness of metamaterials for contactless power transfer enhancement. Hence, it can be concluded that metamaterials can be a potential material to enhance the contactless power transfer system.

References

- Adepoju W, Bhattacharya I, Sanyaolu M et al (2022) Equivalent circuit modeling and experimental analysis of low frequency metamaterial for efficient wireless power transfer. *IEEE Access* 10:87962–87973
- Asheer S, Al-Marwani A, Khattab T et al (2013) Contactless Power and data transfer for electric vehicle. *Int J Adv Res Electr* (2):3164–3173
- Bhattacharya A, Shaw T, Mitra D (2018) Performance enhancement of wireless power transfer system by controlling transmission and reflection properties of metamaterials. In: *IEEE MTT-S international microwave and RF conference (IMaRC)*, pp 1–4
- Bong D (2004) Finite element analysis. *VisionEngineer—finite element analysis*, p 27
- Brown WC (1984) The history of power transmission by radio waves. *IEEE Trans Microw* 32(9):1230–1242
- Chabalko MJ, Besnoff J, Ricketts DS (2015) Magnetic field enhancement in wireless power with metamaterials and magnetic resonant couplers. *IEEE Antennas Wirel Propag Lett* 15:452–455
- Corrêa DC, Resende UC, Bicalho FS (2019) Experiments with a compact wireless power transfer system using strongly coupled magnetic resonance and metamaterials. *IEEE Trans Mag* 55(8):1–4
- Dong Y, Li W, Yang X et al (2017) Design of unit cell for metamaterials applied in a wireless power transfer system. In: *IEEE PELS workshop on emerging technologies: wireless power transfer*, pp 143–147
- Fincan B, Üstün Ö (2015) A study on comparing analytical methods for coil design in high frequency wireless energy transfer. In: *IEEE PELS workshop on emerging technologies: wireless power*, pp 1–5
- Fletcher J, Williams B, Mahmoud M (2005) Airgap fringing flux reduction in inductors using open-circuit copper screens. *IEE Proc Electr Power Appl* 152(4):990–996
- Gregor RB, Parazzoli CG, Nielsen JA et al (2008) Demonstration of impedance matching using a mu-negative (MNG) metamaterial. *IEEE Antennas Wirel Propag Lett* 8:92–95
- Horigome K, Koshiji F, Koshiji K (2014) Comparison of wireless power transmission characteristics using circular-coil array and elliptical coil as a transmission coil. In: *International conference on electronics packaging (ICEP)*, pp 811–814
- Jez R, Polit A (2014) Influence of air-gap length and cross-section on magnetic circuit parameters. In: *Proceedings of the COMSOL conference*, pp 1–6
- Kava GM, Patil SL, Chaskar UM (2015) Efficiency improvement of two coil wireless power transfer system for biomedical implants. In: *International conference on industrial instrumentation and control (ICIC)*, pp 1317–1322

- Khafaga DS, Alhussan AA, El-Kenawy ESM (2022) Solving optimization problems of metamaterial and double T-shape antennas using advanced meta-heuristics algorithms. *IEEE Access* 10:74449–74471
- Lee IG, Kim N, Cho IK et al (2018) Shielding effect of mu-near-zero metamaterial slab to reduce magnetic flux leakage in wireless power transfer system. In: 2018 Asia-Pacific microwave conference (APMC), pp 690–692
- Liu J, Chen Z, Zhou J et al (2020) Compact triplex-layer metamaterials design for wireless power transfer efficiency enhancement. In: *IEEE 19th biennial conference on electromagnetic field computation (CEFC)*, pp 1–4
- Lu C, Huang X, Rong C et al (2020) A dual-band negative permeability and near-zero permeability metamaterials for wireless power transfer system. *IEEE Trans Ind Electron* 68(8):7072–7082
- Lu C, Huang X, Liu M (2021) Investigation of wireless power transfer with non-perfect planar metamaterial. *AEU Int J Electron* 132:153606
- Ma F, Huang M, Wu JH (2017) Acoustic metamaterials with synergetic coupling. *J Appl Phys* 122(21):215102
- Nguyen MQ, Woods P, Hughes Z et al (2014) A mutual inductance approach for optimization of wireless energy transmission. In: *Texas symposium on wireless and microwave circuits and systems*, pp 1–4
- Nishimura SI, de Almeida JV, Vollaire C et al (2014) Enhancing the inductive coupling and efficiency of wireless power transmission system by using metamaterials. *MOMAG* 121–125
- Nuttall JD (2011) Parallel implementation and application of the random finite element method. The University of Manchester, United Kingdom
- Nysveen A, Hernes M (1993) Minimum loss design of a 100 kHz inductor with foil windings. In: *Fifth European conference on power electronics and applications*, pp 106–111
- Ongayo D, Hanif M (2015) Comparison of circular and rectangular coil transformer parameters for wireless power transfer based on finite element analysis. In: *IEEE 13th Brazilian power electronics conference and 1st southern power electronics conference (COBEP/SPEC)*, pp 1–6
- Pendry JB, Schurig D, Smith DR (2006) Controlling electromagnetic fields. *Science* 312(5781):1780–1782
- Rahman SK, Ahmed O, Islam MS et al (2014) Design and construction of wireless power transfer system using magnetic resonant coupling. *Am J Electromagn Appl* 2(2):11–15
- Samath JPK, Alphons A, Vilathgamuwa DM (2014) Coil enhancements for high efficiency wireless power transfer applications. In: *40th annual conference of the IEEE industrial electronics society*, pp 2978–2983
- Sharma D (2018) Wireless power transfer via metamaterial and superconducting coil for electric vehicles. In: *International conference on smart city and emerging technology (ICSCET)*, pp 1–5
- Shinohara N (2014) *Wireless power transfer via radiowaves*. Wiley
- Sibue JR, Ferrieux JP, Meunier G et al (2012) Modeling of losses and current density distribution in conductors of a large air-gap transformer using homogenization and 3-D FEM. *IEEE Trans Magn* 48(2):763–766
- Sun T, Xie X, Wang Z (2013) *Wireless power transfer for medical microsystems*. Springer, New York, p 183
- Tang SC, McDannold NJ (2014) Power loss analysis and comparison of segmented and unsegmented energy coupling coils for wireless energy transfer. *IEEE Trans Emerg Sel* 3(1):215–225
- Wang B, Teo KH (2012) Metamaterials for wireless power transfer. In: *2012 IEEE international workshop on antenna technology (iWAT)*, pp 161–164
- Wang B, Nishino T, Teo KH (2010) Wireless power transmission efficiency enhancement with metamaterials. In: *2010 IEEE international conference on wireless information technology and systems*, pp 1–4
- Wang B, Teo KH, Nishino T, Yerazunis et al (2011) Wireless power transfer with metamaterials. In: *Proceedings of the 5th European conference on antennas and propagation (EUCAP)*, pp 3905–3908. IEEE

- Yu LJ (2014) Finite element analysis of a contactless power transformer with metamaterial. *TELKOMNIKA* 12(1):678–684
- Zainol MZ, Romlie MF, Jalil MRA et al (2016) Design and analysis of a contactless battery charger with planar PCB windings. In: 6th international conference on intelligent and advanced systems (ICIAS), pp 1–5

Chapter 10

Flexural Characteristic of Carbon Powder Bio-composite with Different Matrix Layer Sandwich Panels



Zulzamri Salleh and Muhammad Azmil Syafuan Mazlan

10.1 Introduction

In this modern era, a composite plays an important role to produce a good product with the best mechanical properties. In the engineering applications fields, it is widely used especially in civil construction, marine structure, and offshore use as their characteristics suit for this usage (Bari and Bajaj 2014). Sandwich panels are already applied in design and construction of lightweight transportation systems such as satellites, high speed trains, aircrafts and etc. Sandwich structures were applied in the aerospace industry in 1937 where balsa wood core and cedar plywood face sheets was used in the construction of De Havilland albatross airplane. The first theoretical analysis of the sandwich theory was published during World War II. Theoretical works on sandwich constructions were documented the late 1940s (Reis and Rizkalla 2008). The structure of a sandwich panel is a combination of different materials that are placed together to create the best mechanical properties for the benefit of the sandwich panel structure (Zaid et al. 2015). Further improvement and development can be carried out through the production and engineering process as it plays a dominant role with design, construction, structure and mechanical properties of the product. The faces and core are bonded together by adding an adhesive substance. It is to ensure that the product can achieve a load transfer between the components. It makes use of the properties of each separate component for the structural advantages of the whole assembly, resulting in a very high stiffness-to-weight ratio and a low

Z. Salleh (✉) · M. A. S. Mazlan
Universiti Kuala Lumpur, Malaysian Institute of Marine Engineering Technology, Lumut, Perak, Malaysia
e-mail: zulzamri@unikl.edu.my

M. A. S. Mazlan
e-mail: mazmil.mazlan@s.unikl.edu.my

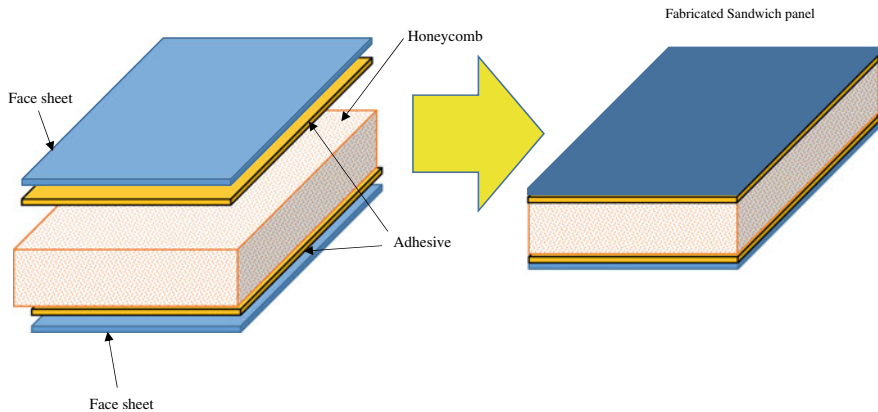


Fig. 10.1 Sandwich panel components

bending strength-to-weight ratio. Generally, aluminum plates, high-pressure laminates, and glass fiber reinforced plastics are used to create the face mask (Arbaoui et al. 2014). The skins are thin, rigid and very solid. Figure 10.1 shows the basic sandwich panels components.

Thus, a development of the sandwich panel itself has been discussed by doing a further research by using multiple layers of a carbon bio-composite made from mangrove carbon powder as their core. The face of the sandwich panel must have characteristics such as being stiff. By adding another materials which is activated carbon from softwood pine, it will improve its mechanical properties and performance so that it can be utilized in marine application.

In this study, carbon powder has been produced from mangrove tree barks. The numerous mangrove-generated products and services have both conventional and commercial uses. A mangrove tree's most direct product is its wood, which is either used as fuel or as building material. Certain sections of the tree are also harvested to manufacture corks and floats, colorants, soap substitutes, synthetic fibers and cosmetics, and even fruit, honey, vinegar, salt, or cooking oil meat. In addition, several species of mangroves have important medicinal properties (Zulkarnain et al. 1993). Activated carbon prepared from mangrove wood showed a fairly high iodine number value compared to the coconut shell value. This value, however, is determined primarily by heating time and temperature, as different temperature or time can result in different iodine number value. A certain temperature and time must be chosen to match the specifications for a particular application which requires a certain amount of iodine quantity from activated carbon prepared from mangrove wood, by heating at 500 °C of 3 h, a total value of iodine can be obtained.

This study highlights the improvement and the development of the material use for construction of sandwich panels. It will refer on knowledge and collected data to analyze the performance and the mechanical properties of the panel. For the model it will follow the American Society of Testing and Material (ASTM) and is

then analyzed using the finite elements method (FEM) to predict its properties. This study will focus on the mechanical behavior and progressive data using the PTC Creo software to analyze the best characteristic of the panel based on the experiment.

10.2 Methodology

In this study, flexural testing has been performed in order to confirm their mechanical testing performance. It is also known as three-point bending based on ASTM C393-00 standard (Scărlătescu et al. 2019). The simulation has been done by using finite element analysis (FEA) using a software for two different types of thickness core sandwich panels (ASTM 2016; Biggs 2000). The details for the specimen can be seen in Fig. 10.2. The dimensions for the specimen are: Face thickness ($t = 2$ mm), 3 types of core thickness = 8 mm, 9 mm, 10 mm, specimen length ($L = 90$ mm) and intermediate layer = 2 mm.

The materials used in this study has been mangrove carbon powder and this is compatible with the softwood pine data which is extracted from the CREO data base. The details for this data are shown in Table 10.1. To run the FEA simulation, one needs to do several processes which are suitable to identify any abnormalities before finalizing the actual parameters. The general process flow can be obtained from Fig. 10.3.

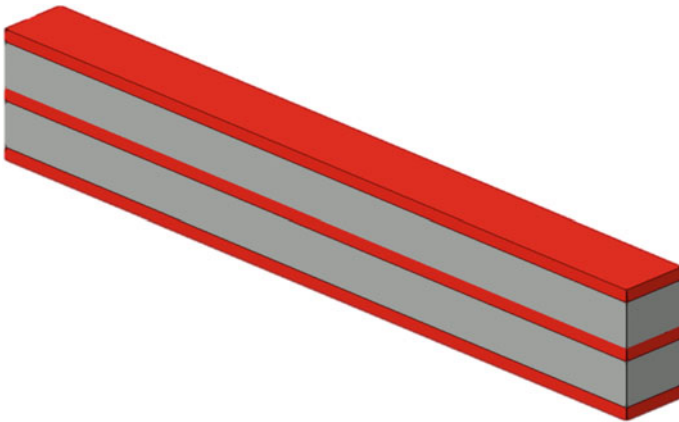
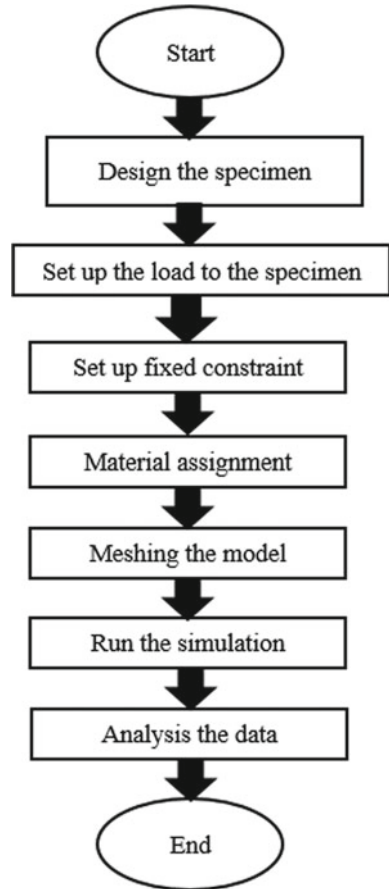


Fig. 10.2 Overview of specimen with a two-layer core

Table 10.1 Softwood pine materials properties data

Mechanical characteristic	Value
Tensile strength (MPa)	104
Bending strength (MPa)	87
Shear strength (MPa)	10
Impact strength (kJ/m ²)	70
Hardness (Brinell)	4
Modulus of elasticity (MPa)	12,000

Fig. 10.3 Process flow FEA simulation



10.3 Results and Discussion

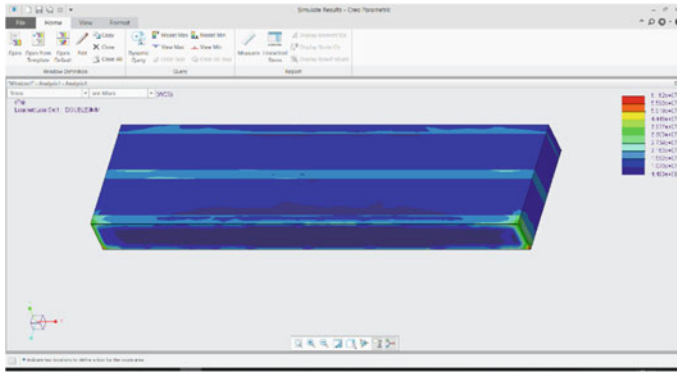
For the double layer with 8 mm core, the critical stress that the specimen can withstand has a value of the value 61.38 MPa, the maximum strain is 8.38×10^{-4} . From the graph, the specimen received the load of 10 kN at the top surface with constant constrain at the bottom surface. While for the sandwich structure with the double layer of the 9 mm carbon content, a higher stress compared to the 8 mm of carbon content was obtained as 61.62 MPa. For the strain, the sandwich structure with the 9 mm carbon content achieved 1.03×10^{-3} . The data for displacement is 3.43×10^{-5} mm when the specimen received the load and the deformation occurred. Based on the simulation data, the pattern shows the value of stress and strain increase when the carbon content increase. For the 10 mm double layer the maximum value of the stress is 64.04 MPa and strain value is 8.87×10^{-4} . This stress is the highest compared to 8 and 9 mm. The overview of the simulation for two layers' and triple layer's sandwich panels with skin thickness of 9 mm can see in Fig. 10.4. While Fig. 10.5 shows the details for auto meshing.

Based on the data gained from the simulation, both with highest carbon content (10 mm) recorded the highest stress and strain. For the double layer with the 10 mm carbon content, the maximum stress is 64.04 MPa while for the triple layer it is 66.22 MPa. For the strain, the triple layer with 10 mm carbon content also recorded the highest value which is 9.04×10^{-4} while for the double layer 8.87×10^{-4} . This data can be simply used for better understanding, the more layer and higher carbon content of the core, the highest maximum point of stress and strain can withstand before the specimen yield of fails. A comparison between two layers and three layers can be referred to Table 10.2.

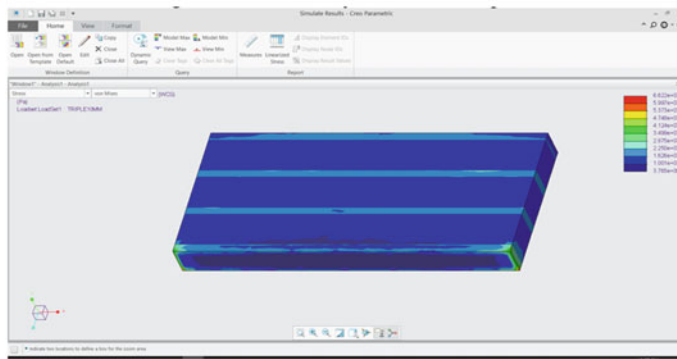
From Figs. 10.6, 10.7 and 10.8, there are differences of value of stress, strain, and displacement between all two types of the specimens respectively. The stress simulation results for all types of sandwich panels show that their mechanical stress values are increasing. When the content of the mangrove wood carbon powder layer's are increased or the sandwich layer's also increased, all the values of maximum stress, maximum strain and maximum displacement also increased as well. The result obtained also shows the behavior of isotropic materials such as softwood reveal a similar behavior when compressive testing has been performing (Salleh and Kee 2021).

10.4 Conclusion

In the experimental study, the sandwich structure with double layer (10 mm) was able to withstand about 64.04 MPa of stress while for the triple layer (10 mm) sandwich structure the limit of the stress is 66.22 MPa. For the displacement, the structure with triple layer (10 mm) recorded 5.29×10^{-5} mm the highest while for double layer (10 mm) 3.74×10^{-5} mm. However, it still experiences the limitation and



(a)



(b)

Fig. 10.4 a Two layers' sandwich panel b three layers' sandwich panel

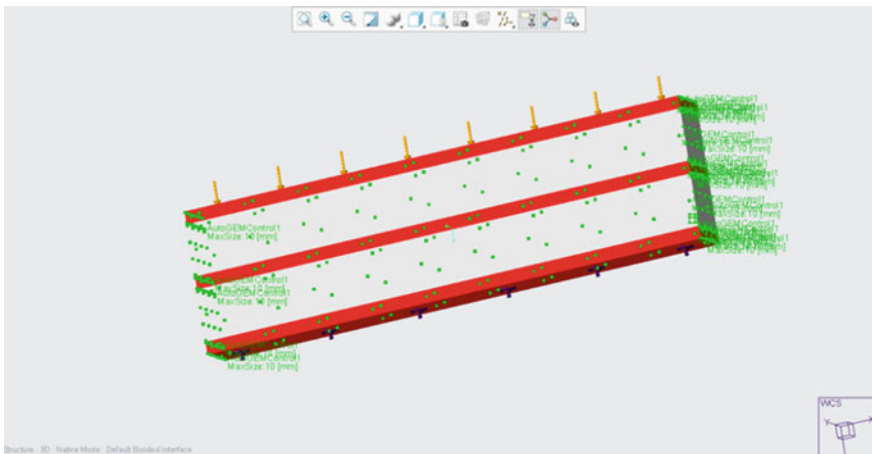


Fig. 10.5 Auto meshing result

Table 10.2 Comparison data between two layers and three layers

Maximum value	Double layer	Triple layer
Stress (MPa)	64.04	66.22
Strain	8.87×10^{-4}	9.04×10^{-4}
Displacement (mm/mm)	3.74×10^{-5}	5.29×10^{-5}

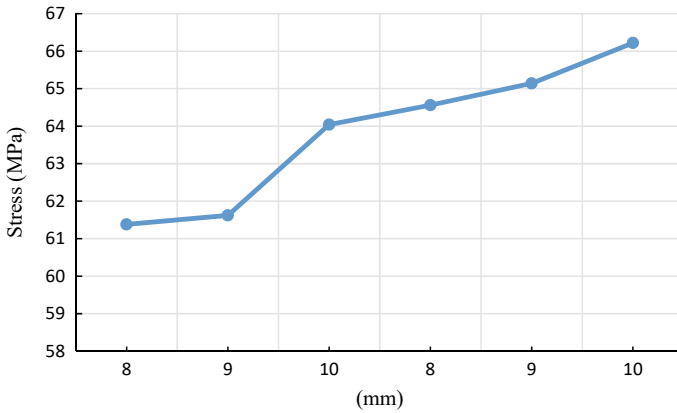


Fig. 10.6 Maximum stress value

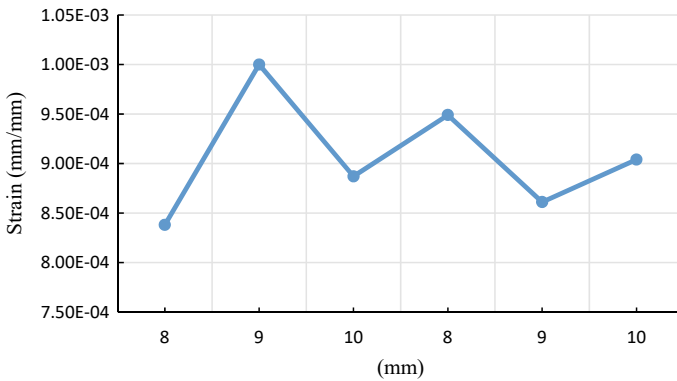


Fig. 10.7 Maximum strain value

deficiencies such as low of impact strength, low tensile strength, brittleness and low conductivity and others. The results show that the simulation for isotropic powder also has similar finding for the mechanical properties such as tensile and flexural testing (Salleh and Kee 2021).

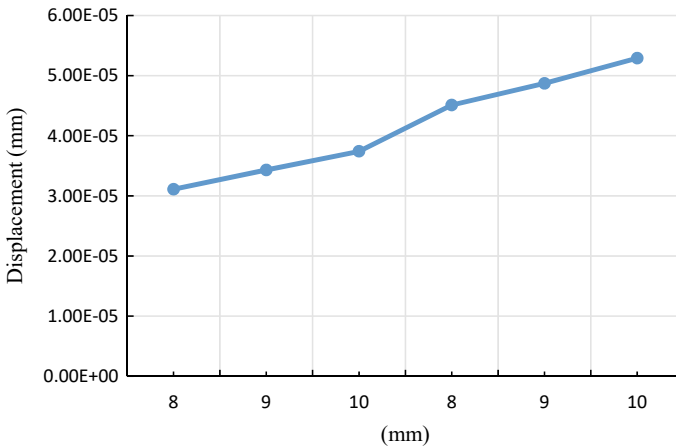


Fig. 10.8 Maximum displacement value

Acknowledgements The author would like to thank the Ministry of Higher Education (MoHE), Malaysia for providing a grant (FRGS/1/2021/TK0/UNIKL/02/20) to the first author in carrying out and completing this work.

References

- Arbaoui J, Schmitt Y, Pierrot JL, Royer FX (2014) Effect of core thickness and intermediate layers on mechanical properties of polypropylene honeycomb multi-layer sandwich structures. *Arch Metall Mater* 59(1):11–16
- ASTM C393/C393M–16/C393/C393M–16 (2016) Standard core shear properties of sandwich constructions by beam flexure. ASTM 1–8
- Bari DD, Bajaj PS (2014) Theoretical flexural behavior of sandwich panel using composite. *Mat Int J Res Eng Tech* 3(4):826–830
- Biggs RM (2000) Finite element modelling and analysis of reinforced-bridge decks
- Reis EM, Rizkalla SH (2008) Material characteristics of 3-D FRP sandwich panels. *Constr Build Mater* 22(6):1009–1018
- Salleh Z, Kee GW (2021) Simulation of three-point bending sandwich composite panels through finite element analysis. *Adv Struc Mat Des Mar Eng* 167:35–44
- Scărlătescu DD, Modrea A, Stanciu MD (2019) Three-point bend test to determine the mechanical behavior of the tubes used in water supply networks. *Proc Manuf* 32:179–186
- Zaid NZM, Rejab MRM, Mohamed NAN (2015) Sandwich structure based on corrugated-core. In: Abstract: the 3rd international conference on mechanical engineering research (ICMER 2015)
- Zulkarnain Z, Hussein MZ, Badri M (1993) Activated carbon from mangrove wood (*Rizophora apiculata*). *J Pre Char* 1(2):169–177

Chapter 11

Risk Assessment of Marine High-Speed Diesel Engine Failures Onboard Naval Vessels Using Failure Mode and Effect Analysis



Muhammad Syafiq Naquiuddin Mohd Zuki, Izuan Ishak,
Iwan Mustaffa Kamal, Muhammad Nasuha Mansor,
and Yaseen Adnan Ahmed

11.1 Introduction

High-speed diesel engines which run at high crankshaft speed, typically running between 1500 to 2500 rpm (Woodyard 2004; McGeorge 1995; Taylor 1998), are commonly used on board of naval and patrol vessels. In this case, in Malaysia these high-speed diesel engines are used especially in ‘Malaysian Marine Enforcement Agencies’ fleets such as the Royal Malaysian Navy (RMN) and Malaysian Maritime Enforcement Agency (MMEA) where the naval and patrol vessel are used for daily

M. S. N. M. Zuki

KL Petrogas Sdn. Bhd., B-3A-32 Block B, Merchant Square 1, Jalan Tropicana Selatan 1, PJU 3,
Tropicana, 47410 Petaling Jaya, Selangor, Malaysia
e-mail: syafiq@klpetrogas.com

I. Ishak · I. M. Kamal (✉) · M. N. Mansor

Universiti Kuala Lumpur, Malaysian Institute of Marine Engineering Technology, Lumut,
Malaysia
e-mail: iwanzamil@unikl.edu.my

I. Ishak

e-mail: izuan.ishak@unikl.edu.my

M. N. Mansor

e-mail: mnasuha@unikl.edu.my

Y. A. Ahmed

Maritime Safety Research Centre, Department of Naval Architecture, Ocean and Marine
Engineering, University of Strathclyde, Glasgow, UK
e-mail: yaseen.ahmed@strath.ac.uk

patrols and surveillances. These aging engines are facing potential breakdowns or in the worst case a total engine failure which at the end will jeopardize their patrol and duty in hand.

MTU engines are commonly used onboard of these RMN and MMEA vessels in maintaining law and order, coordinating search and rescue operations in the country's main sea transportation lines such as the Straits of Malacca, the Straits of Singapore, Malaysian Maritime Zones and on the high seas. But some of the vessels are more than 50 years old and are in an aging state. Most of the aging vessels are powered with MTU 12 V 538 TB81 engines. These MTU engines were popular in the 80s during these vessels design and building phases. MTU derives as *Motoren-und Turbinen-Union* which means "Motor (Engine) and Turbine Union". This company offered high performance and high-speed design with an upper output limit of 9100 kW which was created in 1969 when Daimler-Benz and MAN merged the development and production of relevant engines from MAN and Maybach Mercedes Benz (MTU 1985, 2002, 2009).

Considering these highly likely potential breakdowns, a risk assessment is necessary to prevent or minimize the chances of breakdowns in the future. This risk assessment is crucial to the crew's safety during operation of the ship and this could avoid a catastrophic failure happening to the engine. Risk assessments are used to determine the causes of damage and analysis were carried out to determine the primary failure mode of these high-speed diesel engines. One of the purposes of risk assessment is to know whether the engine is in good condition or not and to identify the potential engine problems that will cause the breakdown of the engine itself. Failure mode and effect analysis (FMEA) is a methodology designed to identify potential failure modes for the high-speed engine, to assess the risk associated with those failure modes, to rank the issues in terms of importance, and to carry out corrective actions to address the most serious failure modes (Patil et al. 2003; Hu-Chen et al. 2013). FMEA is an analysis method determining the causes of damage, where analysis is carried out to determine the primary failure mode. FMEA is also a risk assessment tool that reduces potential failures in systems, processes, designs or services and has been used in a wide range of industries (Hu-Chen et al. 2013). This FMEA was first developed as a formal design methodology in the 1960s by the aerospace industry (Kabir 2017), and has proven to be a useful and powerful tool in assessing potential failures and preventing them from occurring (Faturachman et al. 2013). Initially used by the U.S military after World War II as a process tool, FMEA gradually spread into industry (Saputra et al. 2019). It became widely known within the quality community as a total quality management tool in the 1980s and as a Six Sigma tool in the 1990s (Cicek et al. 2011). FMEA is a living document that should be reviewed and updated whenever the process is changed. To develop the FMEA, initially a survey was done on the functions of each component of the FMEA table which consists of three parts: the first part is the risk identification, the second part is the risk evaluation and the last part is the risk treatment.

In this FMEA, effect analysis was done thoroughly in studying the consequences of those failures. FMEA is widely used in the manufacturing industry in the whole life cycle of a product. The FMEA table consists of risk identification, risk effect,

risk category, risk treatment and risk evaluation. A risk assessment table was made in this research which consists of system by system of the engine such as the air starting system, fuel system, lubricating oil system, exhaust system and cooling system. The risk assessments using the FMEA method were applied to the MTU 12 V 538 TB81 engines which were still the main engines of some of the old vessels belonging to the RMN and MMEA. Once the analysis was done using the FMEA on the MTU 538 engines, the engine operation checklists were generated according to the risk and the remedy identified earlier in the FMEA tables. These operation checklists will help the engine watch keepers in doing their routine daily checks with regards to the engine daily operation. These enhanced daily routine inspections could prevent unexpected breakdown of these high-speed diesel engines.

In general, there are tons of engine failure cases that had occurred, and these incidents indirectly had affected the operation in seas. This research study focused on finding, identifying, and analyzing factors contributing towards the engine failure severity and occurrence especially in the MTU 538 engines. Engine failure of naval vessels is not desirable when the ship's crew operates the ship at high speed for manoeuvring or sailing in high seas. This failure could be dangerous to the ship's crew while the ship is in operation. Problem that causes failure to high-speed diesel engines could lead to a much more disastrous catastrophic failure. In other words, this catastrophic failure means that the engine cannot sustain the high load and start to destroy itself i.e., crankshaft breaks, crankcase explosions etc. Due to this catastrophic failure, it can contribute to a higher maintenance cost where the whole engine must be substituted with a new engine as a replacement. When ships are at high seas, engine failure could happen as well and this kind of failure will make the ship stranded at high seas. Engine failures while naval ships are at operation such as during war or during sailing on patrol could jeopardize the operation or patrol at sea. Engine failures are unexpected events that can lead to profit loss financially and in regards to properties. Fatality or serious injury can also occur toward crews on-board.

Therefore, considering the problems mentioned in the earlier paragraphs, this research was conducted to help identify the major determinants of engine potential failure occurrence. This research proposed a fault tree diagram according to the potential MTU 538 engine failures and to produce the FMEA tables based on the potential engine failure fault tree diagram. In the end, based on the FMEA tables, this research also generated the engine operation checklists for the MTU 538 engines. This study created risk assessment documents for the MTU engine failure as alternative references to the ship's crew to carry out maintenance and repair jobs. The scope of this study is limited on the MTU 538 series engine only.

The MTU series 538 engines were established as a high-speed diesel engine for ship's propulsion purposes. This engine came with 2640 kW per engine of power using the 4 stroke diesel cycle and single acting pistons. The combustion method of this engine is pre-chamber and having an exhaust gas turbocharging with the mode of supercharging. The type of cooling method is water cooling. The arrangement of the cylinders came with a 60° V-engine design configuration, with a total of 16 cylinders, with 8 cylinders in 'A' bank and the other 8 cylinders in 'B' bank.

This engine also came with specific firing order which is A1-B6-A6-B2-A2-B5-A5-B8-A8-B3-A3-B7-A7-B4-A4-B1. The engine bore and stroke are at 185 mm and 200 mm each, having 5.38 L cylinder displacement and the total displacement is at 86 L. The injection pressure of fuel is at 130.5 bar. The MTU 538 series engines have a combustion pressure final at firing speed of around 24 to 28 bar. The air intake temperature to start the combustion is around 32 °C and the water temperature at the charge air cooler is around 27 °C. The valve clearance is at 0 and the valve of this engine is adjusted automatically. The MTU engine of 16 V 538 TB 91 are used by the RMN in 'Handalan' class ships, which are 'Spica –M2' type with a capacity of three engines per ship. The 'Handalan' class is a heavier derivative of the Swedish Spica II (Norrköping) rapid attack boat that has been domestically modified. This class succeeded the Perkasa-class squadron, which was built by 'Kalskrona Varvet' and ordered in 1976. One of the 'Handalan' class ships is the 'KD Pendekar' that has three engines of MTU 16 V 538 TB 91 and is delivering 10,865 HP or 8102 kW with three shafts combined together.

11.2 Methodology

In this research, there are three major activities conducted, which are the (1) fault tree diagram analysis, (2) the FMEA analysis and (3) the generation of the operation checklists. In the first step, to accomplish the objectives set for this research the collected data was analyzed by using a fault tree diagram. A tree diagram is simply a way of representing a sequence of events. Tree diagrams are particularly useful in probability since they record all possible outcomes in a clear and uncomplicated manner (Taylor 1998). All these factors which are related were analyzed by referring to the MTU's 538 engine manual operation and maintenance book (MTU 2009, 2002, 1985, 2013, 2018, 2015, 2012). This was done to collect all the information needed to determine the root causes of the engine part components failures.

Then in the second step, after the development of the fault tree diagram for the MTU 538 engine, a detailed risk assessment analysis was done using FMEA tables. Failure mode and effect analysis is widely used in engineering to represent the risk value. The main objective of FMEA is to spot potential failure modes, evaluate the causes and effects of various component failure modes, and determine what could eliminate or reduce the chance of failure. The results of the analysis can help analysts to identify and correct the failure modes that have a critical effect on the system and improve its performance. In this research the focus is on the MTU 538 series engines that are currently used in 'Handalan' class ships of RMN. This is an important step to determine the potential causes for the damage and remedy action can be proposed to prevent its reoccurrence.

FMEA is a systematic evaluation process to identify where and how it might fail and to assess the relative impact of different failures, in order to identify the parts of the process that are most in need of change. "Failure modes" means the ways, or modes, in which something might fail. Failures are any errors or defects, especially

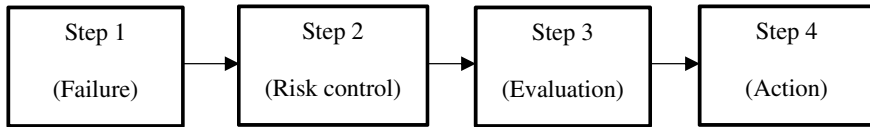


Fig. 11.1 Steps in the risk assessment using FMEA

ones that affect the crew or consumer, and can be potential or actual. “Effects analysis” refers to studying the consequences of those failures. Risk evaluation is important because through evaluation one can know the severity impact of the engine. A FMEA consists of four steps as shown in Fig. 11.1 where:

1. Step 1: Identification of failure (a list of all relevant engine failures with potential causes and risks)
2. Step 2: Risk control options (devising regulatory measures of current risk control)
3. Step 3: How bad and how likely? Assessment of risks (evaluation of risk factors);
4. Step 4: What actions should be taken? Recommendations for decision-making (information about the failure, their associated risks and the cost effectiveness of alternative risk control options is provided).

For example, in the FMEA risk assessments of the turbocharger failure of the MTU 538 engine, the first potential cause of a turbocharger failure is insufficient lubricant to the turbocharger itself. The effect of this insufficient lubricant is that the bearing of the turbocharger will overheat and the consequences of this turbocharger overheating is that the bearing will expand and jammed and finally it will explode. Once the cause, the effect and the consequences were determined, a risk treatment such as how to counter the problem and how to solve that issue is recommended in the FMEA table. In case of the insufficient lubrication to the turbocharger, the risk treatment recommended is that the lubrication oil of the turbocharger must be checked regularly so it will not contribute to the turbocharger failure.

In the third step, after the fault tree diagram and the risk assessment table using the FMEA method were produced, the engine operation checklists were produced based on the information in the FMEA table and the MTU 538 engine’s manual. In these checklists, the information on how specifically the engine component part can be inspected and how to examine the early sign of an engine part failure were determined. These engine checklists are the final step in this research with regards to the risk assessment of these MTU 538 high-speed diesel engine failure. These checklists are important because it will provide the ship’s crew an enhanced knowledge on how to carry out the daily inspection job before engine start-up, during engine running and engine stopping detailing any potential sign for engine failures.

11.3 Results and Discussion

In the first step as mentioned in the methodology, fault tree diagrams were constructed for the (1) cooling system (2) lubrication oil system (3) fuel system (4) turbocharger and exhaust system (5) air starting system and (6) governor system. Examples of the fault tree diagrams for the systems mentioned above are shown in Figs. 11.2, 11.3, 11.4, 11.5 and 11.6.

Example Tree Diagram of Potential Engine Failure (Turbocharger Failure)

The example of the fault tree diagram for the turbocharger failure is described here. In general, with reference to Fig. 11.4, the turbocharger failure can be caused by five potential causes which are the (1) lubrication related problem (2) inclusion of foreign object (3) extreme exhaust gas temperature (4) material/workmanship related problem (5) fresh water-cooling related problem.

In case no. (1), a lack of proper lubrication in a turbocharger can ruin a turbocharger within seconds of operation. All bearings must receive a supply of oil that can lubricate and cool as the shaft rotation speeds can easily approach very high rpm where typically it rotates from 10,000 to 12,000 rpm (MTU 1985). In this category, foreign material can also contribute to insufficient lubrication. Foreign material in the oil includes various sizes of abrasive particles and dilution by the coolant or fuel. Foreign material in the engine lubrication system will first damage the bearings. Sludge in the lubrication oil can block the tiny oil passage in the engine block, connecting rods and the piston cooling pipes. Therefore, this block oil passage can also contribute to insufficient lubrication. Extreme exhaust gas temperature can cause problems too. Even premium oil will decompose if the temperatures are forced high enough during operation or shutdown. When these extreme temperatures reach the center housing of the turbocharger, the deposits will form throughout its interior. As deposits accumulate, oil passages become restricted which reduces the oil flow through the unit. Lack

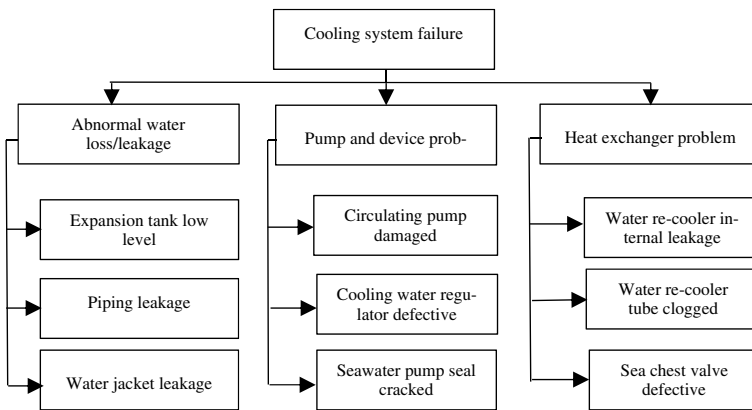


Fig. 11.2 Fault tree diagram for cooling system failure

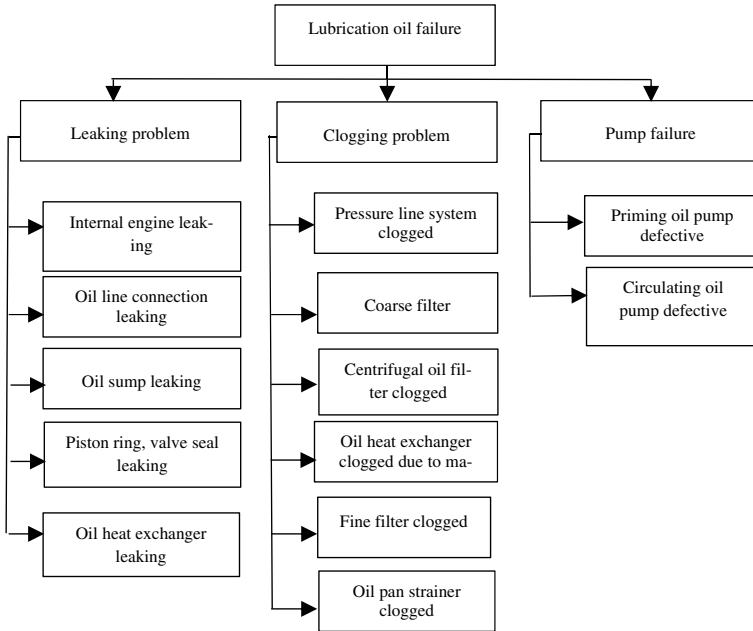


Fig. 11.3 Fault tree diagram for lubrication oil system failure

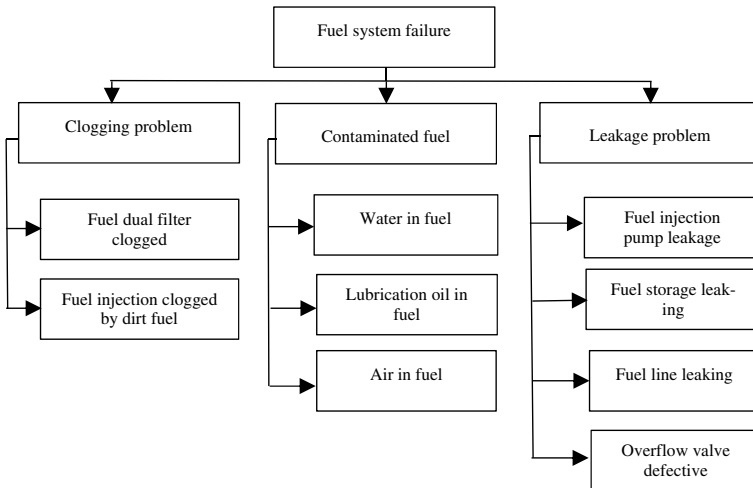


Fig. 11.4 Fault tree diagram for fuel system failure

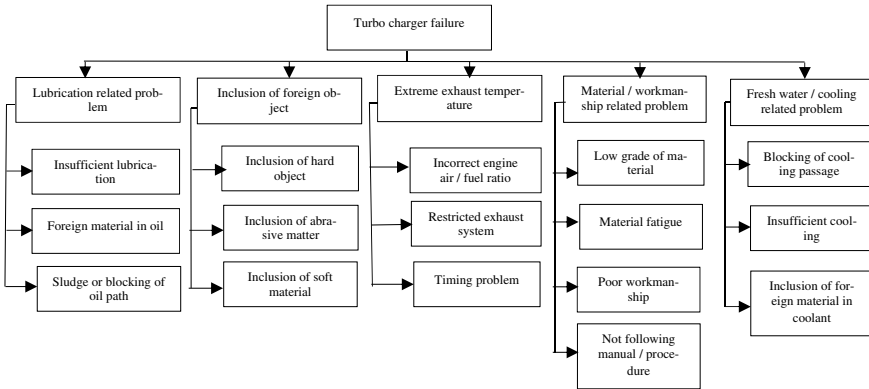


Fig. 11.5 Fault tree diagram for turbocharger system failure

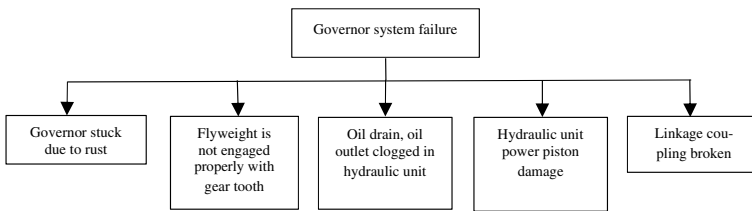


Fig. 11.6 Fault tree diagram for governor system failure

of proper cooling also brings similar symptoms as poor lubrication. These symptoms will cause the casing to discolorate first than the heat will move towards the compressor wheel which than later causes the bearing to seize-up. When a damaged turbo charger is replaced or needs to be dismantled, with a little or no thought given to the cause of the damage, therefore there is a high likelihood of recurrence of the failure resulting in extra downtime and expenses.

Example Risk Assessment Table of FMEA for Turbocharger Failure

In the second step as mentioned in the methodology, FMEA tables were constructed for the (1) cooling system (2) lubrication oil system (3) fuel system (4) turbocharger and exhaust system (5) air starting system and (6) governor system. In the FMEA table, there are three main columns which are the (1) risk identification (2) risk analysis and evaluation and (3) risk treatment. All the information from the fault tree diagrams were transferred to the first column: Risk Identification. In this risk identification, the risks and effects are identified. Then in the second column, i.e., risk analysis and evaluation, scores were given to all issues mentioned in the first column. Scores were given for the severity and the likelihood. The severity number is the impact of the failure which might be low, moderate, high and extreme. The likelihood is the probability number of potential the engine failure might occur. The

likelihood scores were also given in either low, moderate, high and extreme. As a guidance in giving scores to each of the issues, a severity index matrix was used as shown in Table 11.1. In the risk analysis and evaluation column, the risk index was calculated by multiplying the severity with the likelihood i.e., Risk Index = Severity × Likelihood. The risk level than can be identified using the severity index matrix as in Table 11.1. Finally, in the third column, i.e., risk treatment, a treatment category and the recommended action/additional control was proposed. A treatment can be proposed in order to reduce the risk level, either by (1) avoiding (2) transfer (3) reduce or (4) accept. As a guidance for the risk treatment, Table 11.2 which was taken from Faturachman et al. (2013) was used to propose the risk treatment in this research.

An example is shown for turbocharger failures in Table 11.3. With reference to the issue no. 1, insufficient lubrication to turbocharger, the risk and the effect were

Table 11.1 Risk severity matrix

Almost certain	5	Moderate	High	Extreme	Extreme	Extreme
Likely	4	Moderate	Moderate	High	Extreme	Extreme
Possible	3	Low	Moderate	Moderate	High	Extreme
Unlikely	2	Low	Low	Moderate	High	High
Rare	1	Low	Low	Low	Moderate	Moderate
		1	2	3	4	5
		Insignificant	Minor	Moderate	Major	Critical

Table 11.2 Risk treatment category and action to be proposed

Risk treatment		
Treatment category	Description	Action
Avoid	<ol style="list-style-type: none"> 1. This can be done by not taking or continuing activities 2. When a risk is both of high likelihood and high consequences, the organization will wish to avoid or eliminate the risk 	Eliminate the process flow
Transfer	<ol style="list-style-type: none"> 1. This involves another party to share in whole or in part through contracts, insurance, MoU 2. When the likelihood of a risk is low but the consequences is high, the organization will wish to transfer that risk 	Pass over risk to 3rd party
Reduce	<ol style="list-style-type: none"> 1. This can be done with training, testing, control, improve the management system 2. When the level of risk exposure (likelihood) is high but potential loss (impact) associated with it is low, the organization will wish to treat to reduce the risk 	Action required
Accept	<ol style="list-style-type: none"> 1. Where identified risks cannot be eliminated or avoided or no treatment process that can be done 2. When the risk considered to be within the risk appetite of the organization, the organization will accept the risk 	No need action plan

identified as bearing overheating and bearing jamming respectively. The current risk control was identified as periodically checking of lubrication oil using an oil sump dipstick. The scores for the severity and the like hood were given as 4 and 2, making the risk index to be at 8. With the risk index at 8, the risk level for this issue was identified as high using the severity index matrix. The treatment category was proposed to be 'reduce'. An additional control was proposed to reduce the risk level by checking the lubrication oil level periodically and give sufficient amount of lubrication oil.

Example Engine Checklist for Turbocharger

In the final step, the engine operation checklists were produced based on the information in the FMEA table. In these checklists, the information on how specifically the engine component part can be inspected and how to examine the early sign of an engine part failure were determined. An example for the checklist for the turbocharger is described here. In the turbocharger checklist as shown in Table 11.4, there are three main rows which are the (1) item to be check (2) remedy and (3) check box. In the first row, all the issues as in the fault tree diagram and the FMEA table were transferred here in the first row. For example, in the first row for 'Insufficient Lubrication', the remedy was transferred or taken from the proposed additional control in the FMEA table, where the remedy is 'Check lubrication oil level periodically and give sufficient amount of lube oil'. In the third row, a check box is provided for the ship's crew or the engine watch keeper to tick either 'pass' or 'fail'. Symptoms for insufficient lubrication were also provided in the checklist for the crew or watch keeper to look for during the engine operation. Here in this example symptoms for insufficient lubrication are mentioned such as (1) engine lacks power (2) black exhaust smoke (3) blue exhaust smoke and (4) turbocharger noisy.

11.4 Conclusion

A risk assessment using the FMEA method for MTU 538 engines used by the Malaysian Marine Enforcement Agencies such as the RMN and MMEA was proposed. This risk assessment was associated with an enhanced engine operation checklist for the usage of the ship's crew or the engine watch keeper. These operation checklists were generated so that it could be used for the engine crews for daily routine inspections. These enhanced daily routine inspections could prevent unexpected breakdown of these high-speed diesel engines. In this research, all engine system such as the fuel system, lubrication oil system, cooling system, air starting system and governor system have a separate risk assessment FMEA tables. From the FMEA tables, all the risks, effects, and the additional controls were transferred into the engine operation checklists. In addition, it is hoped that this operation checklist for every system could play a vital role in a better and a safer ship operation.

Table 11.3 Example FMEA risk assessment table of turbocharger

No	Risk identification			Risk analysis and evaluation					Risk treatment	
	Issue	Risk	Effect	Current risk control	Severity (impact)	Occ. (likelihood)	Risk index	Risk level	Treatment category	Recommended action/additional control
1	Insufficient lubrication to turbocharger	Bearing overheated	Bearing jammed and failure	Periodically checking of lubrication oil using oil sump dipstick	4	2	8	High	Reduce	Check lubrication oil level periodically and give sufficient amount of lube oil
2	Clogged air filter	Filter body damaged and compressor wheel fractured	Engine lacks power; black exhaust smoke, excessive engine oil consumption, blue exhaust smoke and oil leak from compressor seal	Replace air filter periodically	4	2	8	High	Reduce	Replace air filter periodically
3	Obstructed air intake to turbocharger	Compressor wheel damaged	Turbocharger failed to run	Check air intake before engine start and remove any obstruction	4	1	4	Moderate	Reduce	Check air intake before engine start and remove any obstruction

(continued)

Table 11.3 (continued)

No	Risk identification			Risk analysis and evaluation					Risk treatment	
	Issue	Risk	Effect	Current risk control	Severity (impact)	Occ. (likelihood)	Risk index	Risk level	Treatment category	Recommended action/ additional control
4	Obstructed air outlet duct from compressor to intake manifold	Intake hood overheated	Engine lacks power, black exhaust smoke, turbo noisy	Engine lacks power, black exhaust smoke, turbo noisy	4	2	8	High	Reduce	Remove any obstruction and check regularly before running turbocharger
5	Air leak in duct from air cleaner to compressor	Compressor wheel cracked	Turbo noisy	Replace seals periodically as needed	3	1	3	Low	Reduce	Replace seals or tightened fasteners

Table 11.4 Example of turbocharger checklist

Turbocharger checklist										
DATE :										
Item to be check	Insufficient lubrication to turbocharger	Clogged air filter	Obstructed air intake to turbo	Obstructed air outlet duct from compressor to intake manifold	Obstructed intake	Air leak in duct from air cleaner to compressor	Air leak in duct from compressor to intake manifold	Air leak at intake manifold to engine joint	Obstruction in exhaust manifold	
Remedy	Check lubrication oil level periodically and give sufficient amount of lube oil	Replace air filter	Remove obstruction	Remove obstruction	Remove obstruction	Replace seals or tightened fasteners	Replace seals or tightened fasteners	Replace seals or tightened fasteners	Remove obstruction	
Check box	Pass Fail <input type="checkbox"/> <input type="checkbox"/>	Pass Fail <input type="checkbox"/> <input type="checkbox"/>	Pass Fail <input type="checkbox"/> <input type="checkbox"/>	Pass Fail <input type="checkbox"/> <input type="checkbox"/>	Pass Fail <input type="checkbox"/> <input type="checkbox"/>	Pass Fail <input type="checkbox"/> <input type="checkbox"/>	Pass Fail <input type="checkbox"/> <input type="checkbox"/>	Pass Fail <input type="checkbox"/> <input type="checkbox"/>	Pass Fail <input type="checkbox"/> <input type="checkbox"/>	
SYMPTOMS	Engine lacks power	<input checked="" type="checkbox"/>	<input checked="" type="checkbox"/>	<input checked="" type="checkbox"/>	<input checked="" type="checkbox"/>	<input checked="" type="checkbox"/>	<input checked="" type="checkbox"/>	<input checked="" type="checkbox"/>	<input checked="" type="checkbox"/>	
	Black exhaust smoke	<input checked="" type="checkbox"/>	<input checked="" type="checkbox"/>	<input checked="" type="checkbox"/>	<input checked="" type="checkbox"/>	<input checked="" type="checkbox"/>	<input checked="" type="checkbox"/>	<input checked="" type="checkbox"/>	<input checked="" type="checkbox"/>	
	Excessive engine oil consumption	<input type="checkbox"/>	<input type="checkbox"/>	<input checked="" type="checkbox"/>	<input type="checkbox"/>	<input type="checkbox"/>	<input checked="" type="checkbox"/>	<input checked="" type="checkbox"/>	<input checked="" type="checkbox"/>	
	Blue exhaust smoke	<input checked="" type="checkbox"/>	<input checked="" type="checkbox"/>	<input checked="" type="checkbox"/>	<input type="checkbox"/>	<input type="checkbox"/>	<input checked="" type="checkbox"/>	<input checked="" type="checkbox"/>	<input checked="" type="checkbox"/>	
	Turbo noisy	<input checked="" type="checkbox"/>	<input checked="" type="checkbox"/>	<input checked="" type="checkbox"/>	<input checked="" type="checkbox"/>	<input checked="" type="checkbox"/>	<input checked="" type="checkbox"/>	<input checked="" type="checkbox"/>	<input checked="" type="checkbox"/>	
	Cyclic sound from turbo	<input type="checkbox"/>	<input type="checkbox"/>	<input checked="" type="checkbox"/>	<input type="checkbox"/>	<input type="checkbox"/>	<input type="checkbox"/>	<input type="checkbox"/>	<input type="checkbox"/>	
	Oil leak from compressor seal	<input type="checkbox"/>	<input checked="" type="checkbox"/>	<input checked="" type="checkbox"/>	<input type="checkbox"/>	<input type="checkbox"/>	<input type="checkbox"/>	<input type="checkbox"/>	<input checked="" type="checkbox"/>	

References

Cicek K, Turan HH, Topcu YI, Searslan MN (2011) Risk-based preventive maintenance planning using failure mode and effect analysis (FMEA) for marine engine systems. In: Second international conference on engineering system management and applications, pp 1–6

Faturachman D, Mustafa S, Octaviany F, Theresia DN (2013) Failure mode and effects analysis (FMEA) of diesel engine maritime transportation for ship navigation system improvement. In: International conference on business innovation, entrepreneurship and engineering

Hu-Chen L, Long L, Nan L (2013) Risk evaluation approaches in failure mode and effects analysis: a literature review. *Expert Syst Appl* 40(2):828–838

Kabir S (2017) An overview of fault tree analysis and its application in model based dependability analysis. *Expert Sys. Appl.* 77:114–135

McGeorge HD (1995) *Marine auxiliary machinery*, 7th edn. Butterworth-Heinemann, Oxford

MTU (1985) MTU 12V 538 TB81 manual maintenance plan book, description and services instruction. MTU, Friedrichshafen

MTU (2002) Technical publication diesel engine 8V 4000 G 12V 4000 G 16V 4000 G tolerances and wear limits list. MTU, Friedrichshafen

- MTU (2009) MTU value service technical documentation. MTU, Friedrichshafen
- MTU (2012) Maintenance schedule of 4000 series engine. MTU, Friedrichshafen
- MTU (2013) Operating instruction of 4000 series engine. MTU, Friedrichshafen
- MTU (2015) MTU-12V4000M53 spare parts catalog. MTU, Friedrichshafen
- MTU (2018) MTU diesel engine 12V 4000 Gx0/Gx1 16V 4000 Gx0/Gx1 maintenance manual. MTU, Friedrichshafen
- Patil R, Waghmode LY, Chikali PB, Mulla TS (2003) An overview of fault tree analysis (FTA) method for reliability analysis and life cycle cost management. *IOSR J Mech Civ Eng* 4–18
- Saputra RSH, Priharanto YE, Abrori MZL (2019) Failure mode and effect analysis (FMEA) applied for risk assessment of fuel oil system on diesel engine of fishing vessel. *J Eng Appl Sci* 13(20):14–20
- Taylor DA (1998) *Introduction to marine engineering*, 2nd edn. Elsevier Butterworth-Heinemann, Oxford
- Woodyard D (2004) *Pounder's marine diesel engines and gas turbines*, 8th edn. Elsevier Butterworth-Heinemann, Oxford

Chapter 12

Prediction of the Fibre-Reinforced Polymer Hull on the Wave Slamming Impact



Roslin Ramli, Mohd Hisbany Mohd Hashim, Anizahyati Alisibramulisi, Suhailah Mohamed Noor, and Noorlee Boonadir

Abbreviations

FD	Finite difference
FEA	Finite element analysis
FRP	Fibre reinforced polymer
FSI	Fluid-structure interaction
MEKP	Methyl ethanol ketone peroxide
MetMalaysia	Malaysian meteorological department
UTM	Universal testing machine

R. Ramli (✉) · N. Boonadir
Universiti Kuala Lumpur Malaysian Institute of Marine Engineering Technology, 32200 Lumut,
Perak, Malaysia
e-mail: roslin@unikl.edu.my

N. Boonadir
e-mail: noorlee@unikl.edu.my

M. H. Mohd Hashim · A. Alisibramulisi
Faculty of Civil Engineering, Universiti Teknologi MARA, 40450 Shah Alam, Selangor, Malaysia
e-mail: hisbany@uitm.edu.my

A. Alisibramulisi
e-mail: aniza659@uitm.edu.my

S. Mohamed Noor
Faculty of Civil Engineering, Universiti Teknologi MARA, 13500 Permatang Pauh, Pulau Pinang,
Malaysia
e-mail: suhailahmn@uitm.edu.my

12.1 Introduction

Ships, boats, and small crafts are the primary sea transportation modes in most parts of the world. It is a complicated vehicle meant to transfer people and cargo by water from one destination to another. The hull is the primary body of a ship or boat, which includes the bottom, sides, and deck. However, this research is focused on examining the prediction of the fibre-reinforced polymer (FRP) hull on the wave slamming impact.

The hull is available in various materials, including aluminium, steel, mild steel, wood, and FRP. Note that FRP was selected for the hull lamination in this study due to its corrosion resistance, non-magnetic characteristics, high tensile strength, lightweight, and simplicity of handling compared to aluminium, mild steel, and wood. A structural composite is a strong material that can replace conventional materials such as steel (Coppe et al. 2012).

Thus, the maximum strength FRP configuration was used in an actual boat model simulation with wave impact of slamming on fluid-structure interaction (FSI). The impact of a ship's bottom structure on the water surface is known as slamming. It causes exceptionally high loads on boat or ship structures and is considered during the design. Other than that, hydrodynamics and structural dynamics are involved in slamming occurrences. This event shows complex physics, which is still not well understood.

The complexity of FSI experiments and numerical simulations for ships is currently a key concern in studying full-scale slamming in real-world situations (Volpi et al. 2017). More resolved, higher fidelity simulations and FSI replications are required. However, the results of slam pressure on the bottom hull have shown the significant effects of composite material design on the structural response of slamming.

This research paper aims to predict the impact of bottom slamming on the FRP hull. The wave impact location was based on the Northern Straits of Malacca and the parent hull selected was the planning hull, which is the C945 model.

12.2 Methodology

The hull laminate method will be used in this research, which is a stacked sequence with a $+45^\circ$ layer orientation with different types of fibre mats (tissue mat, chopped strand mat, and woven roving). Thus, using the highest strength FRP composition in real boat model simulation with wave impact of the slamming on FSI was also studied. Slamming is the impact of the bottom structure of a ship onto the sea surface.

The simulation of the FSI was performed for this hydrodynamic diffraction. The fluid interacts with a solid object in the FSI and is a multiphysics combination of

fluid dynamics and structural mechanics. This phenomenon is characterised by interactions between a deformable or moving structure and an external or internal fluid flow, which could be stable or oscillatory.

This FSI is restricted to the slamming's wave effect. Hence, the FSI model is constructed using the 3D slamming technique to produce the wave-induced loads and response on the shell. The combination of a pulsating source distribution over the mean wetted surface of the hull is used in the shell finite element analysis (FEA) idealisation.

ANSYS Aqwa's simulation can effectively predict the interaction between fluids and solids based on pressure (Siyuan 2012; Lefrançois et al. 2014; Xu et al. 2019; Zullah and Lee 2016). Furthermore, it can assess the FSI's wave impact from slamming. Therefore, the methodology is divided into four components: the produced hull, wave components, and FSI simulation.

12.2.1 *Material*

Due to seawater ageing in marine applications, the mechanical characteristics of materials deteriorate in composites (Neşer 2017; Rajak et al. 2019). Note that the properties of the composite material deteriorate because of poor adhesion between the fibre and matrix in the composite structure caused by moisture absorption. These sandwich composite panels with glass or carbon fibre skins and a polymeric core have been used to build whole hulls and marine craft structures (Verma and Goh 2019). Correspondingly, a polymer matrix reinforces the fibres making FRP a composite material (Bai and Jin 2015).

ASTM D 3039 was followed in the processing of the specimen at $S + 45^\circ$. The woven roving 600 (WR600), chopped strand mat 450 (CSM450), and tissue mat (T) were utilised in the specimen $S + 45^\circ$ preparation. Other than that, the catalyst was methyl ethyl ketone peroxide (MEKP), and the polymer is an unsaturated polyester.

There is a kind of isotropic stacking sequence in the specimen $S + 45^\circ$ laminate, with each layer arranged in a stacking pattern. T/CSM450/WR600/CSM450/WR600/CSM450/T is the lamination sequence, and $[0/0/+45^\circ/0/+45^\circ/0/0]$ is the angle orientation, as shown in Table 12.1. The specimen $S + 45^\circ$ complies with earlier studies (Ramli and Mohd Hashim 2017).

12.2.2 *Created Hull*

To construct a hull, the parent hull must include precise information about its size, capabilities, stability, and performance. The planning vessel's parent hull is a C954 type. It was created using the C954 model, which is depicted in Fig. 12.1. An extensive experimentation programme in a towing tank, with or without interceptors, demonstrated that the C954 model had a good performance (Luca and Pensa 2017).

Table 12.1 S + 45° stacking sequence and angle orientation (Ramli et al. 2022)

Stacking sequence	Angle orientation
T	0°
CSM450	0°
WR600	+45°
CSM450	0°
WR600	+45°
CSM450	0°
T	0°

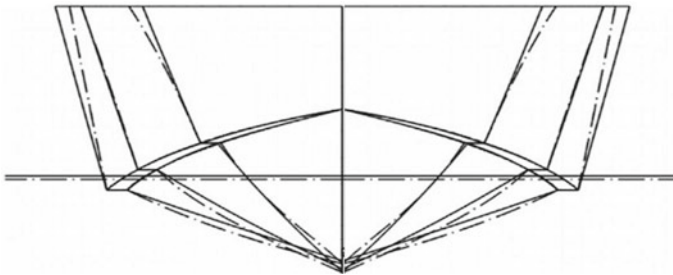


Fig. 12.1 Parent hull C954

Moreover, the planning hull with the chine hull shape was the reason for the good performance during the manoeuvre, as the chine functions as an oscillating dynamic roll.

Table 12.2 shows that the hull parameters had been changed by 4.3 m. On the other hand, the fibre-reinforced polymer (FRP) material was S + 45°. Tensile test results for S + 45° show that the manual and automatic Universal Testing Machines (UTM) have the highest tensile strengths of 151.78 MPa and 137.48 MPa, respectively (Ramli and Mohd Hashim 2017), whereas the American Bureau of Shipping rules section 4 (4.4.2) states that the minimum tensile strength values for the specimen S + 45° are 18,000 psi or 124 MPa. This research uses the FRP laminate method of S + 45°. The material property values are applied to the hull based on the results of the S + 45° test.

The Maxsurf software creates the hull. There are several processes involved in obtaining the required shape: adding up the surface, keying in the size surface, merging in the surface, and smoothening the hull utilising the control point positions for each of the columns. The hull dimensions of the real boat were 4.3 m × 1.4 m × 0.95 m with 8 mm thickness, as shown in Fig. 12.2.

Table 12.2 Parameters of the hull

Parameters	Model 1
Length	4.3 m
Beam	1.4 m
Draft	0.475 m
Depth	0.95 m
Thickness	0.008 m
Longitudinal centre of buoyancy (LCB)	1.539 m
Longitudinal centre of gravity (LCG)	2.15 m
Speed	2.779 knots
Material FRP	S + 45°

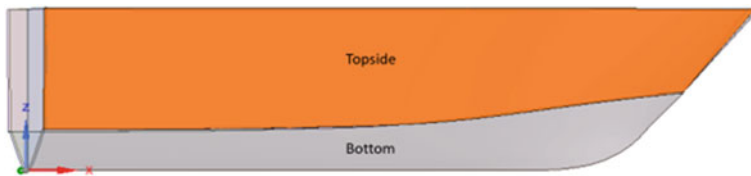


Fig. 12.2 The planing hull in ANSYS Aqwa

12.2.3 Wave Components

The FSI requires wave components and the boat’s position through which it will navigate. Figure 12.3 shows the instances of wave components required in the FSI. Note that the components consist of a significant wave, maximum wave, amplitude wavelength, and wind speed.

Apart from that, the details of the wave component were collected for two months from 4th Oct until the 4th Dec 2020. These were part of quarter 4 of the year, in which the data wave height and wave component were usually collected by the Malaysian Meteorological Department (MetMalaysia) (Yaakob and Zainudin 2010).

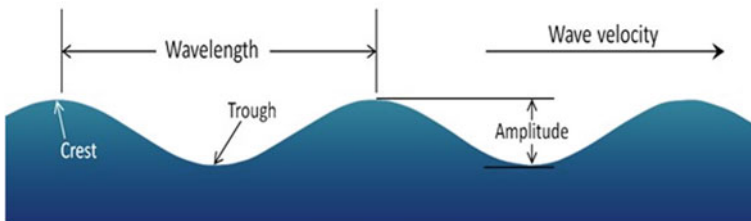


Fig. 12.3 The parameters of water wave (Earle 2019)

Table 12.3 Data of wave components

Deepwater significant wave (Hs) characteristic 60 days	
Location	Northern straits of Malacca
Depth description	Shallow water
Significant wave height (m)	1.0
Shallow water starting depth (m)	3
Wave amplitude (m)	0.5
Wave frequency (Hz)	10
Wavelength (m)	0.94
Maximum wave height (m)	3.5
Minimum wind speed (m/s)	10
Maximum wind speed (m/s)	50
Transition zone starting depth (m)	28
Velocity (m/s)	9.4

The data of significant wave height, maximum wave height, and wind speed on the website MetMalaysia were generated every seven days. The final data of wave components of the Northern Straits of Malacca are shown in Table 12.3.

12.2.4 Hydrodynamic Diffraction—FSI

In the FSI simulation, the ANSYS Aqwa software sets up coordinates in the XY plane, imports the external geometry hull (Rhino.3dm files), and generates the hull. The hull appeared as shown in Fig. 12.4. First, the hull must be divided into the surface and the bottom, with the bottom immersed in the water level. Subsequently, the step to immerse the bottom hull was to add a new XY plane, types from coordinates, and the FD13 point 2 of -500 mm (Z-axis). After that, the file is saved and edited to form the model in the hydrodynamic diffraction analysis.

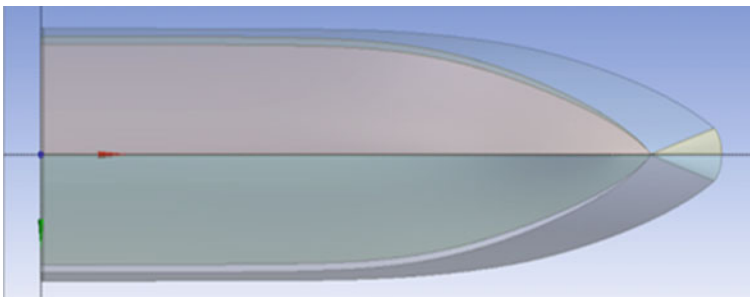
**Fig. 12.4** Setup the coordinate of the hull



Fig. 12.5 The completed mesh of the hull

The mesh element of 4 mm is added with the growth rate of 1.05, while the mesh metric is skewness. Furthermore, the mesh is solved with 26,946 nodes and 3402 elements under programme control from the ANSYS software. Figure 12.5 shows the complete meshed hull.

The analytic parameters, structure selection, wave direction, and wave frequency are all configured. The analysis mode is set to program-controlled, and the hull is selected as a structure. Other than that, the wave direction type was a range of directions with a forward speed of 1.542 m/s and a wave range of -180° to 180° .

The details of wave frequencies are 10 for target encounter frequencies, while 24 is the actual encounter frequencies. Apart from that, it displayed all wave directions and frequencies. The lowest and highest frequency definitions are controlled by the program. In the solution, the hydrodynamic, pressure, and motion are inserted.

12.3 Results and Discussion

The hydrodynamic diffraction analysis of fluid-structure interaction (FSI) is based on a $4.3 \text{ m} \times 1.4 \text{ m} \times 0.91 \text{ m}$ hull with a thickness of 8 mm. The implementation of simulation to the real model to address real impacts found that the maximum hydrodynamic pressure of 14,689.90 MPa occurred at the middle of the hull on the first laminate layer. Figure 12.6 shows the impact of pressure on the hull surface. The impact is more on the bottom of the hull on the starboard side.

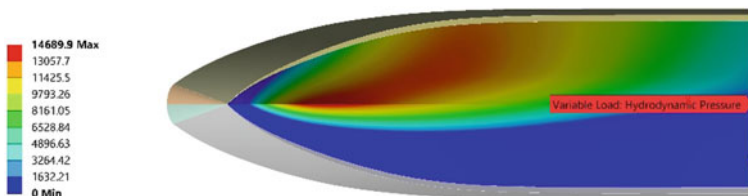


Fig. 12.6 Hydrodynamic pressure (MPa) distribution on the bottom of the hull

The second impact of wave slamming was 13,057.70 MPa, which also occurred on the starboard side. Hence, the impact of the hydrodynamic pressure was more on the starboard side, where the minimum amount was 163.21 MPa. The yellow area is the biggest impact on the starboard side of the hull after and forward, with the impact of the hydrodynamic pressure being 9793.56 MPa.

On the other hand, the port side of the hull has an impact on the middle line of the hull, which is 13057.70 MPa. This is followed by 9793.26 MPa (yellow), 8161.05 MPa (light green), 6528.63 MPa (green), 48,996.63 MPa (cyan), 3264.42 MPa (light blue), 163.21 MPa (dusty blue), and the biggest areas was 0 MPa (dark blue). The dark blue area was 90% on the port side. Moreover, the remaining 10% was combined with the various hydrodynamic pressure. These results are the same for the bottom side of the hull, as shown in Fig. 12.6.

12.4 Conclusion

Based on the real boat model, the hydrodynamic diffraction analysis of fluid-structure interaction (FSI) of the model size of $4.3 \text{ m} \times 1.4 \text{ m} \times 0.95 \text{ m}$ and the 8 mm thickness and a material selection of $S + 45^\circ$ were selected. The real boat hull model is designed according to the parent hull C945 model. Moreover, the wave impact components collected from the Malaysian Meteorological Department (MetMalaysia) website were located in the Northern strait of Malacca. Note that sixty days of data had been collected for accurate results.

The results indicate that subject to moderate slamming loads, the strains of composite bottom panels essentially scale with their static stiffness. However, the most severe slamming events deviated from the static stiffness relationship. Estimates of water impact velocity suggest that impact speeds for these slamming events approach a critical value at which hydrodynamic and inertial effects become significant.

Slamming loads were modelled as a high-intensity peak followed by a lower-intensity hydrostatic pressure moving across the panel at a constant speed. Other than that, hydroelastic effects were ignored or included only as a constantly added mass term. The structural response during the initial loading and later vibration phases was investigated for a constant load of 30 MPa.

Consequently, the FSI occurs when a fluid interacts with a solid structure, exerting pressure that may cause deformation in the structure and, thus, alter the flow of the fluid itself. The maximum impact was 14,689.90 MPa on the starboard side in the slamming wave. Meanwhile, the minimum impact was 163.21 MPa on the port side in the slamming wave.

Acknowledgements The authors would like to express their gratitude and special thanks to the UniKL-Malaysian Institute of Marine Engineering Technology (UniKL-MIMET) for funding this research paper under the Research and Innovation section (R&I) and to her main supervisor and

co-supervisor at UiTM. Lastly, regards and blessings are offered to all those who supported the completion of the paper in any respect.

References

- Bai Y, Jin W (2015) Marine structures, 2nd edn. <https://doi.org/10.1016/C2013-0-13664-1>
- Coppe A, Pais MJ, Haftka RT, Kim NH (2012) Using a simple crack growth model in predicting remaining useful life. *J Aircr* 49(6):1965–1973. <https://doi.org/10.2514/1.c031808>
- De Luca F, Pensa C (2017) The Naples warped hard chine hulls systematic series. *Ocean Eng* 139:205–236. <https://doi.org/10.1016/j.oceaneng.2017.04.038>
- Earle S (2019) Physical geology. SWJ; SEMANT WEB. Pressbooks, Montreal
- Lefrançois A, Léger P, Bouaanani N (2014) Finite element seismic safety assessment of water intake structures. *Finite Elem Anal Des*. <https://doi.org/10.1016/j.finel.2013.12.007>
- Neşer G (2017) Polymer based composites in marine use: history and future trends. *Procedia Eng* 194. <https://doi.org/10.1016/j.proeng.2017.08.111>
- Rajak DK, Pagar DD, Menezes PL, Linul E (2019) Fiber-reinforced polymer composites: manufacturing, properties, and applications. *Polymers*. <https://doi.org/10.3390/polym11101667>
- Ramli R, Mohd Hashim MH (2017) Analysis of tensile strength of different combination of FRP material under seawater conditioning. *J Eng Appl Sci*. <https://doi.org/10.3923/jeasci.2017.4320.4324>
- Ramli R, Mohd Hashim MH, Alisibramulisi A, Mohamed Noor S, Abdul Razak MF (2022) Tensile strength testing of +45° isotropic FRP laminate on different universal testing machines. *Adv Struct Mater*. https://doi.org/10.1007/978-3-030-89988-2_6
- Siyuan M (2012). Studies of composite multihull ship structures using fluid. FAU, Florida
- Verma D, Goh KL (2019) Natural fiber-reinforced polymer composites. In: Biomass, biopolymer-based materials, and bioenergy. <https://doi.org/10.1016/b978-0-08-102426-3.00003-5>
- Volpi S, Diez M, Sadat-Hosseini H, Kim DH, Stern F, Thodal RS, Grenestedt JL (2017) Composite bottom panel slamming of a fast planing hull via tightly coupled fluid-structure interaction simulations and sea trials. *Ocean Eng*. <https://doi.org/10.1016/j.oceaneng.2017.07.053>
- Xu H, Neng P, Yang F (2019) Motion response analysis of mining vessel based on ANSYS/AQWA. *J Phys Conf Ser* 1300(1). <https://doi.org/10.1088/1742-6596/1300/1/012010>
- Yaakob O, Zainudin N (2010) Presentation and validation of remote sensing ocean wave data. *IJRRAS* 373–379
- Zullah MA, Lee Y-H (2016) Fluid-structure interaction simulation of a floating wave energy convertor with water-turbine driven power generation. *J Korean Soc Mar Environ* 40(8):710–720. <https://doi.org/10.5916/jkosme.2016.40.8.710>

Chapter 13

The Effect of Welding Parameters of Flux Core Arc Welding by Utilizing Robotic Welding



Intan Ramli, Mohd Faizal Abdul Razak, Mohd Zaifulrizal Zainol, and Shaiful Bakri Ismail

13.1 Introduction

Welding is a sculptural or manufacturing process that joins materials. Bonding is a process that occurs at the initial border surface of two pieces of materials, such as metals or thermoplastics. Using high heat, the components can melt together and cool, allowing for fusion (Jun et al. 2014). The welding technique is separated into two broad categories: plastic welding (also known as pressure welding) and fusion welding (also known as non-pressure welding). Fusion welding is a popular welding procedure that includes gas welding, electric arc welding, TIG, MIG, and other welding processes (Rogfel et al. 2021). Pressure welding is another basic type of welding in which the ends of the materials to be joined are brought to a plastic condition and then added by applying pressure as in a welding forge. Welding differs from lower wire-joining temperature methods that do not heat the base metal, such as brazing and soldering.

If necessary, a separate filler material of the same composition as the parent materials is added, and the pool is allowed to solidify and create a well-meant structure.

Welding applications are so diverse and extensive that it would not be misleading to argue that there is no metal industry or engineering division that does not use welding

I. Ramli · M. F. Abdul Razak (✉) · M. Z. Zainol · S. B. Ismail
Universiti Kuala Lumpur Malaysia Institute of Marine Engineering Technology, Jalan Pantai Remis, 32200 Lumut, Perak, Malaysia
e-mail: mfaizalar@unikl.edu.my

M. Z. Zainol
e-mail: mzaifulrizal@unikl.edu.my

S. B. Ismail
e-mail: shaifulbakri@unikl.edu.my

in some form or another, including the automobile, manufacturing, aerospace, and construction industries (Winarto et al. 2018). Mostly used in manufacturing, welding is critical in the shipbuilding industry. Welding is one of the most crucial procedures in shipbuilding. If the welds fail, the entire system fails to protect the ship's hull. This process is carried out by qualified welders and efficiently controlled by quality assurance engineers and classification societies.

Various studies on the interaction between welding parameters and bead geometry are given. Voltage, gas flow rate, wire feed rate, and travel speed are welding parameters that influence the bead geometry (Satyaduttsinh et al. 2014). The quality of the weld is determined by the geometry of the beads. Meanwhile, throughout the welding process, the bead geometry is heavily influenced by the various welding parameters. The welding current is an important welding parameter that influences the bead geometry. The effect of welding current on the bead shape is typically determined by the plate thickness and travel speed. The higher the deposition and penetration rate, the higher the current needed during the welding process. It was discovered that a lower electrode diameter produces smoother material transfer. Meanwhile, the voltage parameter has a strong relationship with the arc length. The size of the weld bead is affected by the arc length. The movement of the arc, on the other hand, is determined by the speed of travel. The lesser the penetration, the slower the travel speed. As a result, it leads to the widen of the weld bead (Vidyut et al. 2008).

Because arc welding is typically done by hand, the quality of the welding is dictated by the welder's ability. A welder with extensive experience is required to provide high-quality weldability. This is due to the welder's ability to directly monitor and select welding parameters during the welding process. To address this issue, robotic welding was introduced. One of the benefits of robotic welding is increased efficiency because the robot can do tasks faster than a human worker (Xu et al. 2017). Furthermore, the quality of welding is more constant and accurate when robot welding is used. Other benefits include faster welding speeds and less waste material due to fewer mistakes made during the welding process. Furthermore, the use of robotic welding can improve the worker's safety, because the robot is outfitted with a variety of safety features that can protect the worker from the welding arc, temperature, and brightness (Kim et al. 2003).

Aside from welding parameters and bead shape, other factors to consider are microstructure, fracture morphology, and micro-hardness. This is typically investigated by an hardness test that will is performed following the welding procedure (Winarto et al. 2018). The goal of the hardness test is to provide two critical indications following the welding procedure. The welding material's strength and microstructure are important considerations. Vickers hardness is a technique for determining welds and HAZs. Loads ranging from 1 to 100 kg can be used to create the diamond indentation. The greater the load, the greater the impact of the diamond on the steel sheet. The goal of having a hardness test for welding is to analyze the hardness of the metal and determine the material tensile strength, as well as to confirm that the welded metal meets or surpasses the original metal's strength requirement.

Table 13.1 Welding parameter

Sample no	Travel speed (mm/s)	Weaving parameter (mm)	Voltage (V)	Current (A)
1	1	0.2	22	130
2	2	0.2	22	130
3	3	0.2	22	130
4	1	0.4	22	130
5	2	0.4	22	130
6	3	0.4	22	130
7	1	0.6	22	130
8	2	0.6	22	130
9	3	0.6	22	130

13.2 Methodology

There are three processes involved in these parts namely the sample cutting process, robotic arm welding, microstructure testing, and hardness testing. The material used in this experiment is the low carbon steel AWS A36 using flux core arc welding (FCAW). The material plate is cut into 18 pieces using a swing beam Guillotine Shear device (SB3006) at UniKL MIMET.

13.2.1 Robotic Arm Welding Setting

A robotic welding arm is an automated welding process, which makes it easy for a welder to get the specific measurement and also can reduce the period for any work project. The setting used for the experiment is as follow; firstly, switch on the main power and then set up the parameter such as current, voltage, travel speed, and weaving parameter as shown in Table 13.1. Next, after setting up all the parameters such as current, voltage, travel speed, and weaving parameter as shown in Table 13.1. Next, after setting up all the parameters then turn on the robotic arm and run the material plates in T-joint configuration. In total a number of specimens was obtained.

13.2.2 Experimental Preparation

In this experiment, after using the robotic arm, all the specimens need to be cut into 1 in. stripes using a semi-automatic horizontal band saw. After the cutting process for each specimen, next polish the selected surface to all the material plated using sandpaper GRIT 800, 1000, and 2000 until mirror look is achieved using a polishing machine (Ghalib et al. 2012). This experiment is conducted at STRIDE in Tentera

Laut Diraja Malaysia (TLDM), Lumut. The process for etching the specimen was done using ferric chloride. Firstly, pour some etching liquid in the petri dish and then put the specimen in the petri dish and wait 1 min or 1 min 30 s (Liu et al. 2019). Then, take out the specimen and rinse it with plain water. After the rinse, use the air gun and blower to ensure there is no etching liquid in the welding gap because it can make the specimen easily corroded.

A stereo microscope is a type of optical microscope that offers a three-dimensional vision of a specimen for the consumer to see. The stereomicroscope differs from the compound light microscope by having different objective lenses and oculars, otherwise referred to as a dissecting microscope or a stereo zoom microscope. For each eye, this results in two autonomous optical paths. The multiple angling views for the left and right eyes provides three-dimensional visuals. Compared to the transmitted light that is used by compound light microscopes, stereo microscopes use reflected light from the object being studied. The magnification varies between 7.5 to 75x. With these tools, opaque, thick solid objects are ideal for studying.

13.2.3 Analysis Preparation

This analysis also is conducted at STRIDE (TLDM) using a stereomicroscope to measure the direction bead height, bead width and throat for penetration after etching. Figure 13.1 shows the nine specimens and the stereo microscope that that is used for this analysis. Next, put one specimen on the stereo microscope, adjust the light and distance to get the actual penetration required. For the light, we did not use the support light because it will disturb the size of the image. It also shows the image on the monitor after putting the specimen on a stereomicroscope. This analysis is continued until finish all the specimens. Lastly, collect all the data and make a comparison of the results obtained.

13.2.4 Hardness Test

This method provides important indication after the welding process. There are three type of hardness test namely the Vickers test, Brinell test and Rockwell test as shown in Fig. 13.2. For this experiment, we used the Vickers test. This technique can be used to measure weld and HAZs. The load that is applied in this experiment 98.1 N because of the Vickers HV10. In calculation it has two diagonals, d_1 and d_2 are measured, averaged and the surface area is calculated and then divided by the load applied.

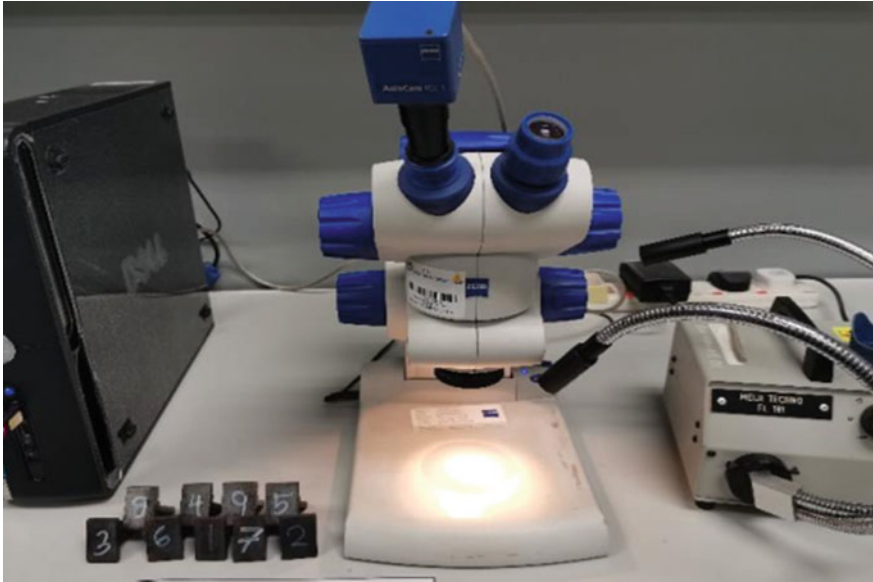


Fig. 13.1 The stereomicroscope



Fig. 13.2 Universal hardness test

13.3 Results and Discussion

The welding is executed using a robotic arm with different weaving parameters and travel speed. The bead geometry is the most important feature in the welding process, especially for automatic systems. In the bead geometry, width, height, and throat are needed in the welding process. There are two testing procedures that were performed in order to analyze the effect of welding parameter on the bead geometry which are microstructure testing and hardness testing (Qing et al. 2021).

13.3.1 Microstructure Testing

This microstructure testing is carried out by measuring the penetration of specimens used in this experiment with a stereomicroscope. Table 13.2 shows the dimensions after using the stereomicroscope on all of the specimens in millimeters.

Figure 13.3 shows the graph of travel speed versus bead geometry. The travel speed start from 1 mm/s, 2 mm/s and 3 mm/s where we can see that with increasing the travel speed, the trend line of bead height, bead width and throat are declining. This is due to the fact that rate of deposition is decreasing when the travel speed is increased and the heat transfer amount is decreasing (Rogfel et al. 2021).

Figure 13.4 indicates that the weaving parameter has a direct effect on the bead geometry profile but from the result does not show a direct correlation for the bead height and throat result (Vidyut et al. 2008). Only bead width shows the direct correlation on weaving parameter to the bead geometry result (Winarto et al. 2018). By applying the same welding parameter set but different weaving value, the data show as the figure above. A weaving value of 0.6 mm shows the highest effect to all the bead geometry, bead height, bead width and throat. The maximum value measured for the bead height is 1.72 mm, for the bead width 1.44 mm and for the throat 1.49 mm. The lowest measurement is for the weaving parameter with a value

Table 13.2 Bead geometry and hardness testing value

Sample no	High (mm)	Width (mm)	Throat (mm)	HV (kgf/mm ²)
1	1.44144	1.12738	1.49158	1514.504778
4	1.21566	1.21089	1.12721	2061.409281
7	1.71522	1.44285	1.40158	2061.409281
2	1.35634	1.03923	1.28693	1756.46708
5	1.39185	1.14904	1.17202	1756.46708
8	1.28055	0.86139	1.09364	1514.504778
3	1.16615	0.73949	1.06486	1756.46708
6	1.13826	0.97589	1.23427	1514.504778
9	1.0764	0.82891	1.13185	1514.504778

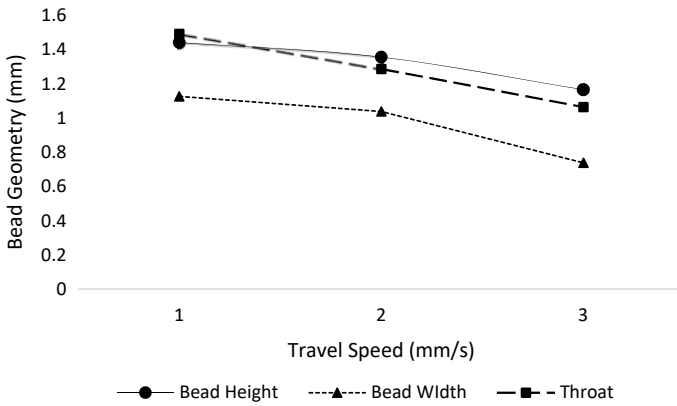


Fig. 13.3 Travel speed versus bead geometry

of 0.4 mm, which affected the bead height and throat only. The value measured is 1.22 mm for bead height and 1.12 mm for the throat value.

Figure 13.5 shows the graph for hardness versus travel speed. The graph shows the result of hv is inclining when the travel speed is increased. The maximum value measured is 2061.41 kgf/mm² for a travel speed value is at 0.6 mm/s while the minimum value hv is 1514.50 kgf/mm² when the value of travel speed is at 0.2 mm/s. This shows that by increasing the travel speed, the value of hv is directly affected to the travel speed (Winarto et al. 2018).

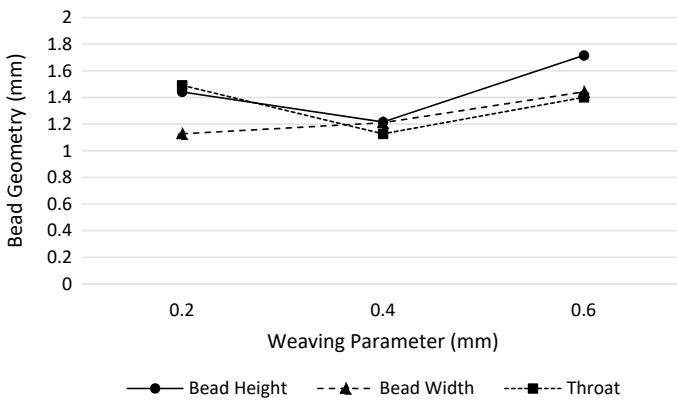


Fig. 13.4 Weaving parameter versus bead geometry

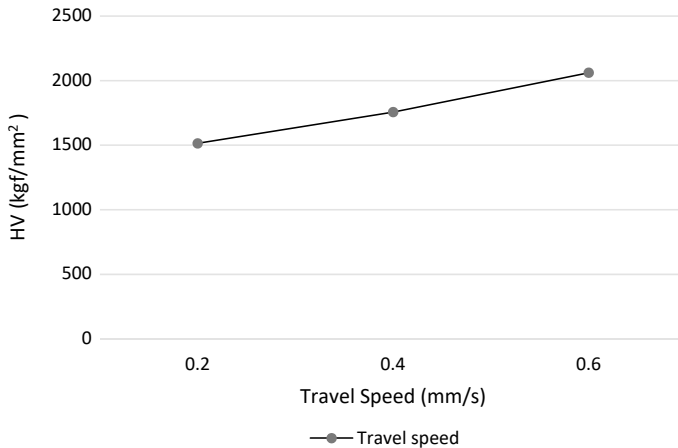


Fig. 13.5 Hardness test versus travel speed

13.4 Conclusion

The objective of this work has been achieved its objective that is to analyze the effect of welding parameter on the bead geometry by using a robotic arm and to identify the hardness of the material after welding by the robotic arm.

Acknowledgements This research has been financially supported by UniKL STRG No STRG of Str 19052 at Campus UniKL MIMET.

References

- Ghalib T, Mohamad YY, Sunhaji KA, Yupiter HPM, Bukhari AJ (2012) Predicting the GMAW 3F T-fillet geometry and its welding parameter. *Procedia Eng* 41:1794–1799
- Jun X, Guangjun Z, Jianwen H, Lin W (2014) Bead geometry prediction for robotic GMAW-based rapid manufacturing through a neural network and a second-order regression analysis. *J Intell Manuf* 25:157–163
- Kim IS, Son JS, Kim IG, Kim JY, Kim OS (2003) A study on relationship between process variables and bead penetration for robotic CO₂ arc welding. *J Mater Process Technol* 136:139–145
- Liu Q, Song J, Hao P (2019) Automatic reading and writing model of welding parameters predicted based on PSO-RFR. *IEEE Xplore* 387–391
- Qing S, Fuxing T, Kai L, Tatsuo Y, Guikai G (2021) Multi-objective optimization of MIG welding and preheat parameters for 6061-T6 Al alloy T-joints using artificial neural networks based on FEM. *MDPI Coatings* 11:1–20
- Rogfel TM, Guillermo AB, Alysson MAS, Sadek CAA (2021) Analysis of GMAW process with deep learning and machine learning techniques. *J Manuf Process* 62:695–703
- Satyaduttsinh PC, Jayesh VD, Tushar MP (2014) A Review on optimization of MIG welding parameters using Taguchi. *Int J Latest Eng Manag Res* 4(1):16–21

- Vidyut D, Dilip KP, Datta GL (2008) Prediction of weld bead profile using neural networks. ICS 1:581–586
- Winarto W, Herry O, Eddy SS (2018) Microstructure and hardness properties of butt and fillet GMAW welded joints on HY80 high strength steel plate. AIP Conf Proc 060020:1–7
- Xu Y, Lv N, Fang G, Du S, Zhao W, Ye Z, Chen S (2017) Welding seam tracking in robotic gas metal arc welding. J Mater Process Technol 248:18–30

Chapter 14

Membranes Technology Development and Challenges in Oily Wastewater Treatment: A Brief Review



Nurshahnawal Yaacob

14.1 Introduction

Fast-growing industrial and agricultural show higher demand for fossil fuels and a variety of substances, which leads to serious environmental problems globally such as polluted oily wastewater (Zhang et al. 2016a). As one of the important contaminants in water, oil causes wastewater problems in environments (Mustafa et al. 2014). Decontamination of wastewater from industry is a key challenge from the environmental and ecological perspective (Sharma et al. 2018). This indicates that there is an increasing demand to treat oily wastewater to preserve the environment from its adverse impacts, and this situation has drawn the scientific community's interest (Modi and Bellare 2019).

Oily wastewater can be treated using conventional treatment methods such as gravity separation and skimming, dissolved air flotation, de-emulsification, coagulation, and flocculation. However, some shortcomings such as low efficacy, high operating costs, deterioration, and concern about decontaminating make the conventional treatment methods less attractive (Makki and Zghair 2014). Compared to conventional treatment methods, pressure-driven membrane filtrations such as microfiltration (MF), ultrafiltration (UF), and nanofiltration (NF) membranes are attracting worldwide attention due to their obvious performance. Nevertheless, though NF membranes have the benefit of maintaining low molecular weight species, the low-pressure MF and UF membranes have an advantage over NF membranes and can be utilized as submerged membranes (Chin et al. 2007).

Various research described the usage of polymeric membranes for wastewater treatment (Ong et al. 2014; Dzinun et al. 2017; Yaacob et al. 2020). Polyethersulfone

N. Yaacob (✉)

Maritime Engineering Technology Section, Universiti Kuala Lumpur, Malaysian Institute of Marine Engineering Technology, Jalan Pantai Remis, 32200 Lumut, Perak, Malaysia
e-mail: nurshahnawal@unikl.edu.my

and polyvinylidene fluoride (PVDF) are the two polymeric membranes that widely monopolize the membrane market despite membrane fouling badly controlling the polymeric membrane's progress because of their intrinsic hydrophobicity. On the other hand, ceramic membranes were unable to discover widespread use owing to their overprice and instability which jeopardizes the membrane's integrity. Hence, polymeric membranes are attracting much attention internationally (Shen et al. 2020).

Membrane filtrations are used to treat wastewater as the growing demand for clean water supply and water scarcity, in recent years (Hossein Razzaghi et al. 2014). Karakulski and Gryta (2017) reported that MF and UF membranes are frequently employed for oily wastewater treatment. These days, photocatalytic membrane reactors (PMRs) with UF membranes are used for the effective removal of organic compounds from water, and the use of UF membranes were cost-efficient for the treatment of oily wastewater because there is no need for chemical additives and environment-friendly (Rani et al. 2021). The treated wastewater can then be utilized in different ways such as by industry in utility plants, farming, and cleaning uses to prevent global water shortage (Rasouli et al. 2017).

14.2 Nanocomposite Membranes

The incorporation of nanoparticles into polymeric membrane matrixes produces nanocomposite membranes (Wen et al. 2019). The usage of titanium dioxide (TiO_2) or zinc oxide (ZnO) nanoparticles in membrane fabrication not only improves the morphology of the membrane but to aid in getting higher permeability. Furthermore, the extremely reactive oxygen species generated by TiO_2 aid oxide molecules to achieve full mineralization and add the antifouling characteristic to the membrane surface (Sakarkar et al. 2020). 3 wt% ZnO/polyvinyl chloride (PVC) nanocomposite membranes prepared by Rabiee et al. (2015) showed improvement in the flux recovery ratio from 69 to >90% indicating that the nanocomposite membranes were less susceptible to being fouled.

14.3 Photocatalytic Membranes

The fabrication of membrane using pure catalysts through methods such as coating or mixing of catalysts over a commercial membrane produces photocatalytic membranes (Iglesias et al. 2016) with photocatalytic ultraviolet (UV) responsive membranes and photocatalytic visible light responsive membranes are the two photocatalytic membranes widely used. For the functional membrane, the photocatalytic ultraviolet (UV) responsive membranes are activated by UV illumination and are mostly concentrating on TiO_2 or ZnO-based photocatalysts (Shi et al. 2019). ZnO has been recognized in photocatalysis and antifouling agent due to the high surface-to-volume ratio of ZnO nanoparticles which makes it an important nanostructure

in many disciplines (Shen et al. 2020). Meanwhile, the non-toxicity, high decontaminating action, economical, chemically inactive, deterioration resistance, and stability make TiO_2 the frequently used photocatalyst in solar or artificial light-driven photocatalysis (Sharma et al. 2018).

Moghadam et al. (2015) reported that 20 wt% TiO_2 /PVDF nanocomposite membranes exhibited improved antifouling properties under UV illumination in comparison to neat PVDF membranes. The flux recovery ratio of 98.1% has confirmed their antifouling property. The membrane hydrophilicity and porous structure also showed improvement because the UV illumination forms surface oxygen defects at the attaching site, which makes the dissociative adsorption of water more favorable at the membrane surface. Oily industrial wastewater was well treated using an 8 wt% TiO_2 /PVDF-trifluoro ethylene (TrFE) nanocomposite membrane in a solar photoreactor as reported by Zioui et al. (2019). The reduction in the contact angle on the polymer matrix with the incorporation of TiO_2 nanoparticles is believed to allow for a higher contact between the nanoparticles and the oily wastewater.

14.4 Photocatalytic Membrane Reactors

Photocatalytic reaction and membrane separation are paired in photocatalytic membrane reactors (PMRs) to perform a transformation of chemicals process. The pairing improves the capabilities of classical photoreactors and membrane filtrations. The membrane enables an uninterrupted process in a system whereby the reaction during photocatalytic, the recovery of photocatalyst, and the separation of the products from the treated wastewater take place in a single step (Molinari et al. 2020). Generally, the two major arrangements for PMR are (i) slurry PMR whereby the reactor contains suspended catalyst particles in the feed solution, and (ii) immobilized PMR whereby the reactor is paired with immobilized catalysts in/on the membrane (immobilized PMR). The succeeding option is more promising since the TiO_2 photocatalyst recovering process can be shortened which eases the operating complexity and practical application expenses (Ong et al. 2014; Zhang et al. 2016b). The former option is associated with photocatalyst regeneration, low photocatalytic efficiency, high membrane resistance, and fouling (Rameshkumar et al. 2020).

A reactor system with TiO_2 suspended is reported to show improved performance than when deposited on the membrane surface. However, the slurry PMR involves a secondary process to free the catalyst from the treated water. In contrast, immobilization of TiO_2 in the membrane matrix can eliminate this additional process despite this approach leading to a decreasing surface area of the available sites for the reaction during photocatalytic. As such, evenly distributing TiO_2 nanoparticles within the membrane is required and can be accomplished through a single-step co-extrusion process. This is important to ensure a higher amount of TiO_2 nanoparticles be exposed to UV light and enable the reaction during photocatalytic to occur (Dzinun et al. 2017).

Soon after, a type of PMR with advantages such as inexpensive installation, energy efficiency, and ease of maintenance known as submerged photocatalytic membrane reactor (SPMR) emerged (Nguyen et al. 2020). In this integrated treatment process, the membrane plays a dual role in which the membrane acts as the support for TiO_2 photocatalyst as well as a physical selective barrier for the degraded products. TOC degradation and oil rejection as high as 80 and >90% were reported using 2 wt% TiO_2 /PVDF hollow fiber membranes using SPMR (Ong et al. 2014).

14.5 Challenges

One of the challenges during the fabrication process of nanocomposite membranes includes the agglomeration of nanoparticles. Agglomeration can lead to a possible reduction in the antifouling ability of TiO_2 nanoparticles and a change in membrane topography and hydrophilicity as a result of the irregular distribution of particles in the membrane (Razmjou et al. 2012).

Challenges on photocatalytic UV-responsive membranes are the risk for the structure of the membrane to experience severe destruction by both reactive oxygen species (e.g., $\cdot\text{OH}$) and UV light and the impacts on the polymeric membranes are harsher. Apart from that, the solar energy usage efficiency is controlled by the TiO_2 or ZnO catalyst bandgap around 3–4% of the solar spectrum (UV region) while about 44–47% of visible light is left unexploited. Additionally, the photocatalytic performance of TiO_2 or ZnO -based catalysts is seriously limited by the rapid recombination of the photogenerated charges and demonstrate low photoactivity in the visible light region (Shi et al. 2019).

14.6 Conclusion

Oil pollution has brought substantial effects on the ecosystem, human security, and economic growth, which caught worldwide attention. With the laws and standards on environmental protection becoming stricter over time, the existing oily wastewater treatment technology can no longer satisfy the higher standard requirement. The development of improved oily wastewater treatment becomes more prominent to protect the environment. Nevertheless, the improved treatment methods are still facing some challenges which need to be overcome.

References

- Chin SS, Lim TM, Chiang K, Fane AG (2007) Factors affecting the performance of a low-pressure submerged membrane photocatalytic reactor. *Chem Eng J* 130:53–63

- Dzinun H, Othman MHD, Ismail AF, Puteh MH, Rahman MA, Jaafar J (2017) Performance evaluation of co-extruded microporous dual-layer hollow fiber membranes using a hybrid membrane photoreactor. *Desalination* 403:46–52
- Hossein Razzaghi M, Safekordi A, Tavakolmoghadam M, Rekabdar F, Hemmati M (2014) Morphological and separation performance study of PVDF/CA blend membranes. *J Memb Sci* 470:547–557
- Iglesias O, Rivero MJ, Urriaga AM, Ortiz I (2016) Membrane-based photocatalytic systems for process intensification. *Chem Eng J* 305:136–148
- Karakulski K, Gryta M (2017) The application of ultrafiltration for treatment of ships generated oily wastewater. *Chem Pap* 71:1165–1173
- Makki HF, Zghair NH (2014) Forward-reverse osmosis processes for oily wastewater treatment. *J Eng* 20:91–212
- Modi A, Bellare J (2019) Efficiently improved oil/water separation using high flux and superior antifouling polysulfone hollow fiber membranes modified with functionalized carbon nanotubes/graphene oxide nanohybrid. *J Environ Chem Eng* 7:102944
- Moghadam MT, Lesage G, Mohammadi T, Mericq JP, Mendret J, Heran M, Faur C, Brosillon S, Hemmati M, Naeimpoor F (2015) Improved antifouling properties of TiO₂/PVDF nanocomposite membranes in UV-coupled ultrafiltration. *J Appl Polym Sci* 132:13–15
- Molinari R, Lavorato C, Argurio P (2020) Application of hybrid membrane processes coupling separation and biological or chemical reaction in advanced wastewater treatment. *Membranes* 10:281
- Mustafa YA, Alwared AI, Ebrahim M (2014) Heterogeneous photocatalytic degradation for treatment of oil from wastewater. *Al-Khwarizmi Eng J* 10:53–61
- Nguyen VH, Tran QB, Nguyen XC, Hai LT, Ho TTT, Shokouhimehr M, Vo DVN, Lam SS, Nguyen HP, Hoang CT, Ly QV, Peng W, Kim SY, Tung TV, Le QV (2020) Submerged photocatalytic membrane reactor with suspended and immobilized N-doped TiO₂ under visible irradiation for diclofenac removal from wastewater. *Process Saf Environ Prot* 142:229–237
- Ong CS, Lau WJ, Goh PS, Ng BC, Ismail AF (2014) Investigation of submerged membrane photocatalytic reactor (sMPR) operating parameters during oily wastewater treatment process. *Desalination* 353:48–56
- Rabiee H, Vatanpour V, Farahani MHDA, Zarrabi H (2015) Improvement in flux and antifouling properties of PVC ultrafiltration membranes by incorporation of zinc oxide (ZnO) nanoparticles. *Sep Purif Technol* 156:299–310
- Rameshkumar S, Henderson R, Padamati RB (2020) improved surface functional and photocatalytic properties of hybrid ZnO-MoS₂-deposited membrane for photocatalysis-assisted dye filtration. *Membranes* 10:106
- Rani CN, Karthikeyan S, Prince Arockia Doss S (2021) Photocatalytic ultrafiltration membrane reactors in water and wastewater treatment—a review. *Chem Eng Process: Process Intensif* 165:108445
- Rasouli Y, Abbasi M, Hashemifard SA (2017) Investigation of in-line coagulation-MF hybrid process for oily wastewater treatment by using novel ceramic membranes. *J Clean Prod* 161:545–559
- Razmjou A, Resosudarmo A, Holmes RL, Li H, Mansouri J, Chen V (2012) The effect of modified TiO₂ nanoparticles on the polyethersulfone ultrafiltration hollow fiber membranes. *Desalination* 287:271–280
- Sakarkar S, Muthukumaran S, Jegatheesan V (2020) Polyvinylidene fluoride and titanium dioxide ultrafiltration photocatalytic membrane: fabrication, morphology, and its application in textile wastewater treatment. *J Environ. Eng (United States)* 146:1–12
- Sharma B, Boruah PK, Yadav A, Das MR (2018) TiO₂-Fe₂O₃ nanocomposite heterojunction for superior charge separation and the photocatalytic inactivation of pathogenic bacteria in water under direct sunlight irradiation. *J Environ Chem Eng* 6:134–145
- Shen L, Huang Z, Liu Y, Li R, Xu Y, Jakaj G, Lin H (2020) Polymeric membranes incorporated with ZnO nanoparticles for membrane fouling mitigation: a brief review. *Front Chem* 8:1–9

- Shi Y, Huang J, Zeng G, Cheng W, Hu J (2019) Photocatalytic membrane in water purification: is it stepping closer to be driven by visible light? *J Memb. Sci* 584:364–392
- Wen Y, Yuan J, Ma X, Wang S, Liu Y (2019) Polymeric nanocomposite membranes for water treatment: a review. *Environ Chem Lett* 17:1539–1551
- Yaacob N, Goh PS, Ismail AF, Mohd Nazri NA, Ng BC, Zainal Abidin MN, Yogarithnam LT (2020) ZrO₂-TiO₂ incorporated PVDF dual-layer hollow fiber membrane for oily wastewater treatment: effect of air gap. *Membranes* 10:124
- Zhang L, Gu J, Song L, Chen L, Huang Y, Zhang J, Chen T (2016a) Underwater superoleophobic carbon nanotubes/core-shell polystyrene@Au nanoparticles composite membrane for flow-through catalytic decomposition and oil/water separation. *J Mater Chem A* 4:10810–10815
- Zhang W, Ding L, Luo J, Jaffrin MY, Tang B (2016b) Membrane fouling in photocatalytic membrane reactors (PMRs) for water and wastewater treatment: a critical review. *Chem Eng J* 302:446–458
- Zioui D, Salazar H, Aoudjit L, Martins PM, Lanceros-Méndez S (2019) Polymer-based membranes for oily wastewater remediation. *Polymers* 12:42

Chapter 15

Compliance to IMO Sulphur Cap Regulations for Vessels of 10 Years of Age and Below



Kogulan Murugan and Aminuddin Md Arof

15.1 Introduction

Since the International Maritime Organization (IMO) started to regulate and implement new regulations to protect the marine environment, various annexures of the International Convention for the Prevention of Pollution from Ships (MARPOL) were gradually enforced. Annex 6 of MARPOL was introduced and entered into force since 2005 to tackle the air pollution of the marine and coastal environment. In 2008, the Annex was further revised to ensure a progressive reduction in the emissions of sulphur oxide (SO_x), nitrogen oxide (NO_x) and particulate matter (PM), while at the same time introduced the concept of emission control area (ECA) in designated maritime regions. The ECA experienced a stricter control of air pollution measures compared to other areas. The amended Annex 6 came into force in 2010. Beginning January 2020, the permitted emissions from ships have continued to be further reduced by the convention with SO_x emission reduced from 3.5% m/m to 0.5% m/m globally and remained at 0.1% m/m in the ECA involving the Baltic Sea, North Sea, North America and United States Caribbean Sea area that was enforced since January 2015. This rule applied to all vessel owners and operators, and they have to observe the stipulated regulations to enable their vessels to sail from one place to another without been detained by the flag state or the port state control authorities. At the same time, the IMO had also issued several guidelines on the compliance methods which are emission gas cleaning systems, switching of combustion fuels from high sulphur to low sulphur and alternative combustion method such as the liquefied natural gas (LNG).

K. Murugan · A. Md Arof (✉)

Universiti Kuala Lumpur, Malaysian Institute of Marine Engineering Technology, 32200 Lumut, Perak, Malaysia

e-mail: aminuddin@unikl.edu.my

15.2 Methodology

This part describes the cost benefit analysis (CBA) of installing scrubbers and utilizing very low sulphur fuel oils (VLSFO). A scenario was set up based on MV Parsifal, which was operated for domestic operation from the Peninsular Malaysia to East Malaysia and vice versa. The main elements used for this analysis are the price of high sulphur fuel oil (HSFO), VLSFO, and estimated initial scrubber installation cost. Apart from it, other costs for operating a vessel involving manpower, annual maintenance, insurance, lubricating oil, management cost and others were considered as the same amount for both scenarios.

15.2.1 Cost Benefit Analysis

Cost benefit analysis (CBA) is a method to differentiate the cost of a project with its benefits. It can be considered as an economic appraisal tool that is normally used by big organizations for their projects. Normally this analysis will be carried out during the design phase of a project that will assist decision making on the potential of the project. For this study, a common formula from CBA is used (Yaramenka et al. 2018). The formula is as per the following:

$$CBR = \frac{\left(\frac{\sum Bi}{(1+d)} \right)}{\left(\frac{\sum Ci}{(1+d)} \right)} \quad (15.1)$$

where *CBR* is a Cost Benefit Ratio, *Bi* is the project benefit in year *i*, where *i* is the number of years. *Ci* is the project cost in year *i*, where *i* is the number of years and *d* is the discount rate. The simple steps in this methodology are:

1. Determine the discounted benefits for each year of the project.
2. Determine the discounted costs for each year of the project.
3. Sum the total discounted benefits for the entire project duration.
4. Sum the total discounted costs for the entire project duration.
5. Divide the total discounted benefits over the total discounted costs.

15.2.2 Scenarios for Analysis

Two scenarios were chosen for this analysis on MV Parsifal in order to comply with the 0.1% sulphur cap as follows:

1. MV Parsifal: HSFO + Scrubber
2. MV Parsifal: VLSFO

Table 15.1 Scrubber installation price in US Dollar

Scrubber type	New built (20 MW)	Old vessel (20 MW)
Open loop	\$2.1 m	\$2.4 m
Close loop	\$2.4 m	\$2.4 m
Hybrid	\$3.0 m	\$3.0 m

Source Mfame Editor (2019). Drewry VLCC scrubber cost insights

MV Parsifal (IMO: 9515395) is a vehicle carrier (RoRo) that was built in 2011, i.e. 10 years before this research was conducted and operated under the flag of Malaysia for domestic trade. The expected potential operations period is about 20 years as the maximum operational lifespan of the vessel is about 30 years. The average fuel consumption is 31 mt/day on sailing, anchor and berth. For this analysis, the Singapore bunker price has been used as the fuel price for HSFO and VLSFO. The price for HSFO is \$294/mt and for VLSFO is \$403/mt based on the result of the average calculation from the price of January 2020 to April 2021. Based on Mfame Editor (2019), the installation costs for a scrubber system are as per Table 15.1. On the other hand, according to Kinch (2020), the installation of a scrubber could cost between US\$1 million to US\$5 million depending on the vessel characteristics. Referring to Table 15.1, the expected cost of scrubber installation is about US\$3 million.

15.2.3 Interview with Industry Experts

For the interview part, the researcher has chosen eight interviewees who were directly involved in maritime transportation and shipping research. In order to get reliable findings, the researcher has selected experts from different sectors such as vessel owners, vessel charterers, vessel operators and researchers. All the interviewees are experts in their respective fields and hold senior positions in their organizations. The interview respondents that participated are listed in Table 15.2.

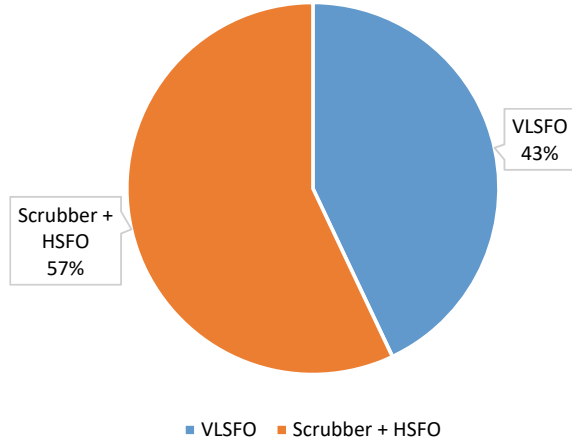
Table 15.2 Interviewee details

Company	Position	Respondent
GIGA Shipping	Chief executive officer	1
GIGA Shipping	Senior operation manager	2
Straits Auto Logistics	Chief executive officer	3
Straits Auto Logistics	Chief operating officer	4
Wilhelmsen Ship Management	Technical superintendent	5
Wilhelmsen Ship Management	Vessel captain	6
Netherlands Maritime University College	Lecturer/researcher	7
UniKL MIMET	Lecturer/researcher	8

Table 15.3 Result of CBA

Compliance	Total benefit	Total cost	Ratio
VLSFO	US\$504m	US\$91.2 m	5.5
Scrubber + HSFO	US\$504m	US\$69.5 m	7.3

Fig. 15.1 Cost benefit ratio from CBA



15.3 Results and Discussion

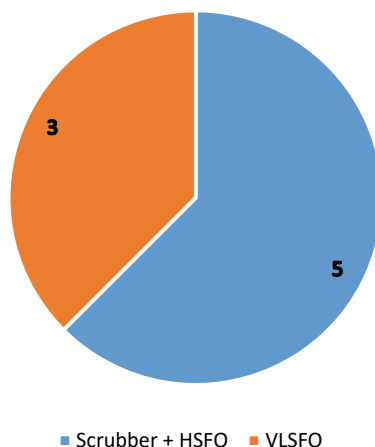
15.3.1 Cost Benefit Analysis Result

Based on the CBA calculation as presented at Table 15.3 and Fig. 15.1, the use of a scrubber with HSFO shows higher ratio which is 7.3 and VLSFO is 5.5. With higher ratio, scrubber compliance indicates a high potential by having high cost benefit ratio. Similarly, 62% or 5 out of 8 respondents have chosen Scrubber + HSFO as presented in Fig. 15.2.

15.3.2 Discussion

In this study, the fuel and scrubber installation were considered as manipulating costs and other elements such as manpower, insurance and others were considered as fixed costs. Therefore, the costs of fuel and scrubber installation were used for the CBA calculation. Eventhough the price of bunker fluctuated from time to time, the average price was taken from the prices between Jan 2020 and March 2020, which was before the Covid-19 pandemic. Based on the CBA calculation, the scrubber system with HSFO has a high potential for cost benefit ratio, which indicates that it can be a more cost effective method for a 10 year old vessel to comply with the rule as compared

Fig. 15.2 Experts choice on alternative for IMO sulphur cap compliance



to the VLSFO compliance. However, this study was carried out with a fixed bunker price for a 5 year period and the scrubber installation cost was based on an estimation considering the operation areas and length of voyage.

The potential of LNG could not be included in this CBA as this propulsion system was totally not practical to retrofit into the available vessels. The requirement for removal and re-installation of equipment to enable the installation of a LNG system on the existing vessel will result in a huge investment cost for the shipowner or ship operator to consider. The safety requirements for the handling of LNG are also very relevant to be considered. On-board crews must have sufficient expertise for the handling and servicing of LNG, and adequate preparation is necessary for crews who do not have such experience or knowledge. It is also important for shore personnel to have similar expertise and training to ensure a secure bunkering/loading and unloading of LNG (Fan and Gu 2019; Paris 2019).

The conversion of the ship's fueling system into LNG largely depends on the global market availability of LNG. Studies suggest that most of the bunkering facilities for LNG are locally developed and located in Europe. Researchers projected that numbers will grow in the near future, with only about 18 exporting countries and about 25 importing countries trading LNG on a global scale by 2011. However, relative to 1990, the LNG trade for the year 2011 was around 5 times more than that of 1990 (Chettri 2019; Kolich and Kurtovic 2019). In other countries such as Singapore, some bunkering facilities are being built in order to ensure the availability of LNG especially to Asian operators.

15.4 Conclusion

The aim of this study is to determine the most cost effective compliance method in adhering to the IMO Sulphur Cap 2020 rule in order to further limit the sulphur oxide emission. Two compliance methods that are widely used globally were chosen for this analysis involving the consumption of VLSFO and consuming HSFO with a scrubber system fitted onboard. Both compliance methods have their own advantages and disadvantages, making it difficult for vessel operator or vessel owner to choose between them.

There were many meetings and conferences that were held among shipping lines to discuss on the alternative approaches. Cost and vessel's life span are the factors that have been considered when determining the compliance method. Additionally, the structure or design of the compliance method is another crucial factor that should be considered before making a decision. The structure or design of the compliance method plays a big role to ensure the suitability with the vessel. Currently, about 60% of the fleets belonging to major players are equipped with scrubber systems with the remaining opting for VLSFO. In the current global market, scrubber technologies are already available in various types that enable the filtration of the sulphur up to 0.1% mass/mass. Through the interview process, it was discovered that the majority of the respondents felt that utilising a recon scrubber system would be the ideal solution to comply with the IMO Sulphur Cap regulation for vessels of 10 years old or below.

As a conclusion for this research, a scrubber system with HSFO would be the most cost effective option in adhering to IMO Sulphur Cap regulation on limiting the global SO_x emission enforced through MARPOL Annex VI for vessels of 10 years old or below. This statement has been proven through the CBA technique and interview with maritime experts.

Acknowledgements We would like to thank GIGA Shipping Sdn. Bhd., especially to Mr. Viknesh Rajaratnam, who has provided invaluable assistance in completing this research. We are also grateful to those who have supported us with their guidance and motivation throughout this project.

References

- Chettri A (2019) The influence of MARPOL annex VI on global ship emission: a study based on the impact in the ECAs. Master's thesis, University of South-Eastern Norway. Faculty of Technology, Natural Sciences, and Maritime Sciences
- Fan L, Gu B (2019) Impacts of the increasingly strict sulphur limit on compliance option choices: the case study of Chinese SECA. *Sustainability* 12(1):165. <https://doi.org/10.3390/su12010165>
- Kinch D (2020) Scrubber installation waiting list 'very long' as IMO 2020 kicks. www.spglobal.com/platts/en/market-insights/latest-news/shipping/010320-scrubber-installation-waiting-list-very-long-as-imo-2020-kicks-in-wartsila. Accessed 15 July 2022
- Kolich D, Kurtovic F (2019) LNG vs scrubber technology in future green ships. https://bib.irb.hr/datoteka/1032238.Kolich_Kurtovic-SMATECH_2019.pdf. Accessed 15 July 2021

- Mfame Editor (2019, September 25). Drewry VLCC scrubber cost insights. <https://mfame.guru/drewry-vlcc-scrubber-cost-insights>. Accessed 15 July 2021
- Paris C (2019, March 14) Shipping companies banking on gas carriers as LNG demand grows. <https://www.wsj.com/articles/shipping-companies-banking-on-gas-carriers-as-lng-demand-grows-11552555800>. Accessed 3 Dec 2020
- Yaramenka K, Mellin A, Malmaeus M, Winnes H (2018) Scrubbers: closing the loop activity 3: task 3 cost benefit analysis. IVL Swedish Environmental Research Institute Ltd., B 2320

Chapter 16

Investigation of Impact of Various Oceanographic Variables on Offshore Platforms Behavior



Md. Redzuan Zoolfakar, Muizzuddin Abdullah, and Sarah Nadiah Rashidi

16.1 Introduction

The oil and gas business, being one of the world's most critical industries, contributes significantly to global gross domestic product (GDP). The extraction and refinery processes are extremely complex, requiring cutting-edge technology to transform oil and gas into finished products such as gasoline for vehicles and aero planes. The only method to reach an oil well and extract the oil is to utilize a drillship or oil rig to drill into the ocean floor.

Activities in the oil and gas value chain can be categorized into three groups which is upstream, midstream and downstream. The term "upstream" refers to the activities of the oil and gas sector that involve exploration and production. A high-potential location is chosen for resource exploration. These analyses are carried out using various techniques, such as infrared (IR) surveys, drill-and-sample assaying, electrical currents, and so on. Seismic surveying is another form of exploration, and it is definitely the most important of all geophysical exploration methods, primarily because it is capable of identifying subsurface structures on a wide range of scales, from large too small. Simple seismic methods are used to determine the shapes and

Md. R. Zoolfakar (✉) · M. Abdullah
Marine Engineering and Electrical Technology, Universiti Kuala Lumpur Malaysian Institute of
Marine Engineering Technology, Lumut, Perak, Malaysia
e-mail: redzuan@unikl.edu.my

M. Abdullah
e-mail: muizzuddin.abdullah@s.unikl.edu.my

S. N. Rashidi
Student Development and Campus Lifestyle, Universiti Kuala Lumpur Malaysian Institute of
Marine Engineering Technology, Lumut, Perak, Malaysia
e-mail: sarahnadiah@unikl.edu.my

physical qualities of the Earth's subsurface strata by analyzing sound waves that have travelled through the Earth and returned to the surface (Joshi et al. 2017).

The word "midstream" refers to the process of oil production between the upstream and downstream stages. Midstream operations also include processing, storing, transporting, and marketing crude oil, natural gas, and natural gas liquids, among other commodities. As a link between the upstream and downstream sectors, the midstream industry is responsible for the transportation and storage of oil and gas between upstream production facilities and downstream refining and processing facilities. Besides using the ship to transfer crude oil or natural gas, midstream can also be done via pipelines, trucks, or trains to the refineries (Devold 2015).

The third and last phase of the oil and gas value chain is known as downstream. Following upstream and midstream processing, crude oil or natural gas is transformed into a final product, such as kerosene, gasoline, diesel, etc., in an oil refinery. The operations of a petroleum refinery start with receiving crude oil from an oil tanker and storing it there in a crude oil tank; they then continue with all petroleum processing and refining operations; they then come to a close with storage before transporting the finished goods from the facility (Gulen 2016). Figure 16.1 shows the three stages of oil and gas production.

When it comes to offshore drilling operations which is the upstream process, offshore platforms are divided into two major groups or types: fixed platforms and moveable platforms. Furthermore, some oceanographic characteristics, such as water depth, wave frequency, and so on, must be addressed before deciding on the sort of offshore platform to be selected and used. For the extraction of natural gas or crude oil in shallow water, fixed offshore platforms are used. These platforms are built on concrete, steel, or steel-and-concrete legs that are fastened to the seabed (Sharma 2019). The second type of offshore drilling rig is a moveable platform or mobile offshore drilling rigs, which may be moved from one location to another. It is a

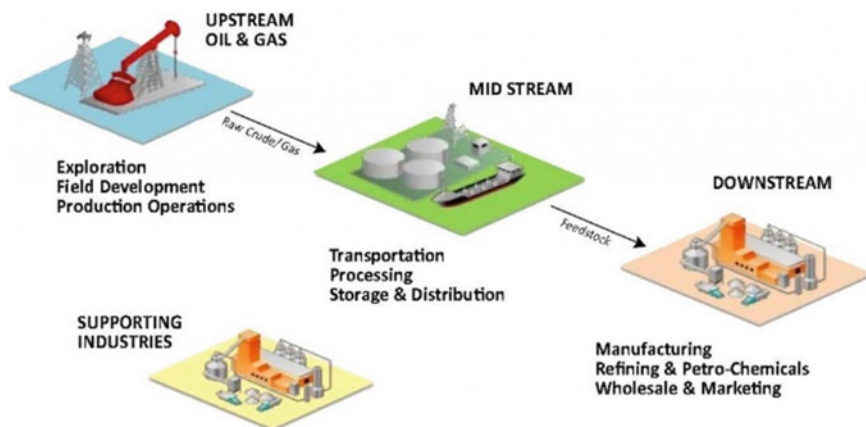


Fig. 16.1 Three stage of oil production (Source Petroleum Industry Structure 2016)

Table 16.1 Parameters

No.	Parameter	Number of variables
1	Type of offshore platform	3

mobile platform/rig used in the exploration process during drilling the oil well to extract the crude oil or natural gas (Sadeghi 2007).

16.2 Methodology

16.2.1 Parameter

Referring to Table 16.1, there are six main parameters that are used in this experiment. These parameters are constant on different types of oceanographic variables throughout the experiment. This parameter is the type of offshore platform which is used in the experiment. The type offshore platform that is used is the spar platform, jacket platform and semi-submersible platform. All three types of offshore platforms (see Table 16.2) that have has been used in this experiment have the same ratio due to the wave tank.

As shown in Table 16.3, the first oceanography variable is the depth of water. It has four different types of water depth, which are 0.6, 0.7, 0.8, and 0.9 m. The second variable is the wave frequency, which has four different types: 0.5, 0.7, 0.9, and 0.11 Hz. The third oceanographic variable is the wave amplitude. It has four different types of wave amplitudes, which are 0.02, 0.04, 0.06, and 0.08 m.

Next is the wave length, which has four different types starting with 0.4, 0.6, 0.8, and 1 m. Lastly is the number of mooring lines applied to the offshore platform, which are 4, 6, and 8. The offshore platform experiences a variety of distinct outcomes as a consequence of each of these oceanographic variables.

16.2.2 Preparation of Offshore Model and Wave Tank

This experiment uses an offshore model, which is described in Fig. 16.2. Every offshore platform model is put to the test separately using various oceanographic variables. In the wave tank, the offshore model is positioned in the middle. The wave tank is a specially designed tank for investigating wave dynamics.

It is sometimes used to show how an offshore platform or ship will react in different wave conditions. The wave tank utilized in this study can be found at Kemaman, Terengganu at the Kolej Kemahiran Tinggi MARA. The wave tank's blueprint was taken from the SOLTEQ wave tank (Model: WTS01). The wave tank is 10 m long, 4 m wide, and 1.3 m high. This wave tank is used to collect data for the experiment. Figure 16.3 shows the real wave tank that has been used for this experiment.

Table 16.2 Type of offshore platform model




No.	Type of offshore platform model	Name
1		Semi-submersible platform 1 m (L) × 1 m (W) × 0.25 m (H)
2		Jacket platform 0.27 m (L) × 0.27 m (W) × 1.6 m (H)
3		Spar platform 0.3 m (L) × 0.3 m (W) × 0.8 m (H)

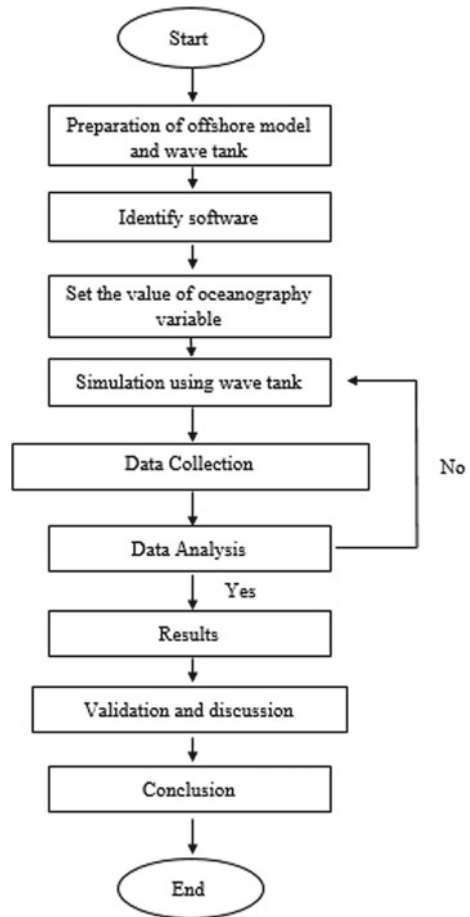
Table 16.3 Oceanography variable

No.	Parameter	Number of variables
1	Water depth	4
2	Wave frequency	4
3	Wave amplitude	4
4	Wave length	4
5	No. of mooring lines	3

16.2.3 Identify Software and Set Data Value

To set the value of oceanographic variable, his experiment requires the use of multiple software tools, including the generated wave. The first is the HR Wallingford’s HR

Fig. 16.2 Flow chart of this experiment



Merlin wave generation software. This software can be used to generate waves with a variety of different characteristics, such as wave frequency and wave amplitude, depending on the configuration.

In addition to the HR Wallingford software, the load cell calibrator system has been used in this experiment. This device is utilized to collect data from all of the offshore platform models utilized in this experiment. Using this device, data is collected as a result of the force generated by the wave striking the platform.

16.2.4 Simulation Using Wave Tank

Start the experiment once all preparations are complete. Figure 16.4 demonstrates the experiment's appearance.

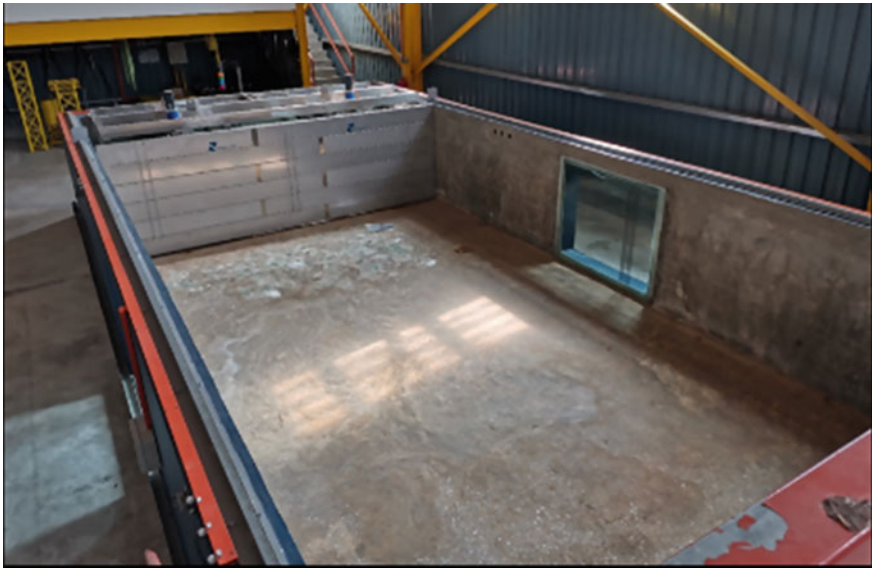


Fig. 16.3 Inside SOLTEQ wave tank at KKTM Kemaman, Terengganu



Fig. 16.4 Semi-submersible platform in the wave tank during the experiment

Table 16.4 Parameter

Time	LC1 (N)	LC2 (N)	LC3 (N)	LC4 (N)
10	- 0.66	- 0.73	1.12	0.44
20	- 4.94	- 0.45	4.66	3.94
30	- 0.87	2.14	4.39	- 2.63
40	- 1.71	- 1.27	5.46	6.28
50	- 3.33	- 0.45	0.16	0
60	- 3.79	2.06	2.11	3.21
70	0.38	1.18	1.59	- 5.26
80	- 3.88	- 0.24	3.59	3.94
90	0.76	1.72	1.46	- 1.46
100	- 4.18	- 1.75	2.83	4.09
110	- 1.49	2.38	4.7	5.4
120	- 4.02	- 1.99	2.49	- 0.29
130	- 2.34	2.83	5.04	- 0.29

16.2.5 Data Collection and Analysis

This test was done with all three kinds of oil platforms: semi-submersible, spar, and jacket. In 130 s, these oil platforms have been run five times with a fixed variable for each type of water depth, wave amplitude, wave frequency, wave length, and number of mooring lines.

The data from the experiment is recorded by the load cells 1, 2, 3, and 4 that are attached to each side of the model. Every 10 s, the data is shown in a table format.

The results shown in Table 16.4 of the experiment are given in newton units, which are a measure of force. Every load cell attached to the model measures how much force the wave is putting on it before the fix variable is set. Based on Table 16.4, the data is collected after the experiment has been done. Depending on the variables and type of offshore platform, each experiment has different results. Based on the parameters used in the experiment, all of the data is used to generate a graphical.

16.3 Results and Discussion

Figure 16.5 shows a graph where each line indicates the kind of oil platform model that was utilized in the experiment as the parameters. According to the graph, the SPAR and semi-submersible oil platforms are more stable than the jacket platform because their lines are close to the zero line. Because of the way they are made, SPAR and semi-submersible platforms are more stable than Jackets for water depth experiments in this situation. The SPAR platform is made up of a large, vertical, buoyant cylinder that can reduce the effects of waves on its structure. The same is

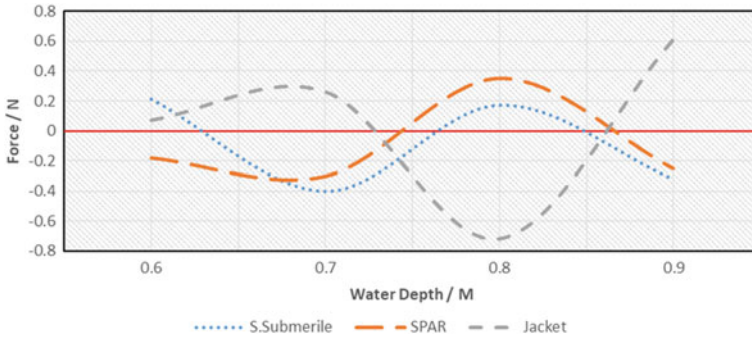


Fig. 16.5 Scatter graph for all platform reacted to different type of water depth

true for semi-submersible platforms, whose design is convenient than that of jacket platforms, which are better for working in shallow water.

As graph in Fig. 16.6 shows, the SPAR platform and the semi-submersible platform are less stable than the jacket platform. The reason for this result is that the jacket platform is made in a more cost-effective and strong way if large waves hit their structure. One of the oil platforms that is connected to the seabed is the Jacket platform. When the sea turns into a storm, the oil platform gets hit by waves with a high amplitude. When things are like that, the jacket platform is better than the SPAR platform and the semi-submersible platform.

Figure 16.7 shows the results of this experiment that the jacket platform is more stable when waves of different frequencies hit it. This is because the jacket platform is built to be stronger than the SPAR platform and is partly submerged. The structure of the jacket platform is attached to the seabed, which makes it more stable. When a lot of waves hit the SPAR platform and the semi-submersible platform at the same time, both platforms' stability and movement are affected, and not in a good way compared to the jacket platform.

At the start of this experiment, the graph in Fig. 16.8 show that all three types of oil platforms exhibited movement due to short wave durations between 0.4 and

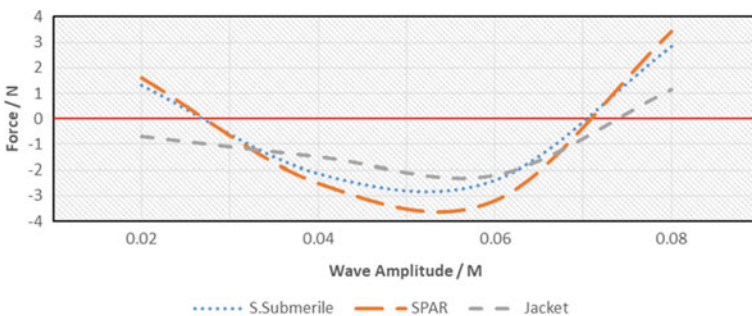


Fig. 16.6 Scatter graph for all platform reacted to different type of wave amplitude

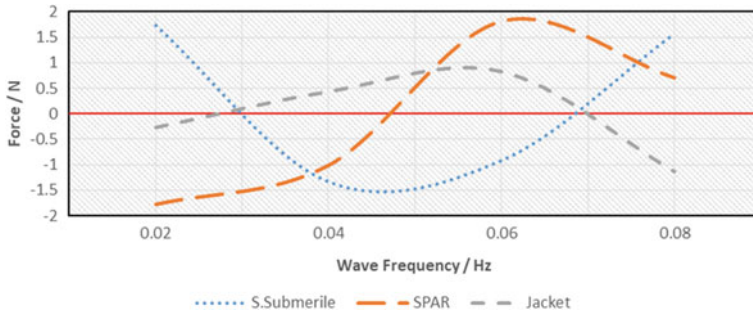


Fig. 16.7 Scatter graph for all platform reacted to different type of wave frequency

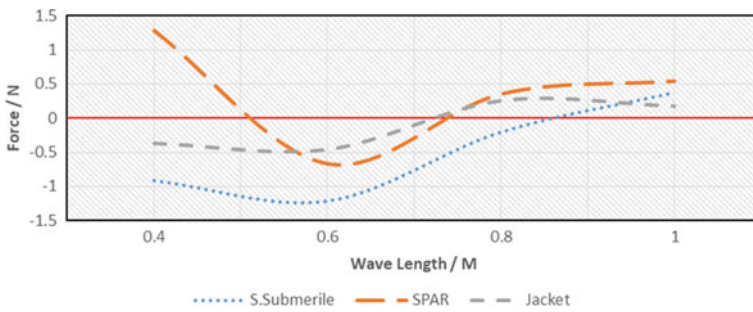


Fig. 16.8 Scatter graph for all platform reacted to different type of wave length

0.6 m. At wave lengths of 0.8 m and 1 m, however, all three types of oil platforms are more stable. The reason for this is that the wave’s frequency increases as its length decreases. When there are more high-frequency waves, the oil platform will move more erratically. This condition describes the events depicted in Fig. 16.8.

At the start of the test, the graph in Fig. 16.9 shows that, when each oil platform had only four mooring lines. These results showed that all of the platforms moved around a lot and were not stable. But when the mooring line is added to 8, the oil platform model becomes more stable compared to the first experiment. When more mooring lines are attached to an oil platform, the platform becomes more stable and steadier. This was demonstrated in this experiment, and the jacket platform was the most stable oil platform in this experiment. The jacket platform is more stable than the other two because its structure is more stable and stronger. This lets it support the plant’s weight better.

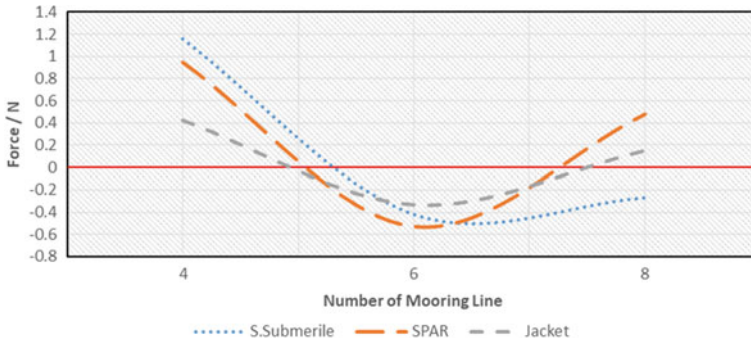


Fig. 16.9 Scatter graph for all platform reacted to different number of mooring line

16.4 Conclusion

The purpose of this research was to compare the capabilities of spar platforms, semi-submersible platforms, and jacket platforms in respect to certain oceanographic factors. These factors included the wave frequency, wave amplitude, wave length, water depth, and the number of mooring lines that were attached. Every sort of oil platform on our globe performs a specific purpose and boasts a unique set of qualities. The owner of an offshore platform must know several things before beginning construction: where the platform will be located, how deep the water will be, how the wave pattern will be at that point, what kind of seabed will be there, and what kind of work the platform will be expected to perform. Some oceanographic variables that had already been set were used in this experiment. Wave frequency, wave amplitude, wave length, water depth, and the number of mooring lines were some of these variables. This experiment also used a wave tank at KKTM Kemaman that was 10 m long, 4 m wide, and 1.3 m high.

It is clear from looking at the results that the experiment parameters led to large variations across runs. To facilitate easier and more precise data analysis, it is common practice to first tabulate the data and then compare the data in the form of graphs.

The experiment reveals that the jacket platform is the most stable option since it makes the best use of the oceanographic variables that were used in the experiment. The behavior of the jacket platform is found to be much more stable when the wave hits the structure.

By contrasting the plots, we were able to determine that the wave frequency and wave amplitude are the two variables primarily responsible for the observed differences in output. When either the wave frequency or the wave amplitude is high, the oil platform is more likely to become unstable.

This experiment was effective in determining the optimal design and operation of an oil platform. The equipment used in this experiment was carefully selected to keep costs to a minimum.

Acknowledgements We would like to thank everyone who played a part, whether directly or indirectly, in the completion of this study, as it is one of the requirements that must be fulfilled by the researcher who is supported by UniKL MIMET with assistance from professionals. As the paper's authors, we appreciate the readers' constructive criticism and new points of view.

References

- Devold H (2015) Oil and gas production handbook: an introduction to oil and gas production, transport, refining and petrochemical industry. ABB AS, Oslo
- Gulen G (2016) Importance of midstream in oil and gas resource development. Curr Sustain/Renew Energy Reports. <https://doi.org/10.1007/s40518-016-0049-x>
- Joshi P et al (2017) Supply chain innovations in the oil and gas industry. IISE 3:1852–1857
- Sadeghi K (2007) An overview of design, analysis, construction and installation of offshore petroleum platforms suitable for cyprus oil/gas fields. J Soc App Sci 2(4):1–16
- Sharma R (2019) An introduction to offshore platforms. IIT Madras. <https://doi.org/10.13140/RG.2.2.31319.21925>

Chapter 17

Soil Nutrient and Management in Oil Palm Plantations and Agronomic Potential of Biochar



Arasu Uttran, Soh Kheang Loh, Muhammad Ahmad,
and Robert Thomas Bachman

17.1 Introduction

The traditionally practiced slash-and-burn agriculture is still common in the humid tropics (Loh 2017), causing seasonal air pollution and more frequent weather extremes. The key difficulties facing world agriculture in the coming decades are growing capacity to produce food for an additional 2.3 billion people by 2050 (FAO) and managing limited natural resources more effectively (Morgan and Connolly 2013).

The oil palm industry still faces challenges in meeting the required global oil demand by 2050 (Corley and Tinker 2016). The current solution primarily relies on land clearing, which appears to be devastating in the long run. Future strategies must not only investigate improving further the oil palm yield via biotechnological means but also enhancing soil biodiversity and reducing GHG emissions.

A. Uttran (✉)

Department of Chemical Engineering, School of Engineering and Computing, Manipal International University, Nilai, Negeri Sembilan, Malaysia
e-mail: arasu.uttran@miu.edu.my

S. K. Loh

Energy and Environment Unit, Engineering and Processing Division, Malaysian Palm Oil Board, Kajang, Selangor, Malaysia
e-mail: lohsk@mpob.gov.my

R. T. Bachman

Malaysian Institute of Chemical and Bioengineering Technology, Universiti Kuala Lumpur, Alor Gajah, Melaka, Malaysia
e-mail: bachmann@unikl.edu.my

M. Ahmad

Department of Chemistry, University of Sahiwal, Sahiwal, Pakistan
e-mail: m.ahmad@uosahiwal.edu.pk

According to Yahya et al. (2010) and (Chiew and Abdul 2002) the use of pesticides and fertilisers in the cultivation of oil palms has significant impact on their production and use of palm biodiesel as a fuel. The related GHG emissions are mainly attributed to uncontrolled release of pesticides during oil palm nursery stage and N fertiliser production. Palm biodiesel produced has a superior life cycle performance compared to *B. napus* (Gandahi and Hanafi 2014), *Jatropha curcas* (Kee et al. 1995) and hydrotreated *B. napus* (Chek et al. 2013).

Biochar is a product of biomass pyrolysis or gasification and is intended for non-fuel applications such as soil remediation. Benefits of using biochar in low fertility mineral soils include improved biomass yield (Omoti et al. 1983; Sogbedji et al. 2001; Blanchart et al. 2005), reduced nutrient loss (Noble et al. 2001; Vengadaramana and Jashothan 2012; Croker et al. 2004), sorption of pesticides (Noble et al. 2000; Siththaphanit et al. 2010; Certini 2005), sorption of phosphate (PO_4^{3-}), nitrate (NO_3^-) and ammonium (NH_4^+) (Jones et al. 2013; Prieto-Fernandez et al. 1993; Sharpley et al. 2001), high nutrients adsorption reusability (Cade-Menun et al. 2000), increased soil pH and water retention (Serrasolsas and Khanna 1995; Kong et al. 2019), suppression of N_2O release (Noble et al. 2001) and acting as a net carbon sink thus mitigating the global warming effect (Shamala and Idris 2009; Naher et al. 2012). Biochar performance in soil is highly variable depending on application rate, feedstock type, pyrolysis temperature and holding time, climatic zone, soil and plant species (Serrasolsas and Khanna 1995; Basu et al. 2018). Table 17.1 summarizes the physicochemical properties of biochar.

Transport distance significantly affects the economic profitability of the intended biochar-pyrolysis system (Jeffries et al. 2003). The environmental impact of biochar compared for conservation versus conventional agriculture in Zambia and confirmed that biochar used in the former is beneficial for climate change mitigation provided that cleaner biochar production technology is adopted to reduce hazardous emissions (Borowicz 2001).

This review aims to provide an overview of the current nutrient management practice in oil palm nurseries and plantations. The second part discusses biochar as a novel tool in nutrient management. At present, there are no publicly available data on biochar performance for oil palm plantations. Data from other crop systems were adopted and used whenever appropriate.

17.2 Nutrient Management in Oil Palm Plantations

The demand for sustainable palm oil as food source has driven oil palm farmers in Southeast Asia to innovate and modify their cultivation methods. The rapidly developed oil palm planted areas have increased the use of land, fertilizers, and labor. It is thus pertinent to implement GAP, establish and standardize optimal crop and nutrient management practices to achieve highest possible oil yield and profitability (Tinker and Nye 2000; Fall et al. 2022).

Table 17.1 a Summary of physical properties of biochar in influencing soil characteristics.
b Summary of chemical properties of biochar in influencing soil characteristics

(a)	
Physical property	Source(s)
Water-holding capacity A combined biochar and coal-derived humic substances increases stability of degraded soil Sandy soil mixed with biochar improves water content	Chen et al. (2009)
Bulk density Biochar changes soil hydrology due to changes in porosity and aggregation The resulted aggregation is preferential by soil organic matters and microorganisms	Azeem et al. (2016), Kasozi et al. (2010)
Soil aggregation Caused by biochar surface charge characteristics upon weathering and affected by overall soil pH Promotes water infiltration and increases water moving through	Kuppusamy et al. (2016), Chen et al. (2009)
Porosity Depends on parent material under the intended conditions: Macropores (> 80 μm)—rapid flow rate through soil and throw in leaching actions, Mesopores (30–80 μm)—water moves in to different soil matrix, Micropores (< 30 μm)—hold water in place	Dünisch et al. (2007), Chen et al. (2009)
Particle size Leaching of organic and inorganic nutrients sorbed to larger biochar particles may be reduced or facilitated by colloidal movement through soil profile Negatively charged colloids facilitate downward migration of metals and organic pollutants through soil	Chen et al. (2009)
(b)	
Chemical property	Source(s)
Cation exchange capacity (CEC) Aged biochar tends to have higher CEC due to high concentration of negative charges on biochar surface and sorption of charged organic matters to biochar surface	Kasozi et al. (2010)

(continued)

Table 17.1 (continued)

(b)	
Chemical property	Source(s)
Oxidation Abiotic process increases oxidation of fresh biochar > biotic process in short term Higher temperature leads to oxidation and negative charge on deeper layer of biochar Fresh biochar (lower surface oxidation) is hydrophobic and tends to adsorb hydrophobic molecules such as organic contaminants	Kuppusamy et al. (2016), Chen et al. (2009)
Nutrient adsorption Biochar adsorbs larger amount of NPK than fresh biomass feedstock Chicken litter biochar (500 °C, activated): effluent (1:100) removes 52% P in a dairy farm Sewage sludge biochar (700 °C) contained less N but more P and K release as well as less water-soluble N, and more water-soluble P and K	Kuppusamy et al. (2016), Chen et al. (2009)
Chemical compositions Determines the following: Volatility, Relationship between H/C and O/C ratios, Surface functional properties, Carbon sequestration potential, Macro- and micro-nutrients availability	Mukherjee and Rattan (2013), Chan et al. (2007)
Electrical conductivity Indication of nutrient bioavailability or presence of excess ash/salt Charges surface active site for nutrient adsorption and microbial rejuvenation	Lehmann et al. (2003)

17.2.1 Nutrient Uptake Mechanism

Plants absorb nutrients via diffusion from the surrounding liquid phase through root systems to the surface of the root. This is followed by passive and active uptake mechanisms across the plasma membrane (Sundram 2010). The uptake mechanisms of most essential nutrients are complex, and their amounts depend on plant's requirements and other factors (Tinker and Nye 2000).

The distribution of the root system in soil influences nutrient uptake, root nutritional composition and root-soil relation (Tinker and Nye 2000). As a monocotyledon plant, oil palms have main roots developed from the bottom of the thickened trunk. The primary roots carry secondary roots (2–4 mm diameter) which in turn produce branched tertiary and quaternary roots (0.1–0.3 mm diameter and 1–4 mm long) (Yahya et al. 2010).

EFB can increase the proliferation of three-year-old DxP palms roots at a depth of 30–45 cm. While individual root orders were not significantly affected, root proliferation in soil environment treated with EFB improved significantly ($p < 0.05$) at 15–45 cm soil depth (Sundram et al. 2015). Besides, the oil palm root tip was significantly more active ($p < 0.05$) than other parts of the primary roots in nutrients absorption (Phosri et al. 2010) thus showing evidence that the fibrous quaternary and tertiary fine roots (diameter ≤ 2 mm) are responsible for nutrient uptake (Blal et al. 1990) while those of primary and secondary roots function as nutrient transporter.

17.2.2 Organic Nutrients in Oil Palm Plantations

Organic nutrients derived from decomposing biomass can be used as organic fertilizer (Ramlah Ali and Dolmat 1991). Mulching of oil palm biomass retains soil moisture, maintains soil temperature, and slowly releases vital nutrients when the biomass undergoes microbial decomposition. This practice improved oil palm yields by 3–35% (Al-Karaki 2013; Mukherjee and Rattan 2013).

Table 17.2 summarizes the nutrient content of EFB. Authors of Blal et al. (1990) reported that mulching with 37 t ha^{-1} of EFB was sufficient to complement current inorganic fertilizer manuring practices. Mulching with EFB could increase the amount of phosphorus (P) in Rengam soil and stimulate the formation of microbial biomass P (4 times more) than that added with phosphate fertilizer alone, but less movement into the inorganic P fractions. On top of that, EFB mulching reduces soil erosion and prevents rain splatter (Chan et al. 2007).

Direct mulching of EFB also causes several problems and has limitations. If EFB stacking is not properly done can lead to rhinoceros beetles which may reduce FFB yield due to beetles' infestation and kill both seedlings and young trees (Chan et al. 2007). Placing them on top of soil also increases the fire and haze risk during prolonged dry weather spells (Chan et al. 2007). Most of the time, the mineralised N could be immobilized by microorganisms, retained by EFB via surface adsorption or lost through NH_3 volatilization and denitrification (Laird et al. 2010).

Some of these drawbacks may be reduced if EFB is composted prior to application using: (1) resistant earthworms (Koe et al. 2001), (2) filamentous fungi (Haryati et al.

Table 17.2 Nutrient content in empty fruit bunches from various sources (Chiew and Abdul 2002)

Nutrient content (%) on dry weight				
Source	N	P	K	Mg
	0.35	0.03	2.29	0.18
	0.34	0.03	2.21	0.17
	0.80	0.10	2.40	0.20
	0.25	0.08	2.03	0.23
Mean	0.44 ± 0.23	0.06 ± 0.03	2.23 ± 0.56	0.20 ± 0.02

Table 17.3 Oil palm empty fruit bunches (OPEFB) and palm oil mill effluent (POME) composting by various techniques (Chen et al. 2009)

Substrates	Microbial systems	Controlling parameters
Palm press fibre, poultry layer deep-litter and broiler floor-litter and urea	Inoculated by bacteria and fungi	Temperature, moisture, C/N, etc
OPEFB, goat dung, cow dung and chicken manure	Inoculated by bacteria, fungal	Temperature (70 °C), C/N (35:1), pH (5.4), etc.
OPEFB	Natural degradation	C/N (30)
OPEFB, fermentation liquid waste and chicken manure and POME	Natural degradation	Moisture (56%), C/N (41, open; 56, closed), etc.
OPEFB, POME and wheat flour	Inoculated by <i>P. Chrysosporium</i> , <i>T. Harzianum</i> , <i>A. niger</i> and <i>Penicillium</i>	pH (5–7), moisture content (60–70%), temperature (30 ± 2 °C), etc.
OPEFB and rice straw	Inoculated by <i>Trichoderma harzianum</i>	Fortified or unfortified
OPEFB and POME	Inoculated by bacteria species	Temperature (> 50 °C), moisture content (65–70%), etc.
OPEFB and POME	Natural degradation	With/without decanter cake slurry

2018) and (3) palm oil mill effluent (POME) (Uttran et al. 2018). Co-composting is accomplished by spraying liquid POME onto EFB at a rate that enables both wastes to be rotten and digested efficiently by microorganisms, while most of the liquid is evaporated towards the end. The good quality compost has a C/N ratio of ≥ 15 –20 (Abdul and Deraman 2013). In recycling by-products of oil palm, the EFB and POME are composted under a controlled environment using different microbial systems (Table 17.3) and mulched as an organic nutrient source for oil palm cultivation. The compost produced can supply N and P (66% and 37%) more effectively than inorganic fertilizer (Md-Som et al. 2013). However, co-composting via windrow method commonly yields a low-quality compost and requires a large processing area. Alternatively, EFB can be converted into biochar, which helps increasing its bulk density, enriching labile carbon for bio sorption, and reducing storage space.

17.2.3 Inorganic Nutrients in Oil Palm Plantations

According to Zainal et al. (2018), the oil palm industry in Malaysia consumes more than 75% of imported inorganic fertilizers (N, P, K and Mg). Soil N can be derived from organic and inorganic fertilizers, bacterial fixation, and atmospheric deposition (Corley and Tinker 2016). The commonly used N fertilizers in oil palm plantations

are ammonium sulphate (AS) and urea for coastal soils. CIRP is most used for oil palms planted on soil with $\text{pH} < 6$ (Chek et al. 2013).

The K compound fertilizer currently in use (KCl or MOP) contains 60% K and is one of the most expensive (Tiraieyari et al. 2014). The cheapest Mg fertilizer source is magnesium sulphate or kieserite which contains 26% Mg. Table 17.4 summarizes the common fertilizers used for oil palm and their nutrient levels.

The nutritional requirements to generate 30 t FFB ha^{-1} are met by an annual application of 4.2 kg AS, 2.7 kg MOP, and at least 5 kg CIRP per oil palm. Additional CIRP is needed to make up for the P immobilised on Al and Ca complexes in the soil, which affects the oil palms' ability to recover PO_4^{3-} (Rugayah et al. 2014).

17.2.4 Nutrient Application System in Oil Palm Plantations

Fertilizer may be applied manually, mechanically and/or using air but the latter is not practiced nowadays due to various shortcomings. Satellite navigational systems may be used for varying application rates with pre-determined parameters. Mechanical broadcasting is commonly used for large, matured oil palm areas where palm rows are easily accessible.

17.2.5 Nutrient Movement and Losses

Fixation of N by microorganism in soil reduces atmospheric N_2 to NH_4^+ . Nitrogenase in prokaryotes is responsible to convert N_2 gas into NH_4^+ but not all organisms contain this enzyme. N is typically present in soil as NH_4^+ , NO_3^- and organic N (Atkinson et al. 2010).

In the presence of oxygen, organic C can be reduced by anaerobic oxidation of organic C to either NH_4^+ (dissimilation) or N_2 (denitrification). The by-product in this process— N_2O —is a potent GHG both in marine and terrestrial environments (Jeffery et al. 2011).

Nitrogen losses from soil can be in the form of a gas (volatilization of NH_3 or denitrification of NO_3^-), or as a solute in runoff through flow or drainage. Soils with low organic matter and pH are net positively charged and adsorb negatively charged NO_3^- , hence reducing nutrient leaching from the root zone (Salt 2004).

P exists in soil as PO_4^{3-} sourced from fertilizer, rainfall, plants, and animal wastes. Movement of P only happens in coarse-structured soil due to high infiltration of water and sandy soil lacking P-sorption sites. Soil with high organic content might also reduce P sorptivity due to organic anions coated active sites for P adsorption (Salt 2004). Other nutrient such as K, Ca and Mg availability factors are summarized in Table 17.5.

Table 17.4 Commonly used fertilizers for oil palm plantation

Nutrient source	Main nutrient	Nutrient content (%)								
		N	P ₂ O ₅	K ₂ O	MgO	CaO	B	Cu	S	Cl
<i>Straight fertilizer</i>										
Urea	N	46	–	–	–	–	–	–	–	–
Ammonium nitrate	N	35	–	–	–	–	–	–	–	–
Sulfate ammonia	N, S	21	–	–	–	–	–	–	–	–
Diammonium phosphate	N, P, S	18	46	–	–	–	–	–	–	–
Rock phosphate	P, Ca	–	30	–	–	45	–	–	–	–
Triple super phosphate	P, Ca	–	46	–	–	20	–	–	–	–
Single super phosphate	P, Ca, S	–	18	–	–	25	–	–	11	–
Muriate of potash	K, Cl	–	–	60	–	–	–	–	–	35
Sulfate of potash	K, S	–	–	50	–	–	–	–	17	–
Langbeinite	K, Mg, S	–	–	22	18	–	–	–	22	–
Kieserite	Mg, S	–	–	–	27	–	–	–	23	–
Dolomite	Mg, Ca	–	–	–	22	30	–	–	–	–
Sulfur	S	–	–	–	–	–	–	–	97	–
Sodium borate	B	–	–	–	–	–	11	–	–	–
Copper sulfate	Cu	–	–	–	–	–	–	25	13	–
<i>Compound fertilizers</i>										
12-12-17-2	N, P, K, Mg	12	12	17	2	–	–	–	–	–
15-15-6-4	N, P, K, Mg	15	15	6	4	–	–	–	–	–
15-15-15	N, P, K	15	15	15	–	–	–	–	–	–
<i>Palm residue^a</i>										
Bunch ash	K, Mg, Ca	–	4	40	6	5	–	–	–	–
Empty fruit bunches	N, K	< 1	0.1	1.2	0.1	0.1	–	–	–	–
Pruned fronds	N, P, K	0.5	0.1	0.8	0.1	0.2	–	–	–	–
Palm oil mill effluent	N, K, Mg	0.4	0.2	1.3	0.4	–	–	–	–	–

Note^a Palm residue nutrient contents are given on a fresh weight basis. Thus, 30 t OPEFB delivers about 100 kg N, 12 kg P, 300 kg K, 20 kg MgO and 21 kg Ca

Table 17.5 Factors that affect potassium, calcium, and magnesium in soil (Kasozi et al. 2010)

	Factors affecting availability
Potassium (K)	<ul style="list-style-type: none"> • Amount of K available in the soil • Highly weathered clay soil has low cation exchange capacity (CEC) and exchangeable K may be limited in these soil • K moves through soil by diffusion, too much moisture in the soil results in K leaching • Warm temperature of soil accelerates the release of K, and K becomes more available at higher temperature • Ample oxygen is needed by plant to uptake K • Under acidic conditions: Al and Mn toxicities lead to poor root formation which prevent K uptake. Limed acidic soil results in higher exchangeable K due to increase of CEC • If Ca and Mg are abundant in the soil, the K saturation on CEC is reduced due to high competition with Ca and Mg
Calcium (Ca)	<ul style="list-style-type: none"> • Soil with low CEC is low in Ca • Acidic soil tends to be low in Ca due to high Al saturation • If the CEC contains < 25% Ca, it is recommended that Ca should be applied to the soil
Magnesium (Mg)	Similar to Ca, Mg is limited in soil that is: <ul style="list-style-type: none"> • Low in Mg • Acidic • High in leaching • Limed with non-Mg material • Contains other cations such as K, Ca, NH_4^+ which compete with Mg

17.2.5.1 Management of Vegetation and Fertilization

Deep roots of plants and trees serve as a “protection net,” bringing nutrients that have been leached and moved to deeper soil horizons back to the surface. Leaching is influenced by the horizontal and vertical distribution of roots in soils that are intercepting and absorbing nutrients. The nutrient efficiency varies among plants as well as the soil condition for the plant (Allen et al. 2004).

A central Amazonian upland soil’s N bioavailability was assessed after it sustained a fruitful oil palm plantation for 15 years without N fertilisation. It was discovered that the mineral N concentration in the upper 2 m was extremely low adjacent to the palm trees, indicating that the palms were effectively absorbing N (Manyà 2012). Atkinson et al. (2010) investigated the effect of fertilizer placement from palm trunk. Result showed that the FFB yield of broadcasting placement 13% higher compared with subsoil placement. As in broadcasting placement, the roots have higher contact with the fertilizer and more efficient nutrient uptake.

Leaching either via batch or continuous process is an important assessment for nutrient cycling in agriculture (Croker et al. 2004). Leaching can result in up to 80% of the applied N nutrients being lost from the rooting zone (Kuppusamy et al. 2016). Large proportion of nutrient losses poses an economic issue concerning fertilizer use efficiency and soil nutrient stocks depletion. Nutrients leached into a river or lake

such as P cause eutrophication resulted in unacceptable water quality (Mia et al. 2017; Lehmann et al. 2003).

According to Mia et al. (2017), factors affecting leaching in soil such as management of vegetation and fertilization, soil structure and texture, rainfall patterns, soil and soil solution chemistry, soil biology and nutrient cycles should be considered first before biochar is added into the soil.

17.2.5.2 Soil Structure and Texture

Soil structure comprises of micro- and macro aggregations depending on the arrangement of primary soil particles into secondary units. Soil aggregates of $< 250 \mu\text{m}$ are microaggregates consisting of plant roots and humin joined together by microbial activity, plant root exudates and actions, fungal hyphae, and earthworm casts. Microaggregate soils are more typically found in disturbed or cultivated soils, and vice versa for macroaggregate soils.

Soil porosity is important to determine the rain infiltration rate and amount of nutrients carried away from the rooting zone. Small pores in soil retain soil solution by capillary force thus reducing leaching and crops water stress. Water percolation rapidly occurs under wet soil conditions but decreases significantly underneath due to lesser macroporosity. Organic N comprising 36–44% of the total N could percolate faster than $\text{NO}_3\text{-N}$ from the topsoil (Dünisch et al. 2007). In general, as biochar contains sufficient organic matter, its presence can reduce soil porosity and increase water retention (Sara de Jesus et al. 2019); hence reducing soil water percolation and leaching of plant nutrients.

17.2.5.3 Rainfall Patterns

Biochar will be effective in reducing leaching losses in regions experiencing higher rainfall. Rainfall patterns are site-specific and influenced by topography and global warming. Changes in weather influence the rainfall patterns which altered the leaching forms at affected sites. The total environmental N losses (denitrified and leached N) increased as the rain precipitation increased for all types of soil.

Soil moisture dynamics are crucial in influencing nutrient-plant canopy interaction. Precipitation variability closely relates to bioavailability of extractable $\text{NO}_3\text{-N}$, $\text{PO}_4\text{-P}$, Ca, Mg and K in soil. As annual precipitation increases, leaching of nutrients becomes more severe, which reduces plant productivity and therefore profitability (Cheng et al. 2006).

17.2.5.4 Soil and Soil Solution Chemistry

The soil chemistry such as soil minerals, clay content and organic matter affects soil leaching. Sandy soil amended with high CEC materials such as bentonite improves

plant biomass growth. However, the nutrient loss mechanisms in clay-amended sands under high rainfall regime needs further investigation (Crocker et al. 2004; Noble et al. 2001).

Column experiments on sandy soil (1.4% clay) amended with clay and bentonite showed total leached $\text{NO}_3\text{-N}$ concentration of 24.3–24.6 mg per column. Addition of bentonite reduced $\text{NH}_4^+\text{-N}$ and total N leachate by 44–49% and 52–67%, respectively, compared to clay and control treatments. This soil was very low in organic matter (0.71%), had limited microbial activity and the nitrification process was slow possibly due to low pH (4.92 with 0.01 M CaCl_2) (Sitthaphanit et al. 2010).

17.2.5.5 Wildfire Effect on Soil Fertility

On soil, wildfires have a variety of effects. They result in a decrease in organic matter, modifications to the soil's structure and porosity, nutrient losses due to volatilization, leaching, erosion, and microbial activity. Complete oxidation of soil organic matter takes place at higher temperature while at 220 °C approximately 37% of organic matter will be lost (Sitthaphanit et al. 2010).

Soils exposed to fire change the pH to almost neutral, resulting in an enrichment of soil P. Burning of soil organic matter converts P into PO_4^{3-} and tends to chemisorb with Al, Fe, and Mn oxides in acidic soils (Cade-Menun et al. 2000; Serrasolsas and Khanna 1995). In neutral or alkaline soils, it binds to Ca-minerals or precipitates out as Ca-phosphate (Certini 2005).

Biochar can be used to create soil that is rich in organic matter and has a large surface area (i.e. exposure of more charged active site) in enhancing the porosity, pH, CEC and water retention capacity of poorer quality soils. It can also reduce nutrient losses and slowly release them to the crops under cultivation (Kong et al. 2019; Dominguez et al. 2020).

17.2.5.6 Soil Biology and Nutrient Cycling

Soil biology relates to microbial activities in soil which are crucial for nutrients uptake of plants and decomposition of bioresidues which then can be accessible to plants.

Basal stem rot (BSR) has been a major problem in oil palm plantations. The *Ganoderma* responsible for BSR attacks matured palms and reduces their productivity. Biological control agent such as *Trichoderma* has been studied to suppress the *Ganoderma* (Shamala and Idris 2009). Another beneficial microorganism for oil palm is arbuscular mycorrhizal fungi (AMF) are present abundantly in natural communities and associate with > 80% of vascular plants (Basu et al. 2018) and play major roles in plant-soil symbiosis (Jeffries et al. 2003). AMF plays an important role in soil formation and contributes to the formation of macroporous soil structures that enhance penetration of water and air and prevent erosion. Most plants could benefit

from AMF activities in soil, but some crops do not respond strongly to inoculation with AMF (Jeffries et al. 2003).

Basal stem rot (BSR) has been a major problem in oil palm plantations. The *Ganoderma* responsible for BSR attacks matured palms and reduces their productivity. Biological control agent such as *Trichoderma* has been studied (Shamala and Idris 2009) to suppress the *Ganoderma*.

An inoculation of *T. Harzianum* (strain FA1132) is capable of controlling BSR disease, also enhances chlorophyll concentration and the weights of oil palm root and leaf (Naher et al. 2012). Another beneficial microorganism for oil palm is arbuscular mycorrhizal fungi (AMF). AMF are present abundantly in natural communities and associate with 80% of vascular plants (Basu et al. 2018).

AMF play a key role in plant-soil symbiosis as they are involved in nutrient acquisition, plant diversity and nutrient cycling (Jeffries et al. 2003; Borowicz 2001). It seems that most plants could benefit from AMF activities in soil. However, in some cases major food crops do not respond strongly to inoculation with AMF (Naher et al. 2012). The combination of AMF and bacteria may have caused a large carbon outflow from the host plant due to severe competition. Sundram (2010) investigated the effect of different AMF mixtures on oil palm growth. There were significant changes in K levels in leaves, but no differences in N and P levels (Sundram 2010; Sundram et al. 2015).

Oil palm plantations have the potential to make oil palm plantations more sustainable and lessen the effects they may have on the ecosystems. When N and P fertilizers are applied in the field, the P uptake is mostly low and largely escapes into water running out of the plantations. The excessive P in surface water might change the natural biodiversity (Phosri et al. 2010).

AMF have been increasingly deployed in agriculture to improve crop yield, health, and soil biological equilibrium (Sundram et al. 2015). Oil palm growers in Malaysia have adopted AMF application in the pre-nursery before transferring seedlings to plantations. AMF colonizes oil palm roots which will help to enhance ecosystem functions later (Chek et al. 2013). This is evident in oil palms planted on tropical acidic soils that grow well with the help of AMF (Blal et al. 1990).

Inoculation of oil palm seedlings with commercial mycorrhizal products at nursery stage offers a threefold higher growth over untreated palms without fertilizer addition (Al-Karaki 2013). Sundram et al. 2015 showed that the *Ganoderma*-infected palms that were inoculated with a combined AMF and endophytic bacteria biocontrol agent could reduce BSR disease by 80%.

Incorporating biochar into soil alters its physical and chemical characteristics (Mukherjee and Rattan 2013; Chan et al. 2007). High surface area of biochar provides space for formation of bonds and complexes with cations and anions of metals and elements in the soil (Arvidsson et al. 2011; Karananidi et al. 2020). Biochar-amended soils show significantly lower bulk density compared to soil without biochar amendment (control) in a column incubation study (Laird et al. 2010).

17.3 Biochar as a Tool in Soil Nutrient Management

17.3.1 Oil Palm Biomass as Biochar Sources

Biochar can be produced from solid bioresidues generated in oil palm plantations and during palm oil milling activities such as OPEFB. Biochar can undergo thermal de-composition under limited supply of oxygen, often at relatively low temperatures (700 °C) (Renck and Lehmann 2004).

As discussed in Sect. 2.2, current GAP is to place pruned OPF on the lips of terraces and apply EFB around young and matured palms to conserve moisture and prevent erosion (Murdi et al. 2011). But improper mulching and disposal practices of these materials also prompt fire hazards, leading to severe haze that releases biomass carbon which in turn might threaten human health. This is especially serious during prolonged dry weather spells (Koe et al. 2001).

An emerging alternative to such practices in oil palm plantations is converting the derived bioresidues into good quality biochar as a soil conditioner. The produced biochars' sorption-relevant properties (e.g. fixed carbon, pH and BET surface area) can be tailor-made to meet specific agriculture needs as potential remedial sources for soil amendment and carbon sequestration (Jones et al. 2013; Prieto-Fernandez et al. 1993; Mukherjee and Rattan 2013; Chan et al. 2007; Lehmann et al. 2003).

Research has shown potential conversion of OPEFB into activated carbon, carbon electrode and molecular sieve carbon. Carbon pellets have high density, porosity, Young's modulus, Rockwell hardness and electrical conductivity comparable to those of commercial carbon electrodes such as Filtra Sob (Abdul and Deraman 2013).

The produced biochar using various methods (Md-Som et al. 2013; Karananidi et al. 2020; Kong et al. 2019; Haryati et al. 2018; Rugayah et al. 2014) showed an increase in pH, electrical conductivity, organic matters, and liming capacity. A growing number of studies and reviews are available on the production and characterization of biochar as well as the measurement of the environmental and agronomical benefits (Atkinson et al. 2010; Jeffery et al. 2011; Lehmann et al. 2011; Meyer et al. 2011; Manyà 2012; Kuppusamy et al. 2016; Mia et al. 2017).

In the following sections, the effects of biochar on nutrient leaching, crop yield and soil biota are reviewed in the context of direct or indirect contribution towards more sustainable oil palm plantation practices.

17.3.2 Biochar Effects on Nutrient Leaching

Charcoal-amended soil increased cowpea biomass production and nutrient uptake via inorganic nutrients such as K, P, Ca, Zn and Cu. Long-term experiments would be needed to establish any post-ash leaching effects of charcoal on bio-mass yield. Ratios of nutrient uptake to leaching increased when charcoal was applied (Lehmann et al. 2003). The OPKS based activated carbon could remove up to 80.7% chemical

oxygen demand of POME, on par with commercial activated carbon (81.5%). It has potential to be an adsorbent to retain nutrients based on its high adsorption capacity. But whether it has capability to slowly releasing the nutrients when required by plants remains uncertain (Shamala and Idris 2009; Fall et al. 2022).

Smaller particles of wood-based biochar retain more nutrients which can be attributed to the fact that smaller particles have a higher specific surface area. Biochar from agricultural residue (*Miscanthus giganteus*) has lower water storing capacity as increasing in particle size (Dünisch et al. 2007). Fresh biochar's oxidation is probably not advanced enough to produce as many negative surface charges in soil as it does in incubators or mature biochar (Cheng et al. 2006).

Biochar may have the ability to minimise leaching of N in deep soil which leads to significant increases in crop yields. The data only allowed for an estimation of N losses because unrecovered N fertiliser may have evaporated or leached below 0.1 m. A higher crop production resulted from an enhanced N retention in compost added plots whereas with biochar more N remained in soil (Renck and Lehmann 2004).

Similarly, bamboo charcoal can adsorb NH_4^+ largely by cation exchange and shows significant difference at various soil depths (multilayered) (Ding et al. 2010). Author of Steiner et al. (2004) reported that nutrients such as P, K, Ca and Mg were higher in charcoal-amended plots even though big amounts of these nutrients were removed from soil in the form of harvested plants. In addition, adding biochar from (*Quercus* spp. and *Carya* spp.) to agricultural soil in the Midwest prevented nutrient leaching and could be a useful strategy for nutrient management in farming. Total N and dissolved P leaching were both reduced by 11% and 69% in the column that received manure and 20 g kg^{-1} of biochar (Laird et al. 2010).

Author of Yao et al. (2012) reported that pyrolyzed sugarcane bagasse (BG), peanut hull (PH) and Brazilian pepperwood (BP) at 600 °C could remove NO_3^- from aqueous solution. Five biochar's produced at different pyrolysis temperatures had the ability to remove PO_4^{3-} with the highest removal efficiency of 3.1%. PH600 and BP600 having good sorption ability were applied in sandy soil at 20 g biochar kg^{-1} soil. In another study, biochars produced from Laurel oak, Loblolly pine and Gamma grass were aged by exposing the biochar containers to rain for 9 months. NH_4^+ and NO_3^- were most abundant in the leachates of soil treated with some biochar. The nutrient release trends of aged and fresh biochars were similar in terms of increased nutrient release from grass versus oak and low versus high temperature biochars (Mukherjee and Zimmerman 2013).

Soil amended with giant reed biochar reduced the cumulative leachate volume by 2.9–11.4% and 7.0–15.4% in NH_4^+-N and $\text{NO}_3^- -\text{N}$. The soil with plant treatments had significantly lowered the total leachate volume compared with control. Biochar addition significantly decreased cumulative $\text{NO}_3^- -\text{N}$ leaching ($p < 0.05$) (Zheng et al. 2013). The proportion of fixed N was 50% in controls (no biochar) and 72% in soil receiving 90 g kg^{-1} biochar produced from logs of *Eucalyptus deglupta*. In soil treated with 90 and 60 g kg^{-1} biochar, respectively, bean yield and biomass output rose by 46% and 39%, respectively. However, when biochar application was raised to 90 g kg^{-1} biochar, the biomass and overall N uptake dropped. Although the results show that applying biochar can reduce the amount of nitrogen in the environment,

overdose can be seen. Long-term R&D is also necessary to have a better knowledge of the impact of biochar on N_2 fixation (Rondon et al. 2007).

Biochar produced from wheat at 525 °C via slow and fast pyrolysis ($> 250 \text{ °C s}^{-1}$) showed that immobilized mineral N was higher (43%) in soil treated with fast biochar as fast biochar was not completely carbonized (Bruun et al. 2012). So far, the data indicate that biochar produced at lower temperatures and fast heating rates has the tendency to adsorb organic and inorganic molecules preventing inorganic nutrient leaching losses.

17.3.3 Biochar Effect on Crop Yield

Studies on the effect of biochar on nutrient uptake are associated with crop productivity. Steiner et al. (2004) reported that the yield of maize grain doubled when planted on forest wood-derived charcoal amended soil in the presence of NPK fertilizer compared with NPK fertilizer only. Another study conducted by Reichenauer et al. (2009) 2 t of rice husk charcoal were applied per hectare of tsunami affected paddy fields in Sri Lanka. Soil treated with rice husk biochar showed the highest number of tillers. The total dry biomass, plant height and productive tillers grown in organic or biochar-amended soil were significantly higher ($p = 0.05$) compared to those of the untreated soil.

By adding biochar at a rate of 1 t ha^{-1} on dry land together with banding to minimize wind erosion risk, some positive effects on wheat fertilizer requirement and yield were observed. Banded biochar increased grain yield by 17% when the fertilizer dose was reduced to half compared with that without biochar added into soil (Blackwell et al. 2010).

When biochar enriched with 15N (biochar- NH_3 complex) was added into soil, the dry matter yield of leaf and root increased by two- to threefold. There were no differences in yields with and without adding biochar into the soil (Taghizadeh-Toosi et al. 2012). Pot experiment conducted by Zheng et al. (2013), the total seedling biomass was significantly higher in biochar (from giant reed)-amended soil compared to control. In general, addition of biochar to soil shows some positive effects in crop yields and productivity (Kong et al. 2014).

17.3.4 Biochar Effect on Microbial Population and Activity

Microbial population in biochar-amended soil has been determined using various methods (Grossman et al. 2010; Halmi and Simarani 2021; Steiner et al. 2004, 2007; Azeem et al. 2016). The two microorganisms' reproduction rate most affected by biochar presence in soil are AMF and ectomycorrhizal fungi (Warnock et al. 2007). Table 17.6 lists the possible mechanisms of microbial response on biochar addition to soil. Biochar showed both advantages and disadvantages in responding to microbial

Table 17.6 Summary of possible mechanism by which microbial abundance is affected by biochar additions to soil (Lehmann et al. 2011)

Mechanism	Rhizobia	Other bacteria	Mycorrhizal fungi	Other fungi
Protection from grazers	nc	(+)	(+)	(+)
Improved hydration	+	+	*	* or ±
Greater P, Ca, Mg, K availability	+	+	—	—
Greater micronutrient availability	+	+	—	*
Higher pH	+	+	nc	nc
Lower pH	—	—	nc	nc or —
Sorption of signaling compounds	* or —	*	*	*
Greater N availability (also through sorption of phenolics and increased nitrification)	—	+ or —	nc	nc
Sorption of microorganism	nc	+	nc	nc
Biofilm formation	+	+	*	*
Sorption of inhibitory compounds	*	+	*	*
Sorption of dissolved organic matter (OM) as an energy source for microorganism	*	*	nc	*

growth in different perspectives (Chen et al. 2009; Kasozi et al. 2010; DeLuca et al. 2012; Jain and Nainawatee 2002). Some areas, like greater abundance of microorganisms in soil amended with biochar (Warnock et al. 2007; Lehmann et al. 2011) was quite well established but others require more attention as shown in Table 17.7.

In short, it is possible to improve soil fertility at oil palm plantations by adding biochar which can act as a soil modifier for better soil nutrient management. Key parameters influencing the properties of biochar, such as type of biomass, technology, pyrolysis, holding time and heating rate as well as biochar application rate in field trials needs to be established.

Table 17.7 Relative levels of existing knowledge on biochar effects on soil biota (Lehmann et al. 2011) and our opinions on suggestions for research priorities

Research area	Level of existing knowledge	Research priority
Microbial abundance	H	L
Faunal abundance	L	H
Root abundance	M	L
Microbial community	M	M
Faunal community	L	M
Microbial function	L	H
Faunal function	NS	H
Root function	M	H
Biochar inoculants	L	H
Biochar enzyme interaction	L	H
Biochar pathogen control	L	H
Environmental risk	L	H

Note L, M, H indicates low, medium and high level of existing knowledge or priority for future research. NS: Not stated

17.4 Conclusion

Oil palm, a major crop in supporting the world population, requires extremely good nutrient management practice at field as it is one of the highest oil yielding crops which demands substantial supply of NPK to ensure healthy growth and high productivity. Systematically planned nutrient management practice is essential to sustain agriculture in general for maximum harnessing of nutrients from organic- and inorganic-based fertilizers-biochar system. Crop-nutrients-soil interaction at different ecosystems is very much dependent on and correlated with physicochemical properties of each individual component involved. Their behaviors, individually and collectively, in a complex soil matrix must be understood in-depth to enable efficient nutrient manipulation and management. With the right biochar candidates, knowledge acquisition, topped with appropriate remediation and management, amending agricultural soil with biochar provides positive symbiosis to retain and increase nutrients uptake in crops cultivation, and provides long-lasting benefits for sustainable farming.

17.5 Recommendations

Very little is known on nutrient management practices in oil palm plantations associating with biochar, hence further exploration is required to strengthen and identify crucial influencing factors for soil quality improvement such as nutrient leaching

mechanism, oil palm root system, fertilizer application method and type of nutrients applied (organic or inorganic). Nutrient leaching mechanism can be assessed by performing actual leaching in laboratory through either batch/continuous mode or both so that real situation on how nutrient is leached in oil palm cultivation can be identified and remedial action be sought. From field trials conducted so far it is evident that there are different and synergistic effects of fertilizers type, characteristics (e.g. particle size) and dosage (based on plant requirement) on root growth and biomass productivity. Be it organic- or inorganic-based nutrients, their advantages and disadvantages can only be evaluated on a level playing field when fairly compared at similar NPK proportions and particle size distribution (uniformity) via nutrient uptake rate through established leaching process. Subsequently, the cost-effectiveness of a combined fertilizer-biochar system can be estimated to determine which fertilizer system is best suited for oil palm with respect to nutrient uptake, yield and productivity, and of course economic return.

Acknowledgements The authors wish to thank MPOB for providing the Graduate Student Assistantship Scheme (GSAS) to Arasu Uttran to conduct this research work for a Master's degree at Universiti Kuala Lumpur (UniKL).

References

- Abdul AA, Deraman M (2013) Pore structure of carbon granules prepared from slow pyrolysis of oil palm empty fruit bunch fibres. *J Oil Palm Res* 25:216–227
- Al-Karaki (2013) Application of mycorrhizae in sustainable date palm cultivation. *Emir J Food Agric* 25:854–862
- Allen SC, Jose S, Nair PKR et al (2004) Safety-net role of tree roots: evidence from a pecan (*Carya illinoensis* k. koch)-cotton (*Gossypium hirsutum* l.) alley cropping system in the southern united states. *For Ecol Manag* 192:395–407
- Arvidsson R, Persson S, Fröling M et al (2011) Life cycle assessment of hydrotreated vegetable oil from rape, oil palm and jatropha. *J Cleaner Prod* 19:129–137
- Atkinson CJ, Fitzgerald JD, Hips NA (2010) Potential mechanisms for achieving agricultural benefits from biochar application to temperate soils: a review. *Plant Soil* 337:1–18
- Azeem M, Hayat R, Hussain Q et al (2016) Effect of biochar amendment on soil microbial biomass, abundance and enzyme activity in the mash bean field. *J Biodivers Environ Sci* 8:1–13
- Basu S, Rabara R, Negi S (2018) AMF: the future prospect for sustainable agriculture. *Physiol Mol Plant Pathol* 102:36–45
- Blackwell P, Krull E, Butler G et al (2010) Effect of banded biochar on dryland wheat production and fertiliser use in south-western Australia: an agronomic and economic perspective. *Aust J Soil Res* 48:531–545
- Blal B, Morel C, Gianinazzi-Pearson V et al (1990) Influence of vesicular-arbuscular mycorrhizae on phosphate fertilizer efficiency in two tropical acid soils planted with micropropagated oil palm (*Elaeis guineensis* jacq.). *Biol Fertil Soils* 9:43–48
- Blanchart E, Albrecht A, Bernoux M et al (2005) Organic matter and biofunctioning in tropical sandy soils and implications for its management. *Researchgate Net*. https://www.researchgate.net/publication/299466431_Organic_matter_and_biofunctioning_in_tropical_sandy_soils_and_implications_for_its_management. Accessed 8 July 2022

- Borowicz VA (2001) Do arbuscular mycorrhizal fungi alter plant—pathogen relations ? *Ecology* 82:3057–3068
- Bruun EW, Per A, Egsgaard H et al (2012) Effects of slow and fast pyrolysis biochar on soil c and n turnover dynamics. *Soil Biol Biochem* 46:3–79
- Cade-Menun BJ, Berch SM, Preston CM et al (2000) Phosphorus forms and related soil chemistry of podzolic soils on northern Vancouver island. i. a comparison of two forest types. *Can J Forest Res* 30:1714–1725
- Certini G (2005) Effects of fire on properties of forest soils: a review. *Oecologia* 143:1–10
- Chan KY, Van-Zwieten L, Meszaros I et al (2007) Agronomic values of greenwaste biochar as a soil amendment. *Aust J Soil Res* 45:629–634
- Chek TC, Ariffin I, Keong YK et al (2013) Evaluation of initial high phosphate rates on growth and early yield of oil palm grown on Sahabat series soil in Sabah. In: Malaysian palm oil board international palm oil congress, Kuala Lumpur
- Chen H, Yao J, Wang F et al (2009) Study on the toxic effects of diphenol compounds on soil microbial activity by a combination of methods. *J Hazard Mater* 167:846–851
- Cheng CH, Lehmann J, Thies JE et al (2006) Oxidation of black carbon by biotic and abiotic processes. *Org Geochem* 37:1477–1488
- Chiew LK, Abdul RZ (2002) The effects of oil palm empty fruit bunches on oil palm nutrition and yield, and soil chemical properties. *J Oil Palm Res* 14:1–9
- Corley RHV, Tinker PB (2016) *The oil palm*. Wiley
- Croker JR, Poss CH, Bhuthorndharaj S (2004) Effects of recycled bentonite addition on soil properties, plant growth and nutrient uptake in a tropical sandy soil. *Plant Soil* 267:155–163
- DeLuca TH, MacKenzie MD, Gundale M et al (2012) Biochar effects on soil nutrient transformations. In: Lehmann J, Joseph S (ed) *Biochar for environmental management: science and technology*, 1st edn. Routledge, London
- Ding Y, Liu YX, Wu WX et al (2010) Evaluation of biochar effects on nitrogen retention and leaching in multi-layered soil columns. *Wat Air Soil Poll* 213:47–55
- Dominguez EL, Uttran A, Loh SK et al (2020) Materials today : proceedings characterisation of industrially produced oil palm kernel shell biochar and its potential as slow release nitrogen-phosphate fertilizer and carbon sink. *Mater Today: Proc* 31:221–227
- Dünisch O, Lima VC, Seehann G et al (2007) Retention properties of wood residues and their potential for soil amelioration. *Wood Sci Technol* 41:169–189
- Fall AF, Nakabonge G, Ssekandi J et al (2022) Roles of arbuscular mycorrhizal fungi on soil fertility: contribution in the improvement of physical, chemical, and biological properties of the soil. *Front Fungal Biol* 3:1–11
- Gandahi AW, Hanafi MM (2014) Bio-composting oil palm waste for improvement of soil fertility. In: Maheshwari DK (ed) *Composting for sustainable agriculture*. Springer
- Grossman JM, O’Neill BE, Tsai SM et al (2010) Amazonian anthrosols support similar microbial communities that differ distinctly from those extant in adjacent, unmodified soils of the same mineralogy. *Microb Ecol* 60:192–205
- Halmi MFA, Simarani K (2021) Responses of soil microbial population and lignocellulolytic enzyme activities to palm kernel shell biochar amendment. *Eurasian Soil Sci* 54:1903–1911
- Haryati Z, Loh SK, Kong SH et al (2018) Pilot scale biochar production from palm kernel shell (pks) in a fixed bed allothermal reactor. *J Oil Palm Res* 30:485–494
- Jain V, Nainawatee HS (2002) Plant flavonoids: signals to legume nodulation and soil microorganisms. *J Plant Biochem Biotechnol* 11:1–10
- Jeffery S, Verheijen F, van-der VM et al (2011) A quantitative review of the effects of biochar application to soils on crop productivity using meta-analysis. *Agric Ecosyst Environ* 144:175–187
- Jeffries P, Gianinazzi S, Perotto S et al (2003) The contribution of arbuscular mycorrhizal fungi in sustainable maintenance of plant health and soil fertility. *Biol Fertil Soils* 37:1–16

- Jones CB, Brad DE, Engel R et al (2013) Factors affecting nitrogen fertilizer volatilization. Landresources Montana Edu. <https://landresources.montana.edu/soilfertility/documents/PDF/pub/UvolfactEB0208.pdf>. Accessed 27 July 2022
- Karananidi P, Md-Som A, Loh SK et al (2020) Flame curtain pyrolysis of oil palm fronds for potential acidic soil amelioration and climate change mitigation. *J Environ Chem Eng* 8:103982
- Kasozi GN, Zimmerman AR, Nkedi-Kizza P et al (2010) Catechol and humic acid sorption onto a range of laboratory-produced black carbons (biochars). *Environ Sci Technol* 44:6189–6195
- Kee KK, Goh KJ, Chew PS (1995) Effects of NK fertiliser on soil pH and exchangeable k status on acid soils in an oil palm plantation in Malaysia. In: Date RA et al (ed) *Plant soil interactions and low ph*. Kluwer Academic
- Koe LCC, Arellano JAF, McGregor JL (2001) Investigating the haze transport from 1997 biomass burning in southeast Asia: its impact upon Singapore. *Atmos Environ* 35:2723–2734
- Kong SH, Loh SK, Bachmann RT et al (2014) Biochar from oil palm biomass: a review of its potential and challenges. *Renew Sustain Energy Rev* 39:729–739
- Kong SH, Loh SK, Bachmann RT et al (2019) Palm kernel shell biochar production, characteristics and carbon sequestration potential. *J Oil Palm Res* 31:September
- Kuppusamy S, Thavamani P, Megharaj M et al (2016) Agronomic and remedial benefits and risks of applying biochar to soil: current knowledge and future research directions. *Environ Int* 87:1–12
- Laird D, Fleming P, Wang B et al (2010) Biochar impact on nutrient leaching from a midwestern agricultural soil. *Geoderma* 158:436–442
- Lehmann J, Rillig MC, Thies J et al (2011) Biochar effects on soil biota—a review. *Soil Biol Biochem* 43:1812–1836
- Lehmann J, da-Silva JJP, Steiner C et al (2003) Nutrient availability and leaching in an archaeological anthrosol and a ferralsol of the central amazon basin: fertilizer, manure and charcoal amendments. *Plant Soil* 249:343–357
- Loh SK (2017) The potential of the Malaysian oil palm biomass as a renewable energy source. *Energy Convers Manage* 141:285–298
- Manyà JJ (2012) Pyrolysis for biochar purposes: a review to establish current knowledge gaps and research needs. *Environ Sci Technol* 46:7939–7954
- Md-Som A, Wang Z, Al-Tabbaa A (2013) Palm frond biochar production and characterisation. *Earth Environ Sci Trans R Soc Edin* 103:39–48
- Meyer S, Glaser B, Quicker P (2011) Technical, economical, and climate-related aspects of biochar production technologies: a literature review. *Environ Sci Technol* 45:9473–9483
- Mia S, Dijkstra FA, Singh B (2017) Long-term aging of biochar: a molecular understanding with agricultural and environmental implications. *Adv Agron* 141
- Morgan JB, Connolly EL (2013) Plant-soil interactions :nutrient uptake. *Nature Educ Knowl* 2:1–5
- Mukherjee A, Rattan L (2013) Biochar impacts on soil physical properties and greenhouse gas emissions. *Agronomy* 3:313–339
- Mukherjee A, Zimmerman AR (2013) Organic carbon and nutrient release from a range of laboratory-produced biochars and biochar-soil mixtures. *Geoderma* 193–194:122–130
- Murdi AA, Hashim Z, Mohammed AT et al (2011) Effective placement of fertilizers for mature oil palm planted on alluvial soils. *Palmoilis*. <http://palmoilis.mpob.gov.my/TOTV3/wp-content/uploads/2020/02/TT-478.pdf#pdfjs.action=download>. Accessed 4 Aug 2022
- Naher L, Tan SG, Yusuf UK et al (2012) Biocontrol agent *Trichoderma harzianum* strain fa 1132 as an enhancer of oil palm growth. *Pertanika J Trop Agri Sci* 35:173–182
- Noble AD, Gillman GP, Ruaysoongnern S (2000) A cation exchange index for assessing degradation of acid soil by further acidification under permanent agriculture in the tropics. *Eur J Soil Sci* 51:233–243
- Noble AD, Gillman GP, Nath S et al (2001) Changes in the surface charge characteristics of degraded soils in the wet tropics through the addition of beneficiated bentonite. *Aus J Soil Res* 39:991–1001
- Omoti U, Ataga DO, Isenmila AE (1983) Leaching losses of nutrients in oil palm plantations determined by tension lysimeters. *Plant Soil* 73:365–376

- Phosri C, Rodriguez A, Sanders IR et al (2010) The role of mycorrhizas in more sustainable oil palm cultivation. *Agric Ecosyst Environ* 135:187–193
- Prieto-Fernandez A, Villar MC, Carballas M et al (1993) Short-term effects of a wildfire on the nitrogen status and its mineralization kinetics in an Atlantic forest soil. *Soil Biol Biochem* 25:1657–1664
- Ramlah Ali AS, Dolmat MT (1991) Status of mycorrhizal research in oil palm. Researchgate. https://www.researchgate.net/publication/264749831_Status_of_Mycorrhizal_Research_in_Oil_Palm. Accessed 27 July 2022
- Reichenauer TG, Panamulla S, Subasinghe S et al (2009) Soil amendments and cultivar selection can improve rice yield in salt-influenced (tsunami-affected) paddy fields in Sri Lanka. *Environ Geochem and Health* 3:573–579
- Renck A, Lehmann J (2004) Rapid water flow and transport of inorganic and organic nitrogen in a highly aggregated tropical soil. *Soil Sci* 169:330–341
- Rondon MA, Lehmann J, Ramírez J et al (2007) Biological nitrogen fixation by common beans (*Phaseolus vulgaris* L.) increases with bio-char additions. *Biol Fertil Soils* 43:699–708
- Rugayah AF, Astimar AA, Norzita N (2014) Preparation and characterisation of activated carbon from palm kernel shell by physical activation with steam. *J Oil Palm Res* 26:251–264
- Salt M (2004) Nutrient movement through SA soil. EPA http://report.epa.sa.gov.au/files/477355_nutrient.pdf. Accessed 26 June 2022
- Sara de Jesus D, Glaser B, Cerri CEP (2019) Effect of biochar particle size on physical, hydrological and chemical properties of loamy and sandy tropical soils. *Agron* 9:165
- Serrasolsas I, Khanna PK (1995) Changes in heated and autoclaved forest soils of s.e. Australia. ii phosphorus and phosphate activity. *Biogeochemistry* 29:24–41
- Shamala S, Idris AS (2009) Trichoderma as a biocontrol agent against ganoderma in oil palm. *Palmoilis*. <http://palmoilis.mpob.gov.my/TOTV3/wp-content/uploads/2020/02/TT-422.pdf#pdfjs.action=download>. Accessed 8 July 2022
- Sharpley AN, McDowell RW, Kleinman PJA (2001) Phosphorus loss from land to water: integrating agricultural and environmental management. *Plant Soil* 237:287–307
- Siththaphanit S, Bell RW, Limpinuntana L (2010) Effect of clay amendments on nitrogen leaching and forms in a sandy soil. In: 19th World congress of soil science—soil solution for a changing world, 3, pp 107–110
- Sogbedji JM, Van-Es HM, Klausner SD et al (2001) Spatial and temporal processes affecting nitrogen availability at the landscape scale. *Soil Tillage Res* 58:233–244
- Steiner C, Teixeira WG, Lehmann J et al (2004) Microbial response to charcoal amendments of highly weathered soils and Amazonian dark earths in central Amazonia—preliminary results. In: Glaser B, Woods WI (ed) *Amazonian dark earths: explorations in space and time* November. Springer
- Steiner C, Teixeira WG, Lehmann J et al (2007) Long term effects of manure, charcoal and mineral fertilization on crop production and fertility on a highly weathered central Amazonian upland soil. *Plant Soil* 291:275–290
- Sundram S (2010) Growth effects by arbuscular mycorrhiza fungi on oil palm (*Elaeis guineensis* Jacq.) seedlings. *J Oil Palm Res* 22:796–802
- Sundram S, Meon S, Abu SI et al (2015) Application of arbuscular mycorrhizal fungi with *Pseudomonas aeruginosa* upmp3 reduces the development of ganoderma basal stem rot disease in oil palm seedlings. *Mycorrhiza* 25:387–397
- Taghizadeh-Toosi A, Clough TJ, Sherlock RR et al (2012) Biochar adsorbed ammonia is bioavailable. *Plant Soil* 350:57–69
- Tinker PB, Nye PH (2000) *Solute movement in the rhizosphere*. Oxford University, New York
- Tiraeyari N, Hamzah A, Abu SB (2014) Organic farming and sustainable agriculture in Malaysia: organic farmers challenges towards adoption. *Asian Soc Sci* 10
- Uttran A, Loh SK, Kong SH et al (2018) Adsorption of npk fertiliser and humic acid on palm kernel shell biochar. *J Oil Palm Res* 30:472–484

- Vengadaramana A, Jashothan PTJ (2012) Effect of organic fertilizers on the water holding capacity of soil in different terrains of Jaffna peninsula in Sri Lanka. *J Nat Prod Plant Resour* 2:500–503
- Warnock DD, Lehmann J, Kuyper TW et al (2007) Mycorrhizal responses to biochar in soil—concepts and mechanisms. *Plant Soil* 300:9–20
- Yahya Z, Husin A, Talib J et al (2010) Oil palm (*Elaeis guineensis*) roots response to mechanization in Bernam series soil. *Am J Appl Sci* 7:343–348
- Yao Y, Gao B, Zhang M et al (2012) Effect of biochar amendment on sorption and leaching of nitrate, ammonium, and phosphate in a sandy soil. *Chemosphere* 89:1467–1471
- Zainal NH, Abdul Aziz A, Idris J et al (2018) Reduction of pome final discharge residual using activated bioadsorbent from oil palm kernel shell. *J Cleaner Prod* 182:830–837
- Zheng H, Wang Z, Deng X et al (2013) Impacts of adding biochar on nitrogen retention and bioavailability in agricultural soil. *Geoderma* 206:32–39

Chapter 18

Performance Analysis on an Arduino-Based Low-Cost Active Dual-Axis Solar Tracking System



Noor Hasyimah Abu Rahim, Muhammad Adam Saifuddin,
and Mohamad Maaroff Bahurdin

18.1 Introduction

Renewable energy has rapidly become a highly important subject area due to world problems nowadays, such as global warming which affects climate change. Somehow, it is difficult to recover from the exponential growth of the world population; thus, this reflects the increased use of electricity. On the other hand, this project is also made to meet the electricity demand somewhere far from the source, for example, on a remote agricultural farm. Modern farms are now also equipped with a variety of automated electrical appliances that require batteries to operate. Drones are one example of a farming tool used as a fertiliser sprayer. To have an efficient electric generator system within this area is considered valuable and practical.

Researchers have undertaken many efforts to improve the efficiency of solar panels. Vast research on the improvement of solar cells by using various types of advanced cells (Mohammad and Karim 2013; Rotar et al. 2018). There are three common PV solar cell types in the market, i.e., mono-crystal silicon solar PV (monocrystalline solar cell), poly-crystal silicon solar PV (polycrystalline solar cell) and thin film solar cell (TFSC). Mono-crystalline, the highest purity silicon solar PV

N. H. A. Rahim (✉) · M. M. Bahurdin
UniKL Robotics and Industrial Automation Center, Universiti Kuala Lumpur, Malaysia France
Institute, Bangi, Selangor, Malaysia
e-mail: noorhasyimah@unikl.edu.my

M. M. Bahurdin
e-mail: maaroff@unikl.edu.my

N. H. A. Rahim · M. A. Saifuddin · M. M. Bahurdin
Industrial Automation Section, Universiti Kuala Lumpur, Malaysia France Institute, Bangi,
Selangor, Malaysia
e-mail: madamsaifuddin@s.unikl.edu.my

cell produced from single-crystal silicon. It also performs better in hot temperatures and low light (Rotar et al. 2018).

There are many studies that have investigated the effectiveness of single-axis solar trackers. The researcher Bawa and Patil (2013) developed a single-axis solar tracker using a hybrid approach. They used a buck converter device to capture the power generated from the panel, and then the fuzzy system will evaluate the maximum power point tracking. Sabran and Fajardo (2018) developed a single-axis sun tracker inspired by the sunflower. To track the sun, they manipulate the light received and use circadian clock calculation. These two works as an input to the controller to instruct the motor to rotate accordingly to the sun position. It goes the same for Kuttybay et al. (2020), where they developed a hybrid tracking system using a light-dependent resistor (LDR), a photosensor, and astronomical calculations of the sun's position in the sky.

The dual-axis solar tracker also implements the same concept as single axis, except the panel can orient in both angles, azimuth, and altitude. Thus, the aim is to make sure the PV is accurately orientated perpendicular to the sun. Studies have shown that the dual-axis PV tracker can yield excellent electric power compared to static PV installation. The study showed that the system they built could yield a minimum of 20% (Sabran and Fajardo 2018) up to 60% (Kuttybay et al. 2020) more than the statics PV installation. Most past studies have only been researched for about one to five days. Only one study by Morón et al. (2017) was found to have conducted a continuous complete study for up to 5 months. The parameters they get from the system they build are voltage, current, light resistance, and temperature. Rotar et al. (2018) found that the PV panel efficiency would decrease if the temperature increased. Next, they calculated the efficient percentage between the tracker PV and the static PV. These percentages reflect the results of their study.

The main purpose of this study was to develop and compare the power gained by two solar harvesting systems, the dual-axis PV panel tracker and fixed PV. Both systems were designed and assembled using on-the-market-ready equipment. Detailed equipment and assembly processes are explained in the methodology section. The remainder of this paper consists of a study of the result and conclusions.

18.2 Methodology

This section covers all the details regarding the design and development of the dual-axis solar tracker and the static PV panel. The exact material name, quantity needed, and cost for this study are shown in Table 18.1. Material listed in this table was for the two system builds, the solar tracker, and the fixed PV. The total material cost for this study is 170.37 USD.

The solar panel chosen was a monocrystalline cell with a 420 mm × 190 mm × 3 mm dimension. The chosen panel has a rated maximum power (P_{\max}) of 20 W, maximum power current of 1.4 A and maximum power voltage of 14 V. Two DC servo motors with metal gear were used in this study. The purpose of these motors

Table 18.1 Material cost (seller website: <https://my.cyton.io/>)

No.	Item name	Quantity	Unit cost (USD)	Total cost (USD)
1	20 W 12 V/5 V DC solar panel (monocrystalline cell)	2 pcs	14.22	28.44
2	RC servo motor (metal gear)	2 pcs	18.97	37.94
3	Arduino Uno Rev3-main board	1 pc	25.84	25.84
4	Light dependent resistor (LDR)	4 pcs	0.12	0.48
5	100 A solar charge controller 12 V/24 V with dual USB port	2 pcs	15.00	30.00
6	Sealed lead acid battery 12 V 7.0 Ah	2 pcs	14.22	28.44
7	Acrylic sheet/Perspex A2 size 3 mm casting grade A	2 pcs	5.93	11.86
8	Plastic box (120 × 80 × 40mm) grey	1 pc	2.37	2.37
9	Other electric and electronic components	1 pc	5.00	5.00
Grand total				170.37

is to rotate the panel in both directions, the latitude and azimuth angle. The chosen controller was the Arduino Uno. Four photoresistor or light dependent resistor (LDR) has a maximum voltage of 150-V DC and a maximum wattage of 90 mW. The light resistance is between 5 and 10 K Ω .

The solar charger is used to control the power collected from the solar panel. The chosen solar charger is a dual MOSFET reverse current protection system with low heat production. The battery voltage is 12 V and has a USB output to a load of 5 V with three maximum amperes. The power collected is then stored in a battery. The seal lead acid (SLA) rechargeable battery was used as this is a typical general-purpose battery.

System Operation

The LDRs act as the sensor to capture the position of the sun. The Arduino then processes the signal from these LDR and evaluates it to instruct the motors to change the panel direction towards the sun.

The process begins with the solar tracker in initial mode. All the LDR can act as a sensor that measures the sun's strength when the sun rises. All four LDRs were placed on one acrylic plate, and there is a separator between the LDRs. The four regions are representing the North, South, East, and West. The LDRs were named LDR1 for North, LDR2 for South, LDR3 for East and LDR4 for West.

If the light intensity of all LDRs is the same, it is likely at noon since the sun is on top of the solar tracker so the LDR can get the same light intensity. If the light intensity is the same at LDR1 and LDR3, the solar tracker would be in the exact location between North and East as the other LDRs with the same light intensity. LDR1 and LDR2 can detect the strength of the sun during the first operation. If the resistance of LDR1 is greater than LDR2, the data is sent to the Arduino, which processes it

and instructs the servo motor controller. The motor controller then instructs the servo motor to move the direction of the solar panel to the north. The same process will occur if the amplitude of LDR2 is higher than LDR1, and the servo motor will shift the solar panel to the South.

After that, the Arduino will receive LDR3 and LDR4 results. If the intensity of LDR3 is greater than LDR4, the panel will be on the East side, and if the intensity of LDR4 is greater than LDR3, the solar panel will be on the Westside. Finally, suppose the day turns into night, and the LDR does not get any lighter intensity. In that case, the solar tracker will return to its initial position, facing an upward direction perpendicular to the sky.

Experimental Setup

The experiment was designed to run for 14 consecutive days, and the parameters to be collected are the hourly voltage, ampere, and power value. The daily data collection is made from 8 a.m. until 6 p.m. Therefore, there were 11 data observations and collection made daily.

Both systems, the solar tracker and fixed PV, were placed at the same testing site. The test site is in an open park and is not covered by any shadow at all. This is to ensure that the PV can receive direct and continuous sunlight. Study materials are not changed or removed until the last day of the test.

18.3 Results and Discussion

The daily average performance result of both systems for 14 days is shown in Table 18.2. Three comparison analyses were made, the voltage, the current and the power. These comparison was based on the overall 14 days data obtained. The details hourly analysis also was made but it just only for a day data analysis. The discussion then summarized by evaluating the tracker efficiency.

Voltage Generated by the PV Panels

The voltage data for both systems is then plotted for ease of discussion as shown in Fig. 18.1. Volt DA for the dual-axis tracker and Volt Fix for the fixed solar panel. Figure 18.1 shows that the solar tracker outperforms the fixed PV system for all days. The highest voltage recorded was 10.07 V by the solar tracker system and the lowest was 6.65 V by the fixed PV system. Even though the solar PV selected is designed to generate a maximum of 14 V, the maximum average voltage acquired is only 10.07 V. The weather condition during the experiment were cloudy and rainy. This 10.07 V was only achieved on day one of the experiment while the rest remain below this value.

The mean for Volt DA is 8.624 V while the Volt Fix is 8.134 V. The solar tracker generated a higher voltage, and the difference is about 0.49 V. The percentage difference in voltage-mean-value was 5.85%. According to Cubas et al. (2015), this percentage difference could not bring significant performance to the solar tracker

Table 18.2 Two weeks averaged performance result

Day	Dual-axis solar tracker			Fixed solar panel		
	Voltage (Volt DA)	Ampere (Amp DA)	Watt (Watt DA)	Voltage (Vol Fix)	Ampere (Amp Fix)	Watt (Watt Fix)
1	10.07	0.87	9.76	9.39	0.8	8.77
2	9.94	0.83	9.11	9.32	0.75	8.24
3	8.33	0.81	7.43	7.68	0.6	6.76
4	8.96	0.73	7.63	8.37	0.66	7.08
5	9.24	0.76	8.33	8.44	0.69	7.36
6	8.16	0.66	7.65	7.96	0.65	7.41
7	7.09	0.62	5.53	6.65	0.57	5.03
8	8.16	0.65	7.22	7.85	0.64	6.94
9	9.42	0.8	8.49	8.85	0.73	7.89
10	6.92	0.59	6.49	6.68	0.58	6.26
11	9.18	0.78	8.22	8.66	0.74	7.76
12	7.54	0.65	6.92	7.3	0.62	6.72
13	8.18	0.67	7.6	7.68	0.64	7.15
14	9.55	0.83	8.9	9.04	0.78	8.3
Average	8.62	0.73	7.81	8.13	0.68	7.26

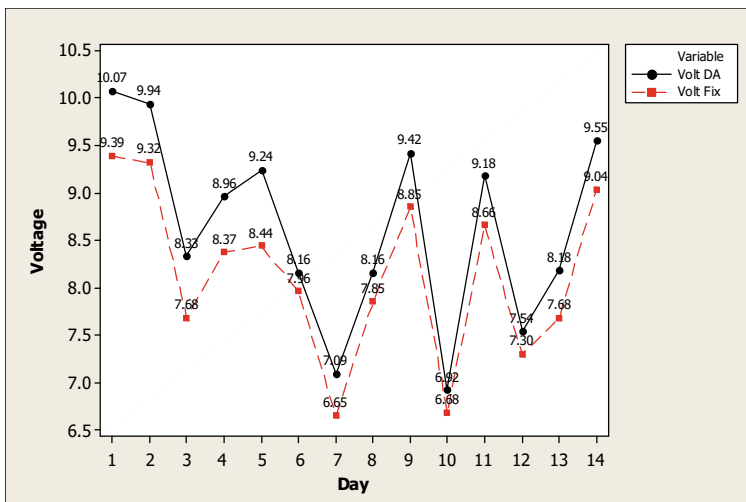


Fig. 18.1 Daily average accumulated voltage

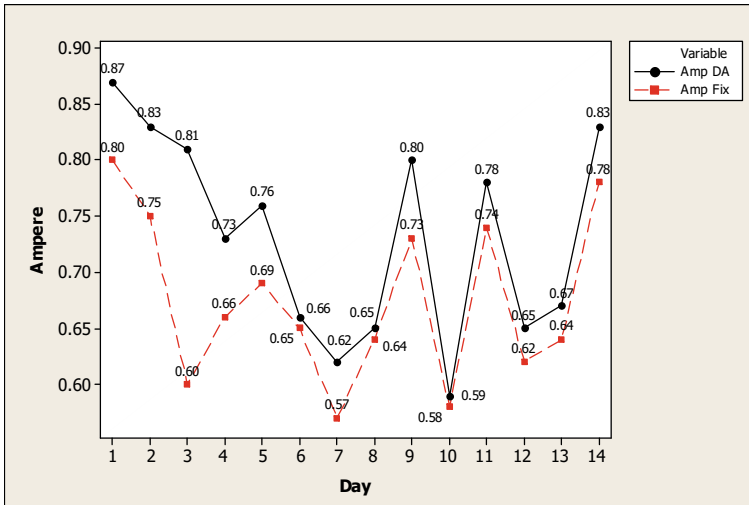


Fig. 18.2 Daily average accumulated ampere

system as the system needs another power to move the panels. This result shows the solar tracker is slightly more efficient for generating higher voltage compared to the fixed PV system. It is found that the solar tracker can generate 61.6% voltage compared to the fixed PV system, which is 58.09% only. The percentage difference between these two solar panels was 3.5%.

Electrical Current Produced by the PV Panels

Figure 18.2 shows the time series plot for averaged ampere value recorded for 14 days. The Amp DA represents the average ampere value for the solar tracker system while the Amp Fix is for the fixed PV system. The highest ampere recorded was 0.87 A on day 1 by the solar tracker system and the lowest was 0.57 A on day 7 by the fixed PV system.

The average mean for Amp DA was 0.7321 A while 0.6750 A for Amp Fix. The difference is about 0.0571 A (7.79%). The solar tracker system was able to generate a maximum of 0.87 A and a minimum of 0.59 A during the experiment duration. The fixed PV system has a maximum of 0.80 A and a minimum is 0.57 A. Comparing the voltage (5.85%) and ampere (7.79%) percentage difference, the ampere percentage difference is higher than the voltage.

The designed solar panel can generate a maximum of 1.5 A. Using the formula output (mean ampere for 14 days) over input times 100, the solar tracker produces 48.80% of the current, while the fixed PV system produces 45.0%. A solar tracker 3.8% outperforms a fixed solar panel.

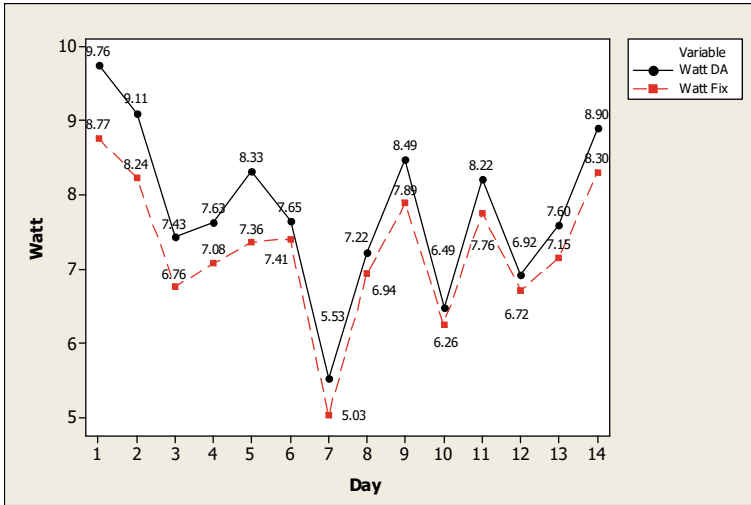


Fig. 18.3 Comparison of daily average accumulated watt

Power Comparison

The power generated by the solar panel is simply a multiplication of voltage and ampere (power = voltage × ampere). Table 18.2, in column Watt Da and Watt Fix, shows the result of power yielded for the 14 days experiment.

The daily averaged ampere for Wat DA and Watt Fix is plotted in time series for better comparison as shown in Fig. 18.3. Briefly, the Watt DA outperforms the Watt Fix for all days. There were 6 days where the power generates more than 7 watts. The lower power rate was recorded because of the weather conditions, and it seems consistent with the value recorded for voltage and ampere.

The solar panel chosen can generate a maximum power of 20 W. Evaluating the performance of this solar panel, the formula output over input times 100 is used. The average power solar tracker can generate 39.05% in these 14 days, while a fixed solar panel can generate only 36.30%. The gap is 2.75% solar tracker lead in 14 days.

Variation of Electrical Power Produced by PV Panels in One Day

The experiment on day 1 was the highest average power generated for both systems. Therefore, a further investigation was made on that day. The hourly data on day 1 are tabulated in Table 18.3. It displays the voltage, current, and power output of the solar tracker as well as the fixed solar panel. The peak performance is at midday. The same power, 17.68 W, is provided by both solar panels. At 8 a.m., relative to a fixed solar panel that begins at 2.8 V, the solar tracker voltage starts at 4.44 V. The fixed solar panel only produces 0.2 A current and 0.56 W power, whereas the solar tracker produces 0.4 A current and 1.78 W electricity. This happens because the sun’s location at 8 a.m. prevents the static solar panel from absorbing all the sunlight, as opposed to the solar tracker, which tracks the sun’s rays and directs the solar panel

at it. The power difference between a solar tracker and a fixed solar panel at 8 a.m. is 1.22 W.

By absorbing the most sunlight in the morning, the solar tracker will maximise the efficiency of the solar panels. The fixed solar panel only produced 0.58 W at 6 p.m. on day one whereas the solar tracker produced 1.14 W. According to this finding, the solar tracker has a major advantage over the permanent PV system in the early morning and late in the evening since its surface will always face the sun.

To calculate the percentage and determine how a solar tracker differs from a fixed solar panel, use the formula output over input times 100. At midday on day 1, both solar panels produced the same results and operated at almost full capacity. The output from both solar trackers is 97.14% of their whole 14 V capacity. Both solar panels produced 88.4% of their 20 W electricity and 86.66% of their total 1.5 A current capacity.

The solar tracker's voltage generated for the day's total average from 8 a.m. to 6 p.m. reaches 76.42% of its maximum capacity (10.7 V). The 9.39 V fixed solar panel, however, only operates at 67.07% of its full potential. The solar tracker made a difference that was roughly 9.35% greater. The complete average solar tracker current production is only 53.33% of the fixed solar panel's maximum, but it still exceeds 58% of the maximum it can accomplish. The average power output from the solar tracker is 48.8%, compared to 44.35% from the fixed solar panel. The solar tracker may provide 4.45% more power than a fixed solar panel on day one, from 8 a.m. to 6 p.m.

Table 18.3 Day 1 hourly data

Day 1 Time	Dual-axis solar tracker			Fixed solar panel		
	Voltage (V)	Current (A)	Power (W)	Voltage (V)	Current (A)	Power (W)
8:00 a.m.	4.44	0.40	1.78	2.80	0.20	0.59
9:00 a.m.	7.79	0.70	5.45	6.20	0.50	3.10
10:00 a.m.	10.21	0.90	9.19	9.30	0.80	7.44
11:00 a.m.	12.31	1.00	12.31	11.90	0.90	10.71
12:00 p.m.	13.60	1.30	17.68	13.60	1.30	17.68
1:00 p.m.	13.58	1.20	16.30	13.55	1.20	16.26
2:00 p.m.	13.33	1.10	14.66	13.32	1.10	14.65
3:00 p.m.	12.34	1.00	12.34	12.34	1.00	12.34
4:00 p.m.	10.09	0.90	9.08	10.09	0.90	9.08
5:00 p.m.	9.31	0.80	7.45	7.31	0.70	5.12
6:00 p.m.	3.81	0.30	1.14	2.90	0.20	0.58
Average	10.07	0.87	9.76	9.39	0.80	8.87

18.3.1 Tracker Efficiency

The efficiency of the tracker was calculated based on the sum of the average total power generated in two weeks. The efficiency (η) is calculated by defining the difference absolute average power of the tracker ($P_{tracker}$) and the fixed panel (P_{fix}), divided by the average P_{fix} and multiply by 100. The equation is $\eta = ((P_{tracker} - P_{fix})/P_{fix}) \times 100$.

The total power generated by the tracker based on Table 18.2 was 7.81 W, while the total energy by the fixed panel was 7.26 W. Based on the formula, the efficiency of the solar tracker is 7.57%.

18.4 Conclusion

This study was about developing and comparing the performance of solar systems. Two systems were built up with similar dimensions, but one is a fixed system, and the other can track the sun. The exact size of photovoltaic (PV) panels was installed in both systems.

The automated dual-axis solar tracker system was successfully built-up using an Arduino as a controller. To locate the sun's position, the LDR was used as a sensor. Two servo motors were installed to tilt and oriented the panel according to proper latitude and azimuth angles. The fixed solar panel was also built with a 30° inclination towards the sunset direction. The total cost to build the solar tracker systems is less than 200 USD. The experiment was run for about 14 days, and hourly data was collected during that experiment duration. The data collected were the values of voltage and ampere acquired.

Both systems can work efficiently with the highest values recorded on day 1. The higher voltage acquired was 10.07 V with 0.87 A, which produce an amount of 9.76 W. The fixed solar panel also shows the highest earned value on the same day. Comparing both data, the dual-axis tracker has significantly generated 4.45% higher power generation than the fixed solar panel in a day. The efficiency of the solar tracker based on the generated power during the two weeks test period (Table 18.2) is about 7.57% better compared to the fixed panel.

Future improvement work for this area is still plentiful in many ways, such as management, control, reduction of construction costs, maintenance methods, and others. Future works are to improvise the methods or techniques for tracking the sun by integrating with other tools and techniques such as adding the pyranometer. It is also interesting to have the performance comparison of different solar trackers that may consist of different methods or techniques. For instance, to compare the performance of single or dual-axis solar trackers built with other techniques.

References

- Bawa D, Patil CY (2013) Fuzzy control based solar tracker using Arduino Uno. *Int J Eng Innov Technol* 2:179–187
- Cubas J, Pindado S, Sanz-Andrés Á (2015) Accurate simulation of MPPT methods performance when applied to commercial photovoltaic panels. *Sci World J* 2015:1–16
- Kuttybay N, Saymbetov A, Mekhilef S, Nurgaliyev M (2020) Optimized single-axis schedule solar tracker. *Energies* 13:1–18
- Mohammad N, Karim T (2013) Design and implementation of hybrid automatic solar-tracking system. *J Sol Energy Eng* 135:1–6
- Morón C, Ferrández D, Saiz P et al (2017) New prototype of photovoltaic solar tracker based on Arduino. *Energies* 10:1298
- Rotar R, Jurj SL, Opritoiu F, Vladutiu M (2018) Position optimization method for a solar tracking device using the cast-shadow principle. In: *SIITME. IEEE*, pp 61–70
- Sabran RU, Fajardo AC (2018) Sunflower inspired solar tracking strategy: a sensorless approach for maximizing photovoltaic panel energy generation. In: *HNICEM. IEEE*, pp 1–6

Chapter 19

Rapid Small-Scale Column Test of Oil Palm Frond Biochar Potential as Heavy Metal Adsorbent



Amelia Md. Som, Zhenzen Wang, Yemi Akinyugha, Padmini Karananidi, Radzi Samsunanwar, and Robert Thomas Bachmann

19.1 Introduction

Malaysia and Indonesia supply more than 80% of the world's palm oil (Zakaria et al. 2018). According to the Malaysian Palm Oil Board (MPOB), a total of 5,737,731 ha of oil palm are planted throughout Malaysia, producing 16,390,517 tonnes of crude palm oil in 2021 (MPOB 2022).

More than 53 million tonnes of oil palm residues are produced, including empty fruit bunches (EFB), palm kernel shells (PKS), oil palm trunks (OPT), and oil palm fronds (OPF) (Nudri et al. 2019). Extensive research has been conducted to identify value-added products that can be generated from these by-products, such as paper pulp and bioethanol from EFB and OPT, furniture from OPT, organic fertiliser from

A. Md. Som (✉) · P. Karananidi · R. Samsunanwar · R. T. Bachmann
Green Chemistry and Sustainable Technology Cluster, Universiti Kuala Lumpur, Malaysian
Institute of Chemical Engineering Technology, Bandar Vendor Taboh Naning, 78000 Alor Gajah,
Melaka, Malaysia
e-mail: ameliamds@unikl.edu.my

P. Karananidi
e-mail: padmini.karananidi@s.unikl.edu.my

R. Samsunanwar
e-mail: radzi.samsunanwar@s.unikl.edu.my

R. T. Bachmann
e-mail: bachmann@unikl.edu.my

Z. Wang
China Academy of Urban Planning and Design, 9 Sanlihe Rd, Beijing, China

Y. Akinyugha
Lagos State Environmental Protection Agency, Oregun, Ikeja 101233, Nigeria

palm oil mill effluent (POME), renewable energy production, and biochar as an adsorbent (Kong et al. 2014).

OPF was reported to be the most abundant oil palm residue constituent (47%) (Roslan 2014). The majority of the OPF is used on the plantation to prevent soil erosion and promote soil conservation (Guangul et al. 2012). Recent studies on the utilisation of oil palm biomass waste as an adsorbent have revealed that carbonised OPF is relatively poorly understood in terms of metal adsorption (Ahmad et al. 2011; Vakili et al. 2014; Marsin et al. 2018). Since ancient times, heavy metals such as Cu^{2+} , Ni^{2+} , Pb^{2+} , and Zn^{2+} have poisoned the environment. Because they are not biodegradable and tend to bioaccumulate in the environment and food chain, their removal from industrial effluents and polluted soil is crucial. One study by Salamatinia et al. (2008) conducted research on the removal of Zn^{2+} and Cu^{2+} from aqueous single metal solutions using original OPF, EFB, and oil palm bark. Metal sorption reached equilibrium after 96 h of contact time, with a reported sorption capacity of 13.2 mg Zn^{2+} per gram OPF, while Cu^{2+} sorption capacity was found to be 11.8 mg/g. According to isotherm modelling, the Freundlich model described the adsorption process slightly better than the Langmuir model, indicating the presence of a heterogeneous surface and binding sites with different energies. The kinetics of diffusion were not fully investigated. In another study, (Som et al. 2012) OPF was pyrolyzed into biochar and the removal of Cu^{2+} , Ni^{2+} , Pb^{2+} , and Zn^{2+} from aqueous single metal solutions was investigated. The Langmuir model predicted adsorption capacities for Pb^{2+} of 83.3 mg/g, Cu^{2+} of 41.4 mg/g, Ni^{2+} of 13.0 mg/g, and Zn^{2+} of 19.7 mg/g. BET surface area increased from 4 to 9 m^2/g , which could explain the observed increase in sorption capacity for Cu^{2+} and Zn^{2+} over Salamatinia et al. (2008). In a more recent study, magnetic elements ($\text{Fe}^{2+}/\text{Fe}^{3+}$) were impregnated into OPF activated carbon and precipitated with hydroxide. The results showed that impregnated OPF activated carbon could remove Pb^{2+} , Zn^{2+} , and Cu^{2+} ions up to 100%, 93%, and 99%, respectively (Zainol et al. 2017).

To conduct a more comprehensive laboratory evaluation of a new adsorbent after batch isotherm tests, a column study is required to provide minimum contact time and optimal operating conditions for the most efficient use of the adsorbent. The rapid small-scale column test is one of several methods for conducting column evaluation for sorbents (RSSCT). It was initially created to simulate the pilot and full-scale performance of granular activated carbon for organic pollutants and natural organic matter (Crittenden et al. 1991). Its smaller volume allows for faster turnaround of results, from days to hours. These columns also take up less space and water than traditional columns. To match the Yoon and Nelson models, the breakthrough point is set at the time when the effluent concentration was 50% of the inlet concentration (Yoon and Nelson 1984). The breakthrough capacity in mg/g was calculated from Goel et al. (2005), see Eq. (19.1)

$$\text{Breakthrough capacity}(\text{mg/g}) = \frac{\text{Breakthrough time}(\text{min}) \times \text{flowrate}(\text{ml}/\text{min}) \times \text{feed concentration}(\text{mg}/\text{ml})}{\text{Mass of adsorbent in the column}(\text{g})} \quad (19.1)$$

A simulation of a pilot and full-scale performance of sorbent by RSSCT can be done by satisfying these equations (ASTM 2021):

$$\frac{EBCT_{sc}}{EBCT_{lc}} = \left[\frac{R_{sc}}{R_{lc}} \right]^2 = \frac{t_{sc}}{t_{lc}} \text{ and } \frac{V_{sc}}{V_{lc}} = \frac{R_{lc}}{R_{sc}} \quad (19.2)$$

where $EBCT$ is the empty bed contact time measured by dividing the volume of column that would be occupied by adsorbent in litres with incoming flow rates in litres per minute. R is the radius of the carbon particles, t is the time to breakthrough point, V is the hydraulic loading rate and sc is the subscript for a small column and lc for the large column.

Yoon and Nelson (1984) came up with a simple theoretical model in order to examine the adsorption behaviour in continuous columns. The model is predicated on the supposition that the rate of reduction in the probability of adsorption for each adsorbate molecule is proportional to the likelihood of adsorbate adsorption and the probability of adsorbate breakthrough on the adsorbent. This is the fundamental assumption that underpins the model. In comparison to Clark's (1987) and Thomas' model (1944), the Yoon-Nelson model is considerably simpler and does not require specific information regarding the type of adsorbent, the characteristics of the adsorbate, or the physical features of the adsorption bed.

The linearised Yoon and Nelson equation is expressed as

$$\ln \frac{C_o}{C_o - C_e} = kt - \tau k \quad (19.3)$$

where C_o is the influent concentration (mg/L), C_e is the effluent concentration (mg/L) and t is the sampling time. The values of k , rate velocity constant (L/min) and τ , time in (min) required for 50% adsorbate breakthrough were determined from the slope and intercept of the linear plot $\ln [C_o/(C_o - C_e)]$ against sampling time (t). Then, using the following equation, the adsorption capacity of a column, q_o (mg/g), is determined as follows (Aksu and Dönmez 2006):

$$q_o = \frac{C_o Q \tau}{1000 m} \quad (19.4)$$

where Q = volumetric flow rate (mL/min) and m = dry weight of OPF biochar in the column (g).

The goal of this research is to investigate the efficacy of OPF biochar as a heavy metal adsorbent using RSSC base on batch studies conducted by Som et al. (2012) and if the results of the experiments will be able to be fit into theoretical model that Yoon and Nelson have developed.

19.2 Methodology

The RSSCT was carried out utilising glass columns with an internal diameter of 0.8 and a length of 30 cm in accordance with ASTM D6586-21 (Fig. 19.1). Before a sample of OPF biochar was taken, it was crushed and sieved through a sieve with a mesh size of between 0.120 and 0.105 mm. To avoid channelling, the ratio of the column diameter to the mean particle size was fixed at 50. Before being sealed with a rubber bung on either end, the biochar was layered between glass wool and 5 mm-diameter borosilicate glass beads at the top and bottom layers. The glass beads in the column assisted in spreading the incoming flow and offering a foundation of support for the media. The biochar was physically packed into the column by tamping as it was added, and its weight was measured both before and after addition. The bio-char column heights were fixed at 16 cm. The experimental design and conditions are as listed in Table 19.1. Deionized water was poured through the columns to wash away small particles and saturate the sample. The loading rates are based on the batch of isotherm results by Som et al. (2012) resulting in three initial feed concentrations for each metal (Table 19.2). The pH of the solution was not modified. The metal solutions were pumped vertically upward at 0.05 ml/min to avoid channelling and ensure uniform solution distribution throughout the column. The columns' effluents were collected every 12 h, and a breakthrough curve was determined. The solution was filtered with Whatman No. 1 filter paper before being tested with a Perkin Elmer 7000 ICP-OES. The adsorption capacity and time required for 50% adsorbate breakthrough were calculated by using Eq. (19.3).

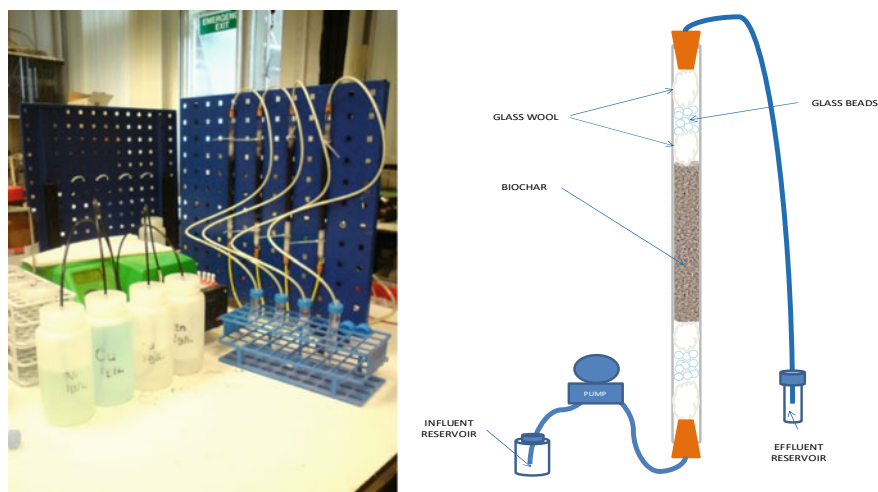


Fig. 19.1 Photographic and schematic illustrations of the RSSCT used to study the removal of Cu^{2+} , Ni^{2+} , Pb^{2+} and Zn^{2+} from aqueous solutions by means of OPF biochar

Table 19.1 RSSCT parameters used in this study

Parameters	Unit	Value
Internal diameter	cm	0.8
Flow rate	ml/min	0.05
Mass of OPF	g	2.6 ± 5%
Bed depth	cm	16
Empty bed contact time (EBCT)	min	2
Radius of biochar	μm	105 ± 5%

19.3 Results and Discussion

The concentration ratio C_e/C_o were plotted in Fig. 19.2a–d to determine the breakthrough capacity. It depicts the breakthrough curves for all four metals at the various concentrations chosen. As the inlet concentrations increase, all graphs show that the breakthrough curve occurs at an earlier time interval. However, breakthrough curves for the 5 mg/L Zn^{2+} column remained undetected until the experiment was completed. The experiment data were fitted into the Yoon and Nelson model, as shown in Eqs. (19.3) and (19.4), to determine k , and q_o . These results were also compared to the batch test results from an earlier study (Som et al. 2012). All calculated data are presented in Table 19.2.

The RSSCT breakthrough capacities (q) calculated based on Goel et al. (2005) and are comparable to the columns adsorption capacities (q_o) computed by using Yoon and Nelson's model for all three Pb^{2+} concentrations in Fig. 19.2a. However, the 250 mg/L feed column appears to have slightly higher q and q_o when compared to the 500 mg/L feed column. The observed breakthrough time of the 500 mg/L column was also longer than Yoon and Nelson's calculated τ value. The 500 mg/L input concentration may have exceeded the column's capacity, resulting in mass transfer and diffusion issues that slowed solute transport.

Nevertheless, the τ value decreased as feed concentration increased indicating faster saturations of the column. There were a limited number of active sites on the biochar column, and an increase in inflow concentration would rapidly saturate the sites. Further adsorption became more difficult as higher activation energy is required for sorption to occur (Clark 1987). A change in concentration will also affect the diffusion process in the column (Goel et al. 2005) and the driving force for adsorption would rise as the inflow concentration rose (Clark 1987). As feed concentration increases, k values decrease; higher k values indicate lower mass transfer resistance and easier metal adsorption.

As shown in Fig. 19.2b, τ and k values for Cu^{2+} columns decreased as feed concentration increased. However, τ value for 500 mg/L column was 30% higher than the actual experimental breakthrough time, and the column also has a much higher q_o in comparison to q . The Cu^{2+} column may experience similar issues as those of the 500 mg/L Pb^{2+} column. The k values for Cu^{2+} columns fluctuated without discernible upward or downward trends. In comparison, the q and q_o values

Table 19.2 RSSCT breakthrough capacity and Yoon and Nelson parameters in comparison to batch sorption studies

Metal	Feed concentration mg/L	Breakthrough time, t min	Breakthrough capacity, q		Yoon and Nelson (1984) parameters							Batch test max sorption capacity	
			mg/g	mmol/g	k (l/min)	τ (min)	q_0 (mg/g)	mmol/g	r^2	mg/g	mmol/g		
Pb ²⁺	500	7560	51	0.25	0.0002	6313.50	43	0.21	0.88	83.3	0.40		
	250	16,320	54	0.26	0.0008	16,893.75	56	0.27	0.81				
	100	18,780	43	0.21	0.0029	18,227.93	42	0.20	0.90				
Cu ²⁺	500	2160	24	0.38	0.0037	2974.86	34	0.53	0.92	41.4	0.65		
	250	3300	13	0.20	0.0045	3846.67	15	0.23	0.82				
	100	10,560	11	0.17	0.0039	10,953.85	11	0.17	0.89				
Ni ²⁺	75	1680	3	0.04	0.0015	1924.93	3	0.05	0.81	13.0	0.22		
	50	2820	2	0.03	0.0042	3119.76	2	0.04	0.86				
	10	55,080	7	0.11	0.0001	47,158.75	< 1	< 0.01	0.96				
Zn ²⁺	20	33,120	10	0.15	0.0008	32,812.50	10	0.15	0.83	19.7	0.30		
	10	50,640	8	0.12	0.0010	44,072.00	7	0.10	0.87				

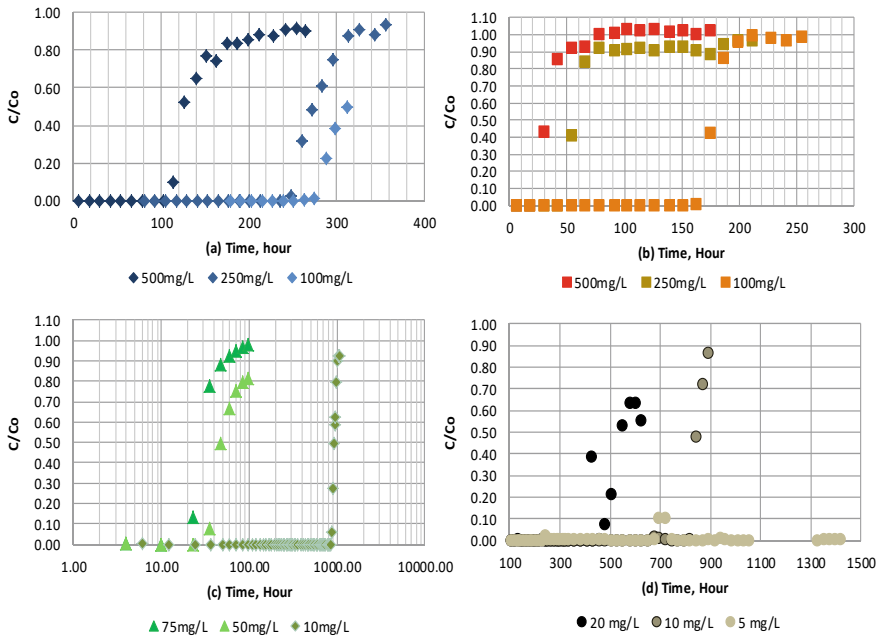


Fig. 19.2 OPF biochar breakthrough curves for **a** Pb²⁺ **b** Cu²⁺ **c** Ni²⁺ and **d** Zn²⁺

for 100 and 250 mg/L feed concentrations columns are similar. Even though every precaution has been taken to reduce the possibility of inaccuracy, these columns may have diffusional problems due to inconsistent column preparation.

The τ values for Ni²⁺ columns decrease as concentration increases, and the actual breakthrough times of the columns in Fig. 19.2c confirm this trend. However, the k value for 10 mg/L column was very low. This column exhibited an extended breakthrough curve, resulting in a greater treated volume of influent. If the concentration is too low, mass transfer and diffusion, and thus adsorption capacity, are significantly reduced. Similar phenomenon occurred in Zn²⁺ 5 mg/L column in Fig. 19.2d. However, the q_o are comparable to those of the actual reading for the 20 and 10 mg/L columns. τ and k values for Zn²⁺ columns also decrease as feed concentration increases.

The data in Table 19.2 also show that the metal adsorption capacities in the columns were lower than in the batch tests, which used a stirring. Adsorbates have a better chance of finding adsorption sites in stirred batch conditions than in static column conditions. It is also possible that the bi-char disintegrated during the vigorous shaking in the batch conditions, exposing more metal adsorption sites. Equation (19.2) can be used to simulate a pilot or full-scale column based on the RSSCT data and the identified breakthrough locations.

19.4 Conclusion

Results from this research reveal that RSSCT can be used to efficiently identify the operating conditions and minimal contact time required for OPF biochar to effectively remove heavy metals from wastewater. Yoon and Nelson's model adequately explained the overall Pb^{2+} , Cu^{2+} , Ni^{2+} and Zn^{2+} adsorption in the OPF biochar using RSSCT, as all experimental data fitted into the model with a linear regression coefficient (r^2) more than 0.81. Cu^{2+} displayed the highest adsorption capacity of 0.53 mmol/g.

Acknowledgements The authors would like to thank Prof. Abir Al-Tabbaa and Dr. Rod Lynch of Cambridge University, Cambridge Commonwealth Trust and MARA, Malaysia for the completion of this research.

References

- Ahmad T, Rafatullah M, Ghazali A, Sulaiman O, Hashim R (2011) Oil palm biomass-based adsorbents for the removal of water pollutants—a review. *J Environ Sci Health C Environ Carcinog Ecotoxicol Rev* 29:177–222
- Aksu Z, Dönmez G (2006) Binary biosorption of Cadmium(II) and Nickel(II) onto dried *Chlorella vulgaris*: co-ion effect on mono-component isotherm parameters. *Process Biochem* 41:860–868
- ASTM (2021) Standard practice for the prediction of contaminant adsorption on GAC in aqueous systems using rapid small-scale column tests
- Clark R (1987) Evaluating the cost and performance of field-scale granular activated carbon systems. *Environ Sci Technol* 21:573–580
- Crittenden J, Reddy P, Arora H, Trynoski J, Hand D, Perram D, Summers R (1991) Predicting GAC performance with rapid small-scale column tests. *J Am Water Work Assoc* 83:77–87
- Goel J, Kadirvelu K, Rajagopal C, Garg V (2005) Removal of Lead(II) by adsorption using treated granular activated carbon: batch and column studies. *J Hazard Mater* 125:211–220
- Guangul F, Sulaiman S, Ramli A (2012) Gasifier selection, design and gasification of oil palm fronds with preheated and unheated gasifying air. *Bioresour Technol*:224–232
- Kong S, Loh S, Bachmann R, Rahim S, Salimon J (2014) Biochar from oil palm biomass: a review of its potential and challenges. *Renew Sustain Energy Rev* 39:729–739
- Marsin F, Aini W, Ibrahim W, Nodeh H, Sutirman Z, Ting N, Sanagi M (2018) Recent advances in the preparation of oil palm waste based adsorbents for removal of environmental pollutants—a review. *Malaysian J Anal Sci* 22:175–184
- MPOB (2022) Economics and industry development division. <https://bepi.mpob.gov.my/index.php/en/>. Accessed 17 Jul 2022
- Nudri N, Bachmann R, Ghani W, Sum D, Azni A (2019) Characterization of oil palm trunk biochar and its suitability for solid fuel applications. *Biomass Convers Biorefin* 10:45–55
- Roslan A (2014) Investigation of oil palm fronds properties for use as biomaterials and biofuels. *Trop Agr Dev* 58:26–29
- Salamatina B, Kamaruddin A, Abdullah A (2008) Modeling of the continuous copper and zinc removal by sorption onto sodium hydroxide-modified oil palm frond in a fixed-bed column. *Chem Eng J* 145:259–266
- Som A, Wang Z, Al-Tabbaa A (2012) Palm frond biochar production and characterisation. *Earth Environ Sci Trans R Soc Edinburgh* 103:39–50

- Thomas H (1944) Heterogeneous ion exchange in a flowing system. *J Am Chem Soc* 66:1664–1666
- Vakili M, Rafatullah M, Ibrahim M, Abdullah A, Salamatinia B, Gholami Z (2014) Oil palm biomass as an adsorbent for heavy metals. In: de Voogt P (ed) *Rev Environ Contam Toxicol* 232:61–88
- Yoon Y, Nelson J (1984) Application of gas adsorption kinetics I. A theoretical model for respirator cartridge service life. *Am Ind Hyg Assoc J* 45(8):509–516
- Zainol M, Amin N, Asmadi M (2017) Preparation and characterization of impregnated magnetic particles on oil palm frond activated carbon for metal ions removal. *Sains Malays*. 46:773–782
- Zakaria K, Sumri N, Salleh K, Balu N (2018) Competitiveness of Malaysian and Indonesian palm oil export in the Balkans: a constant market share analysis. *Oil Palm Ind Econ J* 18:18–25

Chapter 20

Effect of *Zingiber officinale* on Blood Glucose Level, Pancreas, Liver and Kidney Histology Evaluated in Diabetic Induced Dawley Rats: A Systematic Review



Nurul Farisya Abd Aziz, Nur Athirah H. Abdullah,
Nur Jannah Crustia Mohd Halil, Zuhaida Embi, and Ahmad Najib Hasan

20.1 Introduction

20.1.1 Background

The prevalence of diabetic in Malaysia is worrying as the rate of diabetic cases increases every year. In 2015, the rate of diabetic was recorded at 13.4% while the number has grown to 18.3% in 2019 (Nazari 2020). Diabetes mellitus (DM), is a chronic hyperglycaemic disease that affects the production of insulin secretion and action thus can be further divided into type I and type II. Until late 2019, around

N. F. Abd Aziz · N. A. H. Abdullah · N. J. C. Mohd Halil
Biomedical Science, Institute of Medical Science Technology, Universiti Kuala Lumpur, Kuala Lumpur, Malaysia
e-mail: farisya.aziz@s.unikl.edu.my

N. A. H. Abdullah
e-mail: nathirah.abdullah@s.unikl.edu.my

N. J. C. Mohd Halil
e-mail: jannah.halil@s.unikl.edu.my

Z. Embi
Ministry of Health Malaysia, Putrajaya, Malaysia
e-mail: zuhaidaembi@moh.gov.my

A. N. Hasan (✉)
Institute of Medical Science Technology, Universiti Kuala Lumpur, Kuala Lumpur, Malaysia
e-mail: ahmadnajib@unikl.edu.my

1,614,363 patients with diabetes were enrolled in the registry and 99.29% was associated with type 2 diabetes mellitus (T2DM) while the remaining was type 1 diabetes mellitus (T1DM) and other forms of DM patients (Chandran et al. 2020).

T2DM occurs when the pancreatic β -cells secrete insufficient amount of insulin along with insulin resistance. These two factors occur simultaneously in T2DM. High resistance of insulin causes the fatty acid in plasma to elevate and reducing the amount of glucose transported to muscles. Moreover, this condition also causes increase in rate of fat that is broken and subsequently raise the hepatic glucose production. However, T2DM will only occur when the insulin secretion is insufficient and does not match the degree of insulin resistance (Al-Goblan et al. 2014).

Factors that contribute to T2DM primarily are caused by lifestyle such as inactivity, cigarette smoking, consumption of alcohol and unhealthy food (Olokoba et al. 2012). Such lifestyles can be seen clearly in this era which causes Malaysia to be named as the country with the highest rate of obesity among adults in Southeast Asia (15.6%) (Bernama 2020). Insulin resistance and diabetes have a strong link to body mass index. In addition, obese people have higher risk for insulin resistance due to the excessive developing of insulin resistance substances for example nonesterified fatty acids (NEFA), glycerol, pro-inflammatory cytokines and others.

Nowadays, many effective treatments are available for diabetes for instance pharmacotherapy, diet and insulin therapy. Few drugs have been developed to improve peripheral absorption of glucose and enhance insulin secretion. Despite the amount of treatment and therapy, treatment outcome is still far from ideal. Furthermore, some of these treatments have its own downside inclusive of toxicity, drug resistance and side effects. Today, people are becoming more interested in traditional materials and methods as they have almost no negative side effect. Moreover, plants have many beneficiary substances such as flavonoids, terpenoids, alkaloids, carotenoids and glycosides which act as anti-oxidant.

One of the great plants that are used for diabetic is ginger (*Zingiber officinale*). It has been used over 2500 years as spice and medication by Asian, Arabic and Indian herbal traditional remedy for anti-inflammatory, hypolipidemic, anti-nausea, hypocholesterolaemic, anti-arthritic, anti-migraine and anti-thrombotic. Few studies have been conducted on animal to investigate the effect of ginger on diabetic rats and the outcome shows small but significant reduction of blood glucose level on streptozotocin (STZ)-induced diabetic rats. Therefore, this study is being organized to conduct a systematic review on the effectiveness of *Zingiber officinale* on blood glucose level, pancreatic cell and pancreas histology in diabetic induced Sprague Dawley rats.

20.1.2 Problem Statement

Diabetes cases are still increasing every year in Malaysia with female as the leading gender for diabetes which accumulate 57.1% from the total cases in 2019 (Chandran et al. 2020). According to the National Diabetes Registry Report, Malay is recorded

as the highest ethnic with diabetes cases (59.15%) followed by Chinese (19.62%), Indian (13.17%) and other ethnicity (8.05%). Although most of the patients have received treatment accordingly, some of them might show some resistance towards the drug. For example, sulfonylureas can be used for the maximum of 6 years in 44% of the patient before they become ineffective. Lastly, there are many other drugs that can be used but the side effects of the drugs must also be considered.

Due to increasing concern towards this case, natural medication is now being studied to control this condition. Besides, the use of plants is safer rather than chemically synthesized medication. *Zingiber officinale* has proven its effectiveness in previous studies to help reducing the blood sugar level and protecting the pancreas. In conclusion, this study is conducted to carry out a systematic review on the effectiveness of *Zingiber officinale* on blood glucose level, pancreatic cell and pancreas histology in diabetic induced Sprague Dawley rats.

20.1.3 Research Objective

To conduct a systematic review on the effectiveness of *Zingiber officinale* on blood glucose level on pancreas, liver and kidney histology in diabetic induced Sprague Dawley rats.

20.1.4 Zingiber Officinale

Ginger has been proven to have more than 400 different compounds in chemical analysis with many different benefits. The major compounds constituent in ginger are carbohydrates (50–0%), lipids (3–8%), terpenes, and phenolic. Terpenes can be further divided to zingiberene, β -bisabolene, α -farnesene, β -sesquiphellandrene, and α -curcumene, while phenolic compounds include gingerol, paradols, and shogaol, however, the main compounds that are abundant in ginger are gingerols (23–25%) and shogaol (18–25%) (Prasad and Tyagi 2015). The use of ginger has been widely spread to treat various diseases for instance to regulate menstruation and heartbeat, remedy for nausea during pregnancy, gastrointestinal problem, pain reliever for arthritis, muscle soreness, chest pain, low back pain, stomach pain, anti-inflammatory agent and joint problem (Prasad and Tyagi 2015).

20.2 Methodology

20.2.1 Research Design

This research was conducted through a systematic review which is an explicit examination of the evidence on a clearly stated issue, including identifying, selecting, and critically evaluating relevant primary research, as well as obtaining and analysing data from the studies included in the review. In this study, a collection of data is done using electronic databases such as PubMed, Google Scholar, and Science Direct through various keywords. The search is conducted using the following term: “*Zingiber officinale*”, “*Zingiber officinale* AND/OR pancreas/liver/kidney histology”, “*Zingiber officinale* AND/OR blood glucose level”, “Ginger”, “blood glucose level”, “fasting blood glucose level”, “pancreas/liver/kidney”, “pancreas/liver/kidney histology”, “rat”.

After searching the electronic database, there were 2342 articles (Google Scholar = 1993, PubMed = 120, ScienceDirect = 217 and Scopus = 12) found. All articles were screened and chosen according to the inclusion and exclusion criteria as stated below. There were 30 articles that comply with the research objectives and can be used in this research.

20.2.2 Inclusion and Exclusion Criteria

Firstly, only articles such as formal journals, essays and other written items of assessment that were published between the year 2010 and 2021 were selected and used to ensure the data is up to date with the current years. Only journal articles that were written in English were considered in order to avoid any difficulty to understand. Articles that discuss mainly on effect of *Zingiber officinale* with either on glucose level, pancreatic cell and pancreas histology or all on diabetics’ rats were accepted. Lastly, articles that comply with this research objective were screened for confirmation.

All editorials, opinion pieces, non-research papers and conference abstracts were excluded in this paper. Study that uses other substances along with *Zingiber officinale* were cut out as they would influence the result obtained. All studies that were conducted on other than diabetic Sprague Dawley rats were excluded as it is against this research subject.

20.2.3 Data Analysis

A PRISMA flow diagram as shown in Fig. 20.1 explains the flow of the systematic study conducted. The PRISMA consists of the screening process and inclusion

and exclusion criteria for this article selection. This research study used the PICO framework (P: patient or problems; I: intervention being considered; C: comparison intervention; O: outcome measurements).

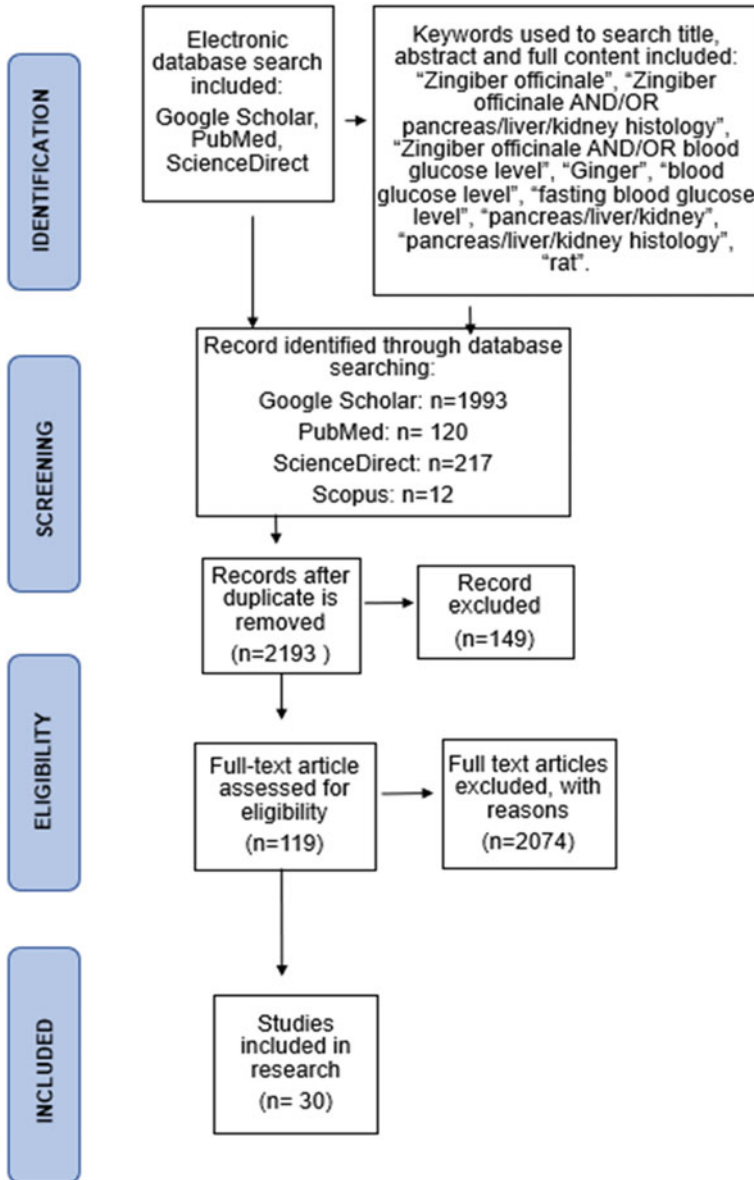


Fig. 20.1 PRISMA flowchart of literature search

20.3 Results and Discussion

20.3.1 Blood Glucose Level

Based on the findings, four studies examined different effects of *Zingiber officinale* on blood glucose level as an outcome to measure. All of the research studies used induced chemical diabetes in rats either alloxan monohydrate or streptozotocin via intraperitoneal (IP), intravenous (IV) and subcutaneous (SC) injection. The duration of treatment ranged within 42 days to 84 days. A research study by Al-Qulaly et al. (2021) stated that the mean (SD) of treated diabetic rats was 275.4 (10.37) compared with diabetic control rats was 319.2 (17.42). This indicates that there was a significant decrease ($p < 0.05$) in the blood glucose level of rats treated with *Zingiber officinale*. Authors of Shalaby and Saifan (2014) reported that oral administration of aqueous ginger extract to diabetic rats at doses of 200 and 400 mg/kg for 6 weeks significantly reduced ($p < 0.05$) the blood glucose levels compared to diabetic rats. The mean (SD) of glucose level in untreated diabetic rats was 225 (4.1), meanwhile diabetic rats treated with 200 mg/kg and 400 mg/kg ginger extract were 157 (3.2) and 155 g (2.5), respectively.

Another study also showed the mean (SD) blood glucose level in untreated diabetic rats was 183 (2.6) as compared to treated diabetic rats after 42 days was 118 (1.6). The supplementation of ginger extract significantly reduced the blood glucose level which revealed the hypoglycemic activity of ginger in diabetic rats (Jafri et al. 2021). This finding is also supported by a study (Bo et al. 2011) that stated that there was a significant reduction ($p < 0.05$) on blood glucose levels treated with *Zingiber officinale* which was 132.0 (8.3) as compared to untreated diabetic rats which was 260 (3.2). It may be concluded from these research studies that there is significant decreased glucose level between the treated and untreated diabetic rats.

20.3.2 Kidney Histology

Based on a research article by Singh et al. (2020), the hematoxylin and eosin stained on the kidney tissues of normal control rats appeared to have normal integrity of glomerulus and convoluted tubules. The diabetic rats demonstrated diminution of glomeruli and necrosis. Accumulation of neutrophil was also found in the tubular region. However, treated rats with *Zingiber officinale* extract 15, 30, 60 mg/kg once daily reduced the glomerular structural, morphological changes and tubular necrosis. Maximum renal protection was seen at a dose of ginger extract at 60 mg/kg.

20.3.3 Pancreas Histology

The pancreas of the control rat group had normal histological structure, and the pancreatic islet cells revealed no histopathological alterations. Anomalies in the pancreas were discovered in diabetic control rats. Red blood cells (RBC) congestion in blood arteries as well as septal thickness was clearly visible. In addition, the islets of Langerhans have undergone significant changes and little vacuolation of their cells has been seen. In comparison, treated rats administered 500 mg/kg BW of ginger showed normal acinar cell and islet of Langerhans structures.

20.3.4 Liver Histology

The liver of the control rat group showed normal hepatocytes arranged in the form of branching cords which were separated by blood sinusoids that radiated from the central vein. The liver cells appeared in the form of polyhedral and contained basophilic granules and a central round vesicle core. The portal space has minimal inflammatory infiltrating cells, a normal proportion of connective tissue cells, and appearance. However, there was a slight enlargement of the blood sinusoids and an increase of Kupffer cells in the liver parenchyma in diabetic rats. The dark stained hepatocyte nuclei were deformed and there was an increase in fibrous tissue and cell infiltrates surrounding the dilated portal vessels.

20.3.5 Discussion

Antidiabetic studies

In this systematic review research, the clinical appearances and the amount of blood glucose, uric acid and serum urea were measured after using chemical diabetic model such as Streptozotocin and Alloxan to induce diabetes in rats. The sign and symptoms such as polyphagia, polydipsia, polyuria, hypoinsulinemia and hyperglycemia convoyed with losing body weight have been seen in adult rats after a few days of STZ induction (Furman 2015) and (Gandhi and Sasikumar 2012).

The Chinese white ginger dichloromethane extract with the highest content of 6-gingerol 34% and 6-gingerol is often referred to as the quality standard for ginger of the pharmacopoeia standard of the People's Republic of China (Liu et al. 2019). Both 6-shogaol and 6-gingerol, which prevent the progression of diabetic complications, inhibited the production of advanced glycation end products (AGE) by removing the precursor of AGE, methylglyoxal (Mao et al. 2019). Ginger is a type of food

and medicine that has many functions such as antioxidant, anti-inflammatory, anti-obesity, anti-diabetic, neuroprotective, and renal protective effects. *Zingiber officinale* is regularly used as a traditional medication in China to treat diarrhoea and bowel infection with less side effects and it is possible for the treatment for diabetes.

In the present study, STZ injection led to significant increase in blood glucose level associated with reduced in serum insulin level. However, *Zingiber officinale* was exposed to decrease blood glucose, develop insulin sensitivity in both nutritional and inherited rodent models of type 2 diabetes (Li et al. 2012). This can be proven by four research articles (Al-Qulaly et al. 2021; Shalaby and Saifan 2014; Jafri et al. 2021 and Bo et al. 2011), which stated that the blood glucose level for the treated group were lower compared to diabetic rats. Many researchers reported that ginger compounds such as 6-gingerol, tannins, polyphenolic in ginger have inhibitory effects on two key major enzymes involved in glucose metabolism which are α -amylase and α -glucosidase. The effectiveness of ginger for these two enzymes has been shown to correlate with phenolic content. Ginger has been shown to regulate the insulin release and promote glucose clearance in insulin responsive peripheral tissues. This is important for maintaining blood glucose homeostasis (Rani et al. 2011). Another hypoglycemic mechanism addressed by ginger extract is the inhibition of hepatic phosphorylase enzyme. It suppresses the breakdown of hepatic glycogen stores and increases the activity of enzymes that improve glycogen synthesis. Ginger has also shown to be able to lower blood glucose levels by suppressing the activity of hepatic the glucose 6-phosphatase enzyme which causes degradation of glucose 6-phosphate to glucose (Khandouzi et al. 2021).

Histopathological Assessment

Based on the results observation, the untreated diabetic rats conveyed morphological changes in glomerulus kidney such as mesangial matrix expansion and epithelium necrosis. A research study by Kengkoom et al. (2021) stated that the renal pathology in human diabetic nephropathy mainly consists of glomerular basement membrane thickening by the lack of immune deposits, mesangial development and glomerulus sclerosis with or without the growth of nodular mesangial sclerosis. These structures have been discovered in kidney rat models induced with diabetes. Elevated uric acid levels in rats can cause glomerular hypertension and renal disease, as well as glomerular injury, arteriolosclerosis and tubulointerstitial fibrosis (Johnson et al. 2013). However, in diabetic rats treated with *Zingiber officinale* reduced morphological alterations are seen in the structure of glomerulus and tubular necrosis in diabetic rats compared to the untreated diabetic group. From the observation, *Zingiber officinale* might be favourable in repairing glomerular damage. Previous findings stated that ginger extract has nephroprotective effect through the inhibition of macrophage infiltration in the glomeruli of kidney tissue which can decrease many substances that promotes renal injury such as tumor necrosis factor alpha (TNF- α), reactive oxygen species (ROS) and interleukin 1 (IL-1). Thus, the inhibition of these molecules were helpful for treating kidney dysfunction in diabetic nephropathy (Wang et al. 2014).

As for the histology study on pancreas, there are no histological alterations found in the pancreas sections of diabetic rats given variety dosages of ginger. The diabetic

untreated rats' sections, on the other hand, showed mild vacuolation of sporadic islets of Langerhans cells. This is due to the nature of ginger that is high in antioxidants; which may be able to prevent tissue damage. In diabetic rats, it has been shown to protect pancreatic tissues against lipid peroxidation. Moreover, histological finding on liver has been proven to preserve the histological architecture of the diabetic liver rats back to normal. Normal hepatocytes and vessels appeared on the portal area regions that have homogenous cytoplasm without lipid deposition and normal central vesicle nuclei. Conversely to the diabetic rats, tiny vesicles showed up next to the hepatocytes of central vein with observation of Kupffer cells. Ginger's antioxidant activity has been shown to have the potential to prevent membranous lipid peroxidation, which can lead to cell damage and necrosis.

20.4 Conclusion

In this study, using a diabetic rat model, it has shown that ginger has the ability to reduce blood glucose level and is helpful in protecting organs. Ginger may be an effective therapy for diabetic people to reduce the risk of some subsequent chronic issues as it only has minor negative effects. In 2020, top four factors that led to CKD in Malaysia are hypertension, diabetes mellitus, increasing BMI and age (Saminathan et al. 2020). This shows how important it is for the future scientists and doctors to develop a plan to utilize ginger as an adjuvant and complementary support in therapy of diabetes. However, this study had some limitations. Most of the researches conducted to identify the effectiveness of ginger to treat diabetes were evaluated through animal studies and only a few studies were conducted on human. Other than that, there is no study that is attempted to evaluate the negative side effect of the consumption of ginger in diabetic patient. Therefore, further research is needed to identify and characterize the active component of ginger; specifically Malaysian ginger variety used by all the papers in this study.

Acknowledgements We would like to thank our parents for giving the endless supports that they have shown us throughout our project. We are thankful for all the memories that we have obtained throughout this competition and these 4 years of study in University Kuala Lumpur, Institute of Medical Science and Technology.

References

- Al-Goblan AS, Al-Alfi MA, Khan MZ (2014) Mechanism linking diabetes mellitus and obesity. *Diabet Metab Syndr* 7:587–591. <https://doi.org/10.2147/DMSO.S67400>
- Al-Qulaly MMM, Abdul-Halim OM, Hassan MMG (2021) Effect of ginger and cinnamon on induced diabetes mellitus in adult male albino rats. *Bull Egypt Soc Physiol Sci* 41:373–388

- Bernama (2020) Obesity rate at worrying levels in Malaysia. <https://www.malaymail.com/news/malaysia/2020/06/22/obesity-overweight-rates-at-worrying-levels-in-malaysia/1877679#:~:text=In%20a%20report%20issued%20in,of%20being%20overweight%20or%20obese.&text=In%20comparison%2C%20Malaysia's%20overweight%20and,per%20ce>. Accessed 22 June 2020
- Bo I, Ap ARG, Ao S (2011) Anti-diabetic and anti-oxidant effects of *Zingiber officinale* on alloxan-induced and insulin-resistant diabetic male rats. *Niger J Physiol Sci* 26(1):89–96
- Chandran A, Abdullah MN, Abdul F (2020) National diabetes registry report 2013–2019. Dis Control Div Ministry Health, Malaysia
- Furman BL (2015) Streptozotocin-induced diabetic models in mice and rats. *Curr Protoc Pharmacol* 70:5.47.1–5.47.20
- Gandhi GR, Sasikumar P (2012) Antidiabetic effect of *Merremia emarginata* Burm. F. in streptozotocin induced diabetic rats. *Asian Pac J Trop Biomed* 2(4):281–286
- Jafri SA, Abass S, Qasim M (2021) Hypoglycemic effect of ginger (*Zingiber officinale*) in Alloxan induced diabetic rats (*Rattus norvegicus*). *Pak Vet J* 31(2):160–162
- Johnson RJ, Nakagawa T, Jalal D, Sánchez-Lozada LG, Kang DH, Ritz E (2013) Uric acid and chronic kidney disease: which is chasing which? *Nephrol Dial Transplant* 28:2221–2228
- Kengkoom K et al (2021) Streptozotocin induces alpha-2u globulin nephropathy in male rats during diabetic kidney disease. *BMC Vet Res* 17(1):1–9
- Khandouzi N, Shidfar F, Rajab A, Rahideh T, Hosseini P, Taheri MM (2021) The effects of ginger on fasting blood sugar, Hemoglobin A1c, Apolipoprotein B, Apolipoprotein A-I and Malondialdehyde in Type 2 diabetic patients. *Iran J Pharm Res* 14(1):131–140
- Li Y, Tran VH, Duke CC, Roufogalis BD (2012) Preventive and protective properties of *Zingiber officinale* (Ginger) in diabetes mellitus, diabetic complications, and associated lipid and other metabolic disorders: a brief review. *Evid Based Complement Alternat Med* 2012:1–10
- Liu Y, Liu J, Zhang Y (2019) Research progress on chemical constituents of *Zingiber officinale* Roscoe. *Biomed Res Int* 2019:1–21
- Mao QQ et al (2019) Bioactive compounds and bioactivities of ginger (*Zingiber officinale* roscoe). *Foods* 8(185):1–21
- Nazari T (2020) Diabetes becoming more and more prevalent in Malaysia. <https://www.therakyatpost.com/2020/05/30/diabetes-becoming-more-and-more-prevalent-in-malaysia>. Accessed 6 April 2023
- Olokoba AB, Obateru OA, Olokoba LB (2012) Type 2 diabetes mellitus: a review of current trends. *Oman Med J* 27(4):269–273
- Prasad S, Tyagi AK (2015) Ginger and its constituents: role in prevention and treatment of gastrointestinal cancer. *Gastroenterol Res Pract*. 2015:1–11
- Rani MP, Padmakumari KP, Sankarikutty B, Cherian OL, Nisha VM, Raghu KG (2011) Inhibitory potential of ginger extracts against enzymes linked to type 2 diabetes, inflammation and induced oxidative stress. *Int J Food Sci Nutr* 62(2):106–110
- Saminathan TA, Hooi LS, Yusoff MFM, Ong LM, Bavandanan S, Hasani WSR, Zhi TEZ, Wong I, Mat RH, Robert TG, Ismail H, Wong NI, Ahmad G, Ambak R, Othman F, Abd Hamid HA, Aris T (2020) Prevalence of chronic kidney disease and its associated factors in Malaysia; findings from a nationwide population-based cross-sectional study. *BMC Nephrol* 21(344):1–12
- Shalaby MA, Saifan HY (2014) Some pharmacological effects of cinnamon and ginger herbs in obese diabetic rats. *J Intercult Ethnopharmacol* 3(4):144–149
- Singh B, Kumar A, Singh H, Kaur S, Kaur S, Singh BH, Arora S, Singh B (2020) Zingerone produces antidiabetic effects and attenuates diabetic nephropathy by reducing oxidative stress and overexpression of NF- κ B, TNF- α , and COX-2 proteins in rats. *J Funct Foods* 74:1–10
- Wang Z et al (2014) Inhibition of macrophage migration inhibitory factor reduces diabetic nephropathy in type II diabetes mice. *Inflammation* 37(6):2020–2029

Chapter 21

The Development of Simulation to Improve the Production Process Efficiency



**Emilya Azrien Samri, Helmi Adly Mohd Noor,
Syed Muhammad Shamin Syed Roslee, Rahimah Kassim,
Fauziah Abdul Rahman, and Zirawani Baharum**

21.1 Introduction

Sime Darby Berhad is Malaysia's largest multinational corporation, and it is one of Southeast Asia's widest plantation company. It was established in 1910 by two businessmen William Sime and Henry Darby contrived Sime Darby. Sime Darby Berhad is a multi-faceted corporation with operations in transportation, motors, industrial machinery, and healthcare. Sime Darby provides engineering services, sales, rentals, maintenance of equipment, administration of port infrastructure, water treatment and distribution, insurance broking, supply of shared services, other commercial projects, car assembly and distribution, and after-sales support. In addition, the company is

E. A. Samri · H. A. Mohd Noor (✉) · S. M. S. Syed Roslee · R. Kassim · F. Abdul Rahman · Z. Baharum
Malaysia Institute of Industrial Technology, Universiti Kuala Lumpur, Pesiaran Sinaran Ilmu,
Bandar Seri Alam, 81750 Johor Bahru, Johor, Malaysia
e-mail: helmiadly@unikl.edu.my

E. A. Samri
e-mail: emilya.samri@s.unikl.edu.my

S. M. S. Syed Roslee
e-mail: shamin.roslee05@s.unikl.edu.my

R. Kassim
e-mail: rahimahk@unikl.edu.my

F. Abdul Rahman
e-mail: fauziahar@unikl.edu.my

Z. Baharum
e-mail: zirawani@unikl.edu.my

also listed on the main board of Bursa Malaysia Securities Berhad. The firm is the biggest multinational corporation in Malaysia and one of the biggest in Southeast Asia. The business is present in Malaysia, other Southeast Asian nations, China, and Australia. The business's headquarters are in Malaysia's Kuala Lumpur (Ravanera and Gorra 2010).

Additionally, the primary commercial activity is oil palm production in the variety sector. Sime Darby Berhad began as a rubber company that also provided engineering services, distributed heavy machinery and vehicles, developed real estate, and produced electricity.

They employ over 100,000 people internationally and operate in close to 20 nations. 38% of sales come from the local market, 25% from Hong Kong, 14% from Singapore, and 11% from Australia. The company has been a leader in the international business sphere thanks to all of its skills and corporate identity. These have a variety of industries that are globally competitive. The history of Sime Darby Plantation Sdn. Bhd. began in the nineteenth century, when intrepid English planters started rubber plantations in Malaya. These pioneers included Alexander Guthrie, Daniel and Smith Harrison, Joseph Crosfield, William Sime, and Henry d'Esterre and Herbert Mitford Darby, who founded the Sime Darby Group in 2007 after the merger of three successful businesses (Kumpulan Guthrie Berhad, Golden Hope Plantations Berhad, and Sime Darby Berhad). Creating a new company with such a completely different mission, vision, and objective (Syed and Philip 2008).

Sime Darby Diamond Jubilee Plantation Sdn. Bhd. in Jasin, Melaka, was established in 1971. H.E. Fraser was the factory manager. There are 16 nations in which the firm conducts its downstream processes, including the refining of crude palm oil (CPO) for use in edible oils and fats products, oleo chemicals, and biodiesel (Potter 2015) stated that maintaining the best quality at all times is key to Sime Darby Plantation's business concept while producing a broad range of goods based on palm oil. Sime Darby Plantation is dedicated to creating and promoting sustainable goods and practises in the palm oil business as the largest producer of certified sustainable palm oil in the world. The firm is constantly looking for new methods to promote the production, acquisition, and use of sustainable oil palm products as one of the founding members of the Roundtable on Sustainable Palm Oil (RSPO). Sime Darby Berhad had the opportunity to expand and build a few manufacturing branches during this time.

The Group changed the name of all of its downstream businesses to Sime Darby Oils (SDO) in March 2019 to fully explore the potential of SDP as a reputable brand known for its sustainability credentials and high product quality. Sime Darby Oils operations manage the trading, production, sales, and marketing of oils and fats products, palm oil-based biodiesel, nutraceuticals, and other variants through a vast global wide range of institutions in eight nations (Malaysia, China, The Netherlands, United Kingdom, South Africa, Thailand, Indonesia, and Papua New Guinea). SDO maintains and runs 11 refineries with a combined capacity of 3.8 million metric tonnes (MT) annually and a total bulking installation capacity of 300,000,000 tonnes within this core business. The company's slogan, "Realizing Possibilities, Together,"

captures its idea of working with partners to make high-quality, enlightening products and to ensure that consumers may live sustainably (Zahraee et al. 2019).

21.1.1 Problem Statement

The aim of this part is to improve the production process efficiency at this firm, located at Jasin, Melaka.

The production process has been facing with a variety of problems according to Tuan Muhammad Mukhtarul 'Arifin Bin Salimin' as Diamond Jubilee Sime Darby Plantation Sdn. Bhd.'s mill director.

1. Process efficiency of the production.
2. The lack of worker in detecting defects.
3. The efficiency in time management.

To solve this issue, the organization needs to take action with contributions such as hired additional employees in the production process of manufacturing activities, adding more machines which contribute directly to one of the biggest impacts. In addition, the organization wants to reduce its workers and computer efficiency in a concept for increasing productivity.

Simulating the proposed production process improvement allows it to be assessed. The organization may recognize by using the simulation which would be better for real work and that the problem can also be resolved to increase performance in manufacturing activities. Khalili and Zahedi (2013) claimed using simulation software would allow to better understand the actual output structure and correctly forecasting the performance of the device over time makes modeling and simulation an excellent method for program planning. Alternatively, it allows to assess the performance and offer data that may be used to gauge capacity. Simulation models are animations of designs that are identical to the real-world systems, and they can help investors better comprehend the designs (Yasir and Mohamed 2018). The production system for a manufacturing firm is the key factor in the competition between the enterprises. Therefore, enhancing the production system is a crucial way to boost an enterprise's ability to compete. The key influencing elements may be identified and improved upon after the simulation results have been examined (Enrico et al. 2010).

21.1.2 Research Objective

The research has three objectives, each of which will lead to the anticipated outcome the researcher needs. The following are the research objectives that should be attained:

1. To identify the production process.
2. To discuss on ways to overcome the problem of the production process.
3. To apply the ProModel Software into the production process.

21.2 Methodology

21.2.1 Research Design

The research development for the research subject will be clarified in this section. A collection of research that involves conceptual analyzes, the product definition, literature review, problem statement and research methodology is given before the beginning of the project.

According to Setyanto (2013), the preliminary analysis is the fundamental process that determines the definition of the project at the beginning of the project. The analysis should be carried out in the process flow, problem statement and draft.

Next phase is the creation of the research project prototype, in the case study Diamond Jubilee Sime Darby Plantation Sdn Bhd, and the construction of a simulation model centered on the collection of data in order to define the plant layout production process. The simulation model will be evaluated before the programme is put into use, and if there are problems with the project, the model may also be tested and given advice.

Finally, the evaluation of the simulation software research methods may be carried out. The evaluations of the whole model would also be conducted by utilizing the performance data for the development of the production process in the manufacturing process.

21.3 Results and Discussion

Depending on the study methodologies employed in the interview sessions, the part would cover research, findings, and results. First, the data would be examined. The research findings will be contrasted with earlier research described in the literature review. The findings of this section are focused on field visits and observations in the development cycle of Diamond Jubilee Sime Darby Plantation Sdn. Bhd. Development to prove the problem and an experiment was carried out by the researchers. The researchers simulated the problems and outcomes of the simulation mentioned in this section after collecting evidence or information based on interviews.

21.3.1 *Research Objective 1*

The research objective 1 is to describe the development cycle at the company. In order to achieve this goal, the researcher did an interview to get the results. The research question for the interview is described in Table 21.1.

21.3.2 *Research Objective 2*

Research objective 2 in this work is to explore how to solve the problems of the production process. The study question below has been created:

Research Question: How to overcome the problem of the operation system at Diamond Jubilee Sime Darby Plantation Sdn. Bhd.?

- **Method.** In order to address the research question two, the researcher developed a simulation for the production process using the Promodel Simulator software.
- **Promodel Simulation.** ProModel describes the production system as a manufacturing location structure, such as machines or workstations, from which parts (or entities) are treated according to some manufacturing definition. The network will also have routes, such as transportation aisles, as well as support facilities, such as operators and material handling equipment used to process and move items. The Promodel Simulator will fix the issue where there is a void in the development cycle by producing a new design or adding an additional design in the production phase.
- **Model Elements.** We must define all the basic modeling elements in constructing this model, and some of the optional elements are shown in Fig. 21.1. The researcher used the position model aspect, entities (parts), arrivals, processes, resources, path networks, and attributes for this study. The model element in order will be used to represent the production process.
- **Building Models.** By completing the corresponding modules chosen in the build menu, models are produced. This module is made up of a number of edit tables and dialogue boxes that are used to offer layout specifications. A setup window is also present for setting up paths and other modelling features for simulation tools.

21.3.3 *Research Objective 3*

The research objective 3 in this research is to apply the Promodel Simulation software into the production process. The research question below was created:

Research Question: How to improve the process of operation system in Diamond Jubilee Sime Darby Plantation Sdn. Bhd. by using the Promodel Simulation software?

Table 21.1 Coding interview

No.	Question	Answer
1	Can you brief about the company background and history?	Diamond Jubilee is one of the subsidiaries of Sime Darby which has five key sectors in the fields of plantation, property, manufacturing, motors and energy and utilities with increasing healthcare business. At Diamond Jubilee our main business is oil palm and the company's initial industry is rubber. That is because in 1910, William Sime of Scotland believed that Malaysia had similar jungle to Brazil, and because of rubber, he chose to create Sime Darby. That is long afterwards. This company produces raw material oil palm and crude oil in another branch at Kempas, Jasin, to make cooking oil. Before starting the next process, the best quality oil needed time to get the right pH result from the laboratory. Sime Darby is listed in Bursa Malaysia and is one of Southeast Asia's largest company. The company was founded in 1971 by H.E. Fraser. That is to say that this company is 49 years old
2	What is the role of the company?	Making Diamond Jubilee Plantation Sdn. Bhd. as sustainable producers of edible oils in the world
3	What is your current position in the company and how long you been in the position?	I'm as a Mill Manager at Diamond Jubilee Sime Darby since 2018 and I was 19 years in this industry
4	What is the main product the company produce?	As a raw product this company manufactures processed palm oil (crude palm oil) and palm kernel oil products, and the product will be manufactured in another division as I said
5	What time did this company start operating?	Every day at 8 a.m. to 12 a.m. for the plantation and at 8 a.m. to 5 p.m. for the office section
6	Does the factory operate under shift pattern?	Yes. There have two shift which is first shift will be at 8 a.m. until 4 p.m. and 4 p.m. until 12 a.m.
7	How many workers handling the operation and their position in the production process?	There are 30 workers per shift at plantation. Which is 60 workers for a day working process and 40 workers for support such as from maintenance and office section. The workers have been divided for 10 production process. Weight bridge until ramp process has 2 workers, sterilization process has 6 workers, threshing process has 6 workers, pressing process has 3 workers and clarifying and handle storage tank process has 3 workers. This is number of workers for only refinery oil process. For kernel needed 10 workers to handle processing stage until dispatch process. So, the balance of the workers will be office department, laboratories, security, maintenance, cleaners and safety department
8	Does this company operate on a full machine or involve worker as well?	Totally half automatic machine for the process, workers needed for monitoring the production process to ensure the machine not stuck and need make a report every day

(continued)

Table 21.1 (continued)

No.	Question	Answer
9	How many machines involved in the process?	For every stage of production have two machine which is the origin and one for backup as a spare part is any obligation
10	How regular the maintenance for the machine?	One a week, every Sunday or based on the report for the last shift
11	How many conveyors, forklift, or other equipment that used in the process?	For every stage of production, we provide many types of conveyors such ribbon and staple
12	How many products that can be produced by a machine at one time?	Unpredictable, depends on palm oil. For average that can be conclude, we can only produce 22% in one hour which is 25 ton
13	Did the production have time- break?	As I said, depends on palm oil it is because they have own season. So, if palm oil less than 200 ton, the production will drag to the next shift
14	Did company have any issues regarding production process?	There are some issues in this company which are the problem of machine production that produce limited production and is the lack of detecting defect (maintenance) which is drag the time production process
15	What is the proper solution of the production issues?	I have no idea but think this company need to upgrade the machine to the new design as oil and gas industry which is the machine known as NIR (infrared technology)
16	How the company transport the goods?	We use pipeline and tanker to deliver the product to the consumer (another branch of Sime Darby)
17	How the company manage the documentation of the production?	By register to MPOB to get the ticket and through the only in the system



Fig. 21.1 Model elements

(a) **Result Statistics**—The researcher’s statistics are classified into 10 processes that result in the production of crude oil and kernel extraction. In other words, without the information gleaned from the observation and interview sessions, the entire process would fall short. In order to update a model element and obtain statistics for comparisons between or more efficient designs, data from interviews and observation is also utilized.

- (b) **Comparison for Total Production in Current Design and Proposed Design**—According to Figs. 21.2 and 21.3, the researcher made an experiment using two end products to get the efficiency of the production process. After the experiment test, the researcher got the result of efficiency production process after making improvements. Improvements have been made towards the system which was reducing the number of processes that have been taken from 13 process into 8 processes, which included the fruit digestion process, clarifying process for crude oil, kernel drying process, kernel crushing process, and kernel separation process. Benefits of minimal process can help the production, produce more products in the same actual time instead of wasting waiting time between a gap process to another process. It also can reduce human error among the workers. Since the simulation is essentially an experimental tool of analysis and predicting the system, the result might not be accurate when the company applied into the system. From the bar graph, the statistics show that the percentage of entities stated of the end product for actual design: crude oil, 79.50% and kernel, 86.63% while the percentage of entities stated of the end product for proposed design: crude oil, 98.77% and kernel, 100%.
- (c) **Comparison for Single Capacity Location States in Current Design and Proposed Design**—Based on Figs. 21.4 and 21.5, the researcher made an experiment by upgrading the process from 13 into 8 processes to get the efficiency of the production process. After the experiment test, the researcher got a result that by upgrading 3 processes which include the oil clarification using ORP sensor (pH sensor), purifying process and silo process indirectly can reduce the number of processes and boost the product within actual time. The best result of the proposed design is an efficiency as much as 100% of ramp, 64.58% of bunch sterilization process, 32.29% of bunch threshing process, 6.6% of pressing process, 33.33% of oil clarification process, 22.92 of kernel recovery process, 52.21% of purifying process and 50.31% of silo process.

Fig. 21.2 Entities states of the end product statistics for current design

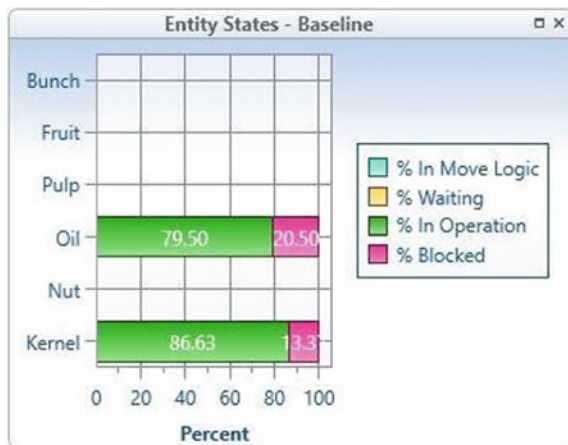




Fig. 21.3 Entities stated of the end product statistics for proposed design



Fig. 21.4 Statistics for single capacity location states in current design

- (d) **Comparison for Multiple Capacity Location Stated in Current Design and Proposed Design**—Figures 21.6 and 21.7 shows the best results of proposed design efficiency as 1.20% busy time of fruit elevator compared to the current design are 53.84% busy time. Furthermore, the percentage decrease is around 52.28 with an addition upgrading fruit digestion process.
- (e) **Comparison for Total Location Utilization in Current Design and Proposed Design**—According to Figs. 21.8 and 21.9, the best results of the proposed design efficiency of ramp utilization as 100%, bunch sterilization as 64.58%, bunch threshing as 32.29%, pressing as 2.70%, oil clarification as 33.33%, kernel recovery s 22.92%, purifying 52.21%, silo as 50.31%, kernel extraction as 21.09%.

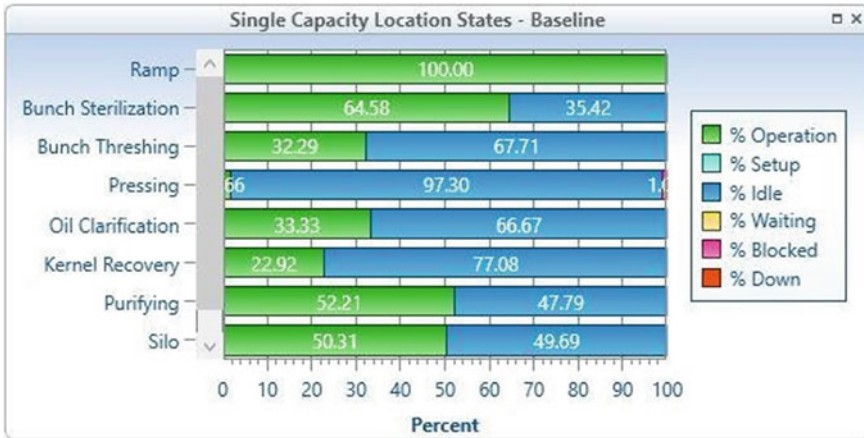


Fig. 21.5 Statistics for single capacity location states in proposed design

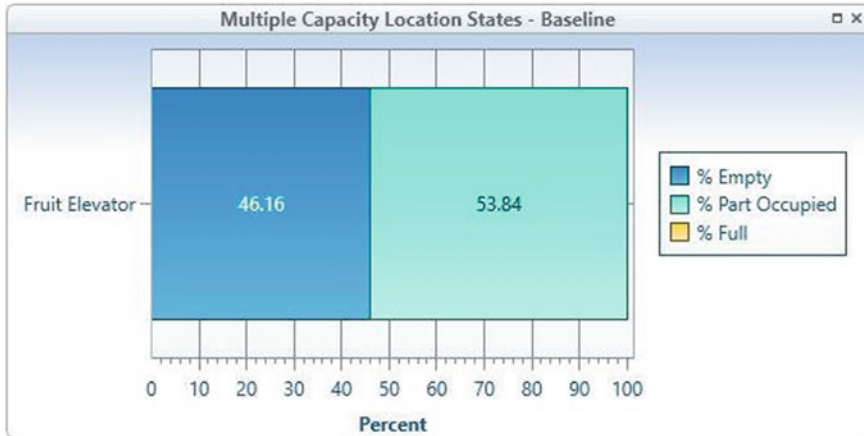


Fig. 21.6 Statistics for multiple capacity location states in current design

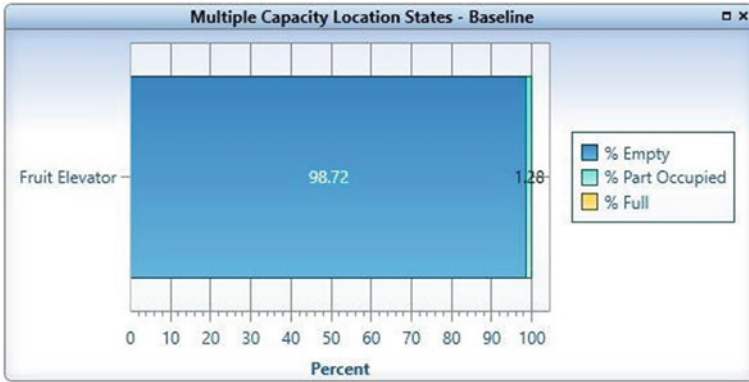


Fig. 21.7 Statistics for multiple capacity location states in proposed design

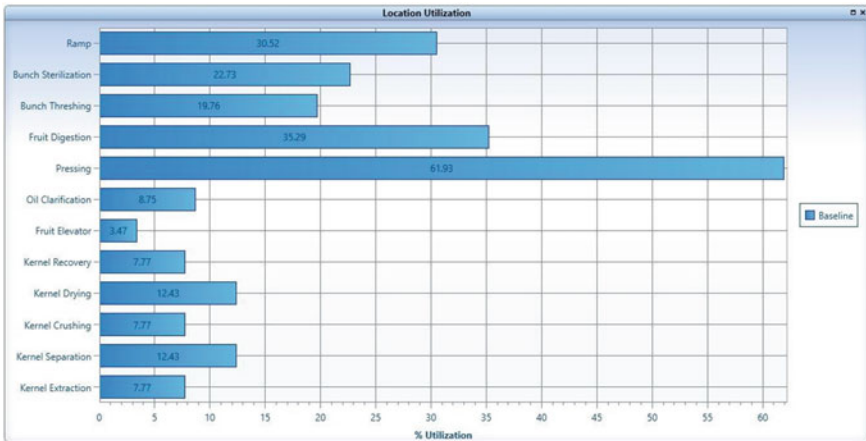


Fig. 21.8 Statistics for location utilization in current design

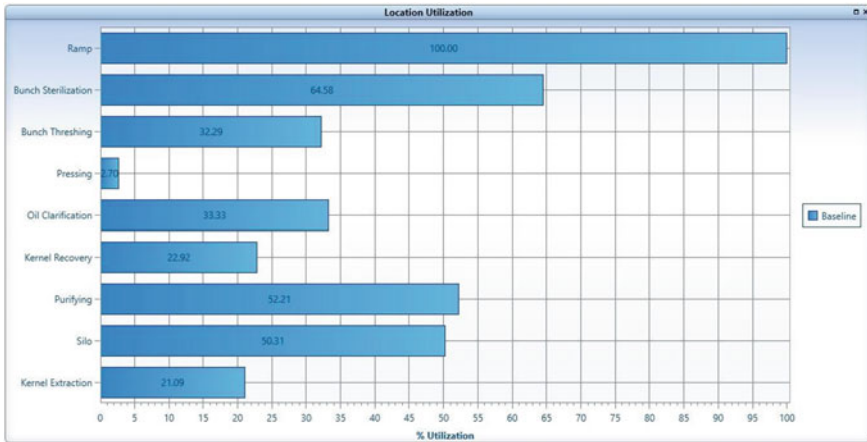


Fig. 21.9 Statistics for location utilization in proposed design

21.4 Conclusion

21.4.1 Overview of the Study

The goal of this research is to investigate the production process operations, create simulation models to determine the plant’s production process efficiency, and discover the differences between the production process’s present and suggested designs. Hopefully, everyone will get something from this study.

21.4.2 Recommendation

Several recommendations and suggestions on the effectiveness of the manufacturing process will be offered at the conclusion of the research based on the findings and analysis of the preceding section.

21.4.2.1 Upgrade the Machine

The study team looked at the production-related issues Diamond Jubilee Sime Darby Plantation Sdn. Bhd. was experiencing. Due to a shortage of machines in the operation of their production process, they experienced a short time difficulty when there are several procedures for raw material input. This occurs because they desire to meet their daily output targets. To make improvements, the researcher suggests the company to reduce the occupation times of each machine while upgrading the

equipment to enhance and improve their operations. The production activities are greatly improved with the addition of a machine. As a result of this development, the company decreases the wastage of unfinished raw materials and spares their workers from working till the wee hours of the morning since it would be more effective if implemented.

21.4.2.2 Usage of More Technology Than Manpower

Based on the observations, the researcher concluded that Diamond Jubilee Sime Darby Plantation Sdn. Bhd. had a cap on the amount of labour that could be utilised in the manufacturing process. Moving items from one activity to another and handling the machine both take time. Because of this, the researcher advised Diamond Jubilee Sime Darby Plantation Sdn. Bhd. to employ more technology to replace the labour force so that items may be moved from one operation to another without concern for the productivity of the labour force. The PH sensor (ORP sensor), which detects the amount of oxygen a liquid can hold, is one type of technology that Diamond Jubilee Sime Darby needs to deploy. Alternatively, they can determine the pH value of an oil instead of waiting for laboratory results. It is much fastest result than manpower.

Acknowledgements The expression of gratitude is made to everyone who has been involved, whether directly or indirectly.

References

- Enrico B, Claudia C, Roberto R, Roberto M (2010) Using WITNESS™ simulation software as a validation tool for an industrial plant layout. In: Proceedings of the 9th international conference on system science and simulation in engineering Iwate
- Khalili MH, Zahedi F (2013) Modeling and simulation of a mattress production line using promodel. In: Proceedings of the 2013 winter simulation conference, Washington, 8–11 Dec 2013
- Potter L (2015) Managing oil palm landscapes: a seven-country survey of the modern palm oil industry in Southeast Asia, Latin America and West Africa. Center for International Forestry Research, Bogor, Indonesia
- Ravanera RR, Gorra V (2010) Commercial pressures on land in Asia: an overview. International Land Coalition, Rome, Italy
- Setyanto AE (2013) Memperkenalkan Kembali Metode Eksperimen dalam Kajian Komunikasi. JIKOM 3(1):37–48
- Syed ZA, Philip KJ (2008) Transnational corporations from Asian developing countries: the internationalisation characteristics and business strategies of Sime Darby Berhad. Int J Bus Sci Appl Manag 3(2):21–36
- Yasir AS, Mohamed NM (2018) Assembly line efficiency improvement by using witness simulation software. IOP Conf Ser: Mater Sci Eng 319:012004
- Zahraee SM, Golroudbary SR, Shiwakoti N et al (2019) An investigation of the environmental sustainability of palm biomass supply chains via dynamic simulation modeling: a case of Malaysia. J Clean Prod 237(117740):1–64

Chapter 22

The Effect of Oil Spill from Current Oil Spill Incidents in Malaysia



Ismila Che Ishak, Aminuddin Md Arof, Md Redzuan Zoolfakar, Mohd Fairoz Rozali, Hayatul Safrah Salleh, Ahmad Shahrul Nizam Isha, and Nur Aqilah Mohd Sabri

22.1 Introduction

Once the oil spill has accidentally been released into the ocean, it can produce huge problems. The oil spill is a dangerous environmental pollution problem that affects the environment and human health (Pham et al. 2021). The oil spills may harm sea creatures, spoil a day at the shorelines and beach, and get seafood dangerous to

I. Che Ishak (✉) · A. Md Arof · N. A. Mohd Sabri
Maritime Management Section, Malaysian Institute of Marine Engineering Technology, Lumut, Perak, Malaysia
e-mail: ismila@unikl.edu.my

A. Md Arof
e-mail: aminuddin@unikl.edu.my

M. R. Zoolfakar
Marine Engineering Technology Section, Malaysian Institute of Marine Engineering Technology, Lumut, Perak, Malaysia
e-mail: redzuan@unikl.edu.my

M. F. Rozali
Marine Department Malaysia, Ibu Pejabat Laut, Peti Surat 12, Jalan Limbungan, 42007 Pelabuhan Klang, Selangor, Malaysia
e-mail: fairoz@marine.gov.my

H. S. Salleh
School of Maritime Business and Management, Universiti Malaysia Terengganu, Mengabang Telipot, 21300 Kuala Terengganu, Terengganu, Malaysia
e-mail: hayatul@umt.edu.my

A. S. N. Isha
Management and Humanities Department, Universiti Teknologi Petronas, Tronoh, Perak, Malaysia
e-mail: shahrul.nizam@utp.edu.my

consume. It takes a long time to clean up the oil and evaluate the effects of pollution, and it prevents the ocean from recovering fast. The oil spills are initiated by numerous causes such as accidental leaks from ships and offshore oil platforms and often result in exorbitant economic costs and damaging marine ecological degradation (Shi et al. 2019). The oil spill from tankers or other ships, which contain the transportation of liquid or bulk such as crude oil, fuel oil, or heating oil is a significant source of hydrocarbon inputs into the oceans, lakes, and rivers (Doshi et al. 2017). Once an oil spill incident happens, it will harm the marine environment as well as the maritime population at large. The suffocating and contaminated effects of oil on flora and fauna could cause such effects on public health, the local economy because of the loss of tourism and aquaculture, and historically or culturally significant sites (Chilvers et al. 2016). Once, the pollution has filled the water, it might activate destruction to marine life, caused marine life to die, interrupt human health, and disturb the ecosystems either on the sea or on land (Abdullah 2014). The oil spill is predicted to pollute a much greater area than primarily projected due to aggressive weather conditions (Chung and Lee 2016). Even though oil spill incidents are infrequent, once it happens, it could lead to a catastrophic phenomenon and impairment of the sea, environment, people, offshore activities, fisheries, and economics, and crop a negative image of the country. The cleaning up of oily wastewater and crude-oil spills is a global challenge (Fan et al. 2021). Therefore, Malaysia is highlighting the commitment to pollution control of coastal and marine environments as we need to meet seawater quality objectives. Malaysia is also devoted to meeting the obligations of the quality environment as essential by the Environmental Quality Act 1974 (Mustafa 2012). Thus, this research aims to investigate the significant effects of the oil spill from the current oil spill incidents in Malaysia gathered from 11 expert agencies who are dealing with the oil spill response in Malaysia.

22.1.1 *Data on the Oil Spill Incidents*

The data on the oil spill incidents in Malaysian water as shown in Table 22.1 were gained from the Department of Environment (DOE) from 2014 to 2022 showing that 130 oil spill incidents have been declared as tier 1 or tier 2 as refer to Table 22.2 (Norazaimah 2019). Statistically, Table 22.1 shows there were 4 oil spill cases in 2022, 7 oil spill cases in 2021, 16 oil spill cases in 2020, 13 cases in 2019, 17 cases in 2018, 22 cases in 2017, 20 cases in 2016, 15 cases in 2015, and 16 cases in 2014. As of now in May 2022, there are no oil spill incidents cases reported as a tier 3 disaster (Azila 2021).

Table 22.1 The tier response (Sullivan et al. 2015)

Year	2022	2021	2020	2019	2018	2017	2016	2015	2014	Total
Cases	4	7	16	13	17	22	20	15	16	130

Table 22.2 The oil spill cases in Malaysian for 2014 to 2020 (Norazaimah 2019; Azila 2021)

Amount of spill	Proximity to operations		
Large of spill			Tier three
Medium of spill		Tier two	
Small of spill	Tier one		

22.2 Literature Review

22.2.1 The Effects of Oil Spill

Once the oil spill incidents occurred, it caused a serious reflection and vulnerability to all of us involving the marine life and ecosystem, economy, social, fishermen, and tourism industry and generated a bad image of the country. The major effects of the oil spill include marine habitats, coastal and health. **(a) Marine Habitats:** Even though major oil spills from tankers are rare occurrences, it remains one of the main worries for the numerous stakeholders in marine environmental protection since of the potentially major impacts of oil spills on marine ecosystems, important socio-economic impacts on communities dependent on coastal resources and high costs of clean-up operations (Goerlandt and Montewka 2015). The oil spill is one of the most serious causes of marine pollution which not only brings huge economic loss to society but also influences the marine ecological environment, leads to damages to ecological balance, and leads to the destruction of nature and the organism immediately or in a long term (Farrington 2014). **(b) Coastal:** Once the oil spill occurred, the spilled oil easily can penetrate the beach sediments. Coastal sand beaches and seashore meadows are the most sensitive to the effects of oil and have threatened habitats, plants, and small animals along the coast. The polluted spilled oil could also affect the shore vegetation and inhibits the absorption of sunlight which is necessary for photosynthesis and growth of the plants (Pezeshki et al. 2000). **(c) Health:** The spilled oil poses direct threats to human health from inhalation or dermal contact with the polluted oil and dispersant chemicals and indirect threats to seafood safety and mental health. An aliphatic and aromatic hydrocarbon are the main components of crude oil. Once the evaporated oil has reached the water surface, it can cause respiratory irritation and central nervous system depression, cause leukemia in humans, nasal tumors, and lung cancers in humans and animals (Solomon and Janssen 2010).

Table 22.3 Likert scale score of 7 points

1	2	3	4	5	6	7
Least important	Less important	Slightly important	Moderate important	Important	Very important	Most important

22.3 Methodology

22.3.1 The Pilot Test

A pilot test involves a small study to test research protocols, data collection instruments, sample recruitment strategies, and other techniques in preparation for research studies (Zailinawati and Schattner 2006). The pilot test involves the distribution of a questionnaire to five samples of the agencies and government authorities which covered the Marine Department, Department of Environment, PIMMAG, and Maritime Academy.

22.3.2 Likert Scale

A Likert scale is used as an important tool in psychology, social survey, and collecting attitudinal data. The Likert scales insist respondents choose amongst the 7-points level of agreement for that statement based on their point of view as shown in Table 22.3. The respondent’s level of agreement with the statement provided is measured in the questionnaires using an application of the Likert scale (Dittrich et al. 2007). The scale is frequently utilized in surveys or questionnaires, for benchmarking feedback in several fields (Pescaroli et al. 2020).

22.3.3 The Proposed Summary of Theoretical Framework

Figure 22.1 supports the proposed summary of the theoretical framework which contains on independent and dependent variables of this research. It covers on the effects of the oil spill towards the current oil spill incidents in Malaysia.

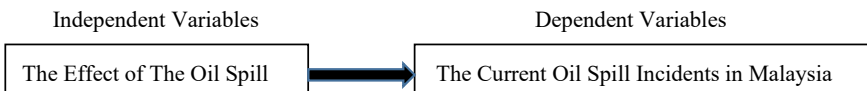


Fig. 22.1 The proposed summary of theoretical framework

22.4 Result and Discussion

The respondent's background shows most of the respondents were male 45 respondents or 76.3%. This is because the predominant gender functions in the maritime field are dominated by a male as this field necessitates masculine employees. The age of 31–40 years old represent most of the respondents or with 32 respondents or 54.2%. This is because at this age most of the respondents have completed their education study by having degree qualifications from various backgrounds to enable them to work in the marine-related field. It shows that most of the respondents have education at a degree level 34 respondents or 57.6%. Meanwhile, for the current position, most of the respondents were in the middle management 25 respondents or 42.4%. Thus, having a position in the middle management inspires the employees to effectively have a good quality working attitude. Meanwhile, the experience of the oil spill with below 3 years or by 27 respondents or 45.8% contributes to the highest responses. This is because not all the respondents are exposed to oil spill incidents directly. Finally, the familiarity of the respondent with the oil spill incidents shows at a moderate level with 33 respondents or 55.9%. Hence, it is anticipated that this respondent profile provides integrity and credibility to the information collected over the questionnaire evaluation circulation.

22.4.1 *The Qualitative Analysis of the Effect of the Oil Spill from the Current Oil Spill Incidents*

Table 22.3 shows most of the respondents have considered the effect of the current oil spill incidents in Malaysia would create damage to the marine life, ecosystem, and pollution of the seawater. Petroleum is known as one of the most significant contaminants in the marine ecosystem, and oil spills have a long-term effect on the marine environment (Yang et al. 2019). This feedback that supports the desired effect was given by 23 respondents out of 59 respondents in Group A. Meanwhile, the second effect involved 18 respondents on the crop effect on the coastal life, fisheries industries, food insecurity, food supply, and marine community as in Group B. The third group highest is Group C which is on the influence on the marine environment by 12 respondents respectively.

22.4.2 *The Quantitative Analysis of the Effect of the Oil Spill from the Current Oil Spill Incidents*

To achieve this aim, question No 1 was applied to rate the effects of the oil spill and the expert respondents were then asked to rate the effect on a five-point Likert scale, beginning with 1 for “Least effective” to 5 for “Most effective”. All the 59

respondents that provided their feedback have given their ratings on the current effect involved allowing for reliable use of descriptive statistical analysis, mean and standard deviation analysis, and Cronbach's alpha on SPSS version 26 software to test the average consistency of the ratings given by all the respondents on the effects. The feedback received was from 11 organizations and shows most of the organization 90.00% has agreed that the response to the current oil spill incidents in Malaysia is moderately effective, Table 22.4.

Table 22.5 indicates that the mean is at 3.51. It shows that the average group score for the effects of the oil spill from the current oil spill incidents in Malaysia is a higher score of 3.51. Meanwhile, the standard deviation is at 1.023 and measures the absolute variability of the data on the effects of the oil spill from the current oil spill incidents. Table 22.6 shows feedback received from all 59 respondents for this section is valid and acceptable. Table 22.7 shows a measure of internal consistency

Table 22.4 The summary of the feedback

Group	Feedbacks	Total feedbacks	Ranking
A	Create damage to the marine life, ecosystem, pollution of the seawater	23	1st Highest
B	Crop effect on the coastal life, fisheries industries, food insecurity, food supply, marine community	18	2nd Highest
C	Influence on the marine environment	12	3rd Highest
D	Consequently, bad influence on human life, loss of income, human health, socio life	12	3rd Highest
E	Raise the cost of cleaning activities, increase manpower cost, increase the recovery process, increase time consumption	11	4th Highest
F	Effect on claim and compensation, profit, and loss management	5	2nd Lowest
G	Impact on availability of the equipment, maintenance of equipment logistics, transportation	8	3rd Lowest
H	The result of the low agency's collaborations, miscommunication, influence from a bad relationship with another agency	10	4th Lowest
I	The outcome of the low management, lack of Standard Operating Procedures (SoP), insufficient practice of the current contingency plan, lack of training and simulation, inaccurate oil spill trajectory	8	3rd Lowest
J	Affect the problem on economics, investment, politics, and damaging relationship with another country	8	3rd Lowest
K	Influence of the forecast of the insufficient meteorological condition and sea state	1	1st Lowest
L	Harmful to tourism activities, economic lost	12	3rd Highest

Table 22.5 Mean and standard deviation analysis

	N	Mean	Standard deviation
The effect of the oil spill	59	3.51	1.023
Valid N (listwise)	59		

Table 22.6 Case processing summary

		N	%
Cases	Valid	59	100.0
	Excluded	0	0.0
	Total	59	100.0

^aListwise deletion based on all variables in the procedure

Table 22.7 Cronbach’s alpha reliability statistic

Cronbach’s alpha	N of items
0.898	

reliability which is useful for understanding the extent to which the ratings from a group of judges held together to measure a common dimension (Osborne and Dillon 2008). Thus, a coefficient alpha of 0.898 from a maximum of 1 simply suggests that the scale scores obtained from the expert respondents are reasonably reliable (Samuel 2010).

22.5 Conclusion

In retrospect, the questionnaire survey can be counted as successfully conducted within less than two months the time taken for all the respondents to deliver their responses. The researcher has conducted an online questionnaire survey via a google form due to the Covid 2019 outbreak which allows the 59 respondents to respond while they are working from home and have sufficient time to respond to this questionnaire survey. A few reminders were sent to the purposive sampling of the response. Based on the analysis, the results show that the top five effects of the oil spill response are as follows. Firstly, the highest is to create damage to the marine life, ecosystem, and pollution of the seawater. Secondly, crops affect coastal life, fisheries industries, food insecurity, food supply, and the marine community. Thirdly, to influence the marine environment. Fourthly, it creates harm to tourism activities and economic loss. Finally, to raise the cost of cleaning activities, increase manpower cost, increase the recovery process, and increase time consumption.

Acknowledgements This research is conducted and supported by the University Kuala Lumpur Malaysia Malaysian Institute of Marine Engineering Technology with cooperation from the UNIKL

academic staff, supporting staff from external organizations together with other associated respondents from several agencies. Without good dedication and cooperation from the team members, it is hard for the research to be finished on time due to the Covid pandemic situation. This research financially obtained funding from the Ministry of Higher Education Malaysia through Fundamental Research Grant Scheme (FRGS) with grant number FRGS/1/2020/SSI03/UNIKL/02/1.

References

- Abdullah HA (2014) Corrosion behavior of steel (St 37-2) by using natural product as inhibitors in petroleum medium. Master Thesis, University of Technology, Iraq
- Azila A (2021) Statistic oil spill. Department of Environment (DOE) Putrajaya. <https://www.doe.gov.my/portalv1/en/>. Accessed 23 Oct 2021
- Chilvers BL, Finlayson G, Ashwell D, Low SI, Morgan KJ, Pearson HE (2016) Is the way an oil spill response is reported in the media important for the final perception of the clean-up? *Mar Pollut Bull* 104:257–261
- Chung SY, Lee G (2016) Combating oil spill accidents in Northeast Asia: a case of the NOWPAP and Hebei Spirit oil spill. *Mar Policy* 72:14–20
- Dittrich R, Francis B, Hatzinger R, Katzenbeisser W (2007) A paired comparison approach for the analysis of sets of Likert-scale responses. *Stat Model* 7(1):3–28
- Doshi B, Repo E, Heiskanen JP, Sirvio JA, Sillanpaa M (2017) Effectiveness of N, O-carboxymethyl chitosan on destabilization of marine diesel, diesel and marine-2T oil for oil spill treatment. *Carbohydr Polym* 167:326–336
- Fan T et al (2021) Robust Graphene@PPS Fibrous membrane for harsh environmental oil/water separation and all-weather cleanup of crude oil spill by joule heat and photothermal effect *ACS Appl* 13(16):19377–19386
- Farrington JW (2014) Oil Pollution in the Marine Environment II: Fates and Effects of Oil Spills *Environment* 56(4):16–31
- Goerlandt F, Montewka J (2015) A framework for risk analysis of maritime transportation systems: a case study for oil spill from tankers in a ship–ship collision. *Saf Sci* 76:42–66
- Mustafa M (2012) The environmental quality act 1974: a significant legal instrument for implementing environmental policy directives of Malaysia. *IIUM Law J* 19(1):1–34
- Norazaimah A (2019) Statistic oil spill. Department of Environment (DOE) Putrajaya <http://www.doe.gov.my/>. Accessed 22 June 2021
- Osborne J, Dillon J (2008) Science education in Europe: critical reflections. King's College London, London
- Pescaroli G, Velazquez O, Ayala A, Galasso C, Kostkova P, Alexander D (2020) A Likert scale-based model for benchmarking operational capacity, organizational resilience, and disaster risk reduction. *Disaster Risk Sci* 11:404–409
- Pezeshki SR, Hester MW, Lin Q, Nyman JA (2000) The effects of oil spill and clean-up on dominant US Gulf coast marsh macrophytes: a review. *Environ Pollut* 108(2):129–139
- Pham LQ, Olekhovich RO, Uspenskaya MV, Vu T (2021) Study on polyvinyl chloride nanofiber's ability for oil spill elimination Iran. *Polym J* 30(5):473–483
- Samuel J (2010) Using SPSS for windows and macintosh: analyzing and understanding data. Prentice Hall Press, United States
- Shi X, Wang Y, Luo M, Zhang C (2019) Assessing the feasibility of marine oil spill contingency plans from an information perspective. *Saf Sci* 112:38–47
- Solomon GM, Janssen S (2010) Health Effects of the Gulf Oil Spill 304(10):1118–1119
- Sullivan B, Gerard J, Engell-Jensen M (2015) Oil and gas industry guidance on voluntary sustainability reporting. www.ipieca.org. Accessed 15 June 2022

- Yang Y et al (2019) Plastics in the marine environment are reservoirs for antibiotic and metal resistance genes. *Environ Int* 123(1):79–86
- Zailinawati D, Schattner P (2006) Doing a pilot study: why is it essential? *Malays Fam Physician* 1(2&3):70–73

Chapter 23

Optimization of the Effect of Hydraulic Hot-Pressing: Process Parameters on Tensile Properties of Kapok Fiber Nonwoven Web Based on Taguchi Experimental Design



Muhammad Abdul Mun'aim Mohd Idrus, Aniq Danish Azli,
Md Redzuan Zoofakar, Raa Khimi Shuib, and Asmalina Mohamed Saat

23.1 Introduction

Kapok fiber (*Ceiba pentandra*) is a renewable resource with a complex structure. It is widely used in daily life because of its excellent performance and favorable cost. Kapok fibers are lightweight, fluffy, and too inelastic to be spun; therefore, they are suitable for stuffing beds, pillows, and cushions (Chaiarekij et al. 2012). In the last few decades, research interest has moved toward natural fibers such as hemp, sisal, jute, flax, and kapok due to several factors, such as low cost, biodegradability, and application potential (Mwaikambo et al. 2000; Ricciardi et al. 2013). These natural

M. A. M. Mohd Idrus (✉) · A. D. Azli · M. R. Zoofakar · A. M. Saat
Malaysian Institute of Marine Engineering Technology, Universiti Kuala Lumpur, Dataran
Industri Teknologi Kejuruteraan Marin, Bandar Teknologi Maritim, Jalan Pantai Remis, 32200
Lumut, Perak, Malaysia
e-mail: mamunaim@unikl.edu.my

A. D. Azli
e-mail: aniq.azli13@s.unikl.edu.my

M. R. Zoofakar
e-mail: redzuan@unikl.edu.my

A. M. Saat
e-mail: asmalina@unikl.edu.my

R. K. Shuib
School of Materials and Mineral Resources Engineering, Universiti Sains Malaysia, 14300
Nibong Tebal, Pulau Pinang, Malaysia
e-mail: raakhimi@usm.my

fibers are attractive, environment-friendly alternatives to fiberglass as reinforcements in composites. Furthermore, natural fibers are renewable and nonabrasive and exhibit excellent mechanical and physical properties. Their application in composite materials tends to increase because they can save costs and are lightweight. Natural fibers show strength and stiffness comparable with those of fiberglass (Venkata Reddy et al. 2008a; Mwaikambo and Ansell 2002). The strength of natural fiber-reinforced composites is related to the strengths of the components and the fiber-matrix interface (Mani et al. 2012; Venkata Reddy et al. 2008b).

Being a potential fiber, raw kapok has been investigated for several applications, including its use as a reinforcement material in the polyester matrix via hybridization with sisal fabrics and glass (Venkata Reddy et al. 2008b). Also, kapok fiber has been mixed with thermoplastic cassava starch (TPCS) to improve the water absorption of the TPCS/kapok fiber composite and enhance its stress at maximum load and Young's modulus (Prachayawarakorn et al. 2013). The wax layer on the kapok fiber surface endows the fiber with excellent hydrophobic-oleophilic characteristics; thus, this fiber is receiving increasing interest as an oil-absorbing material (Wang et al. 2012).

Much research has been conducted to study the kapok fiber polymer composite; however, the research on transforming kapok fiber into nonwoven fiber through the drum carder method is very limited. The comparison of kapok fiber with other fibers in the market shows that kapok fiber is a potential fiber for marine applications such as for fiberglass boat hulls. Among the natural ecological fibers, kapok is the thinnest and lightest and has the highest hollow degree. The fineness of kapok is only half of that of the cotton fiber currently in the market. The structural properties of kapok fiber, including smoothness, antibacterial function, degradability, easy processability, easy ability to tangle, and heat retention, make it more suitable for marine environments. However, Kapok fibers have some weaknesses; they are not well arranged and aligned, making them weak and challenging to use as mat fibers in boat fabrications. This is because the kapok mat density reduces when the fibers are converted into web fabrics. The fiber density is proportional to the fiber mechanical properties. The higher the density of nonwoven fiber fabrics, the better the mechanical properties.

Much effort has been channeled toward building a suitable process for preparing high-density composites or nonwoven fibers. One of the investigated processes is the thermo-hydro-mechanical treatment (Li et al. 2019; Gul et al. 2017; Akbari et al. 2020). This process increases the fiber density using heat, moisture, and mechanical compression. The process can improve the mechanical properties of low-density materials and expand the application range of low-density materials without changing their characteristics. The study on the effect of high-temperature heating, specifically above 175 °C, on the wood strength and brittleness has yielded various results, because of the different chemical properties and anatomies of the material and the different heating methods (Yildiz et al. 2006).

During hot pressing, the thermal energy enhances the fiber plasticity and creates conditions for integrating different bonds; this results in better density and reduces the voids between fibers, thus increasing the fiber strength. Meanwhile, the thermal energy will cause the moisture in the raw board to vaporize (Gul et al. 2017).

Tanaka and Funaki studied the mechanical properties of heat-treated green composites consisting of rice hull and biodegradable resin. They reported that the heat treatment of rice hull at 600 °C improved the composite tensile strength. Tsukasa et al. also studied the mechanical properties of heat-treated Jute fiber and reported that with the increase in the heat-treatment temperature, tensile strength and stiffness decreased due to the occurrence of cracks on the fiber surface (Nagasaka et al. 2020).

Li et al. reported that the hot-pressing temperature affected the average density of compressed wood for different surface-layer thicknesses. They used a temperature range of 90–150 °C and found that the density was higher when the layer was deeper, and the compressed wood had a uniform density at 180 °C. In contrast, at 210 °C, the density was lower when the layer was deeper (Li et al. 2019). The current heat-treatment methods are not similar; therefore, the properties of heat-treated fibers may also significantly vary. However, we found that the pressure during heat treatment represents a gap in heat-treatment research for fiber. We believe that heat treatment under certain pressures is very important to produce better mechanical properties. More research to find and optimize the effect of these parameters is needed.

In the current study, raw kapok fiber was modified into nonwoven web fabric. An Ashford drum carder as shown in Fig. 23.1 was used to process raw kapok into web fabrics, which have inferior bonding and strength. The fabrics had low density and too many voids. Thus, it will be challenging to fabricate composites due to the physical and mechanical drawbacks of the fabrics. The web kapok structure may easily break, and its dimension is not consistent.

Thermal heat treatment via hydraulic hot-pressing under pressure for a specific time can be used to improve the strength of kapok nonwoven web. Some of the properties degraded owing to thermal modification, but the dimensional stability and the bonding strength increased without the addition of outside chemicals or binders to the fiber after the carding process. Thus, this research investigated the effects of heat treatment on tensile strength and the parameter optimization to obtain the highest tensile strength of nonwoven kapok.

23.2 Methodology

23.2.1 Materials

Natural kapok fiber was collected from local sources in Kuala Kangsar, Perak. The kapok fiber properties are presented in Table 23.1. The Ashford wide (30 cm) drum carder was supplied by Ashford Handicraft Ltd., New Zealand.



Fig. 23.1 Kapok fiber web produced using Ashford drum carder

Table 23.1 Physical properties of kapok fiber

Natural fiber	Liner density	Density (g/cm ³)	Strength (g/tex)	Elongation at break (%)
Raw kapok	1.16	0.96	3.6	1.6

23.2.2 *Kapok Fiber Web Production*

A small Ashford wide (30 cm) drum carder was used for the web formation. Moreover, 100% raw kapok fibers were used, mixed with no other fibers. Each portion weighing 40 g was prepared, and the web was collected from the carding machine, kept in a plastic bag, and placed in an oven at 60 °C. The weight of the web produced after carding was about 8 g. The produced samples with 250 mm × 250 mm dimensions all weighed 8 g.

23.2.3 Hydraulic Hot-Pressing Process: Experimental Design

The conditions for the heat-treatment processing of the kapok nonwoven web are presented in Table 23.2. The web kapok fabric was pressed in a hydraulic hot-press machine under 500, 750, and 1000 psi. The temperature was set at three levels: 160, 170, and 180 °C. Meanwhile, the heating time was set at 5, 7.5 and 10 min. Figure 23.2 shows the hot-pressing process of the web kapok fabric into the nonwoven fiber. The surface transformation and physical observation were observed and recorded for further analysis.

Table 23.2 Experiment parameters

	Process parameter	Processing condition levels		
		1	2	3
A	Temperature (°C)	160	170	180
B	Pressure (psi)	500	750	1000
C	Time (min)	5	7.5	10



Fig. 23.2 Hydraulic hot-pressing of web kapok into nonwoven mat with higher strength

The design of experiments is a professional tool for modeling and analyzing the impact of control factors for high-quality manufacturing systems on performance output. It is important for selecting the control factors. Based on the literature review on the factors influencing the mechanical properties of nonwoven fiber and polymer (Gul et al. 2017; Banik 2018; Carvelli et al. 2021), the selected process parameters at three levels were studied using an L_{27} orthogonal array (Table 23.3). A full factorial experimental design will require at least $27 \times 5 = 135$ combinations of runs. However, using Taguchi's factorial experiment approach reduces it to only 27 runs, significantly reducing the experimental cost and time. Experimental observations were further transformed into the ratio of mean (signal) to standard deviation (noise), that is, the signal-to-noise (S/N) ratios, which are logarithmic functions of the desired output; the S/N ratios serve as objective functions for optimization, which helps in data analysis and the prediction of optimum results. The standard S/N ratios generally used are as follows: nominal-is-best, lower-the-better, and higher-the-better. In this paper, the characteristic values are selected as "higher-the-better" (Table 23.2) and are calculated as follows:

$$\text{S/N ratio}(\text{higher} - \text{the} - \text{better}) = -10 \log \frac{1}{n} \left(\sum_{i=1}^n \frac{1}{y^2} \right) \quad (23.1)$$

where n is the number of observations, and y is the value of the characteristic.

23.2.4 Morphology Analysis

Microscopic analysis was performed using a Leica tabletop microscope. Preliminary sample preparation was performed. The samples were characterized via optical microscopy to study the changes in fiber morphology. Several samples were examined to determine and observe the surface changes due to heat treatment. All observations were performed at room temperature.

23.2.5 Tensile Test

Nonwoven kapok fabrics were tensile tested according to ASTM D 5035-06 on an Instron tensile tester, model 3367. Nonwoven fabric specimens prepared via the raveled strip method (50 mm \times 150 mm) were characterized (Fig. 23.3). Tensile tests were performed at a gauge length of 75 mm and a crosshead speed of 10 mm/min. Five specimens were tested to obtain the average tensile properties.

Table 23.3 Experimental design using L₂₇ orthogonal array with experimental results of kapok fabrics tensile strength

Runs	Variables/factors			Response
	Temperature (°C)	Time (min)	Pressure (psi)	Tensile strength (MPa)
1	160	5	500	22.56
2	160	5	500	22.12
3	160	5	500	22.34
4	160	7.5	750	28.32
5	160	7.5	750	27.95
6	160	7.5	750	28.12
7	160	10	1000	31.38
8	160	10	1000	31.25
9	160	10	1000	31.15
10	170	5	750	33.98
11	170	5	750	33.25
12	170	5	750	33.85
13	170	7.5	1000	36.21
14	170	7.5	1000	36.88
15	170	7.5	1000	35.85
16	170	10	500	37.33
17	170	10	500	37.21
18	170	10	500	37.69
19	180	5	1000	35.23
20	180	5	1000	35.11
21	180	5	1000	36.51
22	180	7.5	500	36.45
23	180	7.5	500	35.85
24	180	7.5	500	36.27
25	180	10	750	34.21
26	180	10	750	35.45
27	180	10	750	34.33

**Fig. 23.3** Sample of hot-pressed kapok fiber prepared for tensile test

23.3 Results and Discussion

23.3.1 Data Analysis from Table 23.3: Taguchi Analysis: Tensile Strength (MPa) Versus Temperature, Time, and Pressure

The mean value was used to determine the effect of each process parameter on the tensile strength of nonwoven kapok (Fig. 23.4). From Fig. 23.4a, the tensile strength increased with an increase in heating temperature from 160 to 170 °C and then decreased with further temperature increase up to 180 °C. This result may be due to the thermal degradation of thermally sensitive kapok fiber. Given these results, higher processing temperatures may damage the fiber and decrease its strength. These findings are supported by the burn spot observed at the fiber surface. This burn spot shows that after 170 °C, the fiber started to degrade. Other researchers have reported similar effects in which the diminution in the strength properties was due to the thermal degradation rate and loss of substances after heat treatment (Yildiz et al. 2006). For example, hemicellulose, due to its degradation, is lost, as it is less stable to heat than lignin and cellulose, and this is believed to be the main cause of the tensile strength decrease. Figure 23.4b illustrates the effect of the heating time on the tensile strength; the tensile strength increased as the time increased from 5 to 10 min. The maximum tensile strength occurred at a heating time of 10 min. The 10 min heating time yielded the optimum effect for the nonwoven kapok; it enables better integration between fibers, allowing better bonding between them. Figure 23.4c depicts the effect of hydraulic pressure on the tensile strength; the tensile strength increased with the increase in hydraulic pressure from 500 to 1000 psi. Thus, 1000 psi was the optimum parameter for this process.

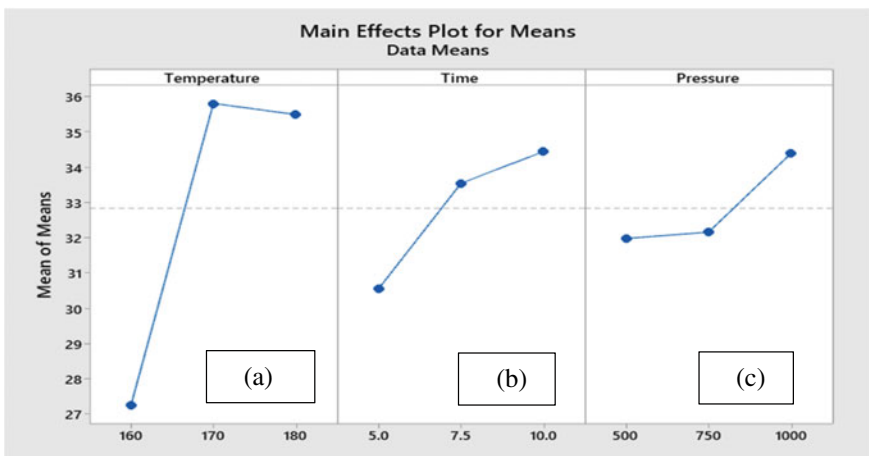


Fig. 23.4 Effect of main process parameters on tensile strength

Table 23.4 Response signal-to-noise ratios for tensile strength (larger is better)

Level	A Temperature (°C)	B Time (min)	C Pressure (psi)
1	28.62	29.52	29.87
2	31.07	30.45	30.11
3	31.00	30.72	30.71
Delta	2.45	1.20	0.84
Rank	1	2	3

The bold text indicates the highest value

23.3.2 S/N Ratio Analysis

In this research, S/N ratio analysis was used to determine the optimal parameters to obtain the highest tensile strength (Table 23.4). The analysis of the results concludes that the largest S/N ratio indicates the optimal processing condition for tensile strength, which is A2B3C3; this optimum level is a combination of 170 °C, 10 min, and 1000 psi.

23.3.3 Analysis of Variance

Table 23.5 presents the results of the analysis of variance (ANOVA). By comparing the percentage contribution of the parameters and the ANOVA results, one can observe that the heating temperature has the greatest influence, since it has the highest F-value and percentage contribution of 95.95%, followed by time (16.85%) and hydraulic pressure (7.34%).

Table 23.5 Analysis of variance results for nonwoven kapok tensile strength (MPa)

Source	DF	Adj SS	Adj MS	F-value
Temperature	2	424.256	212.128	95.55
Time	2	74.830	37.415	16.85
Pressure	2	32.599	16.299	7.34
Error	20	44.403	2.220	
Lack-of-fit	2	40.907	20.454	105.32
Pure error	18	3.496	0.194	
Total	26	576.088		

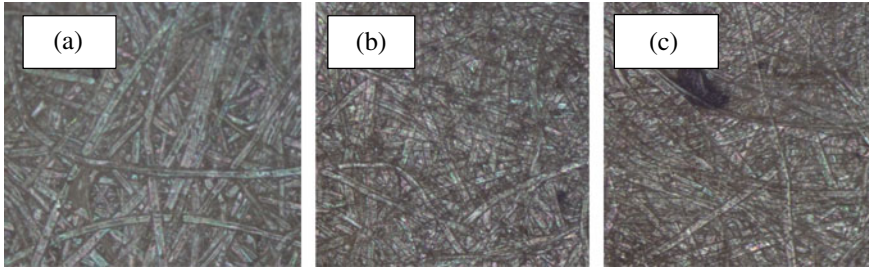


Fig. 23.5 Surface morphologies (100×) of nonwoven kapok samples hot-pressed at **a** 160 °C, **b** 170 °C, and **c** 180 °C

23.3.4 Surface Morphology

Figure 23.5 shows that with increasing temperature, the kapok fiber mats became darker, and the sample pressed at 180 °C had a burn spot. This indicates that the fiber will rapidly degrade as from 180 °C and above. These findings corroborate with the reduced tensile strength of the fiber at 180 °C. When the fiber is being pulled, the existing burn spot will break due to a weak tensile strength. As shown in Table 23.4, The heating temperature at 170 °C was the optimum for the kapok fiber in this study.

23.3.5 Confirmation Experiment

The final step is to predict and verify improvements in the observed S/N ratios using the optimal combination level of process parameters. The S/N ratios for the optimal combination of process parameters can be predicted using the following equation:

$$\eta_{opt} = \eta_m + \sum_{j=1}^k (\eta_j - \eta_m) \quad (23.2)$$

where η_{opt} is the predicted S/N ratio, η_m is the total mean of S/N ratios, η_j is the mean S/N ratio of optimum levels, k is the number of main design parameters that affect the quality characteristics.

The predicted S/N ratios are compared with the experimentally obtained S/N ratios, and the error associated with each performance measure is presented in Table 23.6. The experimental results confirm the validity of the Taguchi method for optimizing the hot-press-forming process parameters. The error between the experimental and predicted values is high (17.98%). Therefore, the tensile strength of the nonwoven kapok needs to be improved by applying the Taguchi experimental design.

Table 23.6 Results of the confirmation test

Performance measure	Optimal process parameter settings	S/N ratio predictive values (dB)	S/N ratio experimental values (dB)	Error (%)
Tensile strength	A2B3C3	32.0375	39.062	17.98

23.3.6 Regression Analysis

This study attempts to derive mathematical models for estimating the tensile strength of nonwoven kapok, a hydraulic hot-press process parameter, using multiple linear regression analysis. Equation (23.3) presents the mathematical models for performance measures.

$$\begin{aligned} \text{Tensile strength(MPa)} = & -46.7 + 0.4123 \text{ Temperature} + 0.779 \text{ Time} \\ & + 0.00483 \text{ Pressure} \\ r^2 = & 0.69 \end{aligned} \quad (23.3)$$

The low equation coefficient $r^2 = 0.69$ confirms the model weakness and suitability; the calculated constants need to be corrected in the future.

23.4 Conclusion

Nonwoven kapok fibers were experimentally investigated, and heating temperature, pressure, and heating time were obtained as the most important hydraulic hot-pressing parameters that influence the fiber tensile properties. On the one hand, as the natural fibers are thermally sensitive, high processing temperature and long heating time will result in thermal degradation. On the other hand, low processing temperature and short heating time will result in insufficient impregnation and wetting of the fiber, which may cause weaker fabrication of the nonwoven kapok web. The experimental results show that the heating temperature has the most significant effect on the fiber, as it determines the strength of the nonwoven kapok after the carding process. The processing pressure also has a significant impact on tensile strength. A high processing pressure of over 1000 psi and a heating time of over 10 min may damage the kapok fiber and lead to its degradation, resulting in poor tensile strength. The heating temperature, heating time, and pressure are significant for increasing the web kapok tensile strength. Moreover, optimum process parameter combinations are obtained from S/N ratios, and mathematical models for the tensile test of hot-pressed nonwoven kapok fiber are proposed. From the results, the most important parameter is heating temperature at 170 °C, followed by heating time at 10 min, and then pressure at 1000 Psi. Establishing the optimal combination of hot-press-forming parameters is beneficial for future research and application of nonwoven kapok.

Acknowledgements This research was funded by Universiti Kuala Lumpur, Malaysia, under Short Term Research Grant (STRG) No: str19051). The study was conducted at the Material Engineering laboratory, Universiti Kuala Lumpur Malaysian Institute of Marine Engineering Technology, and School of Materials, Universiti Sains Malaysia. The authors would like to thank all co-author and the laboratory technicians for their useful contributions to the experimental work.

References

- Akbari E, Ghassemi Kakroudi M, Shahedifar V, Ghiasi H (2020) The influence of different SiC amounts on the microstructure, densification, and mechanical properties of hot-pressed Al₂O₃-SiC composites. *Int J Refract Metal Hard Mater* 91:105235
- Banik N (2018) An experimental effort on the impact of hot press forming process parameters on tensile, flexural & impact properties of bamboo fiber composites with the help of Taguchi experimental design. *Mater Today Proc* 5(9):20210–20216
- Carvelli V, Cesari F, Cavalli E, Guadagnini M, Longo A, Fava G, Zanotti C (2021) Low-velocity impact of hot-pressed PVA fiber-reinforced alkali-activated stone wool composites. *Cement Concr Compos* 114(March):103805
- Chaiarekij S, Apirakchaiskul A, Suvarnakich K, Kiatkamjornwong S (2012) Kapok I: Characteristics of kapok fiber as a potential pulp source for papermaking. *BioResources* 7(1):475–488
- Gul W, Khan A, Shakoor A (2017) Impact of hot-pressing temperature on medium density fiberboard (MDF) performance. *Adv Mater Sci Eng*
- Li R, Huang R, Chang J (2019) Effect of hot-pressing temperature on the density profile of compressed solid wood. *BioResources* 14(1):1482–1493
- Mani GK, Rayappan JBB, Bisoyi DK (2012) Synthesis and characterization of kapok fibers and its composites. *J Appl Sci* 12(16):1661–1665
- Mwaikambo LY, Ansell MP (2002) Chemical modification of hemp, sisal, jute, and kapok fibers by alkalization. *J Appl Polym Sci* 84(12):2222–2234
- Mwaikambo LY, Martuscelli E, Avella M (2000) Kapok/cotton fabric-polypropylene composites. *Polym Testing* 19(8):905–918
- Nagasaka T, Takemura K, Matsumoto K, Katogi H (2020) Mechanical properties of jute fiber using the heat treatment method. *High Perform Optimum Des Struct Mater IV I(December):61–68*
- Prachayawarakorn J, Chaiwatyothin S, Mueangta S, Hanchana A (2013) Effect of jute and kapok fibers on properties of thermoplastic cassava starch composites. *Mater Des* 47:309–315
- Ricciardi MR, Antonucci V, Durante M, Giordano M (2013) A new cost-saving vacuum infusion process for fiber-reinforced composites: pulsed infusion. *J Compos Mater* 48(11):1365–1373
- Venkata Reddy G, Venkata Naidu S, Shobha Rani T (2008a) A study on hardness and flexural properties of kapok/sisal composites. *J Reinf Plast Compos* 28(16):2035–2044
- Venkata Reddy G, Venkata Naidu S, Shobha Rani T (2008b) Impact properties of Kapok based unsaturated polyester hybrid composites. *J Reinf Plast Compos* 27(16–17):1789–1804
- Wang J, Zheng Y, Wang A (2012) Superhydrophobic kapok fiber oil-absorbent: preparation and high oil absorbency. *Chem Eng J* 213:1–7
- Yildiz S, Gezer ED, Yildiz UC (2006) Mechanical and chemical behavior of spruce wood modified by heat. *Build Environ* 41(12):1762–1766